O P T I C A L S T U D I E S

of

G R O W T H & E T C H F E A T U R E S

on

S O M E C R Y S T A L F A C E S

Thesis

Submitted By

Mahmoud Omar

For the Degree

of

Doctor of Philosophy

In the University of London

May 1953

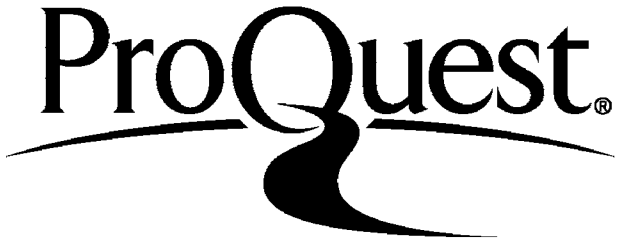

ABSTRACT

The work consists of optical and interferometric studies of growth, slip, and etch phenomena on diamond octahedral faces. For this study special experimental techniques have been developed. These comprise:

(a) Thin film technique for high magnification topographical studies.

(b) Micro-flat for the study of rough surfaces.

The study includes

(1) Evaluation of inter-facial angles of growth hillocks and trigons, so familiar on diamond surfaces. This is carried out by means of multiple beam interferometry, the method competing with goniometry. A similar procedure is adopted to the etch pit.

(2) Cylindrical curvature is discussed and values are obtained for both hillocks and vicinal faces. Trigons are similarly treated, but they are included in another study of a statistical nature (depth versus size).

(3) A theory is developed to account for the existence of trigons. This is first presented as a speculation but is later supported by facts.

(4) Slip has been substantiated to exist in diamond. This has been discovered and studied by means developed in this thesis. The slip plane has been identified as the (111) plane. An opacity has been observed (intimately connected with the slip) which has been duly interpreted.

(5) By artificially etching diamond at a much lower temperature than is usually adopted, etch pits have been observed to be spirally connected. The spirals are oriented in conformity with the crystal symmetry. The susceptibility of the shape and size of the etch pit to the etching temperature has been investigated, also the distribution of depth amongst the etch pits.

(6) The temperature at which the diamond has formed is calculated, and a procedure to be adopted for the complete confirmation is outlined.

C O N T E N T S

INTRODUCTION

Part I

INTERFEROMETRIC STUDY OF DIAMOND SURFACES

Part II

SPECIAL NEW TECHNIQUES

Part III

STUDY OF SLIP IN A DIAMOND

Part IV

STUDY OF ETCH PHENOMENA

INTRODUCTION

CHAPTER ONE.

Diamond.

Diamond both as a crystal and a mineral has a Kingdom of its own. It is an aloof Kingdom and its language is difficult to read. Historically it gained its fame by being an unparallelled gem, and in recent times it has proved to be an unequalled abrasive. The first quality is won by its unusual optical properties (combined high refractive index and dispersion) also by its rarity and durability. The second by its exceptional hardness. In that latter quality it is estimated to be 85 times harder than the next hardest mineral (corundum).(1) Diamond is also a most controversial crystal, both in its origin and mode of crystallization. With respect to its origin there is a big controversy amongst petrologists and geologists as to when, how and where it crystallized. The controversy is even bigger amongst crystallographers as to which particular class of the cubic system it ultimately belongs. The difficulty of the petrologists and geologists has not been lessened by the fact that up to now, diamond has not been grown by artificial means. And the difficulty of the crystallographers has not been finally eased by the fact that x-ray methods revealed its undoubted holohedral structure.(2) When its surface structure, apart from its mode of crystallization, was studied, certain marks were observed on its different habit faces. Then there arose the controversy whether these surface markings were due to growth, or to the fact that diamond in its history has been

etched by an unknown solvent. When two types of diamond were discovered, then it is not known what they really actually represent, and a modern school extensively engaged in its study believes that each type can still be divided in two.[3] The difficulty is accentuated by the suspicion that in the same crystal type I and type II are generally co-existent.[4] It is for the above reasons that crystal growth scientists faced with their own difficulties of explaining how an ordinary crystal grows, have not touched at all upon its growth.

In order to form a background for a good part of the present work we find it necessary to review, substantiate and stress some of its well known features.

Its General Habit Faces:

Diamond crystallizes mostly in the octahedron which represents more than one third of its recovered stones. Octahedral faces are always covered with a tracery of triangular depressions. After Sutton[5] they are called "trigons". These trigons are always situated with their angles pointing to the octahedron edges. Due to the fact that they take the position of etch marks on octahedral faces of other crystals in the cubic system (e.g. Alum and cuprite) they were thought by the earlier crystallographers[6] to be etch marks. Mostly the edges of the octahedron are sharp, but there is a tendency to curvature towards the corners,[5] giving a rounded outline to the whole crystal. Striations are nearly always present down the edges. When these are bold they look like grooves which are sometimes

taken as a sign of twinning.

As the rounded edges and corners of the octahedron become more and more developed, the octahedron faces diminish, and finally disappear. The figure created would approximate to a dodecahedron. But the best way to visualize a dodecahedron, is to imagine triangular plates of diminishing size 'deposited' on all the eight faces of the octahedron. If this happens uniformly, the edges of these layers will be the new faces of the dodecahedron. No wonder that the faces of the dodecahedron are always lined out in striations running parallel to the longer diagonal of the rhombs. It is also conceivable that the edges of the diminishing triangular plates need not exactly fit to give plane new faces. Curvature would be the rule in such a process, and whether the new faces turn out to be convex or concave depends on the thickness of these layers, and how closely they approach each other.(7) Generally they turn out to be slightly convex. When the convexity is noticeable they are called "rounded dodecahedra". This is also how Tolansky explains curvature on crystal faces.(8) Since solution has a rounding effect on crystals,(9) and since these striations or projections are rounded, Fersmann and Goldschmidt used this fact as a support for their solution hypothesis.

Smooth plane faces of the cube are never existent in diamond. When the cube faces exist, they are marked by numerous rectangular depressions called 'tetragons'. These are inverted pyramids and exist in great numbers giving the cube face a

corroded appearance. It is generally believed that the sides of the tetragons are faces of the negative octahedron.

The simple tetrahedron is very rare indeed, and the nearest approach to its form is a distorted octahedron in which four of the eight faces have been unduly developed. Such crystals cause great controversies, because they can be equally described as distorted octahedra, as well as a combination of a positive and negative tetrahedra. It is suspected that a crystal of this type has been used by Fersmann and Goldschmidt to advance their theory of hemihedrism. They describe it as a real tetrahedron but slightly rounded at the corners. They explain the rounding as due to the action of solution, and produce by drawing the etch marks they found on its main faces. This explanation has been strongly attacked by Williams[10] and Sutton.[5] However, Dr. Grenville Wells[7] mentions the use of a tetrahedron in her x-ray experiments. Strangely enough x-rays show its holohedral character.

The Origin of Curvature.

Although diamond surfaces are always quoted for curvature, very few measurements[8] have been made on them.

We have explained one kind of curvature that could arise from the piling of layers, and could arise from the growth of diamond by layer mechanism. The other one is due to a curvature in the growth front boundaries. To account for the frequent curvature of faces and edges Fersmann and Goldschmidt[11]

imagined the diamond to have been immersed in a mother liquor allowing for free movement of crystallization and solution currents. Delicate balance existed between these two kinds of currents such that the material dissolved by one of them could be used by the other, for growth purposes, in a different part of the same crystal. Solution currents mostly acted on the dodecahedron faces leaving bosses, and on the octahedron edges leaving grooves, and on the cube faces leaving cavities. Growth being mainly on the octahedron. This is one reason, perhaps, why they excluded the trigons from being due to etch. These ideas have been recently supported by Shafranovsky.(12)

Sutton stresses that the external forms of diamond are impressed and shaped by the surrounding medium and by forces acting while the diamond was in a plastic state. He agrees with Friedel.(13)

A. Kucharenko(14) attributes the curvature to minute crystal facets whose inclination to one another is very small. Taken as a whole they give the effect of a continuous rounded surface.

Van der Veen(15) made a careful study of diamond surfaces and came to the conclusion that they arise by growth in layers. He also gave a possible explanation for the existence of trigons.

Raman and Ramaseshan(16) (1946) astounded by the extreme curvature of some Indian diamonds developed a theory for the growth of diamond. They conceive the diamond to have resulted from the solidification of carbon which has assumed the liquid form under conditions of high temperature and pressure. They

realise that thermal agitation of atoms in the liquid state would prevent a perfect ordering of the valence bonds within the liquid. Molten carbon would therefore assume a rounded shape. Solidification would be accompanied by a fixation of the valence bonds, but not necessarily with any radical change of shape. According to this view, the form of the rounded diamond is a remnant of the carbon drop modulated by the internal forces.

Structure of Diamond.

According to x-ray finding (2) the structure of diamond consists of two interpenetrating face centred cubic lattices which are displaced with respect to one another along a triagonal axis by one fourth of the cube diagonal. Each carbon atom in the structure has its nucleus located at a point where four triagonal axis intersect, and, therefore, it is quite possible that the electronic configuration of the atoms possesses tetrahedral symmetry. (17) (3)

The length of the C-C bond is 1·54 Å, but the edge of the cubic lattice cell is 3.560 Å in length. Fig.(2) shows such a cell; the planes designated by AAA - are the 111 planes. Fig. (1) shows the structure of diamond with the 111 plane horizontal. To obtain 111 faces, the single vertical C-C bonds are broken.

Some Properties.

According to the above structure these are 8 atoms in the elementary cell ($a = 3.56 \times 10^{-8}$ cm). According to Rinne (17)

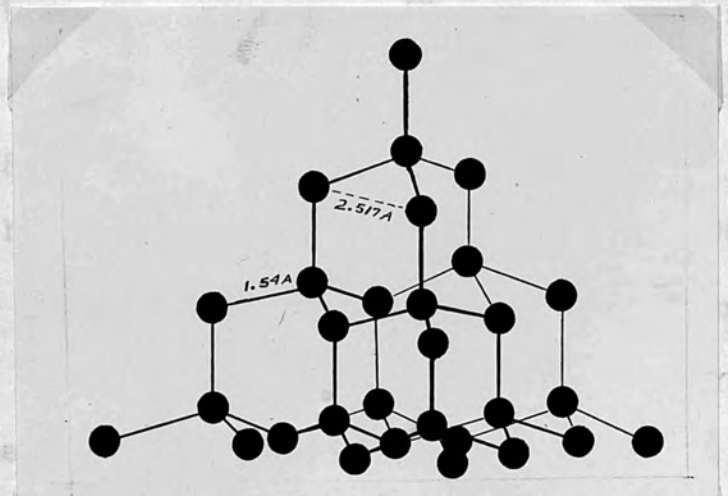

FIG. 1. Structure of the diamond, with the 111 plane horizontal. To obtain 111 faces the single vertical carbon-carbon bonds are broken.

Fig (1).

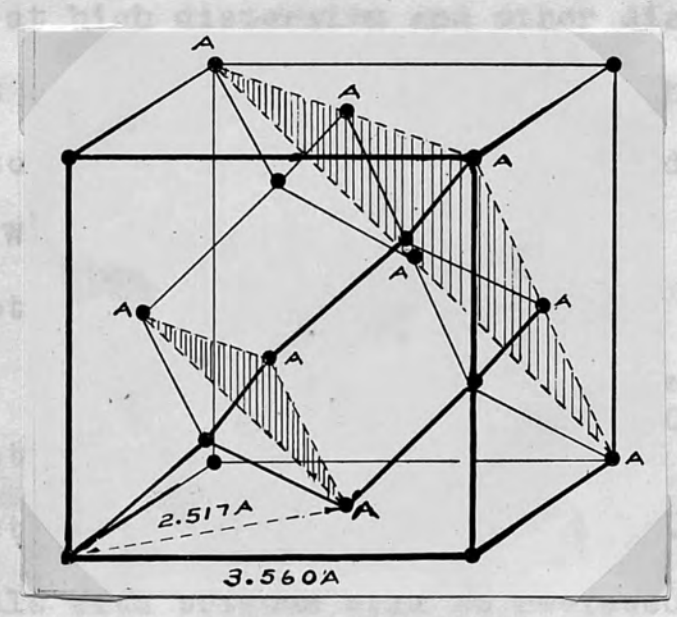

Fig (2).

1 C.C. of the gem contains 180,000 trillion carbon atoms, compared with 1.3 trillion in the carbon vapour at 5500° C . With such packing of the particles of matter, the cohesion between them becomes enormous. The energy necessary to break a C-C bond, as calculated by Harkin [18] has the high value of 6.22×10^{-12} ergs.

Diamond burns in oxygen between 700° and 900° C, but its aptitude to oxygen begins at much lower temperature, and Chapter 14 Part IV of thesis records the etching of diamond at the very low temperature of 5 25° C.

Recent Studies.

In a later work by Tolansky and Wilcock, [8] and by Wilcock alone, [19] interferometric studies of diamond surfaces were undertaken. Perfectly smooth crystals were chosen, and multiple beam fringes at high dispersion and other dispersions were used. They found it convenient to project two or three pictures on the same plate in what is called the "crossed fringe technique". Tolansky and Wilcock found it necessary from their results that growth and not solution would be responsible for the formation of 'trigons'. Further interferometric studies on diamond surfaces constitute the works of Mrs. Wilks, [20] but these were mostly connected with hardness and cleavages. The part of her work that deals with trigons will be reviewed later. A part of the present work constitutes a further study in this field.

CHAPTER TWO

Crystal Growth and Vicinal Faces.

The subject of crystal growth is beset with many difficulties.[21] It is a subject intended to make intelligble how a crystal grows. The essential ideas in this subject were first laid down by Gibbs[22] (1878). His ideas were developed by Volmer,[23] Kossel,[24] Stranski,[25] Becker and Doring,[26] and by Frenkel,[27] (from 1920 - 1945). In the last few years, Burton, Cabrera and Frank,[44] have re-examined some aspects of these theories, and came to the conclusion that such theories will lead to the growth of perfect crystals only under stringent conditions (e.g. high supersaturation). To allow for the growth of ordinary crystals under ordinary conditions, whether in nature or in the laboratory, they had to assume certain imperfections in what is known as 'screw dislocations'.

Closely connected with crystal growth is the kind of growth known as "vicinal growth". It is either a subordinate or an essential growth that appears on crystal faces. It invariably takes the form of flat pyramids whose adjacent faces are inclined to each other at angles of the order of a few minutes of arc. The faces of these pyramids are not all equally developed, but they conform to the symmetry of the crystal on which they are observed, and replace partly or wholly the simple forms of simple indices. They are responsible for the variation of 'interfacial angles' between main faces of the same crystal forms. It is due to them that crystal faces only

approximately obey the law of rational indices.

Pfaff[28] made an extensive study of interfacial angles of some cubic crystals, and came to the conclusion that the observed values differed from one minute to thirty minutes of arc from the theoretical values based on the law of rational indices. Similar results were obtained by Brauns[29] (on octahedra of lead nitrate and spinel, who attributed them to the distorting action of gravity during crystallization. Because some of the vicinal faces possessed smoothness and uniformity comparable with the best faces seen on crystals, some of the early workers, in particular Scacchi[30] considered them to be true lattice planes of low indices which have been dislodged during the cooling process. Another view held by Mallard[31] attributes them to twinning. According to Buckley[9] this last interpretation paints a far more complicated picture of the growth of a crystal.

The nature of the vicinal faces on a growing crystal was studied by Miers.[32] Miers constructed a special goniometer that enabled him to measure interfacial angles to one minute of arc, while the crystal was suspended in the mother liquor. He began with cubic crystals whose theoretical angles were calculable (e.g. Alum) and found that the goniometric reflection from each face of the octahedron resulted not in one but three equally spaced images. They were due to a low triakisoctahedron replacing the true octahedron face of the alum. This was Miers' most important discovery. He also occasionally found an

octahedron face of alum with two sets of triakisoctahedral replacement, the lower set having closer positions to the true lattice plane. In many cases one of the vicinal faces of one set would push the other two aside in a process of elimination. Miers studied other cubic crystals and found that in every case the replacement of the vicinal faces was not gradual but 'per saltum'. He came to the conclusion that the indices of the vicinal faces, however high, were rational. As an example, a plane situated at 6′ 7″ to the true (111) position was calculated to be of the form (251,251,250). He made this calculation by the way of an example not to be seriously taken, because it is obvious that as the indices get higher, variation within experimental limits, may take one from one set of indices to another of slightly different proportions. It is perhaps for these reasons that Hintze (33) originated the idea of describing them by their angular deviations.

Miers also measured the refractive index of the liquid in contact with the growing crystal and came to the conclusion that it is slightly supersaturated. The supersaturation in his experiments (e.g. Sodium nitrate) was less than 1%. According to the recent theories of Frank, growth could not have proceeded except by spiral mechanism. Miers' observation is that the vicinal form becomes flatter where the solution is more concentrated, also that it becomes more acute as the growth proceeds. It is not known with certainty that the dislocation theory has a clear-cut interpretation of these two phenomena.

In a later paper, Hedges[34] using the same kind of goniometer as Miers dealt with Epsom and Rochelle salts, and supported Miers' main views. But he throws some doubt on the rationality of vicinal faces. Shubnikov and Brunowsky[35] have also studied the relationship of vicinal faces to the true lattice planes. They leave quite open the question whether they have rational indices or not. They used x-ray and goniometric as well as geometric methods, and came to the conclusion that good vicinal faces are truly plane, but Tolansky[36] studying quartz by multiple beam interferometry detects a slight cylindrical curvature in the vicinal faces.

Kalb[37] in a series of papers extended the goniometric method to non-cubic crystals, including quartz and topaz. He pays great attention to the relation of the vicinal faces to crystal symmetry. Because of their very low angles, vicinal faces cannot occur in more than one common zone. If two zones of vicinal faces intersect it was perhaps proper to assume that some true crystal plane of low index exists at the junction of the two zones.

Regarding the reason for vicinal faces we are still in doubt. Wulff[38] tried to trace their effects to concentration currents. But Miers[39] found that they do occur whether the crystal grows in a quiet or disturbed environment. Miers, however, gives a plausible reason for their occurrence. He noticed that the solute (e.g. Sodium chlorate) was 45 times more dense in the crystal than in the adjacent liquid. Now

planes of high indices in a space-lattice contain fewer points in unit area, than planes with simple indices. He therefore suggests that vicinal faces grow upon a crystal in preference to simple forms, because the crystallising material descends upon the growing face in a shower which is not very dense.

Judging by their wide occurrence, the vicinal faces do not seem to be a superficial adherence to crystal faces, and they must play a fundamental part in the growth of crystals. It may be due to their agency that the crystal reaches the stable lattice structure beneath.(9) In recent years, and as a result of observations from many quarters, a new idea has gained ground that growth occurs by the deposition of layers on the crystal's main faces, one layer quickly following another. It is not un-natural to suspect that these layers belong to the growth hillocks which are responsible for the vicinal faces. The growth hillocks themselves arise from centres of initiation of growth. If one layer followed another at comparatively long intervals, the resulting crystal surface would be strictly parallel to the close packed surface underneath. If the layers succeed each other at moderate speed, their tips or edges would form the high index plane of the vicinal faces. The inclination of this plane to the low index surface will depend upon two factors, the depth of the advancing layer and the speed of spreading across the surface. In this picture a low index plane cannot exist, except as a stepped surface, in areas far removed from vicinal faces. The steps follow each other at

relatively great distances and may not be individually detected by the optical microscope. Such surfaces or pieces of surfaces give sharp signals in the goniometer which records their low index. At the vicinity of the centres of initiation of growth where the growth hillocks are centred, the layers follow each other far much more closely and may or may not be laterally resolved by the optical microscope. The apparently sloping "sides" of the growth hillocks, when slightly removed from the centres of initiation of growth, are the vicinal faces. This picture allows for the existence of low index as well as high indices on the same crystal face. In the present work vicinal faces are presented as a continuum of growth hillocks.

It is inherent in above picture that in order to have the largest piece of a low index in a certain face, growth hillocks must be "pushed" as wide apart as possible i.e. to the crystal corners. There the vicinal faces of the same growth hillock will not perhaps be equally spread; at least one side spreads towards the main crystal face. The other sides which must necessarily diminish become incorporated in the edges, and this might account for the grooves observed in diamond. An alternative is that growth hillocks arise from ~~a~~ main centres which controls their growth (Cf. Chapter 6).

Growth by Layer Deposition.

The observation of growth by layer mechanism has been observed by R. Marcelin [40] (1918) who studied the growth of p.toluidine from alcoholic solutions, and by Kowarski [41] who

studied the growth of the same substance from vapour. But among the observations in modern times is the film exhibited by Bunn and Emmet.(42) Their study consisted in placing a drop of warm saturated solution on a warm microscopic slide. This was then covered with a thin cover-slip, and observed under the microscope using high magnification and dark ground illumination. Layers could often be seen spreading over the face one after another. Sometimes relatively thick layers which spread at a moderate speed could be seen to be built up from much thinner and more rapidly spreading layers, and it seemed quite likely that the same thing could happen on a molecular or ionic scale.

Growth by Spiral Mechanism.

In 1931 Volmer and Shultze(43) published the results of some well controlled experiments on the growth rate of iodine crystals from the vapour. Below 1% supersaturation the rate of growth was very much less than the expected value, and this necessitated reconsideration of the whole problem of growth by nucleation mechanism.(44) The two dimensional nucleus was accepted in principle but the rate of its formation of a favourable size for its extension on a close packed plane was extremely neglible. Below 1% the crystal will not perceptibely grow for a time as long as the age of the universe. This time will exponentially decrease with larger supersaturations, and at a supersaturation of 50% or more growth could occur at a reasonable rate.

It was contended that if a crystal contains a dislocation with a screw component, the dislocation generally terminates on one of its faces creating an extended ledge. Growth at ordinary supersaturations will take place by the deposition of molecules along this ledge. The point of emergence of the screw dislocation is called the axis. The molecules in the crystal now no longer lie on planes but on screw surfaces about the axis. By the deposition of molecules the ledge rotates creating a spiral. It is generally assumed that dislocations of opposite signs exist on crystal faces. If a pair of opposite sign are closer together than a critical distance (equal to the diameter of the critical nucleus) no growth occurs. If they are further apart than this they send successive closed loops of steps. The loops may be circular but if growth depends on crystallographic orientation, they change into polygons. The ultimate result is the formation of low pyramids whose sides are the vicinal faces. The above theory accounts for growth from the vapour or from solutions, but it does not touch upon growth from the melt. Since then spirals have been observed on a large number of crystals.[45]

Most of the success that accompanied the above theory came from this laboratory.[46] The only independent support came from the electron microscope.[47] The only substance that accompanied the birth of the spiral when it was without theory is Si C. Menzies and Sloat[48] observed it on that crystal as far back as (1929). It is the substance which Verma[46] used to

support the dislocation theory of growth, and it is the substance on which Buckley[49] has observed spirals long before there was any theory for them. Buckley[50] attributes spirals to some macroscopic events occurring in the vapour adjacent to the surface at the moment of solidification. He conceives the possibility of Vortices or swirling motions and eddies being produced by the rapid motion of vapour through numerous narrow orifices provided by the porous mass of the growing crystal.[51]

CHAPTER THREE.

Multiple Beam Interferometry (Theory and Practice).

Three names will always be mentioned in the kind of interferometry in which light is reflected and made to interfere between two surfaces brought into as near close contact. The first is Newton because of his rings. His fringes opened the field. The second is Fizeau because he generalised the wedge. Instead of being symmetrical as it is in Newton's rings, it could be any wedge. If the topography of one of the surfaces be known, the other could be deduced. The reasons generally advanced for attributing the wedge fringes to Fizeau (52) is that he realised their working conditions viz: (1) absolutely monochromatic light (2) properly collimated rays (3) normal incidence. But are these not the conditions for producing Newton's rings. The third is Tolansky who realised what precision these fringes could give once they become sharp and thin by silvering the two surfaces concerned.

Multiple beam interferometry found the modern technique of vacuum evaporation ripe for its use and development. Before its actual birth on the hands of Tolansky it was a latent method and has not been used except perhaps once in the testing of etalon plate flatness. (53) It consists of the use of a light source, relatively powerful, but restricted in size, placed in the focal plane of a lens to produce a collimated beam of light. The use of certain filters makes this light nearly monochromatic.

The fringes are formed by multiple reflections at normal incidence between two silvered surfaces, one being the surface to be examined, and the other an optical glass flat, placed in close proximity to the latter. Owing to the occurrence of multiple reflections, the fringes are very narrow and therefore clearly defined. As they are Fizeau fringes they follow the contour lines of equal distance.

Two - Beam Fringes.

If the reflectivities of the surfaces are low, the first reflected beam from the second surface contributes effectively to the interference, and the problem resolves itself into finding the resultant effect of two coherent wave trains, of the same frequency, with amplitudes r_1 and r_2 (taken to be equal) one lagging behind the other in phase by $\delta = \frac{2\pi}{\lambda} \cdot 2\mu t \cos\theta$, where λ is the wave length, t the separation and μ the refractive index of the medium. The square of the resulting amplitude gives the intensity "brightness" at any point of the film as :

$$I = 4 r^2 \cos^2 \frac{\delta}{2}$$ i.e. of the $(\text{cosine})^2$ type.

Multiple Beam Fringes

The rounded top of these intensity distribution patterns, characteristic of two beam interference, makes the resultant fringes unfavourable for precision measurement, aside from the lack of contrast. Boulouch (1893) first drew attention to the important change in "intensity distribution I" if the reflection

(54)

amplitudes "r_1" and "r_2" of the surfaces are increased by semi-silvering. The beams which arise from multiple reflections in the film can no longer be ignored, and their effect on the intensity distribution is similar to the effect of the many openings in the grating compared with a double slit. The spread of the maxima in (transmission) and the minima (in reflection) becomes much more confined and the fringes can be made extremely sharp.

Multiple reflections have not only immensely improved the two-beam reflection-fringes, but have for the first time made transmission-fringes a practical proposition. Owing to the disparity between the two main interfering beams two beam interference fringes, in transmission, were masked by background intensity and were hardly visible. The power of the transmission fringes lies in the fact that, being bright against a dark background they appear with their natural colours enabling the allocation of orders. They have also been used in such techniques as the crossed fringe technique.[8] Their contrast does not appreciably depend on the absorption of the silvering. For all these reasons they were the first fringes discussed by Tolansky[55] and Brossel.[56] The reflected systems were later treated by Holden[57]; the original counterpart for chemically deposited silver films having already been admirably and ably treated by Hamy.[58]

Intensity Distribution in Multiple Beam Fringes:

Fig (3) is the general case of two partially transparent metal films forming the boundary of three dielectric media. Let the angle of refraction of the main ray at the first boundary be θ , the amplitude reflection factors of surface (I) for light incident from outside or the interspace be r_1 and r_1' respectively, and the phase changes occurring in these reflections be α_1 and α_1' . For passage in film (I) downward and upward, the amplitude transmission factors and phase changes are t_1 , t_1' and β_1 , β_1' . Suffix 2 will apply to surface (2).

The amplitudes of the outer transmitted beams form a geometrical progression with the factor $r_1\, r_2'\, \exp.\{i(\alpha_1' + \alpha_2' + \delta')\}$ where $\delta' = (4\pi n_2 y \cos\theta)/\lambda$ and n_2 is the refractive index of the medium of the film between (I) and (2). The square of the modulus of the sum of this infinite series is the well known Airy intensity distribution (59)

$$I = \left(\frac{T}{1 - R}\right)^2 X \frac{I\ max.}{1 + F \sin^2 (\alpha_1' + \alpha_2' + \delta')/2} \quad \ldots(I)$$

where F is the Fabry-Perot 'coefficient of finesse' $4R/(1 - R)^2$, and $R = r_1'\ r_2'$ and $T = t_1\ t_2$.

Provided the conditions permit a close approximation to Airy summation, then whether the $\sin^2$ term variation is produced by either λ , θ , or y or combinations of these,

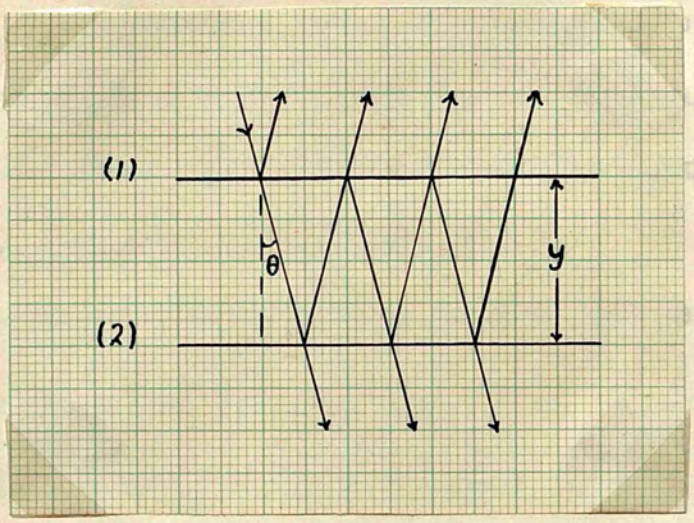

Fig. (3).

the fringe intensity distribution will be the same. These three quantities exist implicitly in δ', and it will be noted that for colour filters the factor $\frac{1}{\lambda}$ is the essential variant; for monochromatic Fabry-Perot fringes the factor θ; and for Fizeau fringes the factor y is the main variable. For fringes of equal chromatic order, as will be seen, the variable is y/λ. To return to our normal use of symbols we restrict ourselves to the normal wedge which is an air film $\mu = n_2 = 1$ and $y \equiv t$. δ' takes the familiar form $\frac{2\pi}{\lambda} . 2\mu t \cos\theta$. Neglecting phase changes at reflection, δ' is the only phase change equivalent to the normal path difference $\delta'/2\pi$. This leads to the familiar expression $n\lambda = 2\mu t \cos\theta$., where n is integral.

But it must be remembered that the actual phase change is

$$\delta = \delta' + \alpha_1' + \alpha_2'$$

where $$\delta = 4\pi\mu t \cos\theta/\lambda + \alpha_1' + \alpha_2' = 2n\pi$$

$$\therefore \quad n\lambda = 2\mu t \cos\theta + \Omega\lambda$$

Ω is dependent upon the wavelength, the incident angle, and the state of polarisation and equals $\frac{1}{2\pi}(\alpha_1' + \alpha_2')$. Reference is made to this function Ω in connection with a new method of estimating order by visual inspection of Fizeau fringes (illustrated in a subsequent section).

Fringes of Equal Chromatic Order.

With λ variable, and if θ is constant and t varies,

fringes are produced in which $\frac{t}{\lambda}$ is constant for each fringe. In the simplified formula, this represents the order n. These are obtained when white light is substituted for the mercury, the filter being removed. The image of the interferometer is at the same time projected on the slit of a spectrograph. Considering the transmitted fringes, each small element behaves as a colour filter, transmitting certain wavelengths only. The transmitted wavelengths are given by

$$n\lambda = 2\mu t \cos\vartheta + \Omega\lambda. \qquad \text{.....(2)}$$

For an air gap illuminated normally the wave number difference between any two transmitted fringes of order n and $(n-1)$ is

$$\Delta\nu = \nu_{n+1} - \nu_n = \frac{\lambda_n - \lambda_{n+1}}{\lambda_n \cdot \lambda_{n+1}}$$

$$= \frac{1}{2t}\left\{1 - (\Omega_{n+1} - \Omega_n)\right\}$$

For silver films it is generally assumed that the phase difference involved in Ω is small. This is justifiable in most cases. According to Faust,[66] the effective order of interference is $(n - \Omega) = \frac{2t}{\lambda_n} = \frac{\lambda_{n+1}}{\lambda_n - \lambda_{n+1}}$

When a silvered wedge is projected on to a spectrograph with its apex is $\perp^r$ to the slit, the fringes produced in the spectrograph are inclined, and the direction of their slope gives the direction of the wedge. This is of immense value in surface topography. Not only is the direction of the wedge determined but the topography across any certain line is

precisely measured. With these fringes which share Fizeau fringes their intensity distribution, Tolansky and Khamsavi[60] examining a cleavage surface of calcite were able to measure a step of 12 A ± 3. By their use was Verma[61] able to measure step heights of unimolecular growth spirals (15 ± 2 A) and Griffin[62] a step height of about 8 A.

High Dispersion Fringes.

When the two surfaces concerned are in closest contact forming a small wedge angle, high dispersion exists. When the general wedge angle reaches the value of zero the local wedge angles created by the features become the sole determining factor. Fringes will run parallel to the wedge apices created by the features. Since the features are the wedge apices themselves, it is clear that the fringes will run parallel to the features. In other words the topography of the surface will be imitated exactly by the fringes. Since there is contrast in the fringes (especially in transmission when the fringes are coloured) which may be lacking in the features, the advantage is extreme visibility. This particular kind of high dispersion is sometimes called the geographical dispersion. To show how it imitates the features fig (4) shows this particular kind of dispersion using green mercury light in transmission. The exact similarity in outline between this picture and fig (5), which is effectively a photo-micrograph of the same area, is quite evident.

Fig. (4). x 165

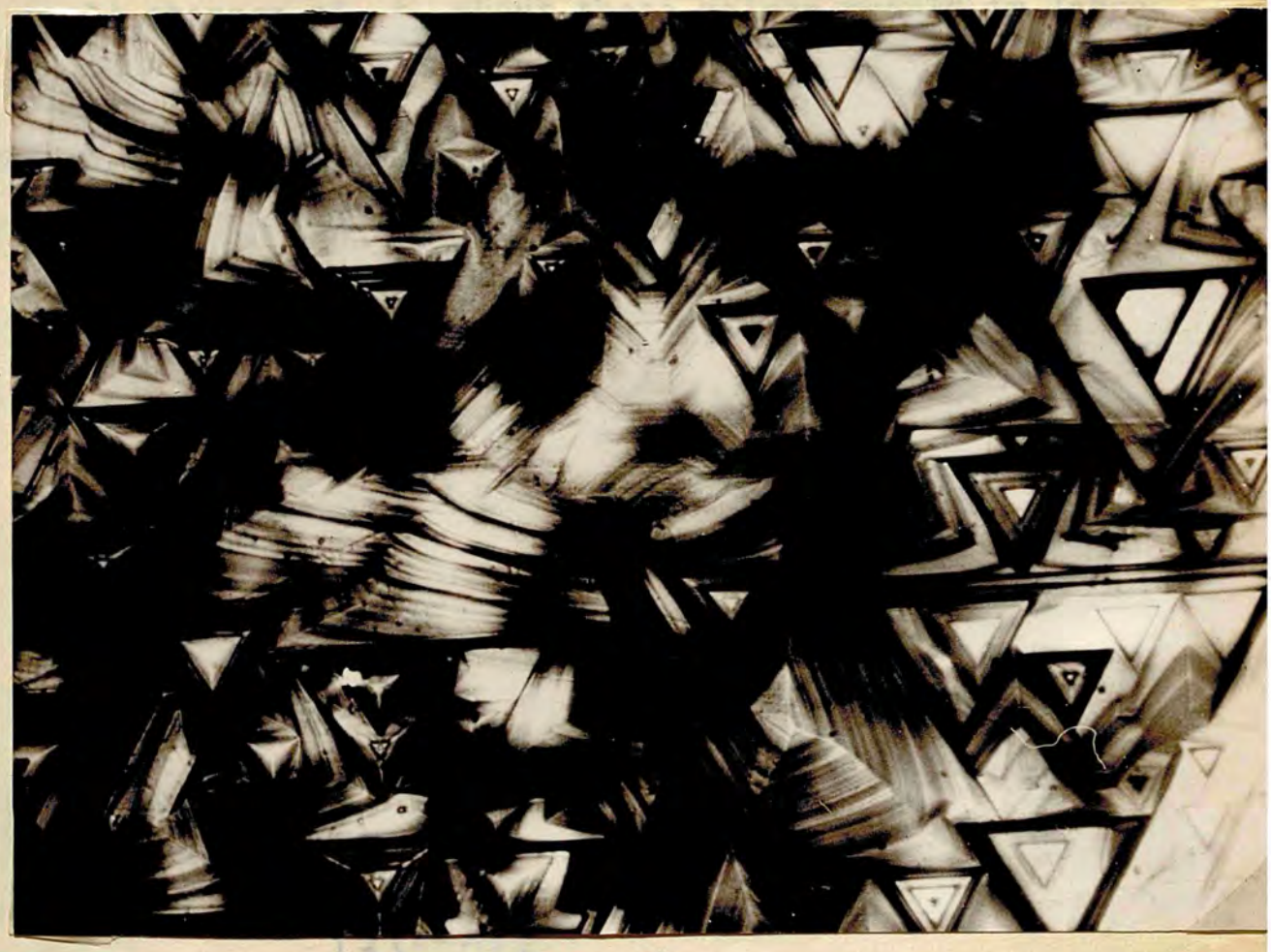

Fig. (5). x 165

Sensitivity of the High Dispersion.

If there is no absorption (T = 1 - R) considering normal incidence and using an air gap, equation (1) is simply

$$I = \frac{I\,max}{(1-R)^2 + 4R\sin^2\frac{\delta}{2}}$$

Transforming the phase change $\alpha_1' + \alpha_2'$ into a gap ε to be added to t $\qquad \delta = \frac{4\pi}{\lambda}(t + \varepsilon)$

The illumination of the surface is maximum at any point when

$$t + \varepsilon = \frac{n\lambda}{2} \qquad n = \text{integer},$$

and small changes of t about these values result in large changes of intensity if R is large. From the shape of the Airy summation this change is greatest when the intensity is half the maximum value i.e. when

$$\sin^2\frac{\delta}{2} = (1-R)^2/4R \qquad \ldots\ldots (3)$$

The change in δ corresponding to a small change Δt in t is

$$\Delta\delta = \frac{4\pi}{\lambda}\cdot\Delta t$$

and the change in intensity is

$$\Delta I = \frac{I_{max.}}{\{2(1-R)^2\}^2}\cdot 8R\sin\frac{\delta}{2}\cdot\frac{\Delta\delta}{2}$$

and for δ small i.e. $R \sim 1$

$$\Delta I = \frac{I \max}{2(1-R)^2} \cdot \frac{\sqrt{R}}{1-R} \Delta\delta$$

For $R = 0.94$

$$\Delta t \text{ (in A)} \simeq 27 \frac{\Delta I}{I} \quad \ldots\ldots (4)$$

As 10% change in intensity is perceptible to the eye it is clear that a step of ~ 3 A should be recognisable. In practice this is seldom attained. In the above calculation, due to Tolansky,[8] t is selected such that approximately half the peak intensity is in field of view. If this happens by chance for a single feature at a certain depth it is clear that it does not happen to all the other features at the same time.

A certain interpretation of phase contrast, due to Wilcock[19] gives for green mercury light and diamond surfaces (unsilvered)

$$\Delta t \text{ (in A)} \simeq 60 \frac{\Delta I}{I} \quad \ldots\ldots (5)$$

This equation allots phase contrast with a maximum resolved step of $\sim$ 6 A compared with $\sim$ 3 A for high dispersion. The order of comparison is probably true. On theoretical grounds phase contrast can resolve a step if its height is greater than 30 A[63] but in practice 15 A[61] and probably

10 A is resolvable.

The Half-Value Width and Effective Number of Beams.

The half value width $\delta_{\frac{1}{2}}$ is defined as the difference between two adjacent values of δ for which $I = \frac{1}{2}$ Imax. If this is so, the half width value, as a fraction of an order is $\frac{\delta_{\frac{1}{2}}}{2\pi}$. The reciprocal of this value is the effective number of beams. If N is sufficiently large, the sine of the angle in equation (3) can be replaced by the arc. This gives -

$$N = \pi \sqrt{R} / (1 - R) \qquad \ldots\ldots (6)$$

For $R = .94$ $N = 50$

Another wording for the half-width is that is the width at half the peak intensity. The half-width as a fraction of an order is

$$W = \frac{1 - R}{\pi \sqrt{R}} \qquad \ldots\ldots (7)$$

Its value for 0.94 reflectivity is $\frac{1}{50}$ and for 90% it is $\frac{1}{30}$.

Limitations of Multiple Beams.

The theory and practice of multiple beam interferometry have been fully described by Tolansky (64) in his book "Multiple

Beam Interferometry", and in a variety of original papers by Tolansky [55] [65] and Brossel [56]. A careful analysis has been carried out by Faust [66] and Wilcock [19] and quite recently a review article appeared [67] in which a summary of multiple beam interferometry has been carried out by Kuhn. From these works and from practice there is a general agreement that multiple beams, work only, in the very small wedge angle, and very small separation, provided in a wedge suitably made. The wedge is composed of the silvered surface to be studied and a silvered optical flat. These are brought close together in a special kind of jig. The wedge is viewed by the use of a robust metallurgical microscope. Any shortcoming in multiple beams must, therefore, be attributed either to (a) the property of the wedge: as a progressively increasing separation and (b) the limit imposed by the resolving power of the microscope.

The condition that the N^{th} reflected beam has suffered a phase change of π, and is therefore opposing the Airy summation has been carried out by Brossel [56]. It is

$$\frac{4}{3} N^3 \alpha^2 y = \frac{\lambda}{2}$$

If x is the separation between adjacent fringes

$$\alpha = \frac{\lambda}{2}/x \qquad \text{and} \qquad y = \frac{3x^2}{2N^3\lambda}$$

This gives an upper limit for $y \equiv t$. The limit becomes progressively smaller, the smaller x^2 is (i.e. the closer the fringes are). This limit depends to a greater extent on the number of beams N, and becomes smaller as the reflectivity R increases.

The use of N effective beams makes the half value width of a fringe

$$x' = \frac{\lambda}{2 N \alpha} = \lambda \Big/ \frac{\alpha_n}{2} \qquad \ldots\ldots\ldots (8)$$

where α_n is the angle which the N^{th} beam forms with the directly transmitted beam. α_n is the angular spread of multiple beams, and a microscope will be able to resolve x' if it has N.A of $\frac{\alpha_n}{2}$.

The displacement of the N^{th} beam compared with the first is

$$x'' = 2 N^2 y \alpha = N y \frac{\alpha_n}{2} \qquad \ldots\ldots (9)$$

α_n occurs in opposite positions in (8) and (9). Equating (8) and (9) gives the maximum numerical aperture allowable. This gives

$$N.A = \frac{\alpha_n}{2} = \left(\frac{\lambda}{N y}\right)^{1/2} \qquad \ldots\ldots (10)$$

If $N = 50$ $\quad t \equiv y = \lambda$ $\quad N.A \sim 0.14$

which is satisfied by a 25 m.m. objective. In practice multiple

beam interferometry is carried out quite easily with the 16 m.m. objective. (N. A 0. 3 m.m.). Equation (10) is a convenient way of approach (64)(67) and is a hint that the gap used must be very small.

Finite Source and Finite Line Width.

If the interferometric gap is small a finite source (i.e. a wide aperture) can be used. Tolansky has shown that if the gap $y = t$ is of the order of one micron, a source stop of 6 m.m. diameter may be used. Another advantage of the small gap is that high temperature mercury lamps having a finite line width may be used. The finite line width in the source is due to the finite range of wavelengths emitted by the source. Its effect on the fringe is another broadening. The broadening is not much, and both these factors are sometimes used to increase intensity.

The Practice of Multiple Beams.

In the practice of multipe beams the specimens are thoroughly cleaned with various reagents depending upon their nature. Absorption has a great effect on the visibility of the fringes, especially in the reflection technique. Further cleanliness is achieved in the silvering plant where a high voltage glow, provided by a large spark coil, is passed between two electrodes to provide the ions necessary for ionic bombardment.

The silvering plant, without which no multiple beams

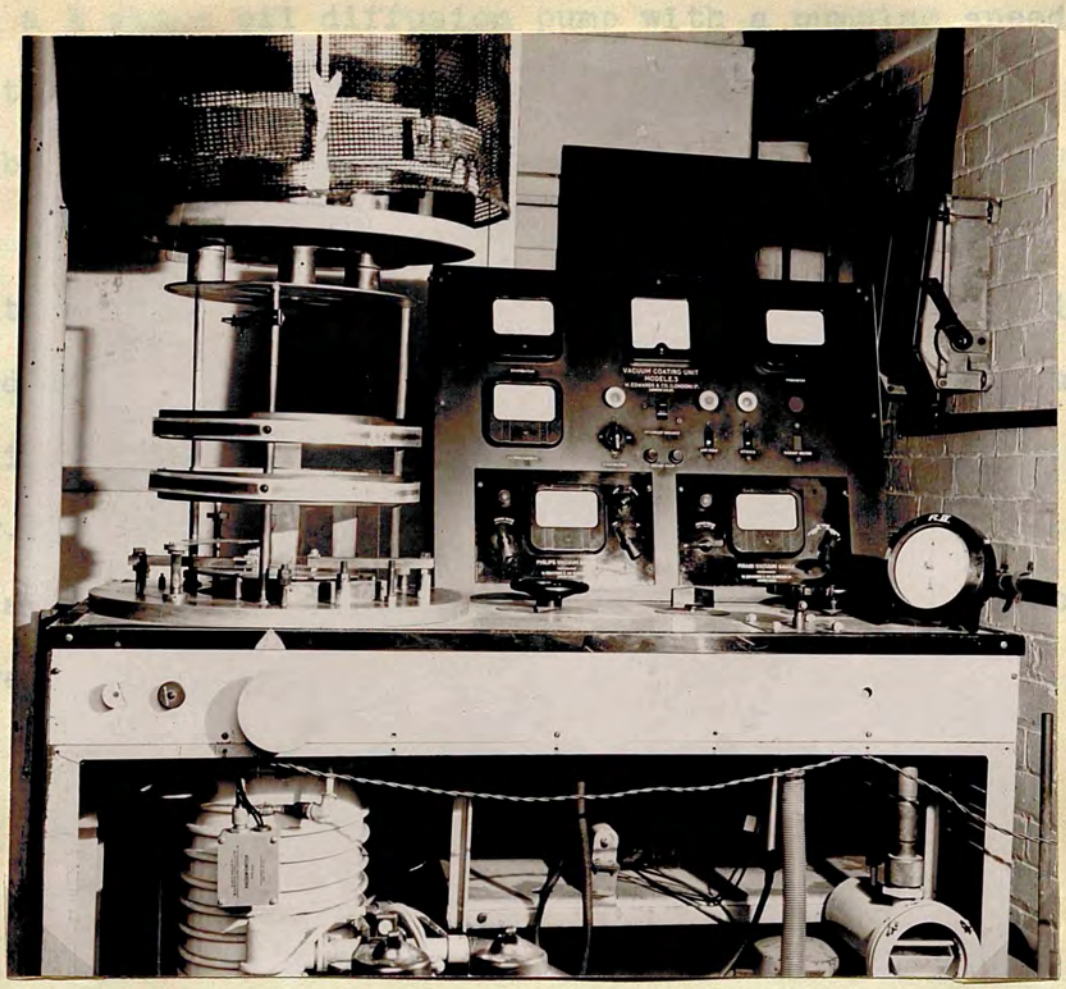

Fig (6).

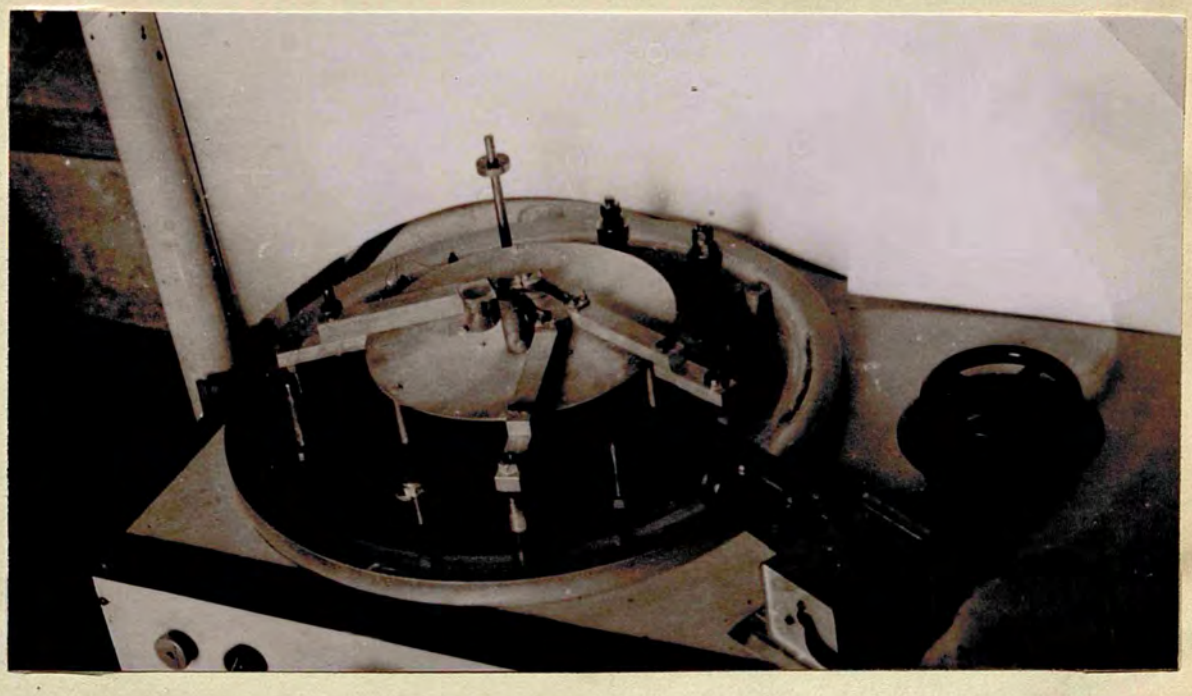

Fig (7).

could be carried out, is photographed in fig (6). The pumping unit is a 3 stage oil diffusion pump with a pumping speed of 1000 litres/sec., backed by a rotary pump. Provision is made on the base plate for several filaments as seen in fig (7), in which a maximum heating current of 150 A mp. passes for evaporation of the silver. The pressure in the chamber is measured by a Philip type ionization guage of the cold cathode type which measures pressures down to 0.5×10^{-4} m.m. of mercury.

I am indebted to my colleage J.A.Belk for the loan of the negative of fig (7).

P A R T I

Interferometric Study

of

Diamond Surfaces.

CHAPTER FOUR.

New Techniques and Methods.

A New High Dispersion Technique.

When the flat is equally inclined to the features, and is as near to them as possible, this particular kind of high dispersion was called the geographical dispersion. When the features are extremely flat, high dispersion does not differ much from the geographical dispersion, and a slight adjustment will procure the symmetry necessary for the latter dispersion. It is when the features are moderately prominent that high dispersion can secure a closer approach to the surface. This can only be done in parts at a time, and at the expense of loss in symmetry in the wedge. The symmetry is necessary if the features are to be imitated interferometrically. When the features are more prominent high dispersion becomes useless, and the geographical dispersion must be resorted to. Other dispersions are only useful in step-height determinations.

The general procedure taken in obtaining a high dispersion picture is to open the aperture of the source as much as possible. The source is the mercury arc, the filter being removed. (8,19) In doing so the sensitivity of multiple beams, represented by equation (3) Chapter 3 is not impaired. Only the fringes broaden, and scan a greater area of the surface. Being broad and of different colours, it is in their capacity to scan the whole surface. This method is applicable if the

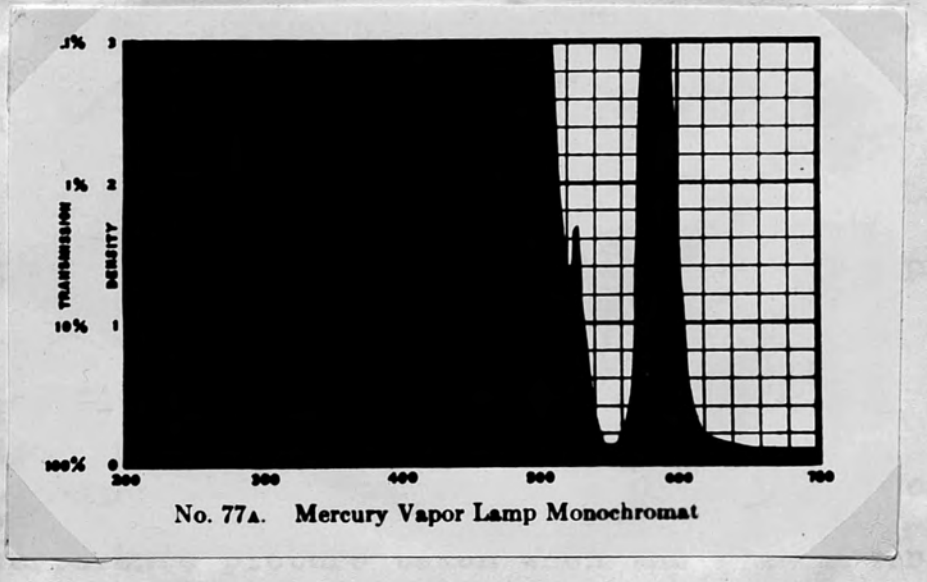

No. 77A. Mercury Vapor Lamp Monochromat

Fig (8).

features are flat, in which case, the optical flat and the surface nearly coincide. It is of no use, however, if the features are prominent, in which case, the geographical dispersion is the only useful dispersion to be used.

Towards the end of work carried out in this thesis, it has been realized that dye colour filters are of immense value in elucidating surface features, if used in conjunction with white light instead of the mercury arc. In particular (Kodak wratten filter 77A) is an ideal filter for the monochromatic green mercury line. When used in conjunction with white light it transmits the two bands illustrated in fig (8). These two bands appear in the interferometer as two broad fringes (green and red) in transmission. Fig (9) represents a part of a diamond octahedron face, taken with this technique, and fig (10) is the phase contrast counterpart. The three photographs (9), (10) and (11) represent the same area. Fig (11) is the interference picture taken when the 77A filter is used in conjunction with the mercury light, and fig (9) is the result when the mercury light is substituted for the pointolite lamp. The extreme similarity of these two pictures is due to the geographical dispersion. Fig (11) is an interferogram taken with the aperture nearly wide open. To complete the high dispersion procedure the colour filter ought to be removed. When this is done it is clear that no gain is achieved - except that lines of the other colours appear and scan the field in the manner represented above.

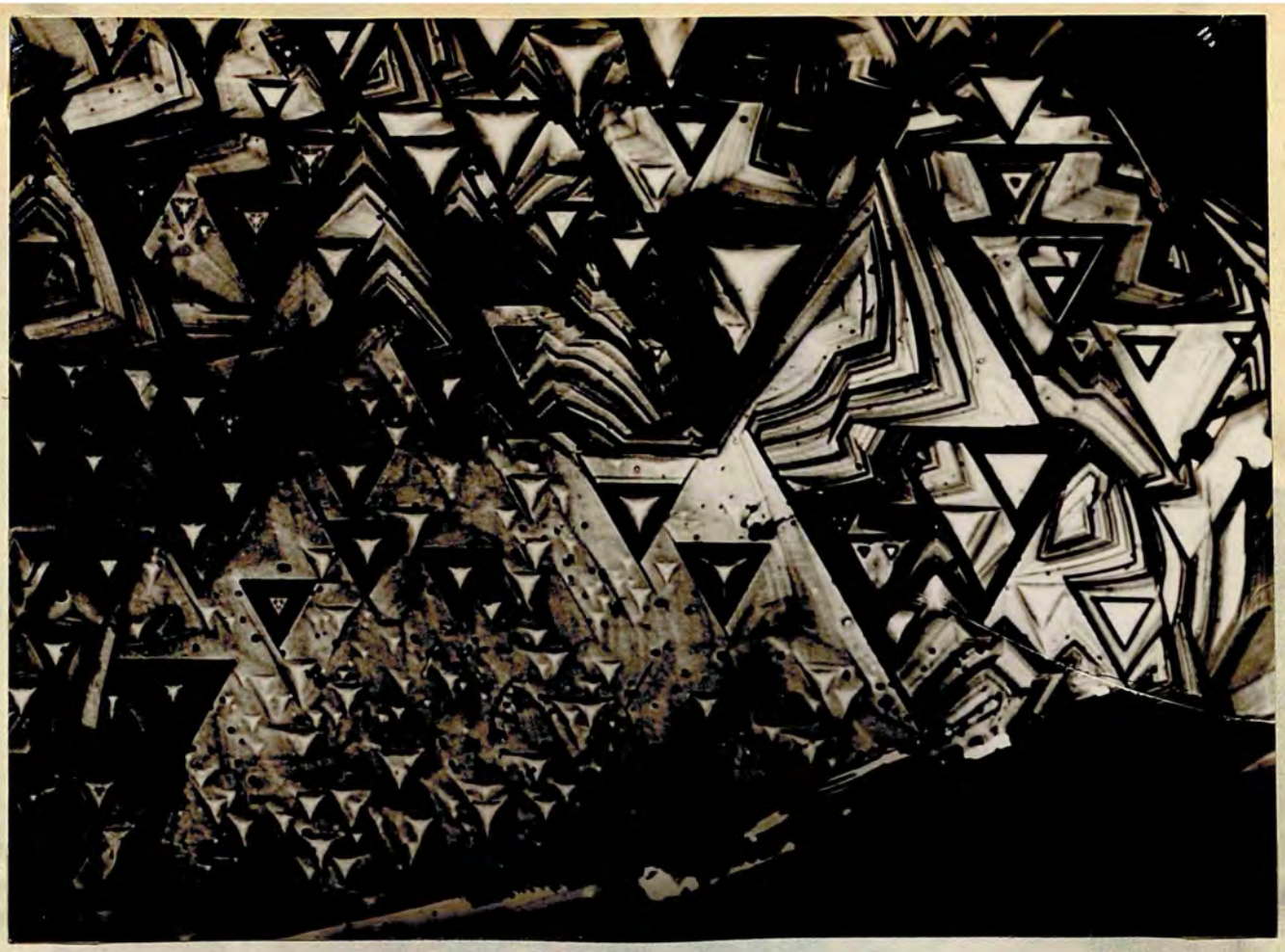

Fig (9). X 100

Fig (11). X 100

Fig (10) x 150

The conclusion to be drawn is the following: What broadening of the source cannot do, spectral broadening will achieve. The two broad colours (green and red) both clear and vivid, intermingle and share the features between them. They are of course of different shades, and fig (9) looks in the microscope as a superior coloured phase contrast.

Description of the Features.

The triangles, with their angles pointing downwards are the trigons familiar on diamond octahedral faces. They are of different sizes and depths. The number of fringes enclosed in any trigon give an estimate to its depth. The triangular features with their angles pointing upwards are growth hillocks. They bound the trigons from all sides, and the origin of both must be the same. But some of the trigons exist with no hillocks around them. These lie in a flat area in the middle of the picture. The area is however curved and not flat as seen from the broad fringes. The hillocks are connected and lie with their tips on top of each other, and the picture looks extremely complicated. The figures constitute part of crystal A (Chapter 5) and as such are not odd features. They represent the diamond texture. The pyramids are spiral looking but could not be identified as spirals. If they arise from numerous multiple dislocations we can easily account for both hillocks and trigons. It is perhaps worthy of observation, at this stage, to notice how the upper tips of the apparently flat triangular

area, develop, or are connected to smaller triangular plateaux in the form of pyramids. If the trigons are due to etch, the hills must be the etch hillocks. From their disposition and shape and from the layers composing them, they do not seem to be what is left over after etching took place. Aside from the impressions presented here the pictures convey no more un-detailed information.

A New Method of Determining Fringe Order.

The following method has been developed during work carried out in this thesis. It has been of real advantage. Another corallory to the method is that it decides the direction of the wedge, The method is based purely on an interesting observation and has an interpretation.

If we look into a Fizeau picture in transmission using the mercury arc without filter, we see three systems of fringes corresponding to the three principal colours of the mercury:

blue	green	yellow
4358	5461	5770 - 90

We shall treat the fringes as purely monochromatic. Clearly coincidences can occur for different orders. The following table consists of integers multiplied by the wave-length. The integer is a subscript to the symbol.

Table I

Blue		Green		Yellow	
b_4	17432	g_3	16383	y_3	17340
b_5	21790	g_4	21844	y_4	23120
b_6	26148	g_5	27305	y_5	28900
b_7	30506	g_6	32766	y_6	34680
b_8	34864	g_7	38227	y_7	40460
b_9	39222	g_8	43688	y_8	46240
b_{10}	43580	g_9	49149	y_9	52020
B_{11}	47938	g_{10}	54610	y_{10}	57800
B_{12}	52296	g_{11}	60071	y_{11}	63580

It is clear from the above table that b_4 is nearly equal to y_3 so that the 4^{th} order fringe for the blue colour will nearly coincide with the 3^{rd} order fringe for the yellow colour; the difference between the total optical paths for the two being only 92 A. b_5 and g_4 will also do the same with a path difference of 54 A. It appears, at this preliminary stage, that the approximate coincidence in the latter two is better than it is in the first two. Experience shows the reverse, and that the 92 A is nearly cancelled out giving an 'absolute' coincidence with a certain characteristic 'rose' colour, while the 54 A difference persists and is in fact

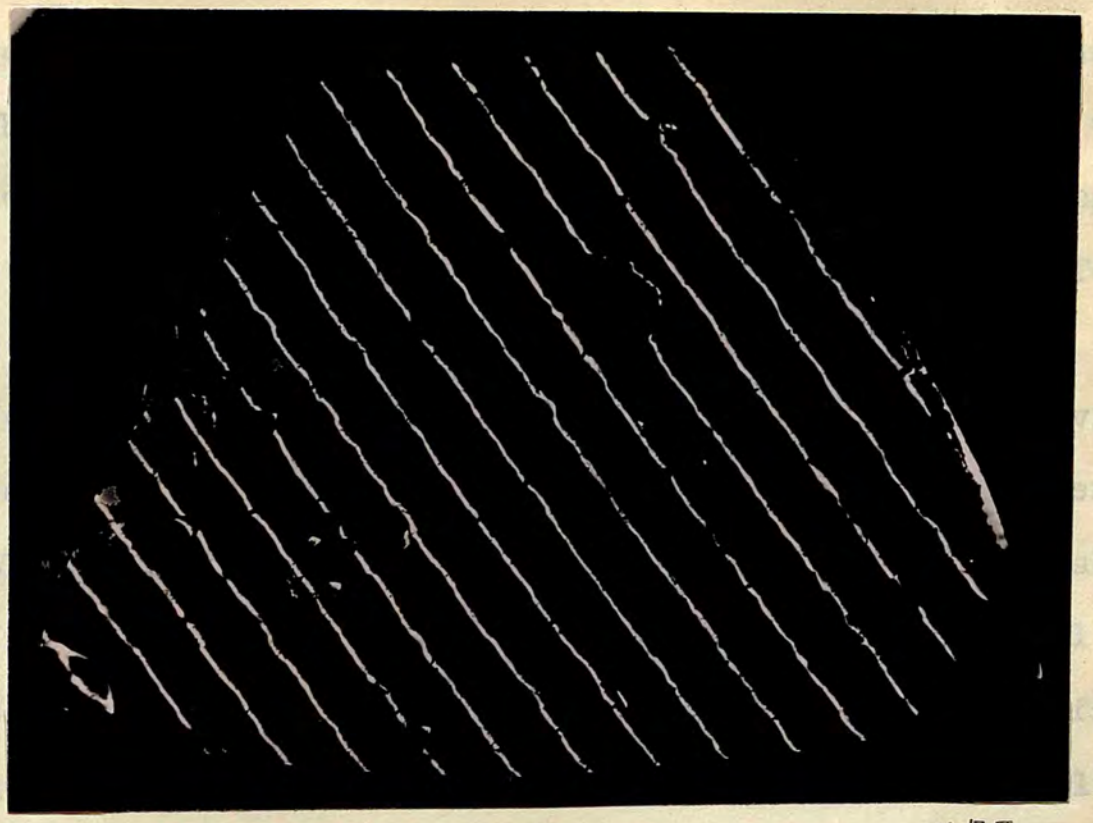

Fig (12). ×55

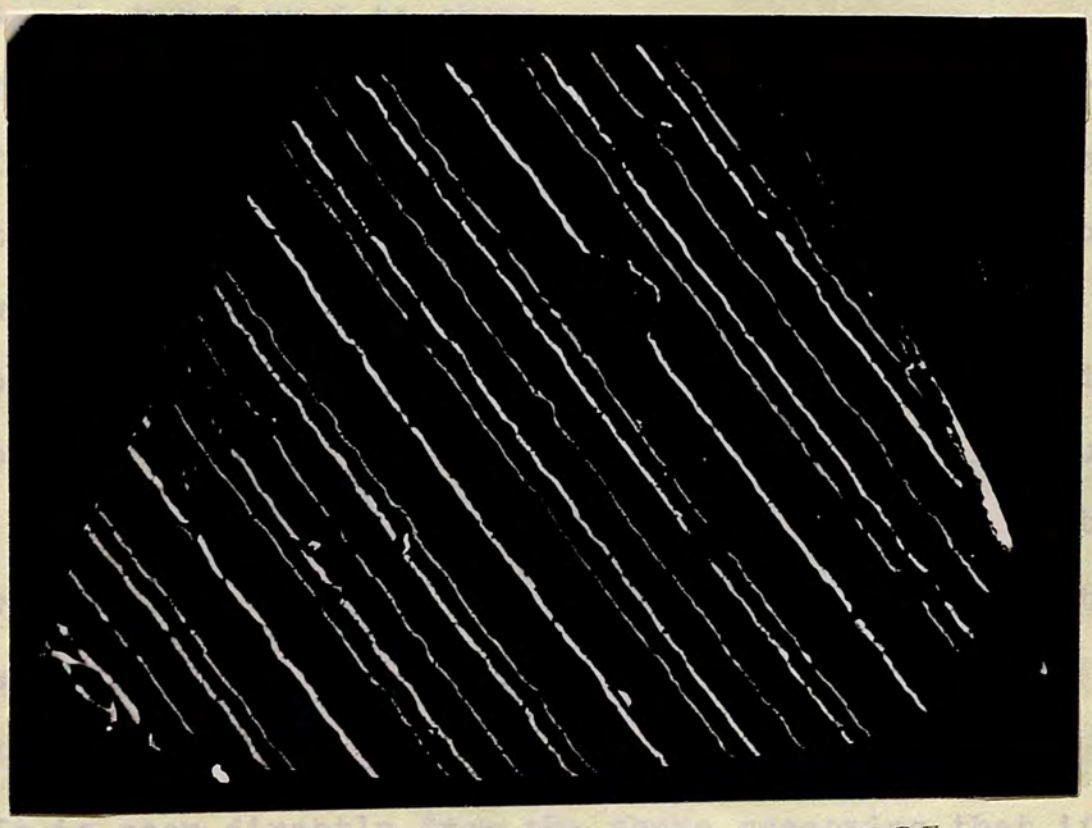

×55

Fig (13).

increased, with a separation of the two colours involved.

Confining our attention to the blue and yellow, we see from the table, that b_8 and y_6 also b_{12} and y_9 are very near together. They also unite in a similar manner giving a characteristic rose - colour. This repeats after every four orders in the blue and extends for some distance in any interferogram based on a wedge starting in the field of view from zero contact in one side. Fig (13) shows an interferogram of a plane diamond octahedron face resting upon an optical flat, in transmission. It is one of the faces of crystal C studied in this thesis. It represents a combination of fig (12) the blue - filtered with an identical figure yellow - filtered. Every fourth line in the blue is thicker on account of the increased intensity of superposition, and its colour is the rose - colour referred to above.

The existence of a certain colour that persists every four fringes in the low order blue, may or may not attract the attention. It would be of little value if it were not for the following observation: The near coincidence of b_5 and g_4 was mentioned. Restricting our attention to the blue and green, we see, (also from the table) that the repition must occur for (b_{10} and g_8) and for (b_{15} and g_{12}). In practice the colours are found just resolved, with the blue directed towards the wedge apex. The repetition of this near coincidence occurs every five blue fringes, as is seen in fig (14).

It is seen directly from the above reasoning that if a

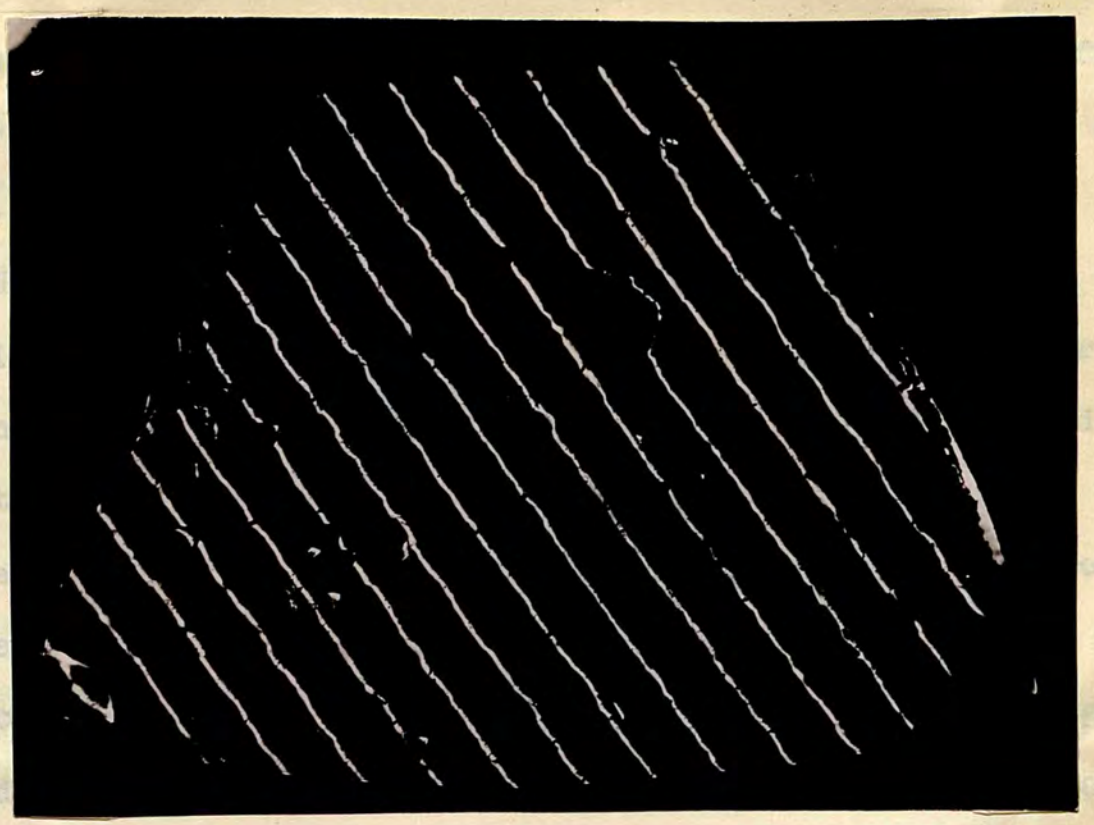

Fig (12). ×55

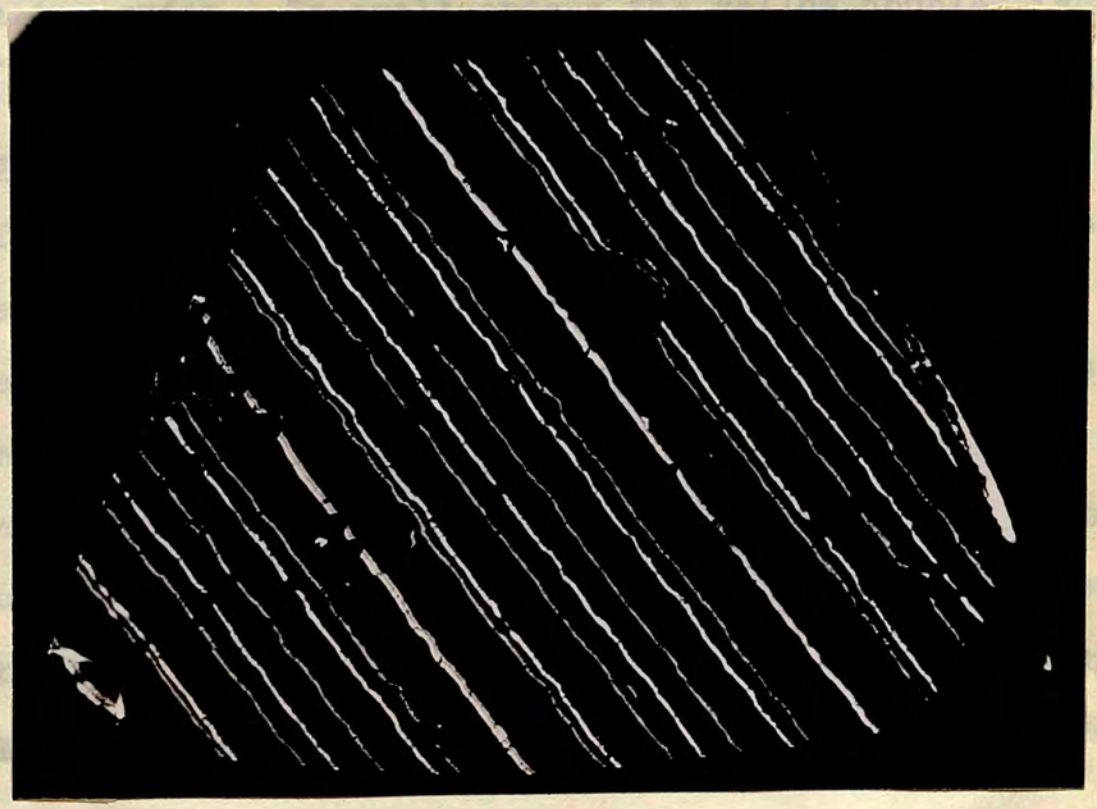

Fig (14). ×55

rose - colour fringe is followed directly by a blue - green fringe its order in the blue is 4. If the rose - colour fringe is directly followed - but one - by a blue-green fringe its order is 8. If it is directly followed but two, its order is 12. And this is sufficient.

Not only is the order of the fringe known by sight, but the direction of the wedge is determined. In this latter meaning it is superior to Brossel's[69] method, which depends upon the broadening (actually upon a noticeable wing) of the fringe towards the wider gap of the wedge, when the source dimension is increased. This wing is barely perceptible when the source dimension is such that broadening of the fringes already exists - and is not perceptible at all, when a narrow gap exists. It is also superior to another method depending upon the increased separation of the yellow doublet with increasing order. In small orders the yellow doublet is not resolvable.

Analysis of the Above Observation.

The complete analysis of the above phenomena is outside the range of this thesis as the lines are singlet (green fringe) doublet (yellow fringe) and triplet (blue fringe). But one or two points must be mentioned. (a) There is a phase change at reflection. This phase change is represented by the function Ω of equation (2) and depends upon the wave-length. It has been considered by Faust[66] to be a retardation. This phase change has been approximately calculated by

Faust [66] for evaporated silver films, but accurately determined by Meggers [68] for sputtered silver films. Accepting the latter values, Meggers' values taking the red cadmium line as showing zero effect are:

Table II

6000 A (y)	5500 A (g)	4000 A (b)
.002	.005	.045

The estimated phase changes are enlisted as fractions of an order under the respecting wavelengths. Identifying the 1st with the yellow, the 2nd with the green and the 3rd with the blue, a relative phase retardation of .043, between the blue and the yellow, should shift the blue towards the wedge apex by $2.179 \times .043 = 93.7$ A . This exactly compensates for the 92 A seen from Table (I) and the coincidence is striking.

(b) When higher orders are observed the spectral resolution increases but as the colours are not monochromatic and are in fact bands emitted by the hot mercury source, the components of any particular colour get further apart. The spectral resolution with increasing order of the two main colours is retarded by the broadening of the resultant intensity cap of either colour, and the resultant separation is hindered. The resolution will not be affected unless the separation of the two colours exceeds a certain limit depending on the width of the band at the moment of the separation. The fact that the

relative phase change due to multiple reflections, is a fixed amount, not depending on the gap, helps in that direction.

(c) According to Table I the relative phase change between the green and blue is less than, but very nearly equal to that between yellow and blue of the preceding orders. The amount calculated (~ 87 A) is added to the 54 A belonging to $b_5 - g_4$. This total amount of 141 A is larger than the natural fringe width (~ 100 A) of %90 silver films, and the separation is affected from the start.

(d) Although theortically there is only absolute coincidence for identical wavelengths, there is in fact considerable tolerance because of the fringe width due to (i) interferometer shape and (ii) Doppler width. The result is that appreciable intensity extends over wings separated perhaps by as much as twice the theoretical value. The persistence of colour in higher orders may be partly due to such an effect.

The above procedure is not restricted to the transmission technique, and both deductions (order of fringe, and direction of the wedge) may still be achieved in reflection. Both theory and experience show that for the highly reflecting silver films, the reflected pattern of the surface topography consists of dark fringes against a bright background. As a rule observation is only satisfactory if monochromatic light falls upon the interferometer, since the superposition of fringe patterns of different colours reduces the visibility. If the unfiltered mercury lamp is used, the minima of the green system

appear purple, those of the yellow system blue, and those of the blue system yellow. These are complementary colour pairs for the blue-white background illumination. The minima of the rose - colour system referred to above is olive - green, and in fact the rose - colour itself is some kind of purple.

CHAPTER FIVE

Study of the Normal Features.

In this chapter certain measurements are carried out on a single octahedron face. Information is obtained upon such items as interfacial angles as well as the profile of both hillocks and trigons. Cylindrical curvature is described and divided into two types, type I and type II. Type I is a result of the curvature of the growth fronts, and type II is the curvature $\perp^{r}$ to it. It is hoped that by this division some confusion may be clarified. The curvature of the growth fronts themselves is very important in connection with the temperature at which diamond was formed. Also certain questions are settled as regards relations existing (if any) between the length of side and depth of a trigon. The enquiry is supposed to answer the following questions: Is every big trigon deep, and every small trigon shallow? If some of the small trigons are deep, to what extent that can be, and if some of the big trigons are shallow, how often shallow they are? What sort of interfacial angle exists between the sides of a trigon or a growth hill? Are the angles crystallographic (i.e. some tens of degrees) or are they vicinal (i.e. a few minutes to half a degree)? All the above features and problems are often interrelated, and the actual values must depend upon the conditions of growth. It is important therefore that these operations be carried out on a single face. Since interferometry is the science of depth it is hoped that through

these measurements we may be able to have a better prespective of the whole phenomena of growth.

An attempt to correlate size (length of side of trigon) and depth has been carried out by Mrs. Wilks[20] using fringes of equal chromatic order, but the number of trigons surveyed was very small. We record at the end of this chapter a survey of 2,000 trigons using Fizeau fringes at the geographical dispersion. These trigons are all on one single face; the face of the crystal which is the subject matter of this chapter.

Description of the Crystal: (Crystal A).

The crystal (fig 15a & b) is a contact twin (macle) of length of side or edge 10.48 mm and thickness 1.82 m.m. Fig (a) is face 1, which is studied here. It is generally conceived that such a crystal arises from the hemitropic rotation of one half of the octahedron through 180° upon a composition plane parallel to (111). This rotation is a convenient means of description but it must not be taken literally as such. According to Sutton[5] who has made a statistical survey of some South African diamonds, the average spread ($^{edge}/_{thickness}$) tends to be 2.49 which is practically double the spread of a perfect octahedron. The spread in our crystal is 5.75 . Sutton[5] does not believe that the macle arises from the growth of an originally twinned nucleus. He conceives the macle to have arisen from the actual rotation of one half of the octahedron, the crystal being squeezed and

Fig. (15 b)

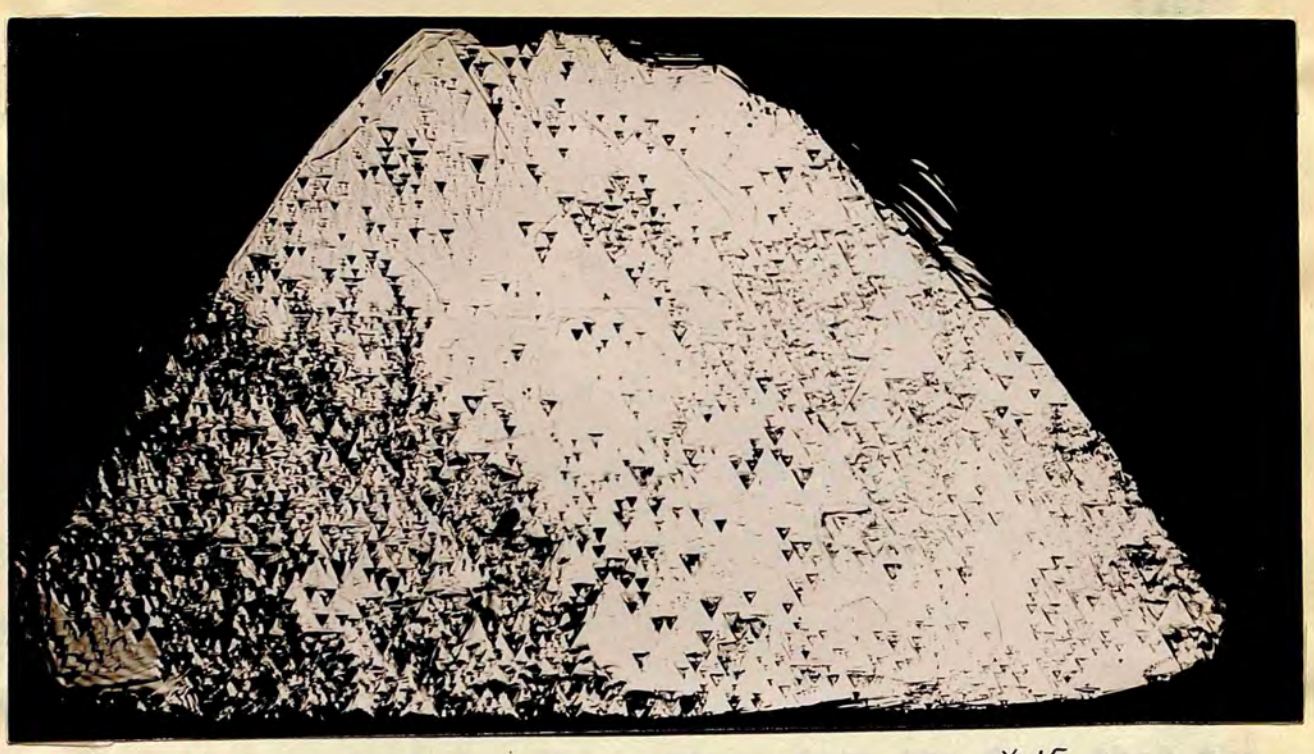

X 15

Fig. (15 a)

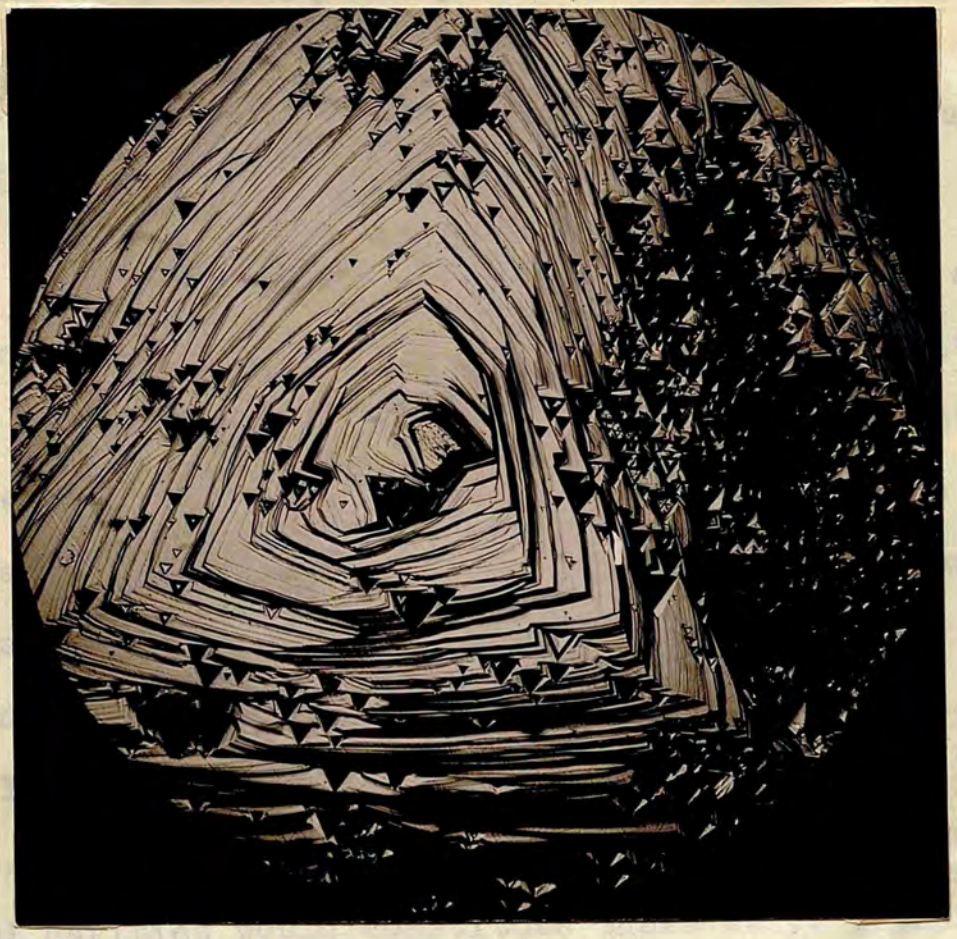

Fig. (15 b) X 28

thus flattened, while it was in a plastic state. Raman considers the macle, to be an outcome of his oblate spheriodal drop of carbon. The thinner this is, the greater will be the probability, during the formation, for one half of the form to swing around through 180° with respect to the other.

If trigons exist on both faces of the macle, as indeed is the case in this crystal, it can easily be differentiated from a portrait stone. Using a low power objective the trigons on the two opposite spread faces of the former are oriented in the same way, whereas in the portrait stone, they are oppositely oriented. This arises from the fact that the trigons always take a certain position with respect to the octahedron edge, and any two parallel octahedron faces, from any one point of view, are oppositely oriented. This is clear in fig (15). Each face is composed of 3 vicinal surfaces.

Experimental Procedure.

The crystal was silvered 90 to 94% reflectivity and tilted in a jig with reference to an optical flat suitably silvered to give sharp fringes in transmission or contrasting interference pattern in reflection. The angle of the tilt was varied until the fringes gave symmetrical patterns inside the trigons, parallel to the edges of these trigons. This is an indication that the general wedge angle has disappeared. What is left, therefore, is local wedge angles created by the features. Trigon edges at the end of the sloping sides of the pyramidal cavities would constitute these wedge apexes. Since

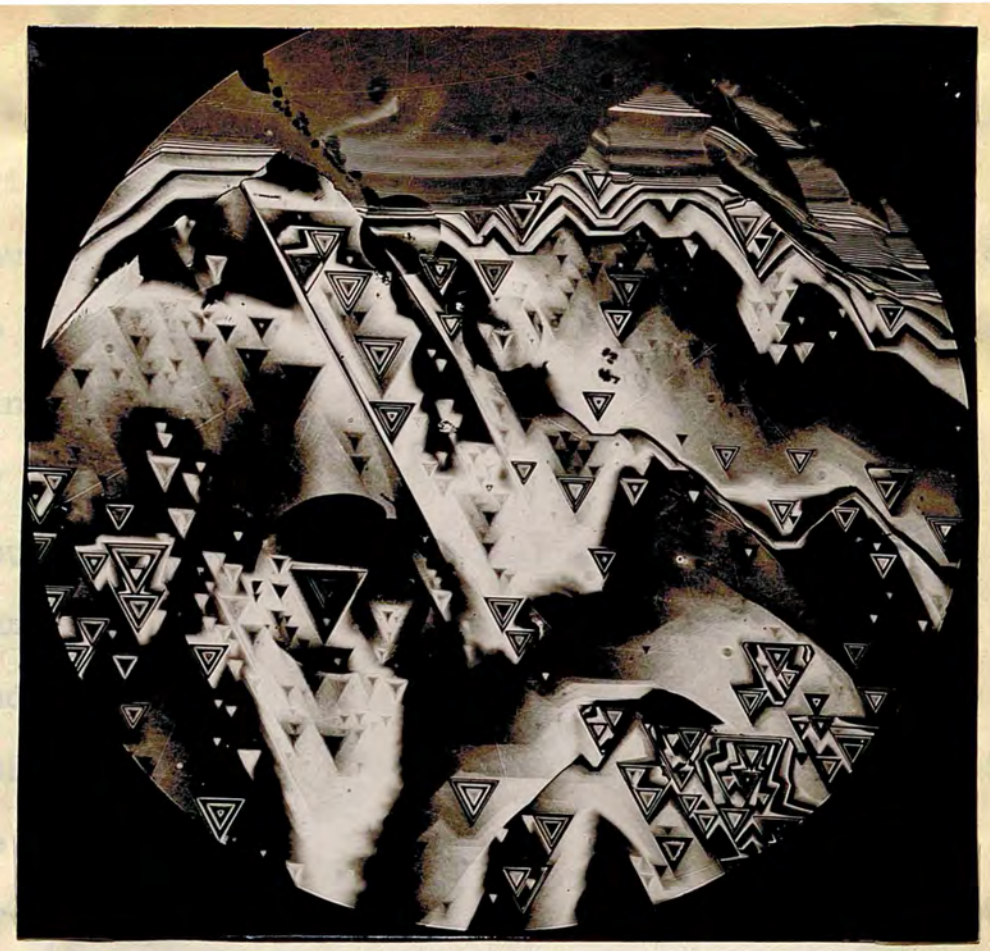

Fig. (16a). x 45

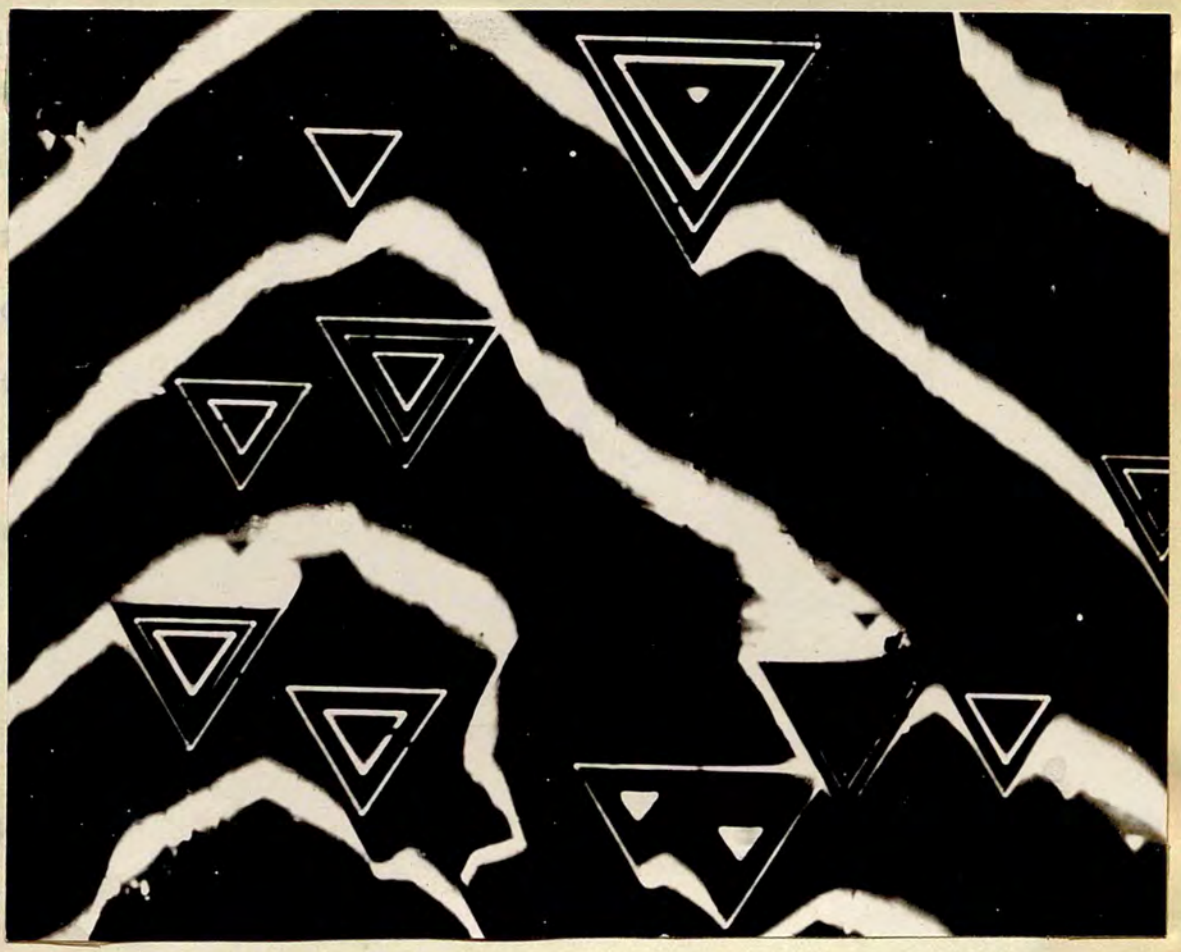

Fig. (16 b). x 225

fringes must be parallel to the wedge apexes, the fringes inside the trigons would be at 60° to each other, and are said to contour the trigons. This is clear in fig (16) of which b shows a group of trigons ranging in depth from $\frac{\lambda}{4}$ to λ. This contouring as we have remarked before (chapters 3 & 4) is a property of the geographical dispersion. Not only are trigons contoured, but growth sheet edges are contoured all over the pyramids. This is clear in fig (17) which shows a micrograph and fig (18) which shows a Fizeau picture of the same area. When the fringes are contouring there is no basic difference between the photo-micrographic picture and the Fizeau picture, except that in the latter pattern only lines that are separated in depth by half a light wave in length appear.

These will be clearly defined and therefore susceptible to exact measurement. The counting of the fringes within a certain feature will give the height or depth of this feature to an accuracy of $\lambda/4$, roughly to 0.1 of a micron. The size of the feature (e.g. length of a side) on a negative (Magnification 50 - 100) can be estimated to 0.1 m.m.

Since the features are flat, and therefore extended, an accuracy of 0.1 m.m. is sufficient in length. This corresponds to 2 - 1 micron on the specimen. But in certain cases where distance between two fringes is the deciding factor, or an actual measurement of an angle is in view, a higher order of accuracy is maintained.

Fig. (17) × 45

Fig. (18) × 45

Evaluation of Interfacial Angles.

The interfacial angle is the angle between the two perpendiculars to two near faces of a pyramid or a trigon. In interferometry the interfacial angle is estimated from the fringes when they cross the boundary between the two faces concerned. The formula which is used is due to Tolansky and Wilcock[64] and is illustrated in fig (19). The sloping lines are the fringes. The interfacial angle is the dihedral angle between the upper and lower faces (meeting at A B) and is -

$$\theta = \frac{\lambda}{2PQ} \quad (\cot \alpha + \cot \beta) \qquad \ldots\ldots (1)$$

The dihedral angle between the sloping side of a pyramid or trigon and the close-packed direction, (unfortunately there is no accepted name for this angle), is obtained from the fringes, only at the geographical dispersion. The fringes are separated in vertical height by $\frac{\lambda}{2}$ and are separated horizontally by the distance $\perp^r$ to them. The ratio of these two quantities gives the tangent to this angle, which we call ϕ . The accuracy of determination of this angle as well as the angle θ (unless the dispersion is constant) depends on the accuracy with which we can measure the distance between two fringes.

Equation (1) (also fig (19) is a general equation that belongs to any dispersion. If the fringes are contouring (the geographical dispersion) equation (1) is still valid, and

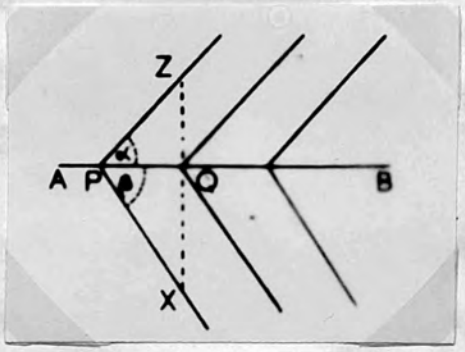

Fig. (19)

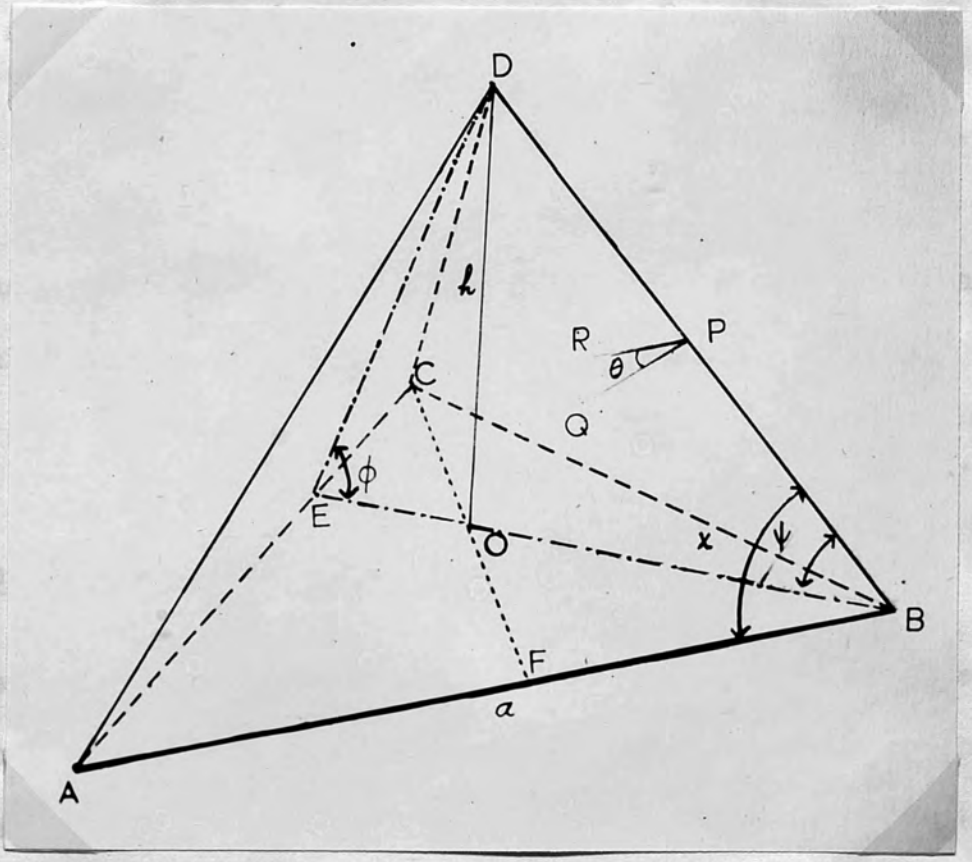

Fig. (20)

fig (19) may still represent this special dispersion. In this latter case considering a trigon or a 60° pyramid both α and $\beta = 30^\circ$ and

$$\theta = \frac{\lambda}{2PQ} \cdot 2\sqrt{3} = \frac{\lambda}{PQ} \cdot \sqrt{3} \quad \ldots\ldots(2)$$

In this special case fig (19) will also give the angle between the sloping faces (above and below A B) and the close packed plane, e.g. now to the left of the figure (in 3 dimensions it is the plane of the paper). As mentioned before tan ϕ equals $\frac{\lambda}{2}$ divided by the separation of the fringes. This separation in the figure $=$ PQ sin β (or) PQ sin α. If ϕ is small, and taking $\alpha = \beta = 30^\circ$

$$\phi = \lambda/2 \Big/ PQ \cdot \tfrac{1}{2} = \frac{\lambda}{PQ} \quad \ldots\ldots (3)$$

Equations (2) and (3) show that in the special case of a regular flat trigon or a flat 60° pyramid,

$$\theta = \sqrt{3} \cdot \phi \quad \ldots\ldots (4)$$

The General Case of a Flat Pyramid or Trigon.

The equations of interferometry are approximate equations only applicable in the case of flat features i.e. when ϕ and θ are small. To find the order of accuracy of the above formulae, and to establish an independent means of arriving at the same result, and therefore support their issue, it was found necessary to treat the problem from the point of view

of solid geometry. Since it is easy to derive the height $\underline{h}$ (by interferometry), and length of side $\underline{a}$ (by knowing the true magnification), it is convenient to take, as a parameter, the value $\frac{h}{a} = \alpha$. In actual calculation of these angles, by the method of parameters, only cases have been considered where the slope of the pyramid (elevation or cavity) has been approximately uniform, and where the height of the summit is known with accuracy. In fig (29) the pyramid is ABCD, where D is its top and ABC the close packed plane. The equations are derived with respect to a flat pyramid whose base Δ A B C is equilateral (with circumcentre O; A B = a)

(i) O D $\perp^r$ to plane A B C (base); O D = h

(ii) P Q lies in plane A D B ; P Q $\perp^r$ to B D

P R " " " C D B ; P R $\perp^r$ B D

$\underline{\angle R P Q} = \theta$

(θ is the dihedral angle between planes C D B, A D B; this is the interfacial angle between 2 faces of the pyramid)

(iii) $\phi = \underline{\angle DEB}$ = dihedral angle between base and any other face

Formulae 1 :

(a) $$\tan \phi = \frac{h}{DE} = \frac{3h}{BE} = \frac{3h}{\frac{(a\sqrt{3})}{2}} = 2\sqrt{3}\,\alpha, \quad (\alpha = \frac{h}{a})$$

For $h \ll a$

$$\underset{\text{(radians)}}{\phi} = (2\sqrt{3}\,\alpha)\left(1 - \frac{12\alpha^2}{3} + \frac{144\alpha^4}{5} - \ldots\right)$$

(b) $\tan \psi = \frac{\sqrt{3}h}{a} = \sqrt{3}\alpha$

$\tan \chi = \frac{2h}{a \sin \phi}$

$\sin \frac{\theta}{2} = \frac{1}{2 \sin \chi}$

$\cos^2 \frac{\theta}{2} = \frac{-1}{4 \sin^2 \chi} + 1$; $\cos(\pi - \theta) = -\cos\theta =$

$1 - 2\cos^2 \frac{\theta}{2} = \frac{1}{2 \sin^2 \chi} - 1$

i.e. $\cos(\pi - \theta) = -\frac{1}{2} + \frac{1}{8\alpha^2} \sin^2 \phi = -\frac{1}{2} + \frac{3}{2(1+12\alpha^2)}$

The above equations are sufficient to calculate both ϕ and θ depending on the measurement of the parameter $\alpha = \frac{h}{a}$, but it is more convenient to use other parameters derived from α.

Parameters: $\alpha = \frac{h}{a}$; $\beta = 2\sqrt{3}\alpha$; $\gamma = \beta^2 = 12\alpha^2$

Formulae 2:

I (a) $\tan \phi = \beta$

(b) $\phi = \beta\left(1 - \frac{\gamma}{3} + \frac{\gamma^2}{5} - \frac{\gamma^3}{7} + \frac{\gamma^4}{9} - \ldots\right)$ ..... (5)

II (a) $\cos(\pi - \theta) = \frac{3}{2(1+\gamma)} - \frac{1}{2}$

(b) $\frac{\pi}{2} - \frac{\theta}{2} = 3\alpha\left(1 - \frac{7\gamma}{8} + \frac{427}{640}\gamma^2 - \ldots\right)$

i.e. $\theta = \pi - 6\alpha\left(1 - \frac{7\gamma}{8} + \frac{427}{640}\gamma^2 - \ldots\right)$ .....(6)

Neglecting γ i.e. neglecting terms containing $\frac{h^2}{a^2}$ we see that equation (5) and (6) give the following ratio:

$$\theta = 6\alpha / 2\sqrt{3}\alpha \cdot \phi = \sqrt{3}\phi \qquad \ldots\ldots (5)$$

This is the same result obtained by applying the interferometric equations and is, therefore, an independent test for their validity. This is of course subject to the condition that γ may be neglected. In some of the calculations carried out in this chapter the neglect of the γ term amounted only to an error of 0.25%.

EXAMPLE: of Interfacial Angles.

The trigon at the top of fig (21a) is of the same order of size, but indentical in depth, to the trigon at the extreme right. Both are similar in another respect. They are more inclined to the close-packed direction towards their bottom. The close-packed direction is the (111) plane, and the bottom of the trigon is the apex represented by a dot. That the trigons are flat towards their bottom seems to be the general tendency of nearly all trigons. In some of them there is another flattening towards their extremities (at the top). The extremity of a trigon we may call its base. From continuity considerations we expect that it gets progressively flatter mostly towards its apex and sometimes towards its base also. The dot is a fringe, and distance between the two outer fringes is considerably less than the distance between the two inner fringes. The two trigons are one wavelength deep and are of medium size. These trigons, it will be seen afterwards, are mostly composed of layers on the average 24. The average thickness of layers in these trigons is therefore 200 A

X 206

Fig. (21 a)

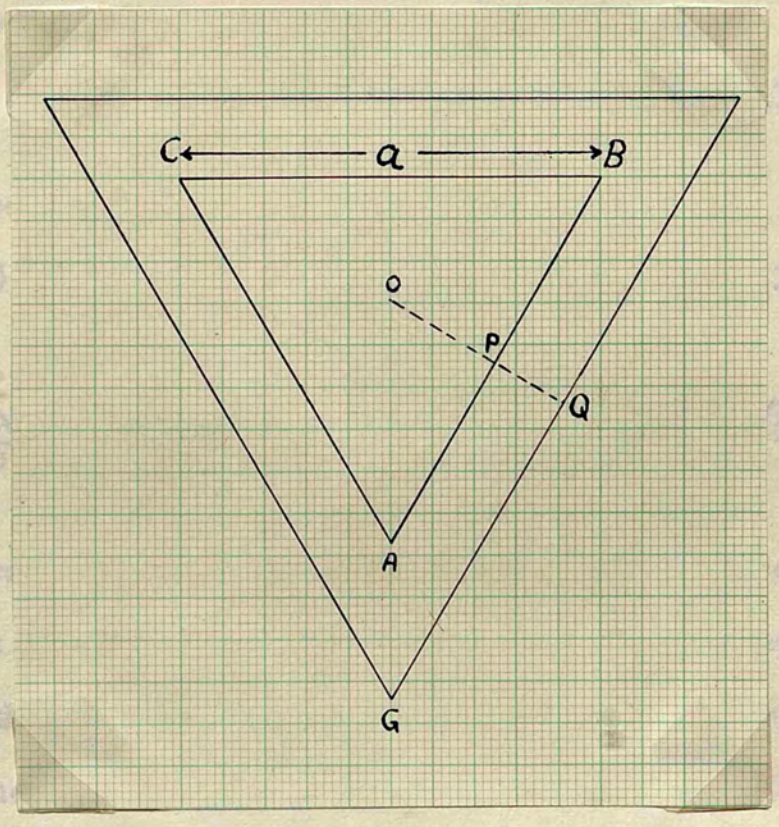

Fig. (21 b)

and sharp discontinuities are rare. The difference in dispersion between the outer and inner fringes cannot be due to any other reason except a gradual change of slope. There cannot be a constant interfacial angle between the sloping sides, but it is convenient to treat such trigons as if they have two different slopes; one between the two top fringes and one between the two bottom fringes. One fringe is common to both. The following results belong to the top trigon alone. The values of ϕ and θ obtained at the bottom (apex) are:

(a) by the method of parameters,

$$h = \tfrac{1}{2}\lambda = 0.273\,\mu \; ; \qquad a = 51\,\mu$$

$$\alpha = \frac{h}{a} = \frac{0.273}{51} = 0.00535$$

$$\tan \phi = 2\sqrt{3}\,\alpha = 0.0185 \quad \therefore \phi = 1^\circ\ 3'$$

$$\theta = 6\alpha = 1.84^\circ \text{ i.e. } \theta = 1^\circ\ 50'$$

Since $\frac{h}{a} \sim \frac{1}{200}$ the 2nd order terms are neglected.

(b) The two equations of interferometry give:

$$\tan \phi = \frac{\lambda/2}{OP} = \frac{0.273}{14.5} = .0188 \quad \therefore \phi = 1^\circ\ 4'$$

$$\theta = \frac{\lambda}{20\,A}(\cot 30 + \cot 30) = \frac{0.546}{2 \times 29} \times 2\sqrt{3} \quad \therefore \theta = 1^\circ.85$$

The results are indentical to within $1'$ of arc. In the above estimates mean values have been used for geometrically identical lengths. As longer distances are involved in the method of parameters the accuracy is greatest, and the neglect of the 2nd., order terms (even if $\frac{h}{a}$ is as high as $\frac{1}{30}$) amounts

to less than 1%. However, the method of parameters cannot be always applied, and the equations developed by Tolansky had to be used. The values at the top, by the above method, are:

$$\tan \phi = \frac{\lambda/2}{P\,Q} = \frac{0.273}{9.7} = .0281 \quad \therefore \phi = 1^{\circ}\ 37'$$

$$\theta = \frac{\lambda}{2\,AG} \times 2\sqrt{3} = \frac{0.546 \times 2\sqrt{3}}{2 \times 21.3} \therefore \theta = 2^{\circ}.54$$

The trigon in the middle of the picture has a ϕ - value of $58'$ and a θ - value of $1^{\circ}\ 40'$. The trigon to its left has a steeper wall than either of the above but is characterised with a very flat centre. Its wall is steepest in the middle and represents the general trend of trigons.

Cylindrical Curvature.

Newton's rings are generally demonstrated by the use of a thin plano-convex lens. If the convex part is conceived as a growth hill then the flat part of the lens is the close-packed plane. Newton's rings are an example of the geographical dispersion. If the convex surface is cylindrical Fig (22) may represent the cross-section of the wedge where the dots are the fringes. If the distances d_1 and d_2 between three consecutive fringes be known, the radius of the surface $\perp^r$ to the fringes may be deduced. This radius is the radius of cylindrical curvature and it is stressed to be the radius of a cross-section $\perp^r$ to the fringes. Recently (70) this radius

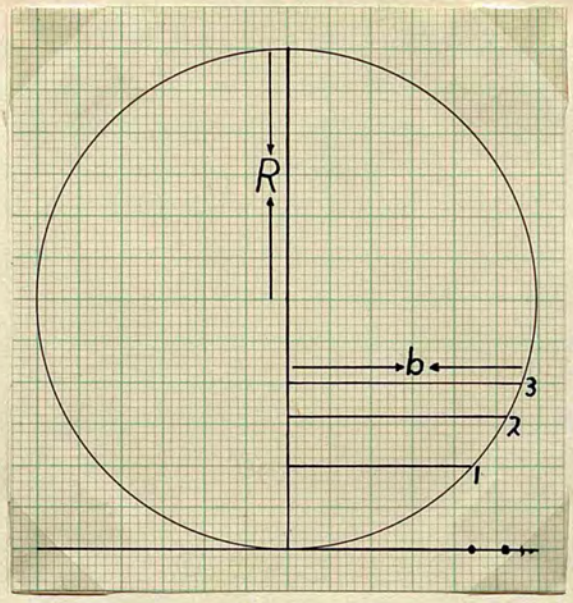

Fig. (22)

Fig. (23 a) × 500

× 225

Fig. (23 b)

has been published as:

$$R_{(approx.)} = \frac{1}{2\lambda}\left[d_1\, d_2\, (d_1 + d_2)\right] / (d_1 - d_2) \qquad \ldots\ldots (x)$$

This equation is suspected to be incorrect by a facter of 2. The above equation in its form 'x' has been used in another work of a similar nature,(19) and since this form may be used again and again until it replaces the true form, it has been found advisable from the point of issue of this thesis, that the equation be derived from the very first principles.

Equation for the Cylindrical Curvature.

Neglecting phase change at reflection, and taking R to be the radius of curvature, and denoting the 1^{st} distance by b, where n is an integer

$$\frac{b_1^2}{2R} = \frac{\lambda}{2}\, n_1$$

$$\frac{b_2^2}{2R} = \frac{\lambda}{2}\,(n_1 + 1)$$

$$\therefore R = \frac{b_2^2 - b_1^2}{\lambda} = \frac{(b_2 - b_1)(b_2 + b_1)}{\lambda}$$

$$\therefore R = \frac{d_1}{\lambda}(b_2 + b_1) = \frac{d_1}{\lambda}(2b_1 + d_1) \qquad \ldots\ldots (1)$$

similarly $R = \frac{d_2}{\lambda}(b_3 + b_2) = \frac{d_2}{\lambda}(2b_2 + d_2)$

$$= \frac{d_2}{\lambda}(2b_1 + 2d_1 + d_2)$$

$$= \frac{d_2}{\lambda}\left[(2b_1 + d_1) + (d_1 + d_2)\right] \quad \ldots (2)$$

From (1) and (2) $$R = \frac{d_2}{\lambda}\left[\frac{R.\lambda}{d_1} + d_1 + d_2\right]$$

$$\therefore \quad R\left(1 - \frac{d_2}{d_1}\right) = \frac{d_2}{\lambda}\,(d_1 + d_2)$$

$$\therefore \quad R\,\frac{(d_1 - d_2)}{d_1} = \frac{d_2}{\lambda}\,(d_1 + d_2)$$

$$\therefore \quad R_{approx} = \frac{d_1\, d_2}{\lambda}\left[\frac{d_1 + d_2}{d_1 - d_2}\right] \quad \ldots\ldots \text{(y)}$$

The approximation applied is the ordinary approximation used in Newton's rings. The equation (y) derived, gives a value for R twice that given by (x).

Two Kinds of Cylindrical Curvature.

There are two kinds of cylindrical curvature. Growth features exhibit both kinds. Type I arises from the piling of curved growth fronts. It is a curvature parallel to the edges and could be measured by interferometry by arranging the fringes to be $\perp^r$ to the growth sheet edges. Type II arises from the same cause but could also arise from the piling of straight wave fronts. It is a curvature perpendicular to the growth sheet edges. This can also be measured by interferometry by arranging the fringes to lie $//^{\ell}$ to the growth sheet fronts. This can only be achieved at the geographical dispersion and it is this kind of curvature that is generally measured in this thesis. Equation (y) will always apply provided there are no missed orders. This kind of curvature

has been sufficiently explained (Chapter (1), the introduction), and could arise by the piling of straight edges. Diamond surfaces are affected by both curvatures.

Example of Cylindrical Curvature.

Since trigons are characterised by straight edges and at the geographical dispersion are lined with straight fringes parallel to the edges, cylindrical curvature type II is the only curvature that arises. It is interesting to know the order of curvature inside the trigons, and perhaps fig (21)^{a} with its associate fig (21)^{b} provide the means for presenting such an example.

$O P = d_1 = 14.5\ \mu$ $\qquad P Q = d_2 = 9.7\ \mu$

$$R_{approx.} = \frac{d_1 d_2}{\lambda}\left[\frac{d_1 + d_2}{d_1 - d_2}\right]$$

$$= \frac{14.5 \times 9.7}{.546} \times \frac{24.2}{4.8}$$

$$= 1290\ \mu = 1.29 \text{ m.m.}$$

This value is not odd, and represents the general order of magnitude of this transverse curvature; not only in trigons but in growth hillocks around the trigons. The trigon at the extreme right has even a larger curvature and its $R_{approx.} =$ 0.54 m.m. The nearly equidistant fringes near the edges of the larger trigon at the left represent a cylindrical curvature

of 1.4 m.m. Fig (23a) shows an interferogram from which type II cylindrical curvature may be estimated for a growth hillock, the radius of curvature at one side varies between $\frac{1}{2}$ and $\frac{3}{4}$ m.m. The treatment is similar to that adopted in the case of trigons Fig (23b) shows another growth hillock lined with fringes for evaluation of type I cylindrical curvature. The two curvatures are generally quite different, but are of the same order. Type I is the direct result of the curvature of growth fronts adjacent to it; both have approximate values, but the latter is estimated by geometrical means.

Curvature of Growth Fronts and Temperature.

In the theory advanced by Burton, Cabrera and Frank[44] the number of kinks increases as the inclination θ of the step relative to a close-packed direction increases. The mean distance x_o (θ) between kinks decreases and becomes:

$$x_o\ (\theta) = x_o \left\{ 1 - \frac{1}{2} \left(x_o/a\right)^2 \theta^2 \right\},$$

where a is the intermolecular distance in the direction of the step, and

$$x_o = \frac{1}{2}\ a \left\{ \exp\left(W/KT\right) + 2 \right\} \sim \frac{1}{2}\ a \exp\left(W/kT\right)$$

where (W) is the energy necessary to form a kink, (k) is Boltzmann's constant, and (T) absolute temperature.

From the above, following a simplified geometrical construction,[71] it is easy to arrive at the following relation

$$\frac{\rho}{P} = 1 + \frac{1}{4} \exp.\left(\frac{2W}{kT}\right) = 1 + \frac{1}{4} \exp\left(\frac{\phi}{kT}\right) \quad \text{----(7)}$$

In a close-packed step in a (1,1,1) face of a f.c.c. crystal, $2W = \phi$, (44) where ϕ is the nearest neighbour interaction.

Another name for ϕ is that it is the molecular binding energy. In the above ρ is the radius of curvature of the boundary of a polygonal growth sheet, and (P) is the normal distance of the growth front from the initiating centre. The equation tells that for high temperatures we should expect more curved growth fronts.

The Surface Energy of Diamond.

Diamond is the hardest known substance. It has an extremely high melting point (Mp). Of all substances it has the lowest atomic volume (V). Bloom (72) considers the cohesion in elementary solids to be proportional to Mp/V. We expect, therefore, its atoms to be tightly bound. More tightly bound than the atoms of any other solid. The result of excessive cohesion, is high surface energy. Harkins (18) obtained the surface energy of diamond by calculating the energy utilized in splitting a diamond crystal along some definite plane to give two surfaces. Since for each cm^2 of the plane two cm^2 of surface are formed, the surface energy would be half the cohesional energy.

If the diamond crystal is split in the 111 plane in a

position equidistant from the carbon atoms on the two sides of the plane, fig (1) shows the bonds before rupture $\perp^r$ to the plane. Rupture is to be assumed occurring in a plane $//^l$ to the base of the figure. Fig (2) shows the arrangement of atoms just above or just below the plane. It is clear that only one carbon-carbon bond is ruptured for each carbon atom on one of the sides of the plane. Harkins calculated that 1.825×10^{15} such bonds would be cut per cm^2. Harkins also used in his calculation 90,000 calories as the energy required to rupture 12 gms of carbon. This figure is of some theoretical and practical importance, and has been foreseen by Crookes (110) to be the heat of volatilisation per mole of carbon. Harkins concluded that the cohesional energy for (111) plane of diamond would be 11310 erg/cm^2. This latter calculation although simple is original, and we must attribute to him also the value of the energy necessary to break a C - C bond. This is simply $11310 \div 1.825 \times 10^{15} = 6.18 \times 10^{-12}$ ergs, seeing that one bond projects per atom.

The Binding Energy of the Carbon Atom in Diamond.

It is clear from the views and results of the above section that the binding energy ϕ is simply $6.18 \times 10^{-12} \div 2 = 3.09 \times 10^{-12}$ ergs. This value may not attract the attention, but when taken in conjunction with Boltzmann's constant k which is 1.38×10^{-16} erg. deg^{-1}, must be realized as a huge amount. We write again equation (7).

This is:

$$\frac{\rho}{p} = 1 + \frac{1}{4} e^{\frac{\phi}{kT}}$$

For growth under typical conditions, which according to Burton, Cabrera and Frank (70) is such that the temperature lies between 0.5 and 0.8 times T_b, the boiling point in degrees absolute, $\phi/kT \sim 4$. This gives $\frac{\rho}{p} \sim 15$, which is a normal value observed on crystal faces e.g. quartz (71). Diamond is exceptional in the curvature of its growth fronts, but the centres of initiation are small and near. Admitting that $\frac{\rho}{p} = 15$ is acceptable on diamond octahedron faces,

$$\frac{\phi}{kT} = \frac{3.09 \times 10^{-12}}{1.38 \times 10^{-16} \times T} = 4$$

This gives T the unusually high figure of 5600°K.

The Temperature of Formation of Diamond.

A number of determinations of $\frac{\rho}{p}$ has been carried out on different growth hillocks on crystals A and D. Some results are found in the table below. The procedure was to secure the geographical dispersion over these hillocks. When this is done the fringes are parallel to the growth sheet fronts. The fringes being visible and clearly defined, it is easy to measure ρ. In the table 2 a is the chord, in microns, and S is the sagitta. $\rho = \frac{a^2}{2s}$ microns. In most of the photographs the top of the hill is marked with a frings. The marking of the top facilitates the calculation of p, but this is not necessary

as the edges of the vicinal faces of these hillocks could be extended visually and located by the use of the crossed eye-piece of the comparator. The value of $\frac{\rho}{p}$ is independent of the magnification, and could be calculated directly from the negative if the magnification is not known. To refer to actual values on the surface is only useful in prespective.

Table III

Crystal	Hillock	2a	S	$\frac{a^2}{2S}$	p	P/p
A	1	50	1.05	298	23.1	12.8
	1	71.5	1.45	442	35.8	12.4
	2	19.2 x2	1.05	176	14	12.6
	2	36.6 x2	2.1	319	25.5	12.6
	3	36.2	1.0	164	13.1	12.5
	3	64.4	1.67	312	24.2	12.8
D	1	28.8 x2	0.85	488	17.7	27.6
	1	51.8 x2	1.44	925	33	28.0
	2	27.7 x2	0.80	480	17.7	27.1
	2	51.8 x2	1.45	924	32.6	28.3

Other values are found in the appendix, but the above is sufficient to show that P/p is constant, within the error of measurement, for the same crystal, and differs with different crystals. Professor Bernal (Birkbeck College) has been interested in the above approach, and suggested solving it by a practical example. According to his suggestion, approach

has been made to South Africa through the intervention of Mr. P. Grodzinski, of the Diamond Research Dept., (London). Dr. J.F.H. Custers of the Industrial Distributors (Johannesburg) has prepared the following specimens out of the above suggested test:

3	diamonds	from	Wesselton Mine
2	"	"	Bultfontein "
2	"	"	Williamson "

The author is not sure if he has carried Prof. Bernal's suggestion rightly, but it must be recalled that the Wesselton Mine is not far from the city of Kimberley and that the Bultfontein Mine is only five miles away from Wesselton Mine. The diamonds originating from these two mines are distinctly different in spite of the fact that they belong to the same locality. The Williamson Mine is situated in Tanganika about 1,800 miles from Johannesburg. Until such a measurement is made on diamonds (a) of the same mine (b) of two different mines of the same locality (c) compared with those of a mine of a distant locality, no weight should be given to the results of applying a formula such as the formula used. The results are provisional until they are supported by practical measurements.

If the above formula is correct it is in its power to be a sensitive and quick method of measuring the temperature of formation of diamond in different mines (a small change in temperature changes the value of $\frac{\rho}{p}$ perceptibly). In that direction

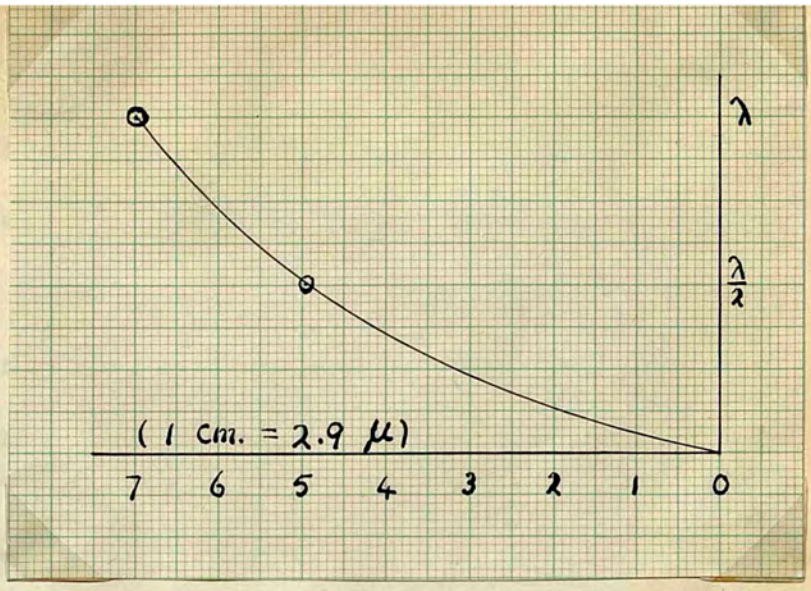

Fig. (24)

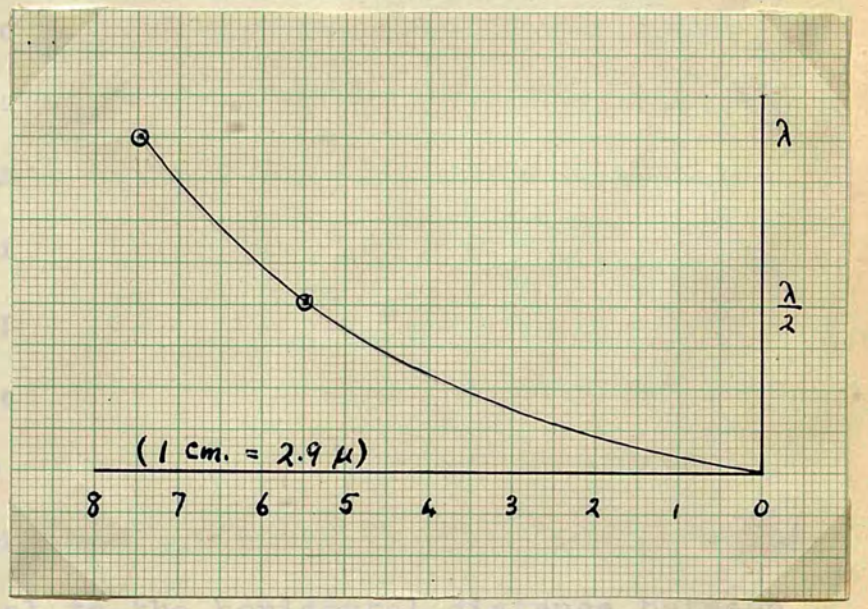

Fig. (25)

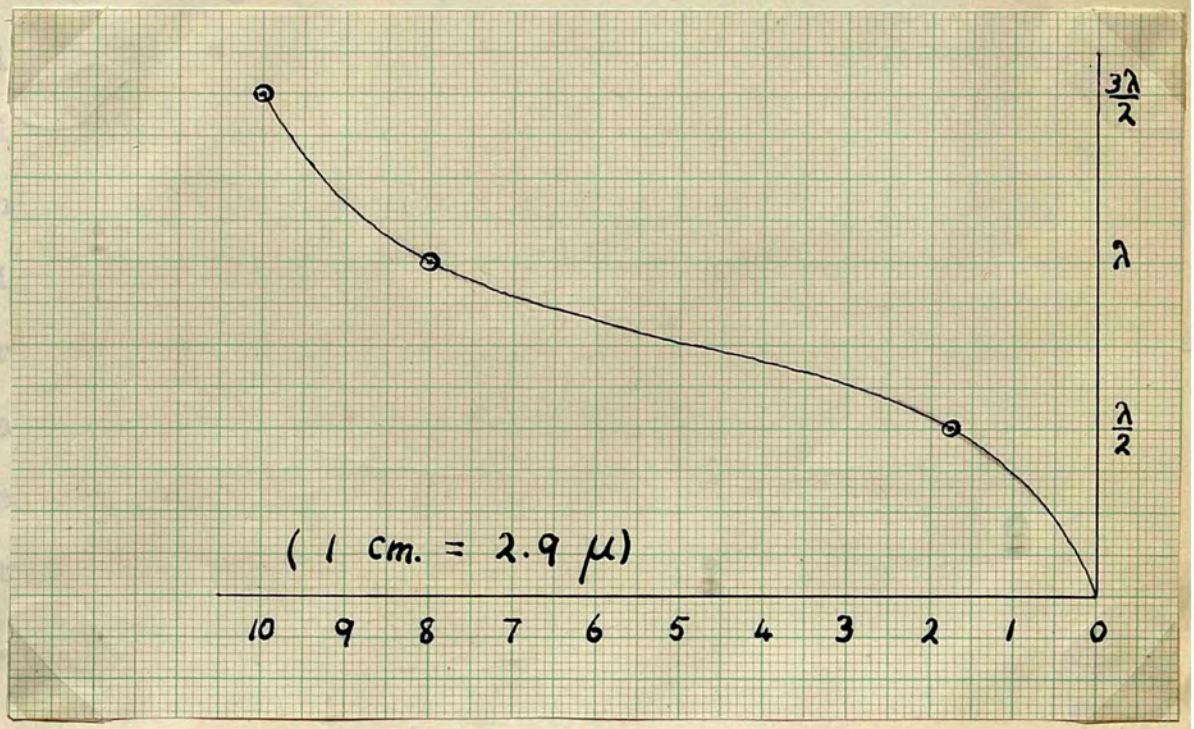

Fig. (26)

following a suggestion of Prof. Bernal, the author measured the curvature of the edges of crystal A. Crystal A is a macle. The face A is composed of 3 vicinal faces meeting in the geometrical centre of the face. The value of $\frac{\rho}{p}$ obtained from such a measurement is 12.4 and is in absolute accord with the measurements in Table III.

Profile of Both Hillocks and Trigons.

The increase or decrease of the gradient of the growth pyramids towards their summit has been observed in the interferograms. As the pyramid gradient can be measured most conveniently by means of multiple beam interferometry taken at the geographical dispersion (c.f. the trigons) it is easy to see how the profile of a pyramid or a trigon may be obtained.

As the fringes are imitating the growth fronts exactly, and are separated in vertical height by $\frac{\lambda}{2}$, the local gradient is inversely proportional to the horizontal distance between the successive fringes. The profile is attained in the accompaning figures along a line $\perp^r$ to the growth sheet edges, by plotting the number n of the fringe, counted from the initiating centre of a pyramid (or from the apex of a trigon) against its normal distance, p, from the centre of apex. In case there is a continuity between the side of a hillock, and one side of a trigon, one centre is sufficient. The vertical axis in both crystal and figures is the same. Fig (24), (25) and (26) represent the profile of pyramids and fig (27), (28) and (29)

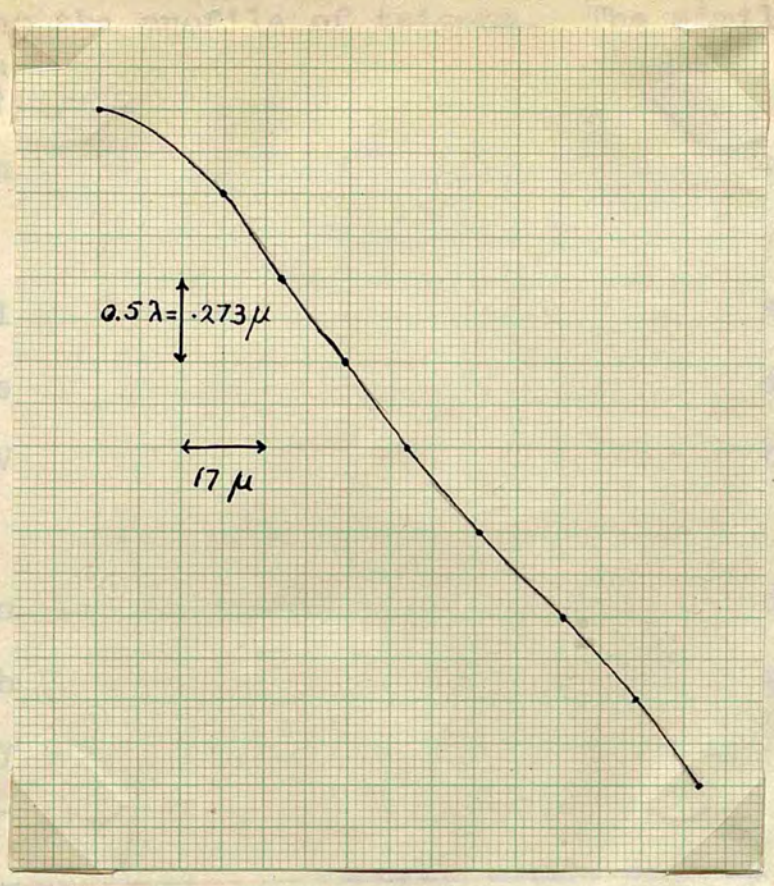

Fig. (28)

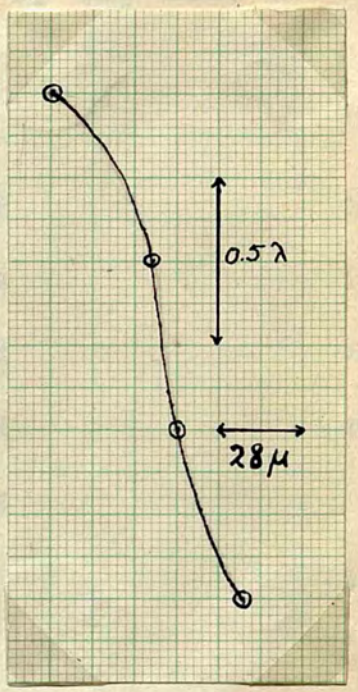

Fig. (27)

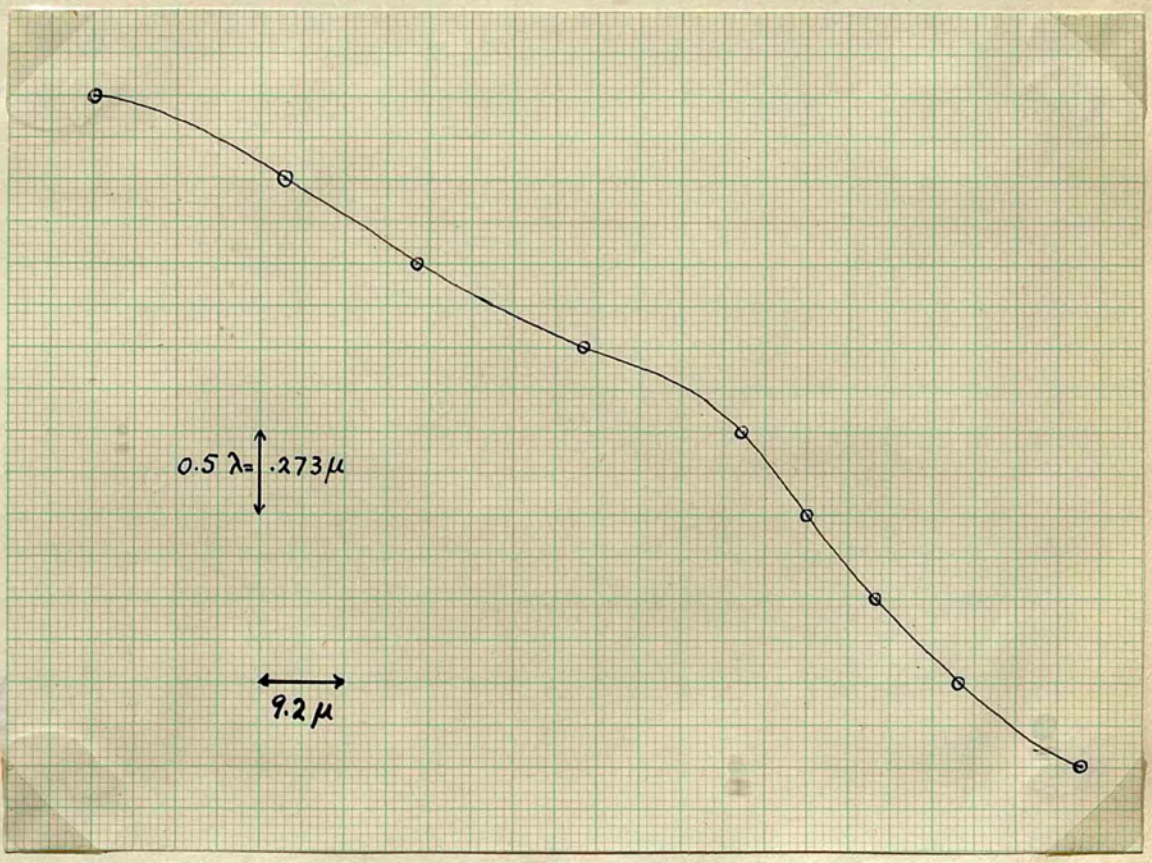

Fig. (29)

represent the profile of trigons. The similarity is evident. Fig (30 a & b) represents the profile of a pyramid by the side of a trigon. The continuity of outline is astonishing. There is only one interpretation : the trigons are due to growth. Their vicinal faces are the lower sides of the growth hillocks. Both the ϕ and θ values for some pyramids are gathered in table IV , aside with some of the values obtained, from before, for the trigons. The values differ amongst the members of the two principal divisions, but they are of order of magnitude for both features. T refers to top layers, M to medium and B to bottom layers.

Table IV

Pyramids				Trigons			
ϕ		θ		ϕ		θ	
		2° 18'	B			2° 32'	T
		1° 43'	T			1° 50'	B
Crystal A				Crystal A			
		1° 43'	B			1° 40'	
		2° 4'	T				
				½ Trigons		1° 18'	
				Crystal A		1° 18'	
						1° 30'	
						1° 39'	
						1° 39'	
Crystal D	T	18'		Crystal C		1° 37'	
	B	27'					

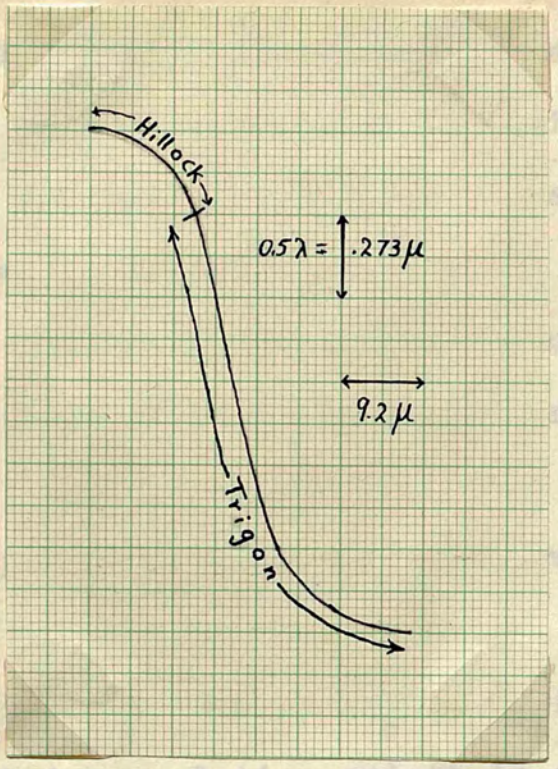

Fig. (30 a)

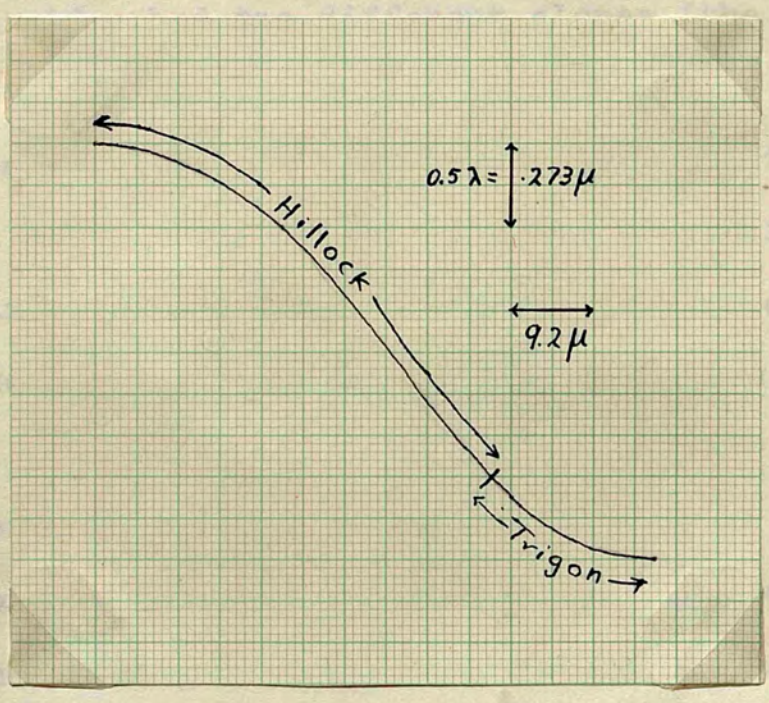

Fig. (30 b)

Statistical Study of Depth versus Length of Trigons.

A study of the profile of trigons has been carried out by Mrs. Wilks using the sensitive means of the fringes of equal chromatic order. The profile would of course be affected by the dispersion of the spectrograph and she was limited to the study of relatively shallow trigons. She also measured the depth and length of side of some trigons. Her conclusions are the following:

There are three types of trigons (1) shallow trigons (2) deep tetrahedra (3) flat bottomed trigons.

(a) The depths of the shallow trigons are proportional to the surface area, but no relation exists in the case of the deep trigons.

(b) Very few of the deep tetrahedra are regular tetrahedra. Sometimes the sides had two different slopes (the gentler slope being towards the surface). In some cases, she made two cross-sections for the same trigon, one including the apex, and another one $//^{l}$ to it. Her conclusions were not clear. In some cases the slope flattened out near the bottom of the trigon although the bottom was pointed.

(c) The flat - bottomed trigons were rare.

Her most important conclusions are in (b). If a trigon has two slopes, and since growth pyramids have sometimes two slopes, this is a plea for growth as the origin of trigons. That growth hills have two slopes is clear from results reached

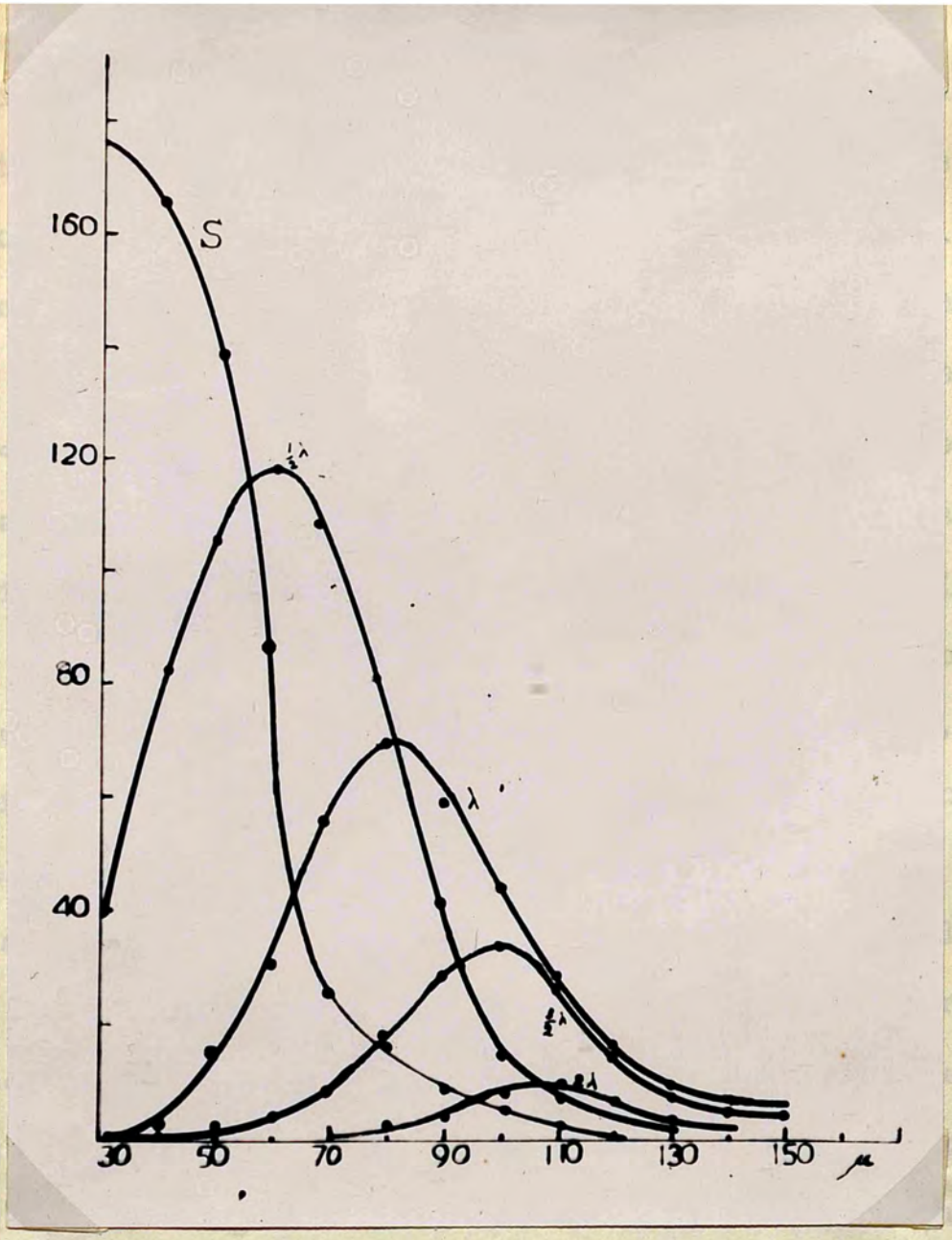

Fig. (31 a)

Fig. (31 D) ×45

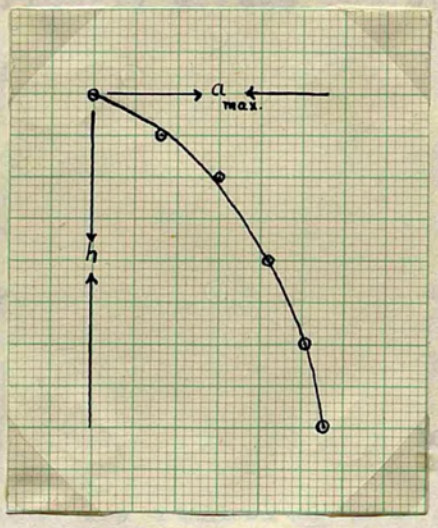

Fig. (31 c)

in this chapter on some hillocks (c.f. the profiles) and from observations in the following chapter. The author is not in a position to judge her result "a" as the trigons studied here are deeper than $\lambda/2$, but can make the following comment: If the area in shallow trigons is $\propto$ depth, then the length of the side is $\propto (\text{depth})^{\frac{1}{2}}$ i.e. $a \propto \sqrt{h}$. This is a parabolic relation which means the trigons are steeper than what is necessitated by the linear relation $a \propto h$. The observation made in a previous section is that the trigon is generally shallower at the bottom than it is at the top. Being due to growth, the piling of layers at the edge (where it is steep) does not increase much its extension, but increases its depth. This result is, therefore, a property of the profile of shallow trigons. Her result (c) is important only in one minor respect. In connection with the work carried in the following section, the depth of a trigon is estimated from counting the fringes enclosed by the trigons. In a flat bottomed trigon, orders in the fringes would perhaps be missed. Since this type is rare, this does not seriously affect the statistical procedure adopted in the following section.

Depth versus Size.

The depth and length of side has been carried out on 1788 trigons. Experimental procedure is easy and needs no further comment. The interferograms are seen in figs (16) and (21a). The results are gathered in the following table, and the graphs that show the relation are grouped in fig (31)a.

Fig. (31 b_1) x 250

Fig. (31 b_2) x 250

Fig. (31 b_3) ×250

"S" refers to shallow trigons that are less than $\frac{\lambda}{2}$ in depth. The graphs show the vertical columns. The length of side was estimated to the nearest round number in ranges that started every 5μ from 30μ to 165μ. As the accuracy in depth is only $\frac{\lambda}{4}$, the 30 and 35μ were grouped together for convenience of presentation. The table shows that for the $30 - 35\mu$ trigons there is no triangle deeper than $\frac{\lambda}{2}$. For the next higher order size only two (λ - trangles) appear. In the $50 - 55\mu$ type, 18 such (λ - triangles) appear, and the $1\frac{1}{2}\lambda$ triangles begin to appear and so on. It is also seen that large trigons can be shallow indeed. Some of the small shallow trigons are definitely missing, and the total number (R.H. of the table) is more likely to be continually decreasing from ~~the~~ top to bottom. Trigons that are revealed by the light profile to be deeper than 3λ have not been included. As the layers bounding any trigon are resolvable in the microscope, and could be counted, it has been revealed that they range in thickness from $\frac{\lambda}{48}$ to $\frac{\lambda}{12}$. Some discontinuities were met but these were rare.

The results of the statistical survey could be accounted for by growth, i.e. by the piling of layers around the trigons. A theory for the growth of these trigons is proposed in the following chapter. Every trigon (T) is surrounded by hillocks (H) fig (31-b). Taking maximum values in fig (31-a) as representative, fig (31-c) is drawn between depth and length of edge. Its shape is exactly that of the profile.

a (microns) / h		S	$\frac{1}{2}\lambda$	λ	$\frac{3}{2}\lambda$	2λ	$\frac{5}{2}\lambda$	3λ	Total
30 & 35		177	40						217
40	45	165	82	2			NUMBER		249
50	55	141	107	18	1				267
60	65	79	119	36	3				237
70	75	24	103	57	8				192
80	85	18	76	70	18	2			184
90	95	8	40	58	28	3			137
100	105	5	15	43	34	8			105
110	115	2	5	26	28	10	3		74
120	125	0	3	17	16	6	3		45
130	135	6	2	7	9	7	4	2	31
140	145	1	2	5	7	3	2	2	22
150	155	0	0	6	4	3	3	1	17
160	165	0	1	3	3	1	1	2	11

Conclusion.

Thus it may be concluded that a "multiple-beam goniometer" has been erected on the surface. This shows that inter-facial angles of growth hillocks of diamond surfaces can be a few degrees. These angles are intermediate between those of the vicinal faces and crystal faces. The radius of curvature is small and can be 1 m.m. or less, but $\frac{\rho}{p}$ values are comparable with those of other crystals.

CHAPTER SIX

Speculation over the Origin of Trigons.

Mode of Growth of Diamond.

Although it may not be appropriate at this stage to outline a proposed theory for the growth of diamond, the more descriptions are given of other crystals the more we are lost in details and the further we are removed from some features of particular interest described in detail in the last chapter.

The theory deals with growth on the octahedron face only, and its guide is the triangular line markings known as trigons. The author has had experience with iodine crystals grown from solution. According to Barret (73) the homopolar character with its covalent bond exists in I_2. Unfortunately they do not last long enough to be photographed, eventually disappearing in the form of vapour. The crystals grow in denderitic trees which soon fill the microscopic slide with parallel limbs. The limbs are made of rows of growth hillocks and enclose geometrical depressions similar in nature to the trigons. The trigons described in the preceding chapter are mostly pyramidical depressions, and the difference between them and the flat trigons, is a difference in degree rather than in form or origin. They arise together side by side on the same crystal face.

Formation of Trigons I.

Fig (32) represents a parallel growth of crystallites

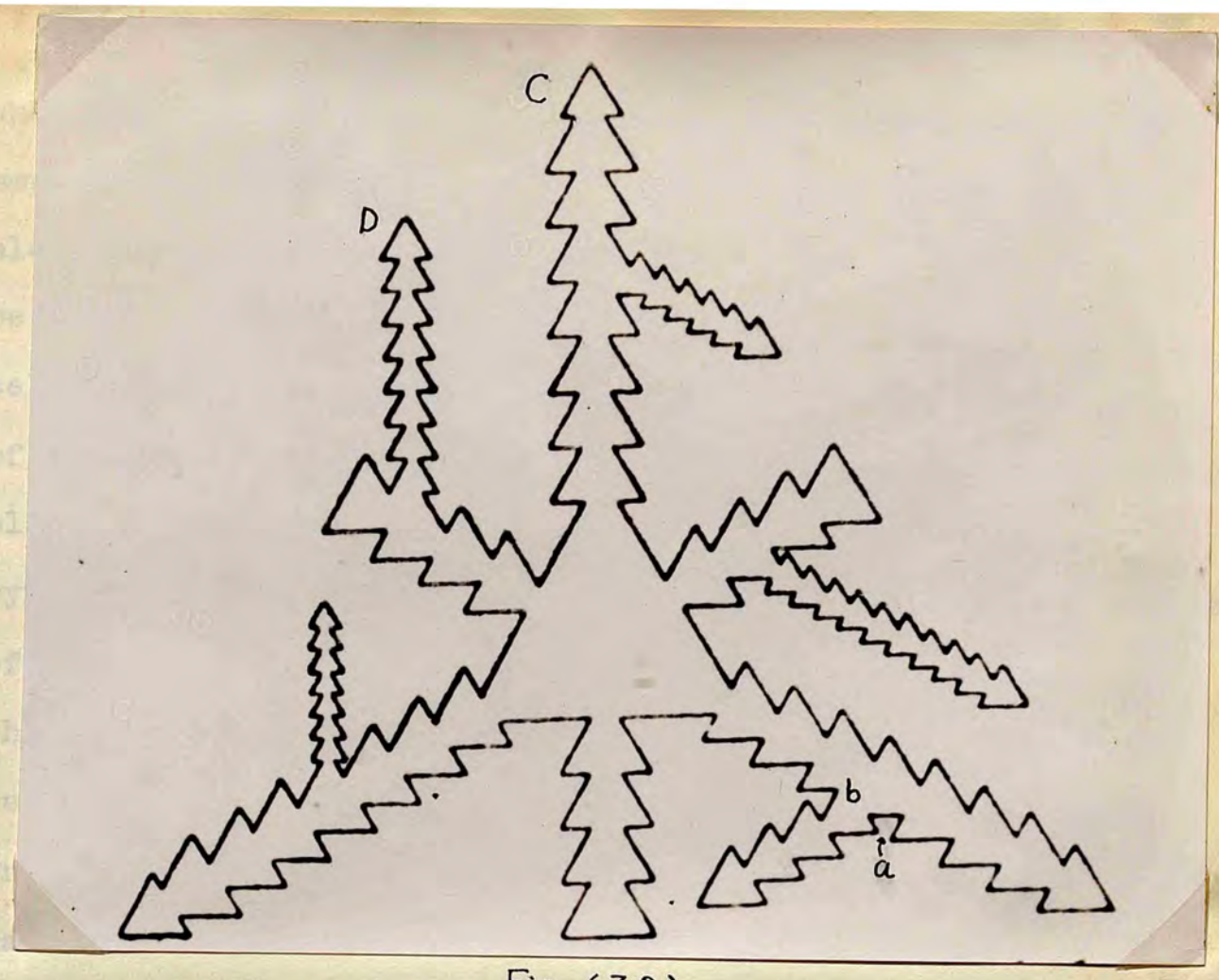

Fig. (32)

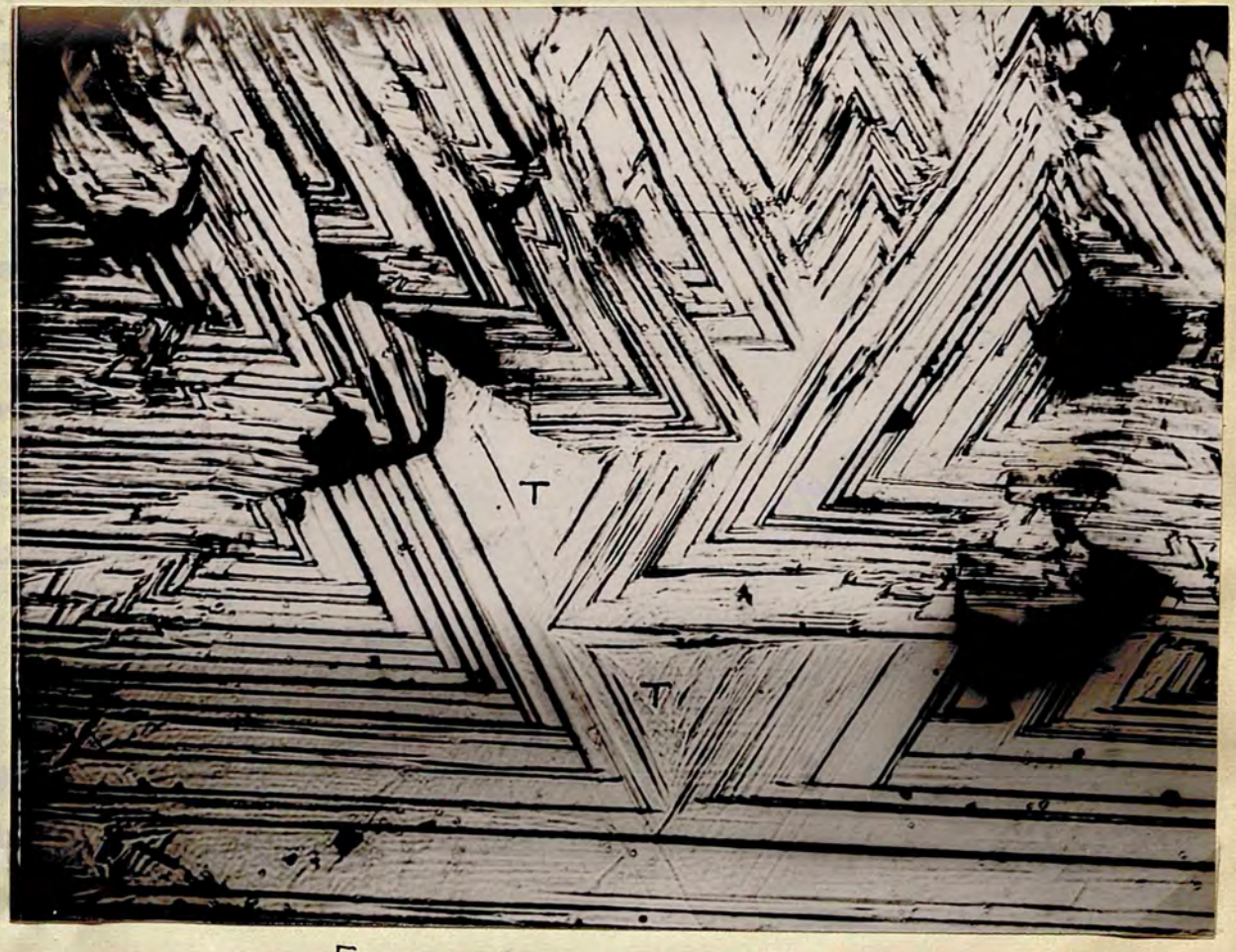

Fig. (33) x72.

when a particular condition of growth arises tending to emphasize a particular plane. Here parallel growth extends along certain directions in this plane. These are seen to be the directions of three diad axis, the crystallites themselves are all oriented with a triad axis normal to the plane of the figure. If we let the plane of the figure be the (111) plane on diamond, and replace the crystallites with flat pyramids, starting from the central triangle, we have a picture of what may happen on a diamond octahedron face. To supply the necessary dynamics, we imagine this central triangle to be based on a centre of initiation of growth. Growth will proceed only from the corners of the main triangle in the manner outlined. The branches connected to the sides of the main triangle have no place here and must be imagined non-existent. The primary branches are those leading to the face corners. Secondary branchings sprout from these in the manners outlined. The secondary branches may lead into tertiary branches, but these are not indicated in the figure. If the process is continued the whole face will be full of pyramidal cavities of varying sizes. Some of the cavities or trigons are already in the formation at a & b. The whole figure represents a denderitic tree, and is characterized by growth at the corner.

If the above picture is a two-dimensional picture the depressions such as a & b will be flat bottomed. These depressions are in the right orientation for trigons, and may

quite possibly be trigons. The observation is not limited to diamond but occurs in other crystals and fig (33) represents such trigons (T) in dendritic formations on the (111) face of a pyrite crystal. These have been proved by light profile methods (chapter 12) to be depressions. It is clear from fig (32) that if the branches are made of hillocks, and are not just triangular plates, the trigons enclosed such as a & b will be pyramidical in character. Two branches like c & d (imagined of the same size and in close proximity) will enclose a series of trigons as is occasionally observed on diamond surfaces. This is clear in the upper left hand arm of the cross in fig (34).

The whole picture of fig (32) is retained in its present guise, because it serves the double purpose of presenting the octahedron face in its relation to parallel growth by actual crystallite formations. (74) One of the theories recently published based on electron-micrographs, considers these crystallites and attributes them to minute drops of carbon. No picture is offered however for the formation of trigons as in the simple manner outlined in fig (32). The theory advanced in the present section, does not propose crystallite formations for pure or industrial diamond. It only makes use of the diagram.

Formation of Trigons 2.

Fig (32) of the preceding section is conceived originally

Fig. (34) x 400

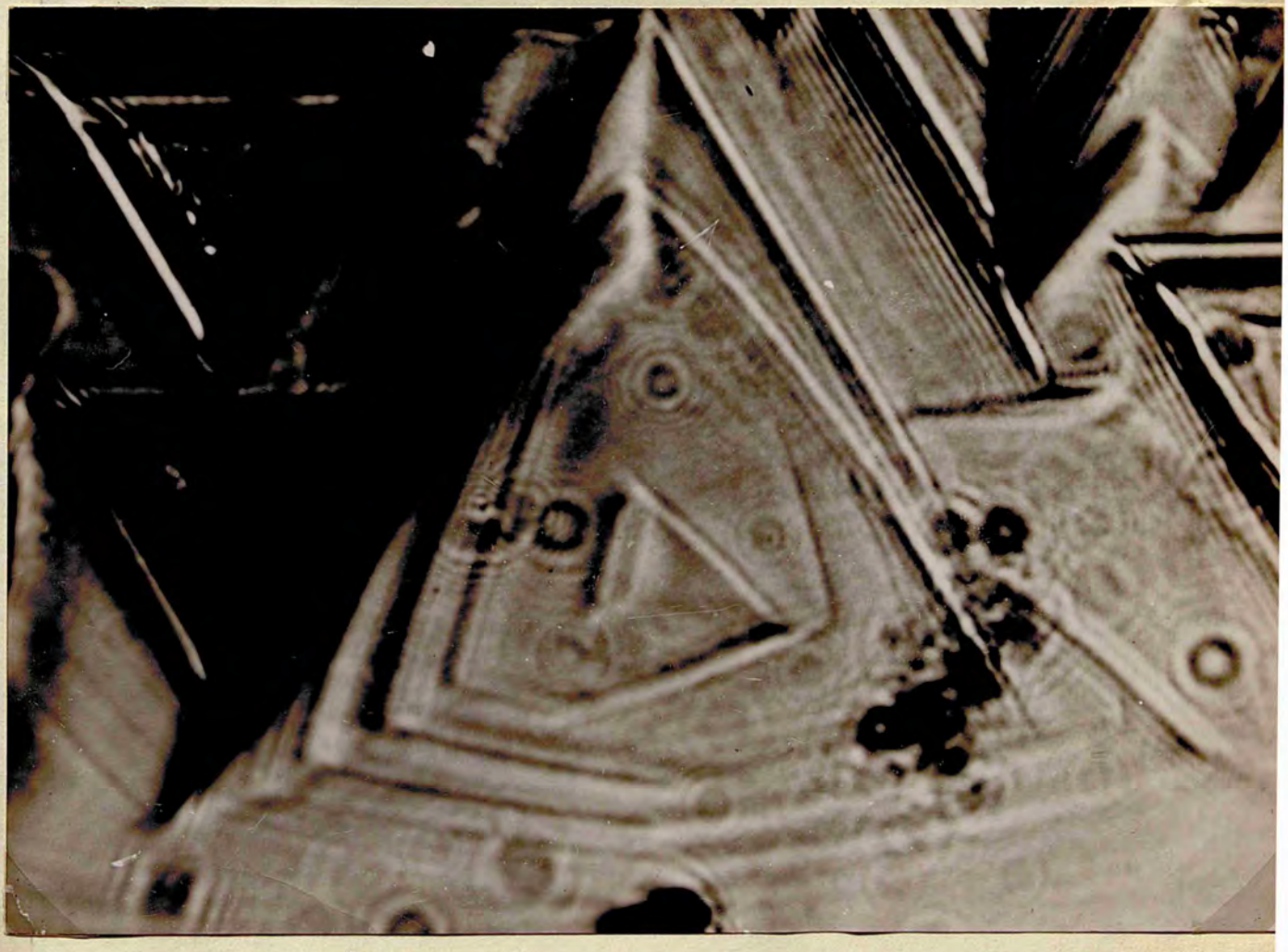

Fig. (35) x 840

to be a two-dimensional figure, and may account for the formation of mono-layer flat trigons. To give it the third dimension, in conformity with observation, we cannot imagine another mono-layer deposited on top of the previous layer and bounded by the outline previously reached. If such is the case and if growth is continued, the trigons must have vertical walls, and moreover they will be surrounded by thick triangular pieces, sharply and vertically cut, and not by pyramidical hillocks as actually observed. To give the picture the third dimension, therefore, and to account for the formation of all sorts of trigons, the triangular layers must be conceived at the start to be flat hillocks. How flat hillocks give birth, at the corner, to other flat hillocks will be analysed fully later. Flat denderitic trees as such, with limbs that need not be straight may be responsible for the formation of trigons on a plane surface that does not depart, apart from local irregularities, from the flat nature (when growth is no longer persued). The denderitic limbs of fig (32) as well as the rows of trigons which must form, are mostly parallel to the $\perp^r$ to the sides of the face, which is not the rule in diamond. Trigons when they do arise are generally in rows parallel and not $\perp^r$ to the sides. Moreover the crystal face tends as a rule to develop into three vicinal faces meeting at a point. The trigons will then lie mostly in rows at the edges of this major growth hill, as has been observed by Tolansky.(8) The features observed in the previous chapter are of this nature;

Formation of Trigons 3.

The success of any theory is that it explains most of the features encountered, when no other theory does. The theory must be based on reasonable premises, and must be built by logical deductions, and must at the end, and stage by stage, be supported by observation. The theory must not be limited by our present knowledge, else no advancement in science is possible. Crystal growth by layer mechanism is based upon persistent centres of initiation of growth. The persistency is stressed because, without it, no growth in the form of hillocks is possible. Since these hillocks can extend or co-operate with other hillocks in the formation of vicinal faces, any theory of crystal growth must account for and accomodate the vicinal faces. As fresh nucleation is not easy to arise on close-packed surfaces, the dislocation theory of crystal growth met with great success. Its success is all the more because observations of spirals is in the fashion of to-day's science. Moreover the dislocation theory explains the occurrence of growth hillocks and thus gives an interpretation to vicinal faces.

The theory proposed here does not use dislocation models as no spirals, up to now, have been observed on diamond. The only growth hillock that looks like a spiral is reproduced in fig (35) belonging to crystal A. The theory starts with a two-dimensional nucleus that has expanded to a certain size. This is exaggerated and denoted by A in fig (36). One

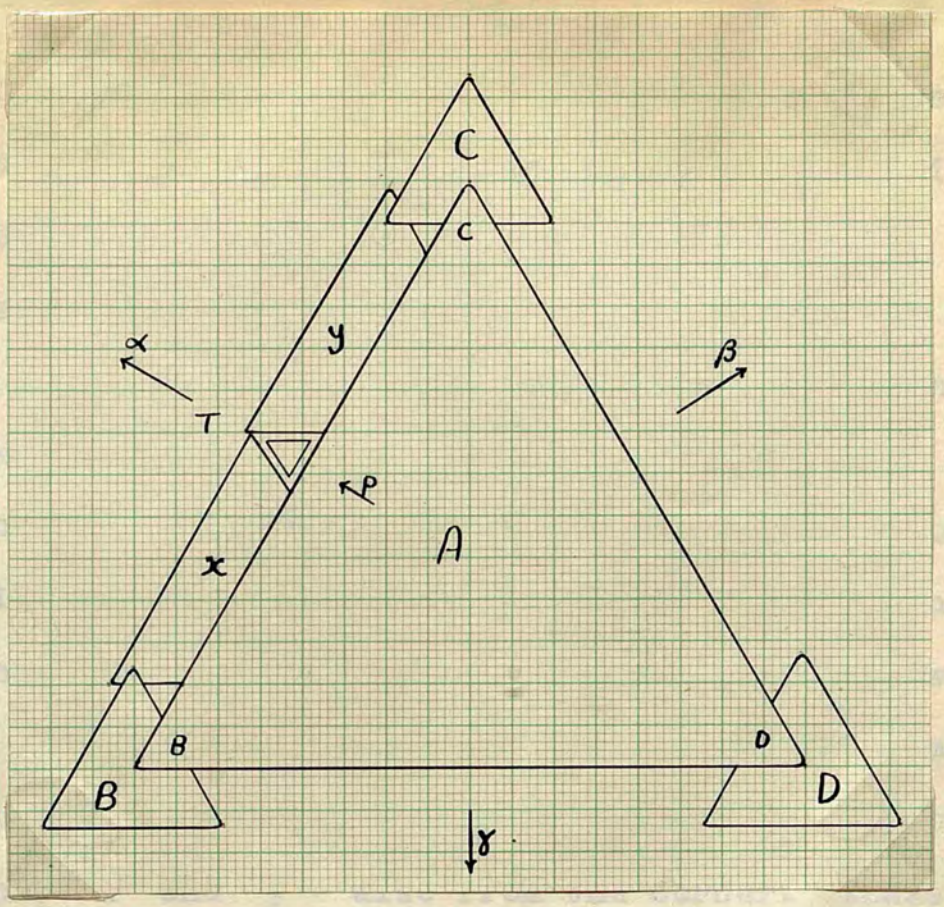

Fig. (36)

Fig. (15 c) x 66

supposition is only made: It is in the capacity of the corner to start a new nucleation. Considering one corner this will expand and become a triangular plate B. During this time another layer starts at the centre of A. A step has been created. Since the step existed before the initiation of B, nothing new has occurred. A new layer will be formed at B, after which a new layer will be formed on A, and so on. A and B will rise together with A higher than B, and the bridge connecting A and B will disappear, leaving two growth hillocks. In a like-manner C may develop at the same time. Both B and C have in their capacity the power to start new hillocks x and y - also from the corner. These will be extended in the direction of BC - CB which is a direction of quick growth. These will meet with the slowly moving side BC which should advance in the direction p. A trigon T is formed by the meeting of the 3 layers at 60°. This is in comformity with Tolansky's (8) interpretation. Moreover a step exists, as A is higher than B and C, which in turn are higher than x and y. After the underneath layer of A has met the underneath layers of x and y, growth is upheld at p, and the layers will pile up forming a bunched step. This observation is of wide occurrence and is seen in most of the Fizeau pictures of crystal A. These bunched steps, Tolansky calls "sharp edged shelves". Since x and y at the end are both hillocks, their sides are sloping towards T. The slope is accentuated by the slope from higher levels at B and C towards T. The edge B C will appear thin at B and C

but thick by the side of T at p as actually observed on diamond surfaces (c.f. chapter 5). B C will form an extension to one side of the trigon (see Fig. 31 D). This has also been observed by Tolansky, and he calls it "basal extension or striation". He describes also curving down of the surfaces, below the striation towards the hollow of the pit. This curving down is none other than the sloping rounded corners of both x and y.

Formation of Trigons 4.

It is seen from the above how a trigon may develop at the edge of a growth hill. The theory explains its orientation, and its shape. The shape will be pyramidical and its inner structure is a series of steps. It explains the hillocks that abide by the side of trigons. It also describes in detail observations made on diamond in a previous work by Tolansky and Wilcock (8) using the very sensitive means of multiple beams. They used extremely high dispersion over very flat trigons which must be some ten atomic layers deep. The description they give is explained by the model presented here. The fact that hillocks like x and y are never complete and are elongated, makes them incorporated in the sides of the steps of the major pyramid, and explains both figures (15b) and (34). But there is more in this theory than the explanation of the existence of a mere trigon. It explains the existence of thousands in a certain limited locality. The locality will rise up like a major pyramid. If growth is continued in

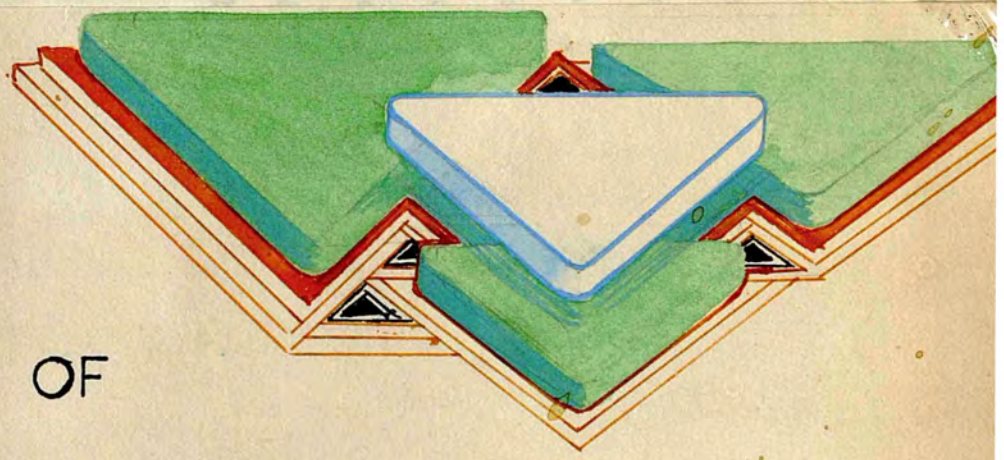

THEORY OF

FORMATION OF TRIGONS.

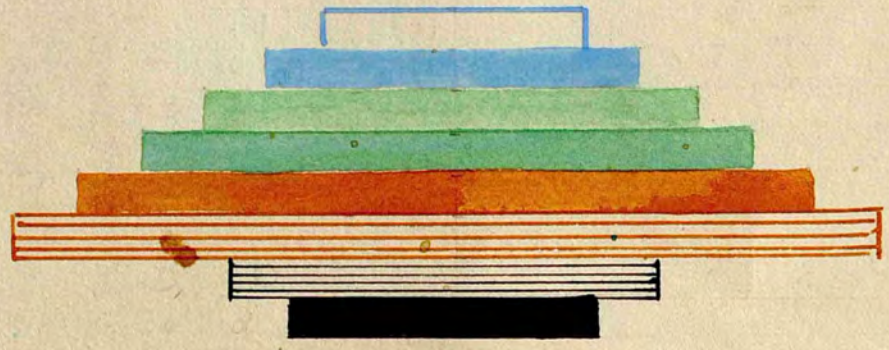

the outlined fashion, from all the corners of the principal sheet A, and from the corners of the other subsidiary growth sheets (B, C and D) there is no end to the subdivision, and there will be steps sloping downwards in the directions α, β and γ. A will develop as a major growth hill whose edges and corridors are lined with trigons, as observed in all diamond features. The edges like B C cannot be horizontal plateaux, and Wilcock (19) has observed a variation of height along the length of steps. In one example the variation in height amounted to 80 Å in 800 μ.

For the purpose of clarity, two pictures are reproduced here (both in the same orientation). One an enlarged part of fig (15b) (chapter 5) and the other/a new hillock belonging fig(37) to crystal B, studied in the next chapter. In the first/are 15 C seen elongated side hillocks of the type x, y. These remain elongated so long as subdivision does not directly occur. When subdivision is the rule they tend to be regular triangles as seen in the right of figure (15 C). This latter behaviour is the rule in fig (37) in which subdivision starts from the very centre. It is seen clearly how small triangular plates or hillocks in that figure are related and connected to other triangular plates or hillocks (the Δ's are the hillocks and the ∇'s are the trigons). The edges of the main hillock of fig (37) are not continuous straight lines but are dissected. According to the theory outlined, above, we should expect a slope towards the mid point of the sides of the main growth

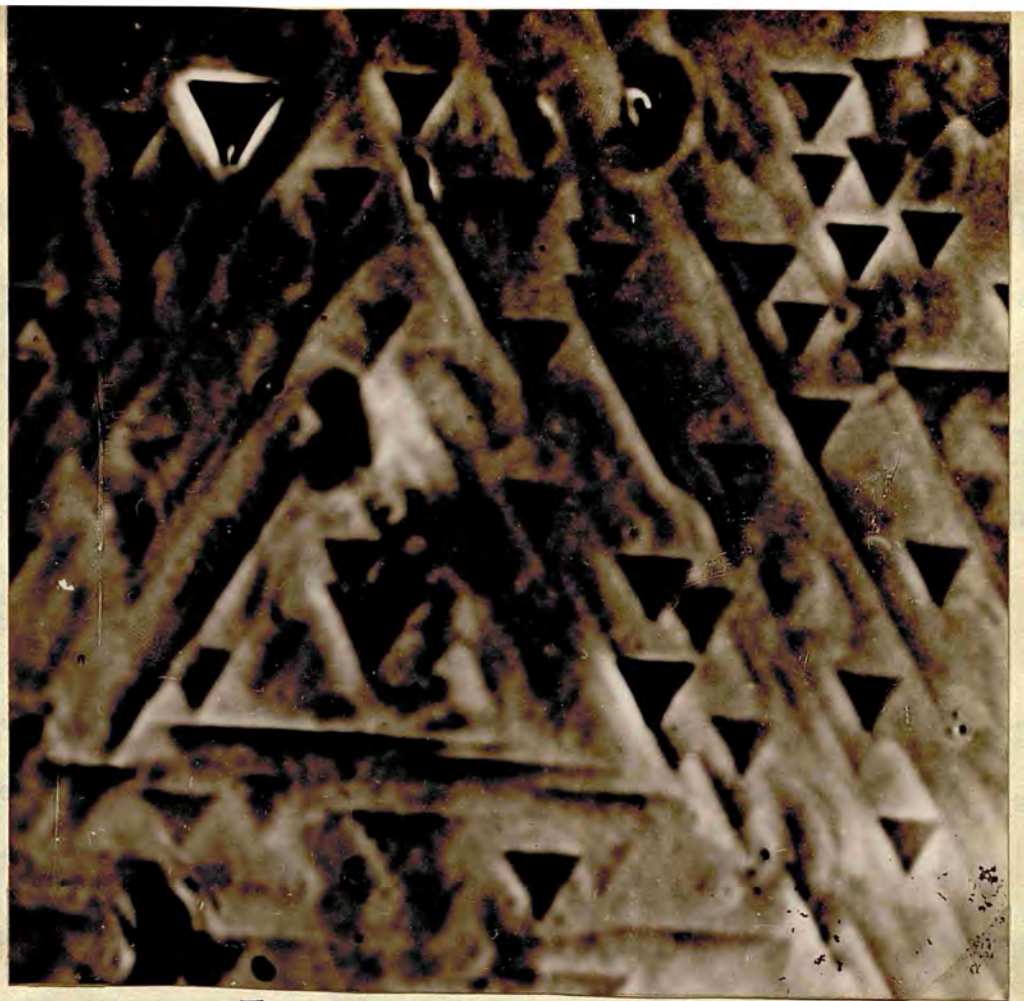

Fig. (37) ×750

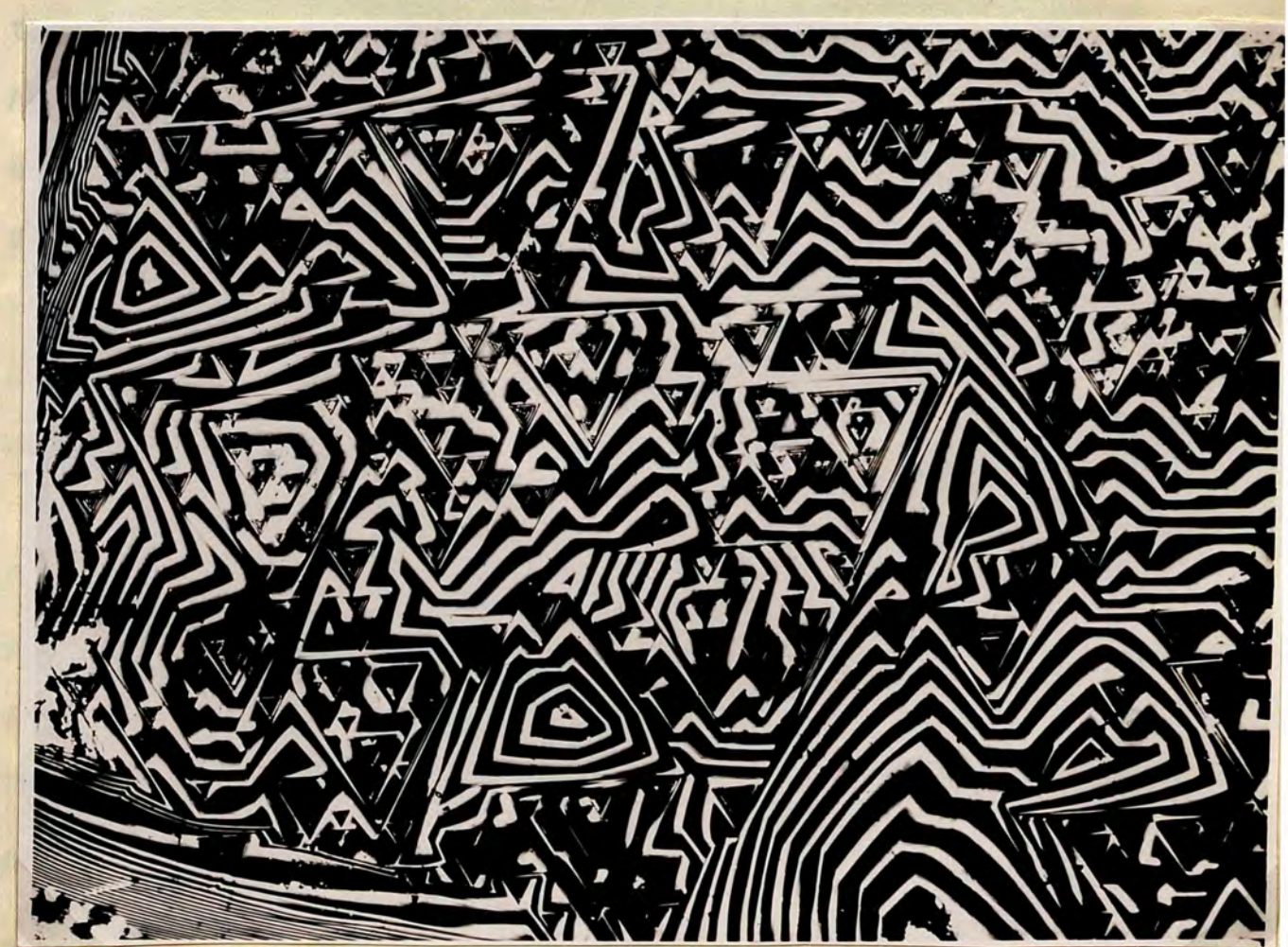

Fig. (38) X 110

hill. This expectation need not materialise as there is equal chance for the subdivision (fig 36) to start from B till C or from C till B. Slope and steps will only be manifested in the α, β and γ directions. In these directions subdivision from points like B and C, or points between, is directed to one such main direction such as α.

Support from Other Crystals in the Present Work.

Ample support in detail is provided in crystal B of the following chapter. Crystal (D) whose hillocks have been recorded in connection with the temperature at which the diamond has formed (previous chapter) gives a general support to the above arguments. Fizeau fringes (fig 38) show that the features are not different from those exhibited in crystal A. Crystal F fig (39a) and (39b) which is a type II diamond shows that we are in front of the same features irrespective of the type. The features are even more prominent than they are in type I diamond. The crystal is amongst the crystals studied by Dr. Grenville Wells, and is noted there for bad morphology. Another type II crystal is referred to in chapter 8.

But the most interesting observation comes in crystal E fig (40). This is the crystal on which slip was discovered, and the slip line is seen as a sharp dark line cutting trigon B. The crystal although large is composed only of 3 trigons. Trigon C is partly shown at the bottom of the picture. Strangely enough two centres of initiation exist x and y.

Fig. (39 a) X30

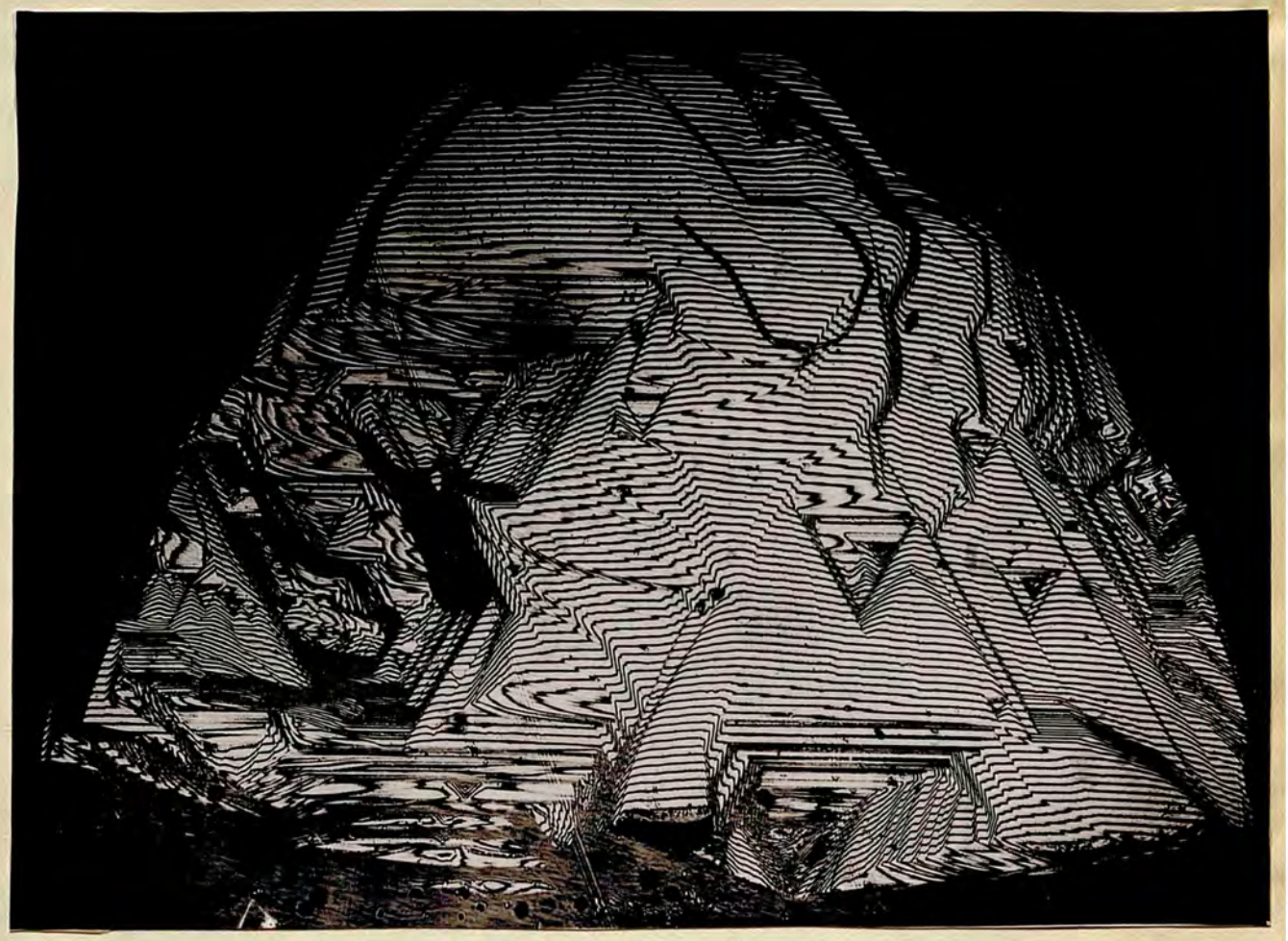

Fig. (39 b) X30

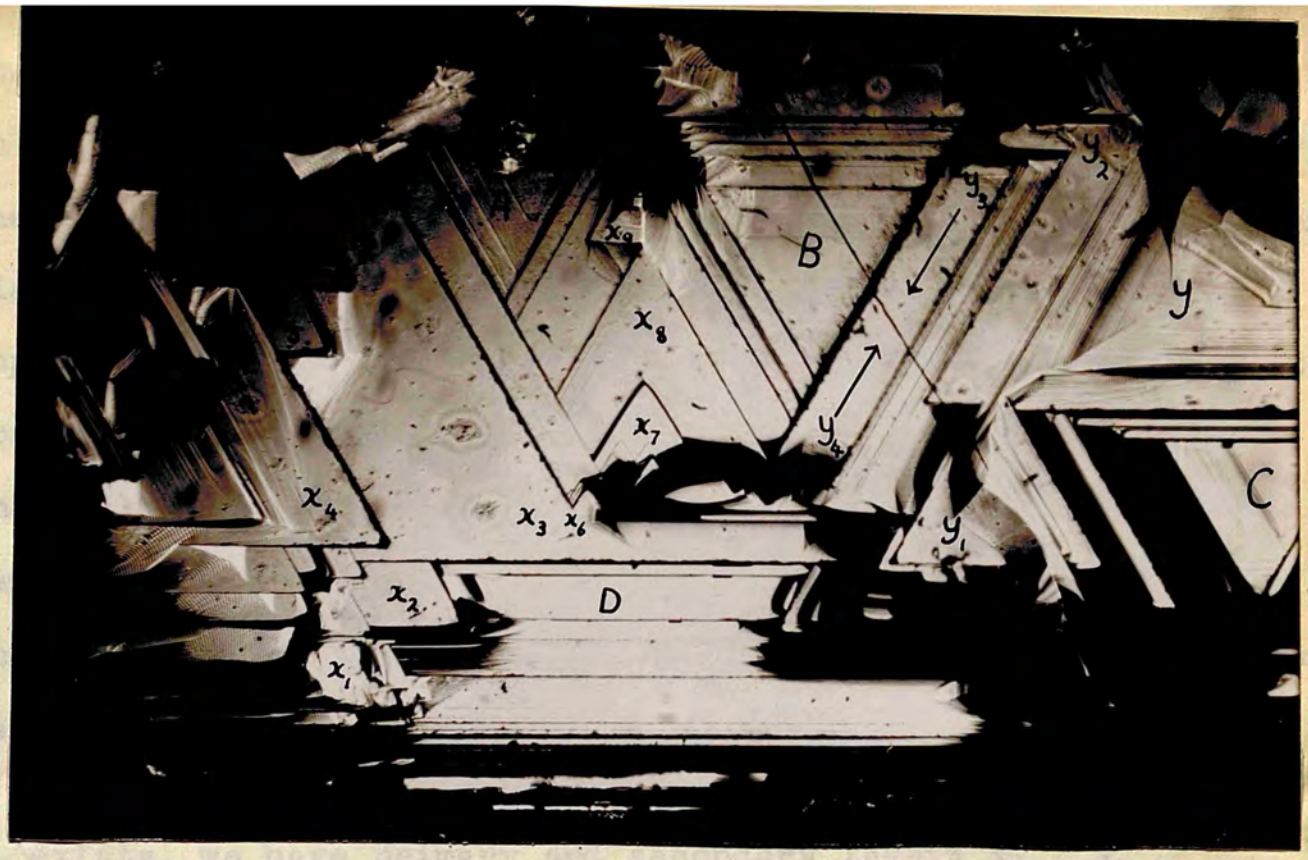

X 10

Fig. (40)

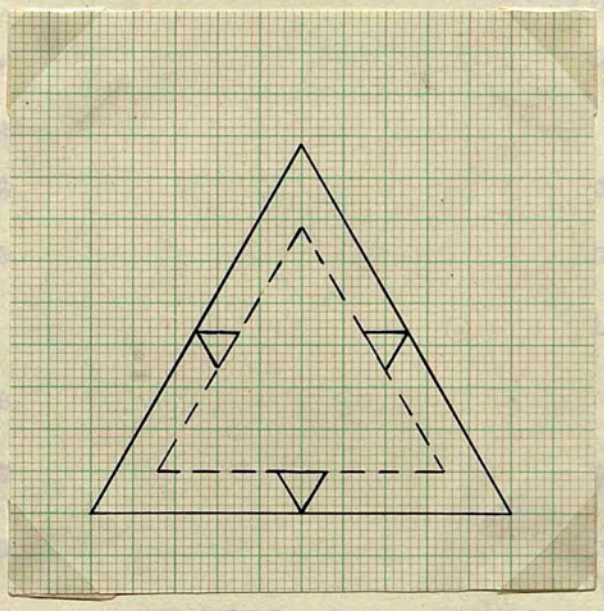

Fig (42 b)

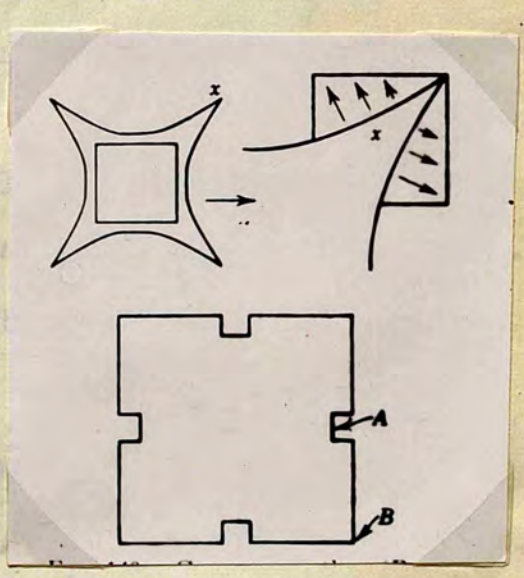

Fig. (42 a)

Centre y is responsible for y_1 between which some connection in the form of a bridge exists. These are both responsible for the existence of trigon C. From the upper tips of the triangular plates of y , other hillocks y_2 and y_3 arise. These fall on top of each other and form a hillock with a double profile, but corridors can extend from them downwards. From the tips of these corridors, other hillocks y_4 are forming. If the lower layers of y_3 and y_4 advance in the directions of the arrows, they can enclose a small trigon on the corridor where the arrows meet.

Turning to the left hand side of the picture where centre x exists, we have primary and secondary layers x_1 , x_2 , x_3 , x_4 and x_5 advancing. The primary layers x_1 and x_2 with the extended layer x_3 , co-operate with the primary layers of y_1 , to constitute the beginning of a major trigon formation D at the bottom of the picture. Such unfinished trigons exist, on the face, near the edges in some diamonds and exclude etch as responsible agent.

At the tip end of the top layer of x_3 we see clearly a small hillock x_6 initiated. At the right of x_6 there are other small hillocks. It is not certain whether they belong to the x or y centres. However, other previous layers of the x type (x_7 and x_8) have advanced. x_8 has not developed out of x_7 , but they are both advancing on top of each other. At the top of x_8 we see another growth hillock x_9 initiated. Because of its prominence it is quite possible to have arisen from other powerful centres

at the top. The crystal is only part of a macle.

On account of the large features, crystal E has provided complete confirmation of the theory presented in this chapter as a mere speculation. We see that in trigon A, the left hand base is extended. This is the trigon with a "basal extension" observed by Tolansky.(8) In conformity with the theory presented in this chapter, the extension should appear thick in contact with the trigon and thin away from it, as actually observed here.

Support from Grey Diamonds.

Fig (41a) and (41b) are from the coating of a grey diamond. It contains the diamond characteristic features, and so the coating is pure diamond. The crystal is nearly a complete octahedron with apparantly straight edges. Its weight is 0.2 grams. When looking at these stones they do not appear to be clear, their colour being grey and dull. Some of the coated diamonds have an opening or a window from which one can see the clear stone from inside. Sometimes the coating is cleaved and fig (34) of this chapter is from such a part. That the coating is pure diamond has also been testified by observations made by Custers.(75) He also testified the existence of foreign material of very tiny particles embedded in the diamond. He concluded that they may be pure carbon either in the amorphous state, or in the form of graphite, and Gradzinski(76) proved by

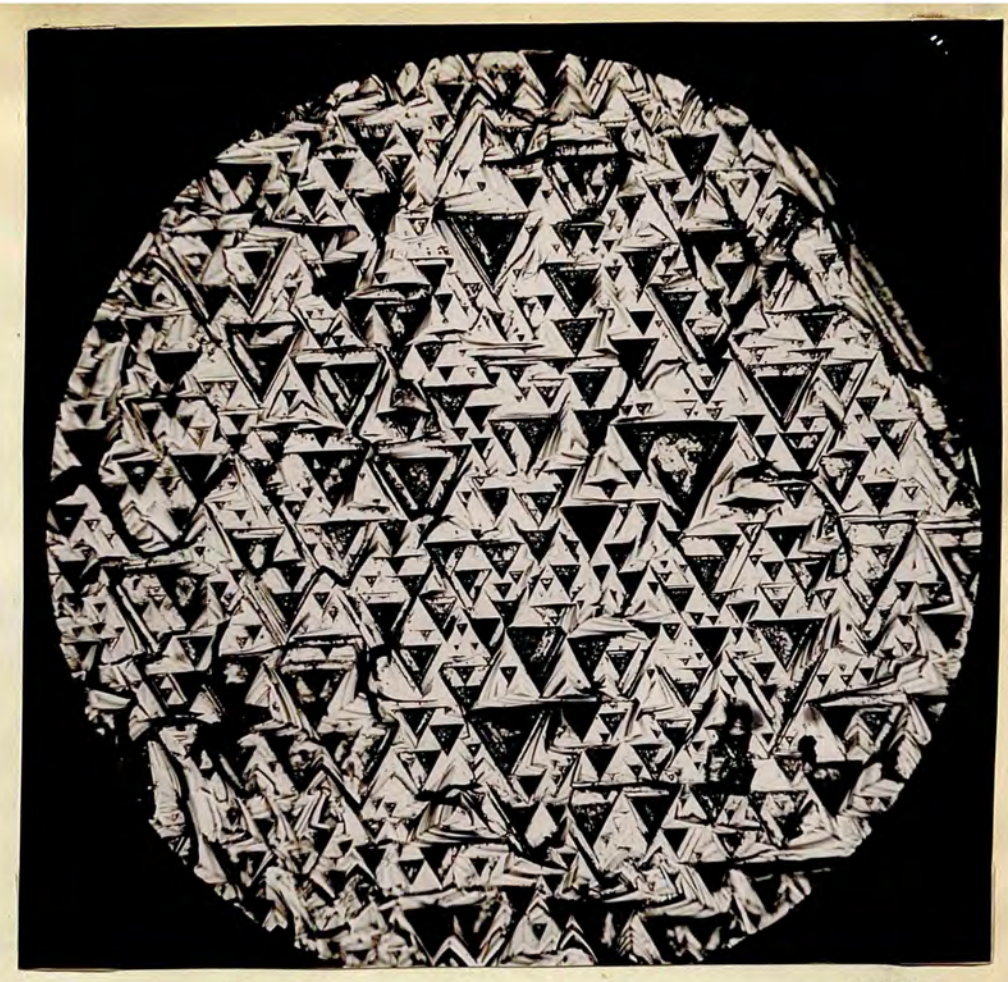

Fig. (41 a) ×170

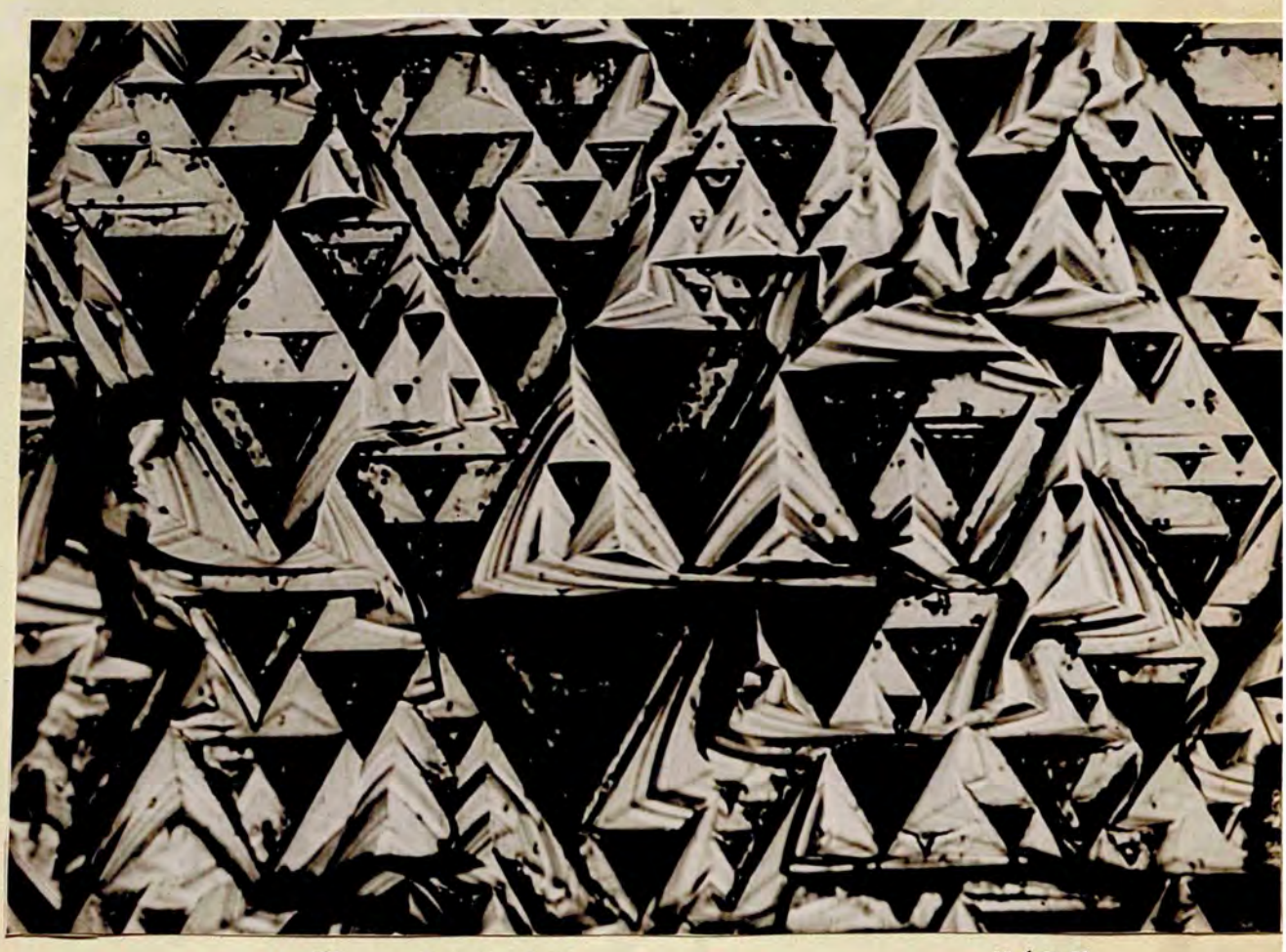

Fig. (41 b) ×625

an experiment that the material of the coating is lighter than the bulk material of the stone. Dr. Grenville Wells (7) comments on the observations of Custers, and thinks that they may be gaseous bubbles. When the coating was powdered and examined by x-ray methods (75) a slight indication of foreign material appeared. Growth cavities in the form of triangles (the black △'s in figs 41a and 41b) are a very common feature of nearly all the coated stones. (75) Custers did not observe the diamond hillocks around the trigons, and made a theory for the growth of the faces of these diamonds. The theory is not clear and perhaps the dark spots observed by Custers (75) as lying in rows are none else than small trigons.

Looking at figs (41a) and (41b) we see how the hillocks lie with their tips on top of each other as expected according to our model. Since no black spots occur on the top or walls of the pyramids, the black colour cannot indicate graphitization. Since it appears only in the trigons, which are depressions, it is quite possible to be due to the enclosed mother liquor between the branches of the denderitic tree.

The growth sheet boundaries of the layers forming the growth hillocks are very much curved, and the radius of curvature in typical cases is as small as 0.1 m.m., but it must be remembered that the hillocks are also very small, and the value of $\frac{\rho}{p}$ is moderate, being only $\sim$ 14. If the theory proposed in chapter 5 as to the origin of curvature is correct, this would mean that the coating has formed at the ordinary temperature of 5670 K.

Support from Previous Observers: (Papapetrou).

Although the above theory for the growth of diamond octahedral faces, is presented in the thesis as a speculation over the origin of trigons, there is more in it than a mere speculation. First it is supported by observation not only on the crystals studied here, but also on the crystals that were well chosen and offered such good results on the hands of Tolansky (8) and Wilcock (19). It can and will be supported by any other observation on any diamond octahedral face.

In this paragraph the support comes from the work of Papapetrou.(77) In Buckley's view Papapetrou's paper constitutes one of the most serious contributions yet to what is possibly the most elusive of crystal - growth problems. The paper begins with the polyhedral or plane - surfaced denderitic growth of a substance like rock-salt. The top of fig (42a) represents a flat minute cube of rock salt. This is followed by one with pointed extensions at the four corners such as at x. Then, in the second stage, the four pointed extensions, have by a change in the direction and speed of growth, become four small, but plane cubes, seated on the corners of the original cube as seen in the bottom of fig (42a). Each small cube then proceeds along the same lines (i.e. via the pointed extensions) to develop more cubes. These views are identical with the author's views on the growth of diamond octahedral feature. The only difference is that in the case of rock salt, the holes

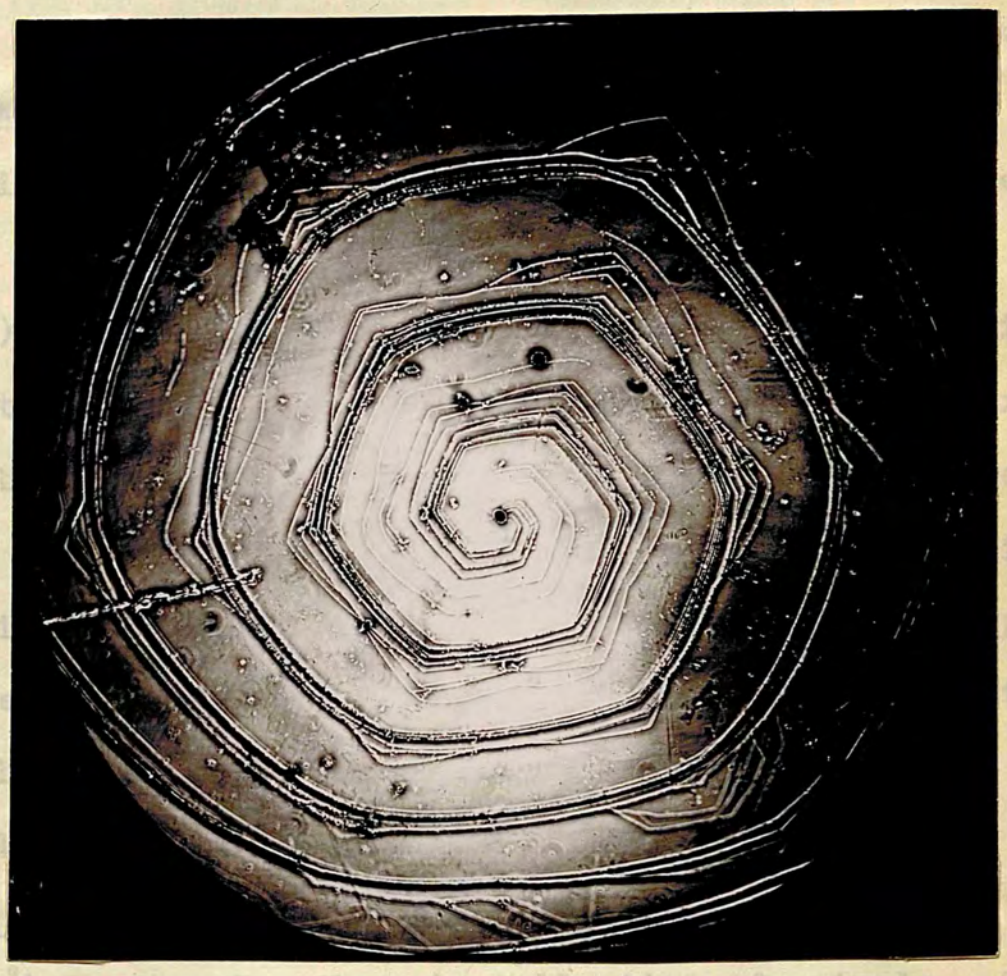

X 150

Fig. (4 2 c)

created at the sides such A, do not close. Our holes fig (42 b) are "closed" immediately and they are the trigons. Papapetrou was compelled to introduce diffusion into his equations, and perhaps the remarks made by Buckley refer to the ingenuity of placing on a theoretical basis, the branching formation of denderitic structure. The sides of the wedge-shaped extensions to the cube corners such as x represent lattice planes of fairly low indices which extinguish themselves through rapid growth.

Vogel's Views.

Denderites may be formed from the vapour or melt. They can also be formed from solution.(9) In one component system (e.g. melts) Vogel's(112) view is that the heat of solidification would affect different parts of a crystal to a different extent. The heat liberated would escape more readily on the cube corner than on the edge and much more so than on the face. Rapidity of growth will facilitate accumulation of heat at certain points and so render denderites more likely. The high conductivity of diamond to heat will not favour dendritic growth, but this may be counter-balanced by the unusually high latent heat.

Exaggerated Growth at the Corners in Spirals.

Fig (42c) is from Dr. Verma's collection of spirals. This may be due to dissociation of steps at the corners. According to our model this is nothing else but exaggerated growth at these parts.

CHAPTER SEVEN

Study of Unusual Features.

Crystal B is an octahedron, two of its parallel faces are exceptionally well developed. They have grown at the expense of the other six faces which now form the sides of the crystal. Looking at it from above the crystal is a hexagonal plate, the sides of which are not all equal. Its upper and lower faces are exceptionally smooth and admirably suited for multiple beam interferometry. In practice it is called a "flat" or a "portrait stone". The stone is South African of alluvial origin. The area of either face is roughly 1 cm^2, and its extensions in the 3 mutual directions: 1.26 cm, 1.02 cm and 0.98 cm. Its thickness is 1.8 m.m.

Visual Inspection.

Looking at it aslant with a hand lens and a source of light, striations could be seen on one face $//^{\ell}$ to an edge. The other face showed no marks. These striations would probably be the edges of growth sheets on the octahedron face. By looking into it under the microscope with narrow bright field or wide oblique illumination, using low or moderate powers, and focussing on one face at a time, one could see on either face three groups of striations parallel to three alternate edges of the hexagon, but the edges that are parallel to the striations on one face, have no stiations parallel to them on the other face. This is the property of the octahedron. Looking at the

octahedron from one fixed direction, if one face is △ the other face parallel to it is ▽ , and since growth sheet edges are parallel to the octahedron edges, this is what should be expected. One can also see other smaller and fainter striations forming into groups and giving the effects of closed triangular patterns. But these triangles were very faint indeed, and the technique used by Griffin (62) was tried. This consists in silvering the crystal, then observing it using narrow field pencil, and defocussing. The patterns improved but were very difficult to photograph on account of the poor contrast. Since the edges of these triangles are parallel to the striations which fall between them and the octahedron edges, they are in conformity with the triangular outline of the octahedron face and would, therefore, be the edges of plateaux of growth hills, and not the edges of triangular depressions or trigons.

With the same illumination under greater magnifications, one could see that the surface is full of exceedingly small triangles, having a tendency to lie in rows. Since these minute triangles are oppositely oriented to the much larger triangular growth patterns they would be depressions i.e. they are the well known and famous trigons in miniature. These are shown as seen, by phase contrast later, in fig (55). The disparity in size between the two types of triangles is great; judging by the visibility which is poor in both, the depth of the small trigons would be of the same order of thickness as the big triangular growth sheets. This thickness (or depth)

would probably be of the order of 100 A or so.

All these deductions are natural, and may be true or untrue, but it must be left for interferometry, (and in particular multiple beam interferometry) to decide, as no other means will.

The Growth Hills.

The crystal was silvered to (90 - 94) per cent reflectivity and matched with a similarly silvered optical flat $\frac{\lambda}{40}$. Such percentage is very suitable for transmission fringes. Fig (43) is the high dispersion picture of face 1 using the full aperture with an unfiltered mercury lamp. It was adjusted in the geographical sense for further use later. The triangular features in this picture are the growth plateaux referred to above. On account of the small magnification the small trigons do not appear as also many of the other structural details. By simply narrowing the pencil of light, and using a colour filter, at this geographical dispersion, an interferogram is obtained giving the extent of depth over the entire face. Fig (44) is such a picture using a blue filter (which transmits the blue line λ 4358 A).

Since the fringes are closed in the central part, and since it is known that growth centres add their growth fronts, and since there are several initiating centres on the face, it is reasonable to assume that the highest point is somewhere in

× $6\frac{2}{3}$

Fig. (43)

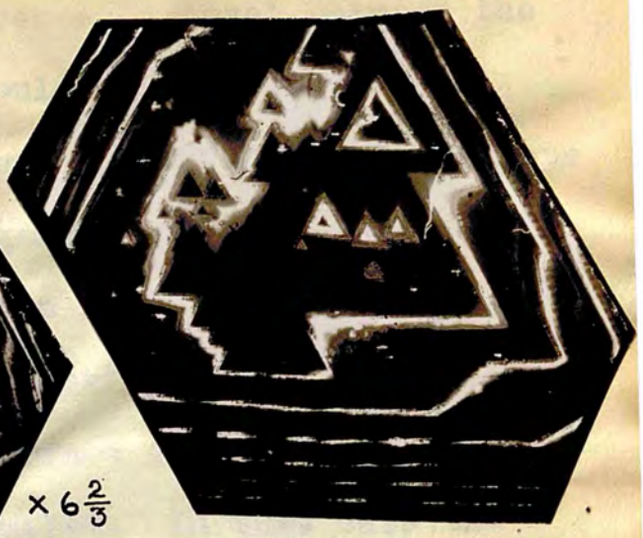

Fig. (44)

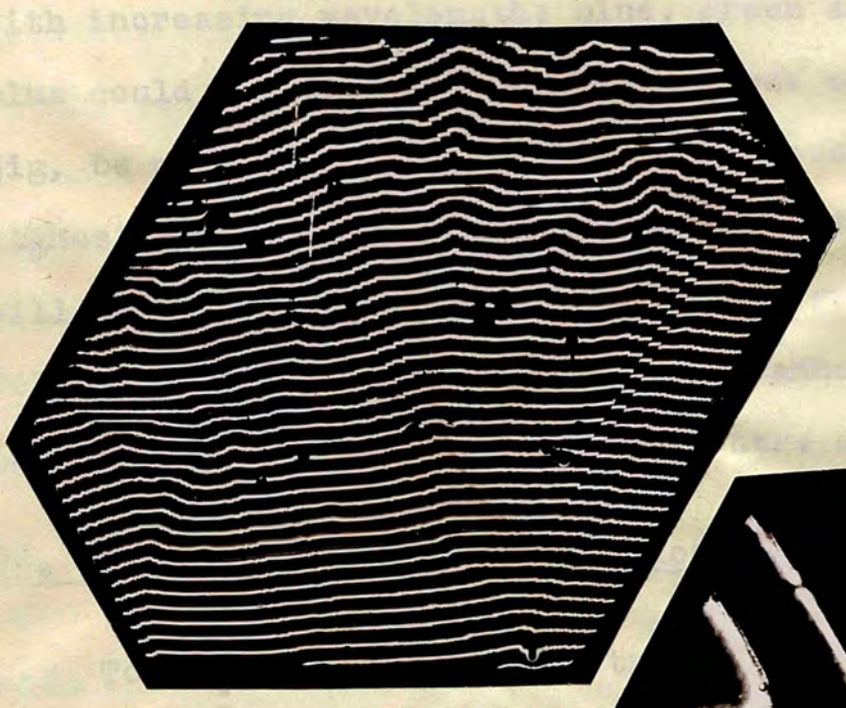

Fig. (45) × 7·6

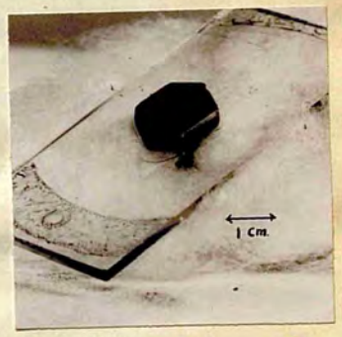

CRYSTAL B

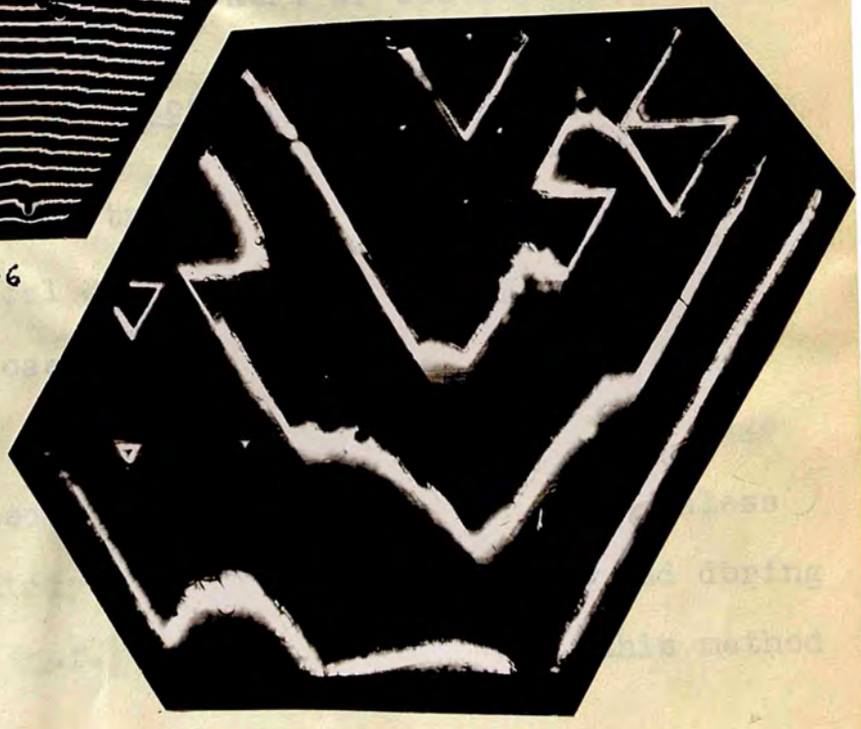

Fig. (46) × 7·6

the middle of the face. The difference in level between the highest area and the lowest zone would be of the order of $6 \times 0.218 = 1.32 \mu$, and there is evidence of bunching of steps at the right-hand and left-hand edges.

When the geographical dispersion is used, especially if the features are flat, it is always useful to work with the flat in close proximity with the surface i.e. when the yellow fringe appears single and not a doublet. In this case the order of colours, starting from the highest feature (nearest to the flat) downwards, will be the natural order of colours with increasing wavelength: blue, green and then yellow. The blue could then, by a proper adjustment of the screws of the jig, be made the colour of the points suspected to be the highest on the face, when the colour of the lower portions will be green, then yellow; then blue, green, yellow for the following order and so on. In this manner it has been testified that the highest point is in the centre of the face.

The Triangular Plateaux are Hillocks.

To prove that the large triangles are hillocks, dispersions other than the geographical dispersion had to be used. The line markings which compose these triangles were revealed to be small surface steps. To decide the direction of the wedge Brossel's method[69] was used, but this method is useless unless the gap is made deliberately big, and a method developed during work in thesis was used (c.f. chapter 4). With this method

not only is the direction of the wedge decided, but the order of the fringes deduced. Fig (45) is such a picture taken with blue mercury light. It represents the crystal's back surface (face 2). The short line at the bottom of the picture is blue fringe of order $n = 1$. Its relation to figures (43) (44) is a rotation where the upper and lower edges remain in their respective positions. From the sequence of order in the fringes in fig (45) the wedge apex is in the lower part of the picture. To the right the fringes cross steps. These steps are parallel to the right-hand edge, and represent edges of growth fronts whose main initiating centre is near the centre of the top edge. That edge is also an octahedron edge. In diamond centres of initiation of growth are mostly inside the surface, and rarely at an edge, but Willis (71) has observed this tendency on (R) and (r) faces of natural quartz.

As the fringes cross these steps in a descending direction, they move towards the wedge apex as is actually observed. Such is indeed the case with respect to the growth hill centred upon the upper edge. The point of initiation of this growth hill is also the point of initiation of the steps. It is the main initiating centre of the whole face, and as will be seen later, represents the highest point on the surface. Fig (47) is a different interferogram of this growth hill at a greater magnification, but rotated through 60°, and taken with the green mercury line (λ 5461 A). It is clearly seen how the fringes kink one way as they climb the steps and kink the

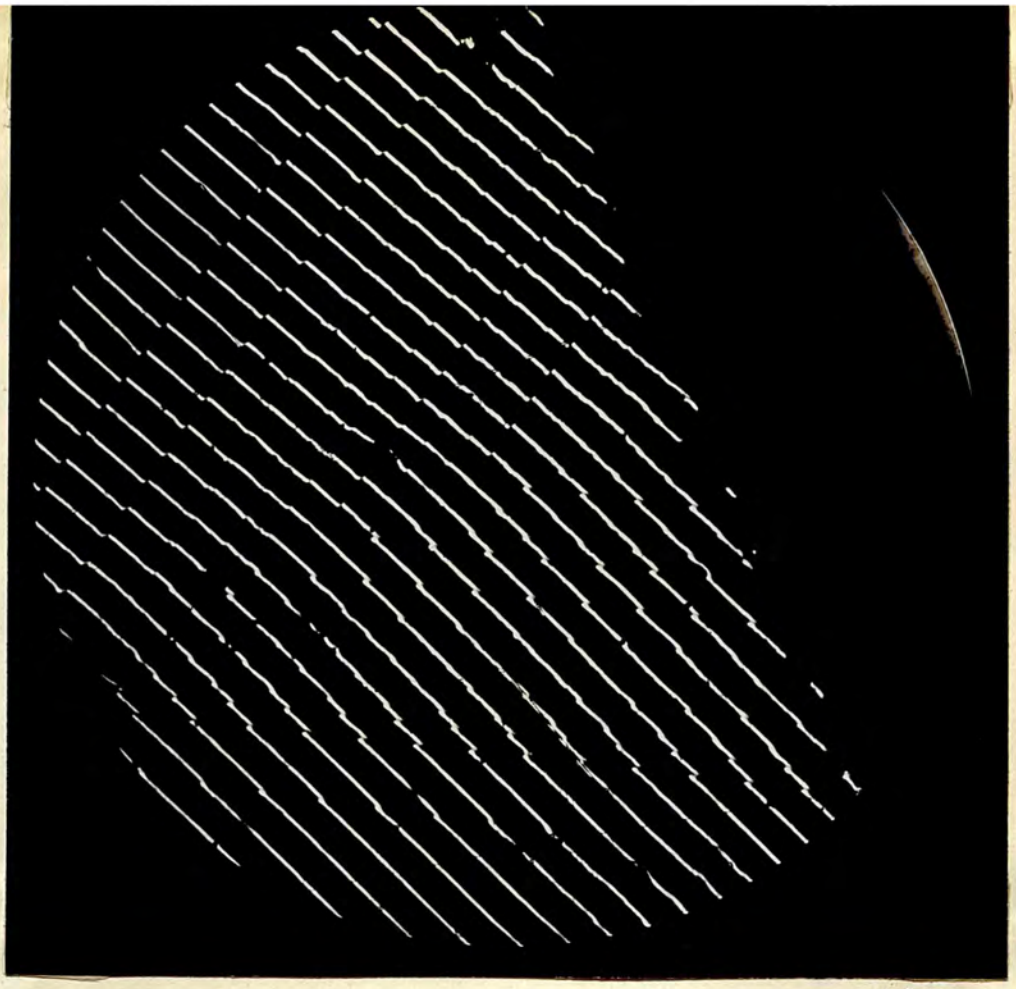

Fig. (47) ×45

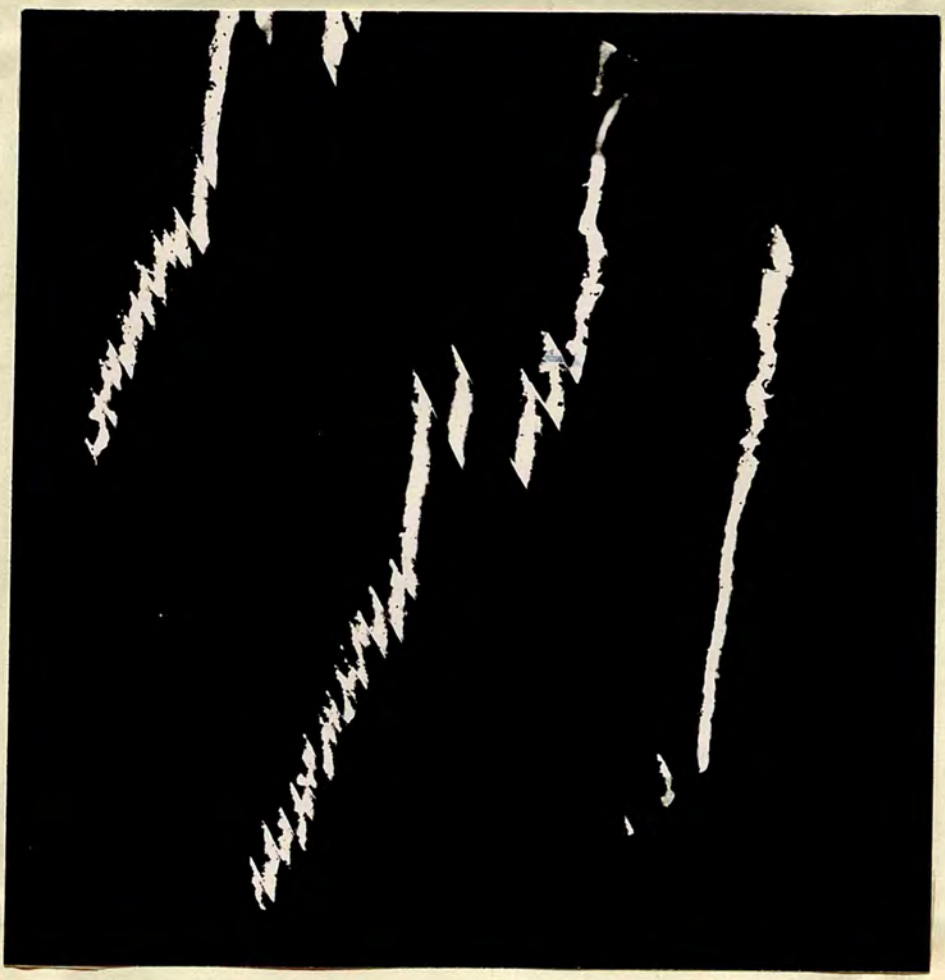

Fig. (48) ×45

other way as they descend. The prominent step-heights are fairly constant and amount to (200 ± 10)A. Fig (46) is an interferogram taken with green mercury line, at the geographical dispersion, of the whole of this face, and it is clearly seen that the point of initiation referred to above, and represented by a dot-fringe (at the centre of the upper edge), is the highest point on the surface. The fringes show that the surface is divided into 2 parts which form two vicinal faces of the main growth hill, whose initiating centre is the centre referred to above, and therefore furthers a small interesting study in vicinal faces.

Vicinal Faces.

Chapter (2) is an ample introduction to vicinal faces. The only record of vicinal faces supplied with some numerical data on diamond is in the work carried out by Tolansky and Wilcock.[8] Their crystal was from Sierra Leone. There it was mentioned that vicinal faces came to a point forming a tetrahedron, the inclination s of whose sides with respect to each other are very small. They give as an example a measurement of 0.9 minutes of arc. In Wilcocks thesis[19] the inclination of the vicinal faces of that same crystal to the true octahedron face was evaluated as 30", which correlates with the interfacial angle of 0.9′ (c.f. chapter 5).

Confining our attention to the vicinal face which comprises the left-hand side of fig (46) where the fringes are straight

(aside from the triangular depression to the left) we see that the distances between the fringes are not equal. This signifies a cylindrical curvature. The curvature which is a property of the diamond surfaces, is probably, in part, due to unequal distances between the edges of growth sheets and the unequal thicknesses of the growth sheets (c.f. chapter 1). In fig (47) which represents the top of the main growth pyramid the fringes are staight and exactly parallel which shows that the growth sheets are plane parallel plateaux. It is seen (fig 47) that the edges of these plateaux are not equidistant from each other. Although the main steps are of constant height, there are smaller steps in the middle whose height is probably half the above estimate. Also evidence will be produced later that there is bunching of steps in the other neighbouring vicinal face. Since the fringes are closer at the top of fig (46), the inclination of the vicinal surface to the close packed surface is greatest. The angle is 1'. In the middle where the dispersion is constant, and therefore the accuracy greater, this angle is 25". At the bottom the angle is only 18". The cylindrical curvature is 9 metres at the top, 100 metres at the bottom and nearly straight in the middle (with a radius of curvature about 200 metres).

That the inclination away from the close packed direction increases perceptibly towards the summit of the growth pyramid is similar to a result observed by Tolansky (36) on a single R face of Brazilian quartz. He was able to show, by virtue

of the sensitivity of multiple beams, that quartz vicinal faces are not truly plane, and possessed a slight cylindrical curvature with a radius of curvature of 20 - 60 metres. The derivation of cylindrical curvature, here, is carried out in a simple and clear manner.

The increase of the gradient of the growth pyramid towards the summit, has also been observed by Willis[71] on R faces of quartz, but this cannot be the rule in diamond unless observations substantiate it. As a matter of fact the rule breaks in the right hand vicinal face as seen in fig (46). Dynamically the gradient θ is determined by two factors[71]:

(a) The rate g at which the growth sheets are initiated at the active centre or centres.

(b) The velocity v of the growth fronts as they spread across the face.

Thus the gradient is steep if g is large and v small; for g small and v large, the vicinal sides of the pyramid make a small angle with the close-packed (111) face.

Due to numerous centres of growth in the right hand region in fig (46) g has become great, and due to these numerous centres again v has been small from the start. Before they co-operate, the numerous centres must hinder the main flow. The result is thickening of growth sheets due to piling from above and hindering from below. The ultimate result is a "bunching effect".

That an increase in gradient occurs towards the edges is

clear from the nearness of the two end fringes towards each other. This is seen in the R.H. portion of fig (46). That this is accompanied by bunching, is also evident from the large step heights in that region as seen in the right hand portion of figure (45). There the major steps run to $\frac{\lambda}{12}$ or $\frac{\lambda}{8}$ where near the main initiating centre they are $\frac{\lambda}{60}$ in the small steps and $\frac{\lambda}{30}$ in the main steps as stated above.

Identifying the centre of face of fig (44) with the highest point on the surface, we see that face "1" comprises the meeting of 3 vicinal faces which are not equally inclined to the close-packed direction. Also the interfacial angle along an edge between the lower and R.H. vicinal faces, is not constant, and violently varies from 0.5' at the face centre to 1.6' directly lower down. Moreover the vicinal form is flatter in the face centre than it is at the edges.

Thus it may be concluded that vicinal faces on diamond are not either plane or continuously curved. They arise from the combined effect of centres of initiation of growth. The growth layers cannot be parallel to any other plane except the close packed direction. The profile of the growth fronts depends on the thickness of the layers and how far they reach up each other. In other words it depends on the rate of the material received and the prelimenary local obstacles in different directions. The combined profile of growth fronts is the profile of the whole crystal face. The only kind of cylindrical curvature, encountered here, has thus been explained

and accounted for. It has also been testified that the vicinal form can be more acute or less acute at the face centre.

The Minute Triangles are Depressions.

Fig (48) represents a group of descending steps from top to bottom. They are part of the steps at the right hand edge of Fig (45). The wedge apex is to the left and the fringes in going over the steps if followed from top to bottom are deviated towards the wedge apex. The shift of the fringes proves that the steps are descending. The amount of shift estimated as fraction of an order gives their heights. The large steps at the bottom are due to the bunching of growth sheets in that locality. The fringe width is due to the unevenness of the surface of the steps, due to minute surface irregularities. If the minute triangles are depressions the areas around them represent either a true or a relative elevation. The fringe in passing over these little ups and downs is virtually dissected. The edge of the fringe which passes over an elevation is directed away from the apex of the wedge, and the edge of it that passes over a depression is deviated towards the wedge apex. The result is a ragged appearance and a false broadening, as indeed apparent in fig (48). As the reflectivities of the silver films used are in the range of 90 to 94% the fringe width should be between $\frac{1}{30}$ and $\frac{1}{50}$ of an order (c.f. chapter 3). The fringe broadening, limits the precision of measurement to an estimate rather than to an exact

value of the depths. All the inverted triangles are without exception 'shifted' towards the side of the fringe-shift over the steps, so they are all depressions, and moreover their depth is about the same order as height of the smaller steps.

No prominent elevations around the trigons exist. If they do exist, there should be a similar shift towards the other side of the wedge, but no observation as such has been experienced, showing that their heights must be smaller than the fringe width. The trigons that have 'separated' from the fringes are the white triangles that appear to the left of middle fringe of fig (48) (tenth step from below). They constitute two consecutive rows and are less than $\frac{1}{25}$ of an order (less than 100 A). Only one of them seems to be deeper than the above estimate. As the average density of trigons on the surface is $2.4 \times 10^5 / cm^2$, we see that only a few amongst thousands have the above depth. The others must be definitely shallower.

Thin Film Technique.

The use of thin films for high magnification topographical study has been published by the author in conjunction with Professor Tolansky (78). It is included in Part II of this thesis. One of the phases of the thin film is that it can be used for high contrast study in the manner in which multiple beam high dispersion acts. During the setting of the silvered crystal in the canada balsam used for mounting, a drop accidentally

×375

Fig. (49)

formed and spread over the surface. Instead of wiping it out and cleaning the crystal again, it was silvered with the appropriate percentage, and fig (49) is the result of interference in the thin film, taken with unfiltered mercury light. It represents a step downwards from top to bottom. The trigons are the triangles pointing with their angles downwards, and it is always good to remember that a trigon points unmistakably to a downward step. The advantage of the thin film is availability of high power, and in this picture it is seen the trigons do not all form at the edges of the steps. As a matter of ~~a~~ fact a minority do so; most of the trigons are formed in the corridors of the major steps. This does not contradict the observation made by Tolansky (8) that the trigons formation is connected with some shelving in the form of steps. The shelves probably exist here but they must be near molecular dimensions, and cannot be seen. The picture shows that it is not an easy and levelled road to jump at any theory dealing with the formation of trigons. But one thing is certain: that they are connected with triangular sheets advancing upwards in both steps. These are clearly seen in the upper part of the upper step and the right of the lower step. These triangular sheets are responsible for the fommation of the incomplete trigon at the edge of the step, also for closing upon the trigon already formed in a previous layer formation in the middle of the upper step. This trigon will never be closed, but will widen and deepen.

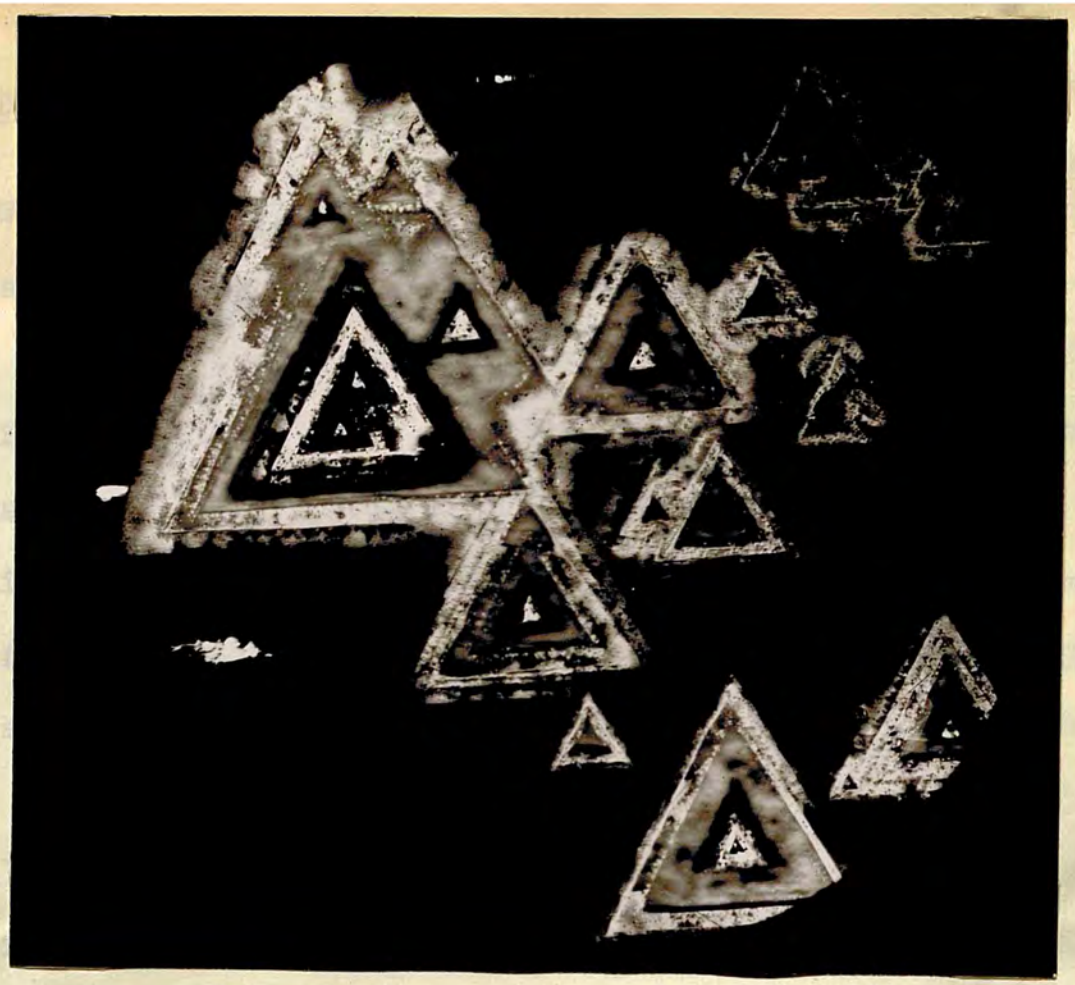

Fig. (50) X 30

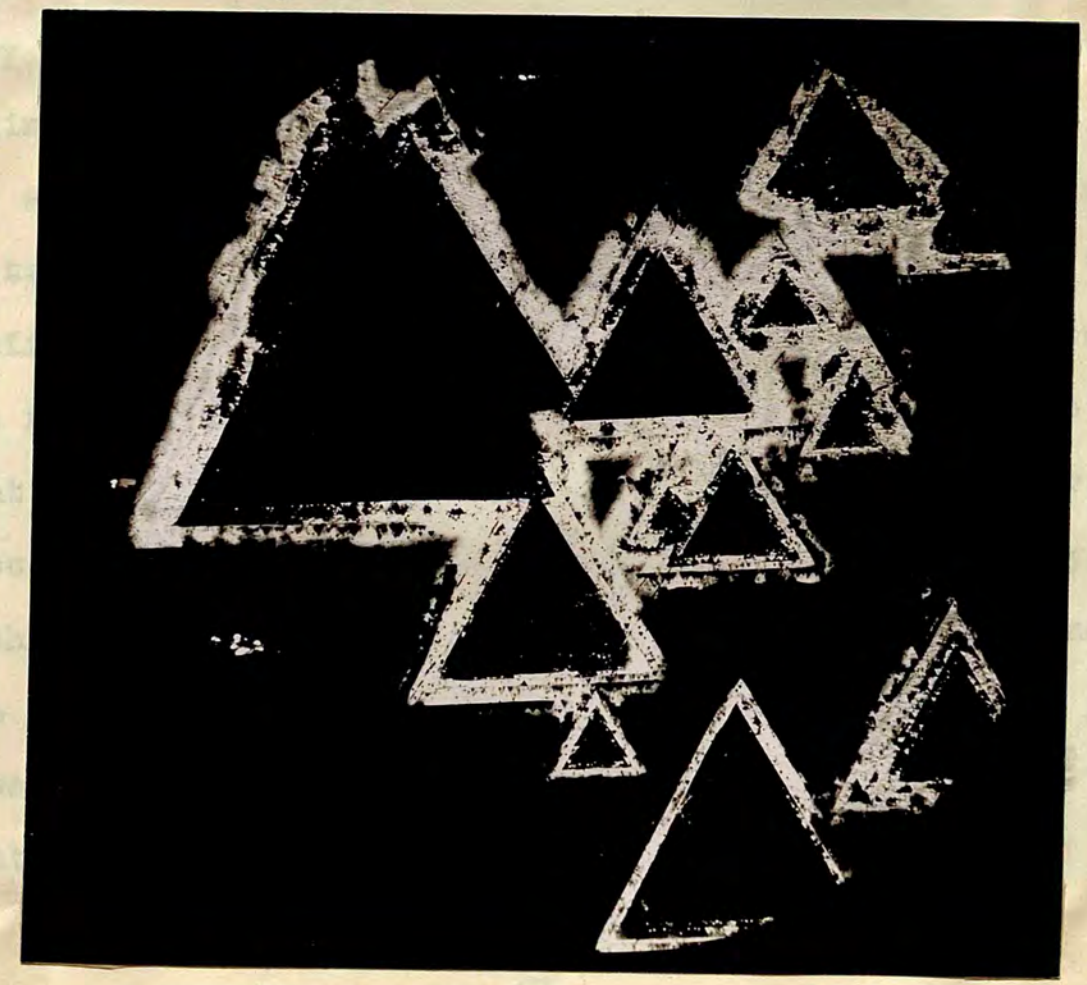

Fig. (51) X 30

High Dispersion Study of Growth Hills.

We have resorted to the geographical high dispersion because the features could not be revealed or recorded by any other means. Apart from the immense contrast obtained, the interferometric picture has the extra dimension of depth. But the magnifications exposed in fig (43) and (44) are not enough for high resolution, and some of the features under greater magnifications are recorded in the following pages. Fig (50) represents a group of growth hills that exist in figs (43,44) taken here with the unfiltered mercury light, and fig (51) reveals the same area taken with monochromatic green light. They range in length of side from 2/3 m.m. to 0.1 m.m. They are all at the same level and their heights do not exceed $\frac{\lambda}{2}$ Every one of them has a core at the centre from which it originated. The central small triangle has a satellite to its left, and the biggest triangle has a double core and a satellite to its right. The central part of this large triangle is magnified in fig (52)^{a}. Worthy of observation is that the core does not develop into a larger triangular complete sheet. It might mean that growth does not proceed by extended wave fronts as occurs in other crystals e.g. in pyrite (a cubic crystal which, although different in structure, imitates diamond in some features) and fig (52)^{b} taken from a (111) face of pyrite illustrates what is meant. The triangles (revealed by the light profile) are hills and not depressions.

Fig. (52 a)

x 150

Fig. (52 b)

x 38

But the most astonishing observation that was referred to in the introductory part of this chapter, comes to life in fig (52a). Innumerable tiny triangles that were described as trigons, hardly leave a single space unoccupied by them. They are oppositely oriented to the much larger triangular plateaux. On the corridors of the completed growth sheets they exist in rows, evenly distributed. If this is due to etch it is surprising that etch figures do not overlap. Another observation is that the linear plateaus in which these figures exist do not seem to be coplanar in the crystallographic sense, also parts of the same plateau are not of the same breadth along any of the corridors. This is accentuated in fig (53) which shows a single growth hill, taken with unfiltered mercury light. One of the growth hillocks is reproduced under greater magnification in fig (54). This shows that growth in the central grey portion (the one surrounding the core) proceeds from the corner. This behaviour is very clear in the upper corner which develops as a fresh triangular plate clearly defined. That growth proceeds in a particular manner is evident from the fact that the edges of the layers of any one single pyramid are not either exactly parallel or continuous.

The development that occurs in fig (54) is not restricted to the layer with the grey shade. The outer (white) and lower levelled area, has two projections advancing from the top to the base as seen in the R.H. portion. Clearly growth by layer mechanism in the usual manner does not arise. Another ob-

Fig. (53) ×30

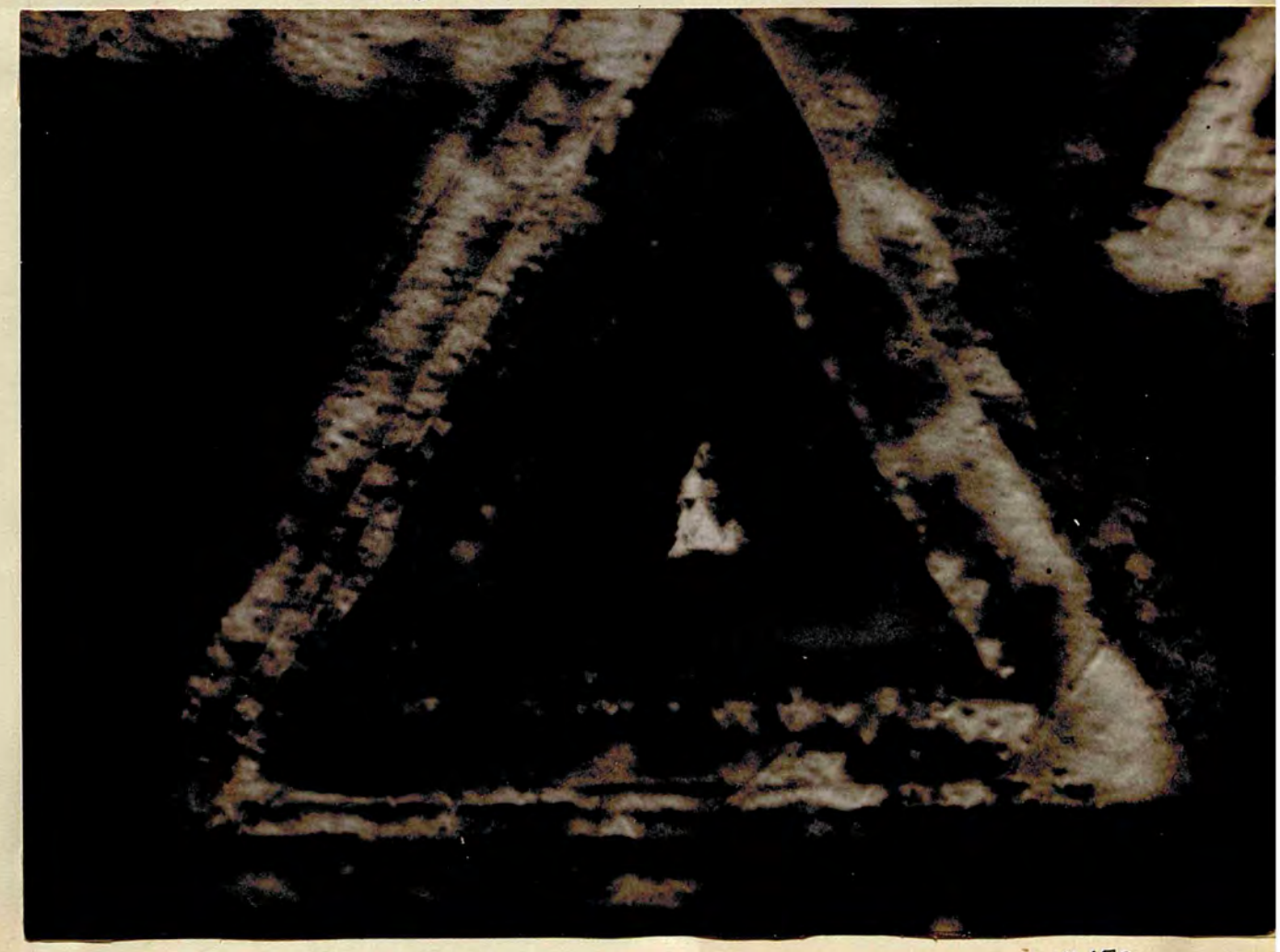

Fig. (54) ×150

servation is that the tiny triangles referred to develop at the core as well as the corridors of the major triangles, and not a single core amongst the twenty hillocks or so on both faces is devoid of them. According to an interferometric study carried out in a previous section, the depth of these trigons rarely exceeds 100 A. Their sizes range from 2 to 20 μ.

The above observations must be accounted for and incorporated in any theory of growth of diamond. The theory must also explain the occurrence of these minute triangles or trigons.

Observations by Phase Contrast.

Having realised that the triangular plateaux are stepped hillocks and that the minute triangles are depressions (and since they are in the right orientation for trigons they must be trigons) it is natural to seek means by which we may be able to see and record these features at higher magnifications. As will be seen in the next chapter these features are imitated in a perceptibly shallower form in other diamonds, and probably the electron microscope can reveal their inner structure; but having no access to such an expensive instrument we have resorted to the phase contrast of the optical microscope. The loss in resolution is slightly counterbalanced by the fact that greater areas of the surface are revealed and thus the relation between different parts could perhaps best be correlated.

Fig (55) shows the smaller companion in a double hillock.

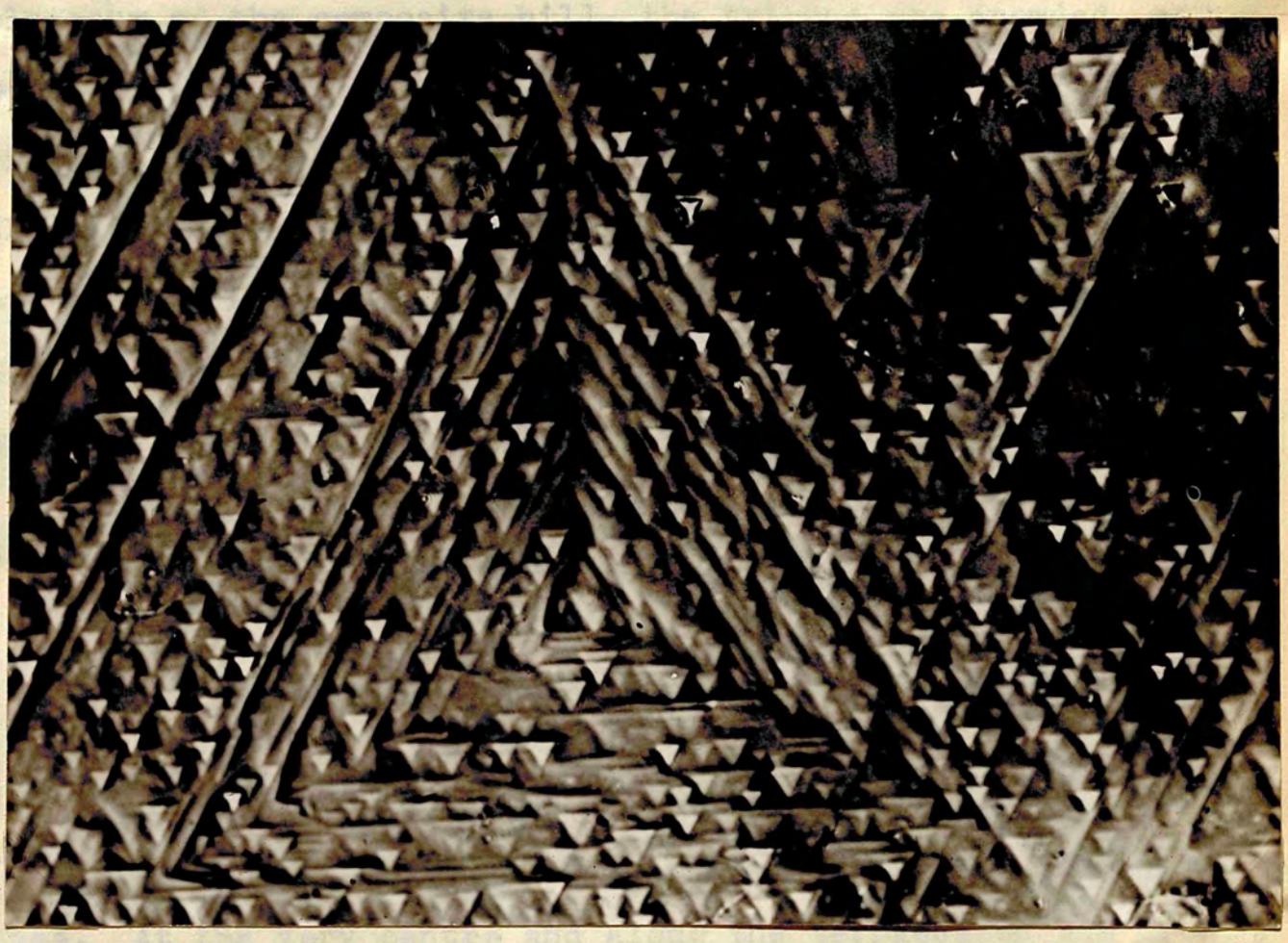

X 250

Fig. (55)

It is the smallest hillock that can be contained in such a size of picture. At the left are the major steps of the composite hill. To the right is part of the space between this hillock and its major companion. This area is a depression and in it the trigons are not evenly distributed. This is probably due to interference from the other hillock. On the terraces of the included hillock as well as on the major plateaux of the composite hill, the trigons are crowded, and more or less, evenly distributed. The trigon formation begins from the very centre so they accompany the growth sheets as they are developed. In the whole literature of diamond such orderly features have not been described or correlated. The trigons are nearly all flat-bottomed and in their very nascent stage.

Conclusions and Deductions.

Thus it may be concluded that growth hills appear on the flat faces of a portrait stone. The growth hills are similar in that they are composed of triangular plates superimposed on top of each other; the plates are parallel to the octahedron face. At the very centre and along the terraces of the growth hills, triangular depressions occur which are the trigons so famous on diamond octahedral faces. The existence of trigons at the very centre and along the edges of growth hills seems to be connected with the mechanism of growth. The phenomena is of wide occurrence and Tolansky has reported the existence

of trigons at edges of growth sheets in the case of a diamond octahedral face, made of three vicinal faces meeting at a point. This was referred to in a proposed theory of growth in the preceding chapter. One of the growth hills referred to here was reproduced there to support the theory. The author expressed some of these views in a diamond conference held at Oxford.(79) There he was given crystal B of this chapter. Crystal B confirmed these views exclusively. There is of course no need to repeat what has been conducted in chapter 6, and it is fair to end this chapter by the following comments.

Three explanations exist for such a phenomena:

(1) The trigons have been produced by etch. Their position with respect to the octahedron edge is similar to that taken by etch figures on other crystals of the cubic system (e.g. alum and cuprite). The etch figures take the symmetry of the crystal and should be equilateral triangles on the octahedral faces of crystals belonging to the cubic system. If the growth hillocks are due to compound dislocations, then according to recent observations in other quarters (80, 81) mostly on Si C crystals, we should expect etching to develop at the centre of growth hills and along the edges of growth sheets.

(2) The trigons are a growth phenomena. They arise when growth sheets meet at angles of 60°. When growth sheets meet an obstacle they are upheld. Secondary growth starts from the sides of this stationary front, and a flat bottomed trigon is

enclosed. This explanation is due to Tolansky[8] and Wilcock,[19] and does not account for the existence of pyramidical trigons.

(3) On the octahedral faces of diamond growth starts by means of triangular plates which can be small in size. From the tips of these triangular plates other triangular plates are developed. From the tips of these secondary plates other tertiary plates are developed and so on. This may be called growth from the corner outwards, and is some kind of denderitic growth. If the triangular plates are in comformity with the octahedron face it is clear that they can enclose triangular spacings between their branches in the exact position of trigons. The theory explains that the primary nucleus builds up into a growth hillock. The growth hillock must be lined with trigons at the edges. It must also incorporate the trigons from the very centre.

Proposition (1) has been dealt with at length by Tolansky[8] and Wilcock,[19] and by Wilcock alone. More than one trigon has been observed whose depth is exactly the same as the depth of the outer levelled area. It is inconceivable, it was reasoned, that solution will etch both areas to exactly the same extent. The trigons were found mostly connected with surface steps. The steps are a growth phenomena, and it is natural that trigons be due to the same cause. The triangles produced by etching diamond artificially are appositely oriented to these natural trigons.

Proposition (2) does not account for the existence of the

pyramidical trigon, and does not explain the existence of hillocks around the trigons. It does not tell what sort of obstacles, or disturbances are responsible even for the existence of the flat trigons.

Proposition (3) explains all the morphological features that were observed during work carried out in thesis. It explains all the observations that were partly responsible for proposition, (2). It accounts for the occurrence and behaviour of vicinal growth on diamond octhedron faces. It explains why a powerful centre of initiation is as a rule the centre of 'gravity' of the whole face. Although growth occurs at the corners, it is not contended that material must arrive from the active centre. The active centre has only the precedence that it has arisen first and that it is continually growing but not necessarily in extension. If it does not grow, and the other parts grow, it must end by being a depression. Growth from its corners will provide the secondary centres. The secondary centres take their material from the solution or vapour. There must be a compelling need for growth from the corner such as local depression in temperature at the corner. These secondary sources being late in development will be on the average lower than the primary source, but they are receiving material all the time. Growth proceeds from their tips and the tertiary centres develop and act in a likewise manner. So it is a continuous wave front that is advancing. Only that it is a dissected wave front full of corners and

×850

Fig. (56)

steps in three mutual directions (c.f. fig 56). The whole group will form up and build as a pyramid full of triangular depressions (c.f. fig 55), as has been fully explained in chapter 6 . It is necessary to mention that the primary source ought not to be more distinguished than the other secondary sources. From fig (55) they all look alike. The primary source cannot nourish these secondary sources, nor will it control them. The wave front spreads only by sub-division, but the material is not transferred. Through the material received, all the centres will rise up keeping their relative proportion in height.

An explanation has thus been given for a very intricate phenomena. The phenomena is of wide occurrence on diamond octahedral faces, but such orderly features are very rare.

CHAPTER EIGHT

Study of Extremely Faint Features.

The small features encountered in the previous chapter - it was mentioned - exist in an even more elementary form in other crystals. The importance of the present chapter lies in its capacity of providing such data. If the growth marks provided by crystal B of the previous chapter exist in a more elementary form in crystal C of this chapter, the growth marks must be of near molecular dimensions. When details are near molecular dimensions (a few atomic layers high or deep) they are bound to give the true pattern of the diamond texture. It is true that multiple-beam interferometry has a decided gain of resolution in depth, but this resolution in depth is supplied upon patterns provided by the optical microscope. The lack of lateral resolution of that microscope affects multiple beams in another manner that was explained before (c.f. chapter 3).

Both phase contrast and multiple-beam high dispersion tell that there is something on the surface. Phase contrast reveals its outline and interferometry decides its depth (or height). We are sure therefore of the shape and depth or height of a certain feature. We know its scale but we do not know its inner structure. The fact that features of both crystals B and C are also imitated in a much more grosser form in other crystals (e.g. crystal A of chapter 5) tells that we are dealing with the true texture of the diamond surfaces and therefore with the true mode of growth.

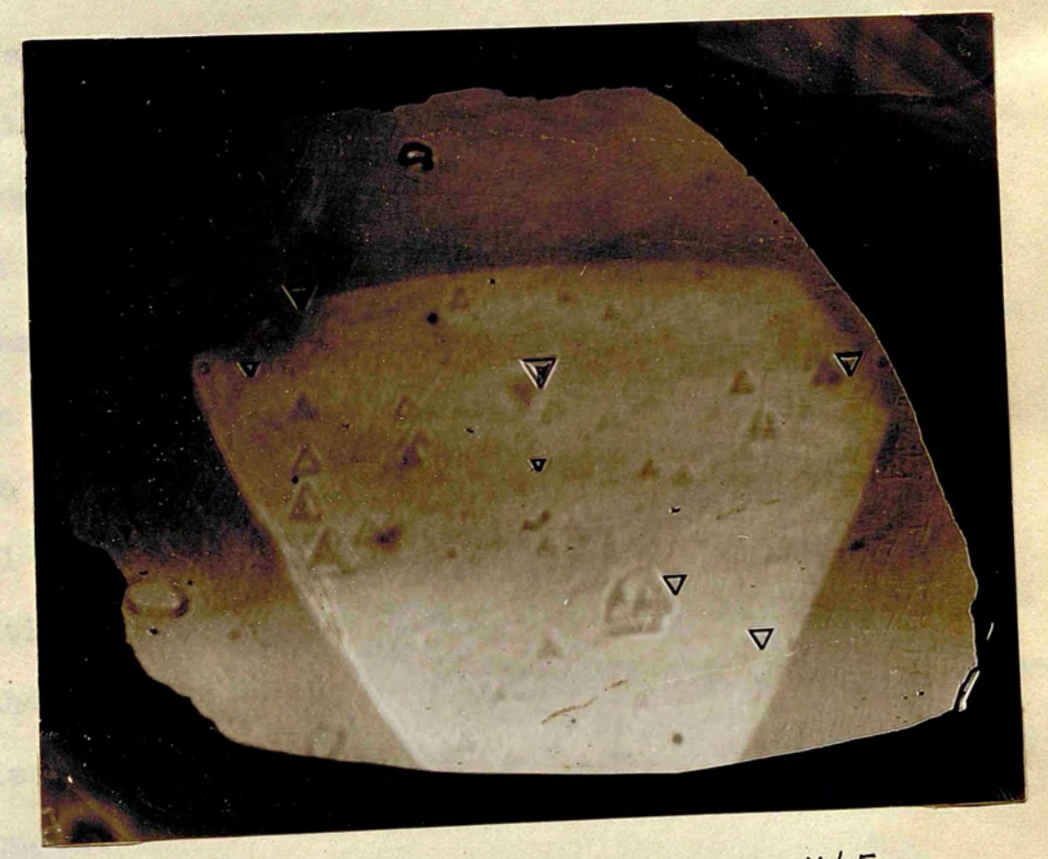

×45

Fig. (57)

Description of the Crystal.

The crystal is a small octahedron belonging to the passage of the regular octahedron to a regular tetrahedron by the diminution in point of size of four of its planes, and the increase that has taken place in the four others. The diminution is not great and a good part of any of the larger faces can still be photographed in transmission by light falling on the smaller face. Two of these parallel faces have been studied in detail both in Part I of this thesis and Part IV to follow. Since there were no features on any of the surfaces except some isolated and neat trigons (fig 57) and the crystal gave always extremely parallel fringes when casually matched with a flat - it was judged that we are probably in front of a true lattice plane in diamond. Such a surface would be invaluable as an optical flat in the study of diamond surfaces. It adds to the essential qualities of an optical flat - smoothness and flatness - the further necessary quality in the study of diamond surfaces, viz: indestructibility and insusceptibility to abrasion.

Test of Flatness.

For this purpose one of its faces was matched against an optical $(\frac{\lambda}{40})$ flat. When the dispersion was small the fringes were extremely straight and parallel. This is not a sufficient judge of flatness. When higher dispersions were tried the fringes remained straight and parallel but another phenomena appeared (fig 58a). The fringes were full of kinks. The kinks were difficult to explain and revealed structure. The estimated

kink by sight would be $\frac{\lambda}{40}$, but no such kinks in $\frac{\lambda}{40}$ flats have ever been observed. In such flats the irregularities in local areas would be $\frac{\lambda}{200}$ and would appear as an inner structure in the fringes, only to be revealed by sensitive means. When an extremely high dispersion was tried the surface appeared to be full of small triangles (oriented as trigons) and the kinks must be due to them.

(19)

Estimation of Depth (or Height).

The trigons on this crystal are much shallower than any trigons observed on diamond surfaces. If it were not for the very high dispersion on a basically plane crystallographic surface, and if it were not for very critical phase contrast illumination used afterwards, they would definitely have passed unnoticed. These trigons exist in nearly all octahedron faces of diamond but they are not always detected. When it was mentioned on account of observations, on this crystal, that probably a smooth atomically plane (111) surface does not exist on diamond - and this was in a Diamond Conference held in Oxford - we were given crystal (B) to test. Crystal (B) described in the preceding chapter, has been used in a variety of experimental research in other fields. It was chosen on account of its perfect morphological texture. If there is any crystal to break this "rule" it would be that crystal. On the contrary the trigons on crystal (B) were not difficult to see and some of its trigons were more than 100 A deep. But the

(79)

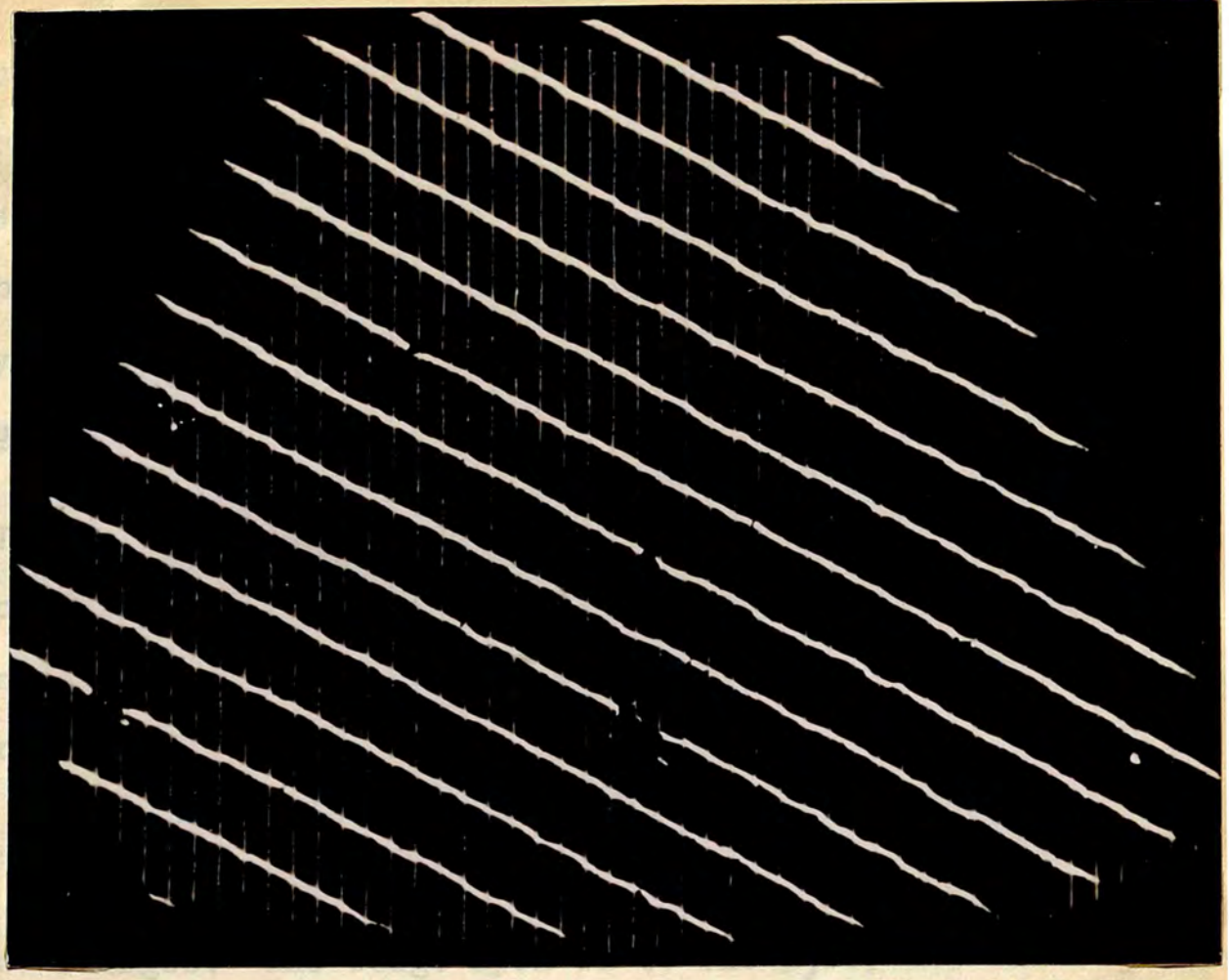

×75

Fig. (58 a)

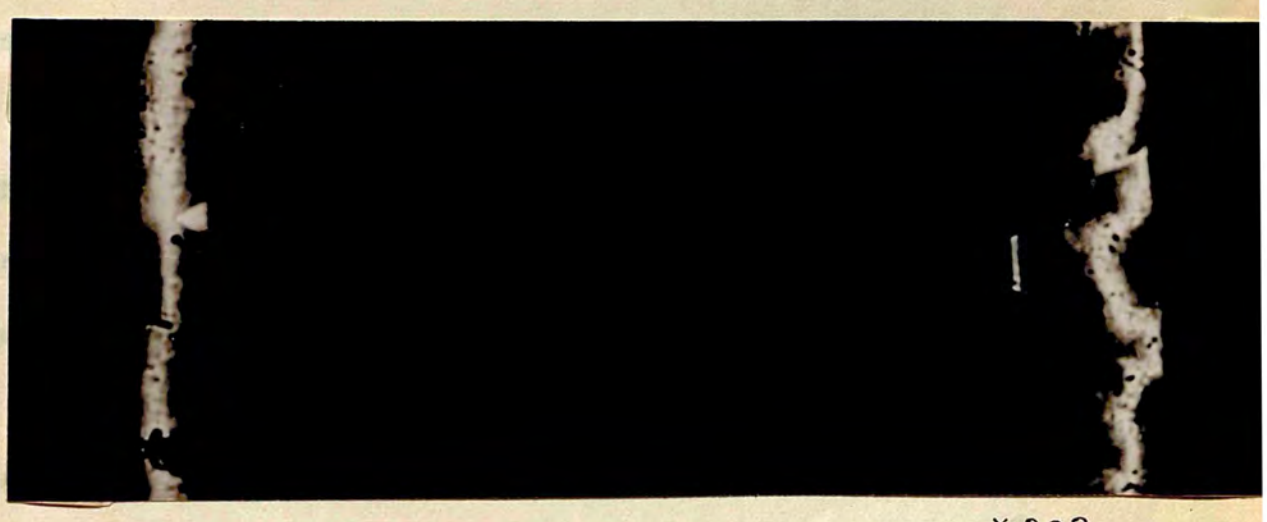

×208

Fig. (58 b)

trigons encountered in crystal (C) of this chapter are of a different class. They are nearly (invisible) trigons and the deepest trigons observed here-and not many are so - are comparable in depth with some of the shallowest trigons observed on crystal (B).

Fizeau Fringes.

To get an estimate of the ultimate depth of these trigons, and to prove that they are depressions, Fizeau fringes were obtained between a silvered crystal face, and an approximately silvered optical flat. Transmission technique was used. The wedge angle was adjusted until there were two fringes in the whole field of view. Fig (58b) is such an interferogram showing the two fringes. The wedge apex is to the right, and the triangle that separated from the fringes is the deepest in a large area of the surface. The dispersion that separates a certain triangle is critical. If it is increased, the triangle would be well separated but the fringe thickness would increase, which would affect the precision of measurement. If it is decreased the triangle will not separate. As the fringe width is $\lambda/100$ the separation of the trigon from the centre of gravity of the fringe is of that order. This triangle is about 50 A deep, all other trigons are shallower. They are depicted in the fringe as kinks towards the apex of the wedge. As the isolated trigon is in that direction, it is a depression and all the other trigons are depressions. But the fringes show also kinks towards

the wider gap of the wedge; only the kinks away from the wedge apex are less prominent than the kinks towards the wedge apex. If these other kinks are due to hillocks around the trigons the heights of these hillocks is as a rule less than the depth of the trigons'. The phase contrast picture shows that these hillocks do exist. In this case there would be no reference surface on the crystal to which heights or depths be referred, and the estimate of 50 A for the depth of the deepest triangle must be referred to a hypothetical mean surface. In other words its real depth below the true octahedron surface is decidedly less, and it is quite possible that its real depth, of which we have no means to tell, is about 2/3 or so the above estimate. For this reason, fringes of equal chromatic order were produced involving the use of a high dispersion spectrograph (Hilger E_1) the result of which appears in the following section.

Fringes of Equal Chromatic Order.

Fig (59a) and (59b) show fringes of equal chromatic order. In Fizeau fringes the third order yellow fringe and fourth order blue fringe nearly coincide. The linear area of this (double) fringe was projected parallel, in a vertical position, on to the slit of above mentioned spectrograph. Two fringes appeared in the spectrograph, yellow and blue. The yellow fringe is underneath the two yellow lines faintly seen above mark 20 in fig (59a). The blue fringe appears near the blue line which

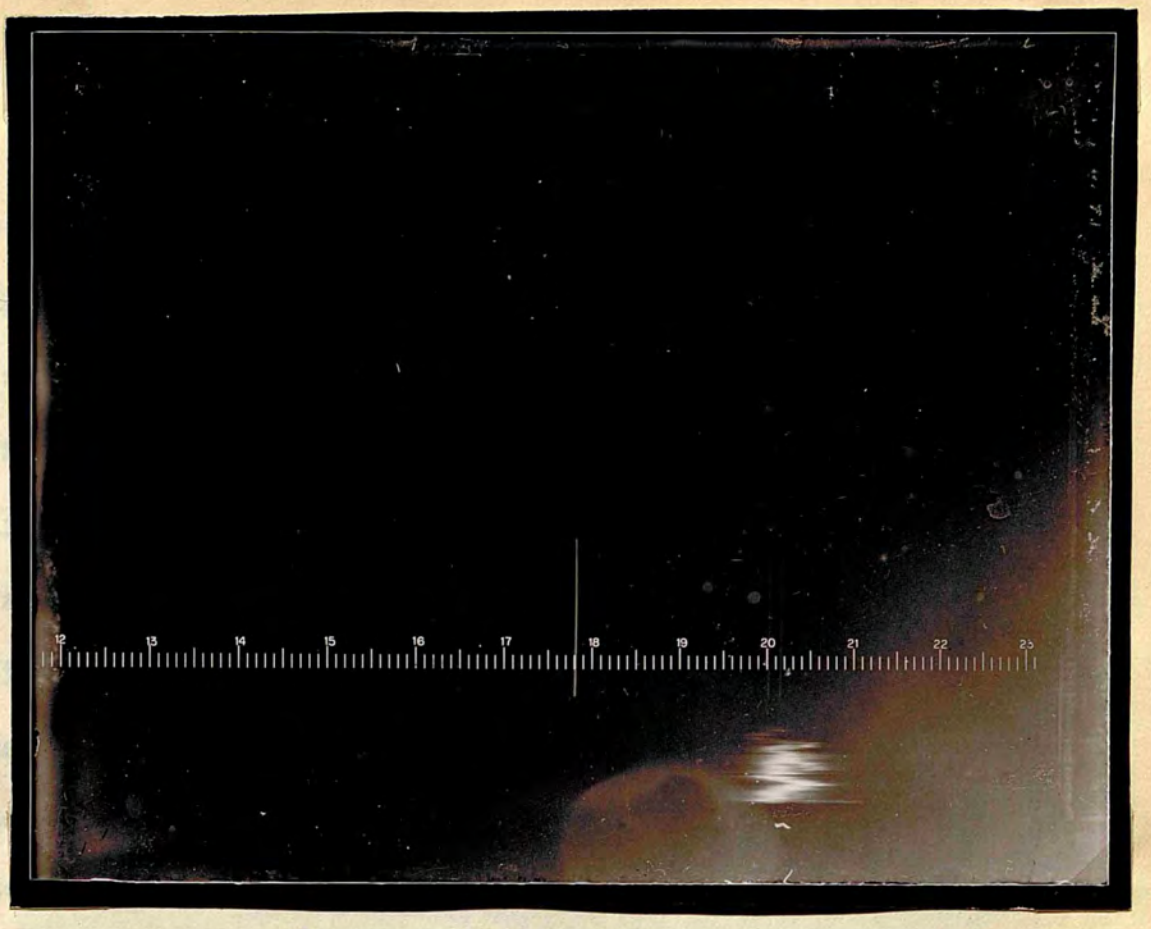

Fig. (59 a)

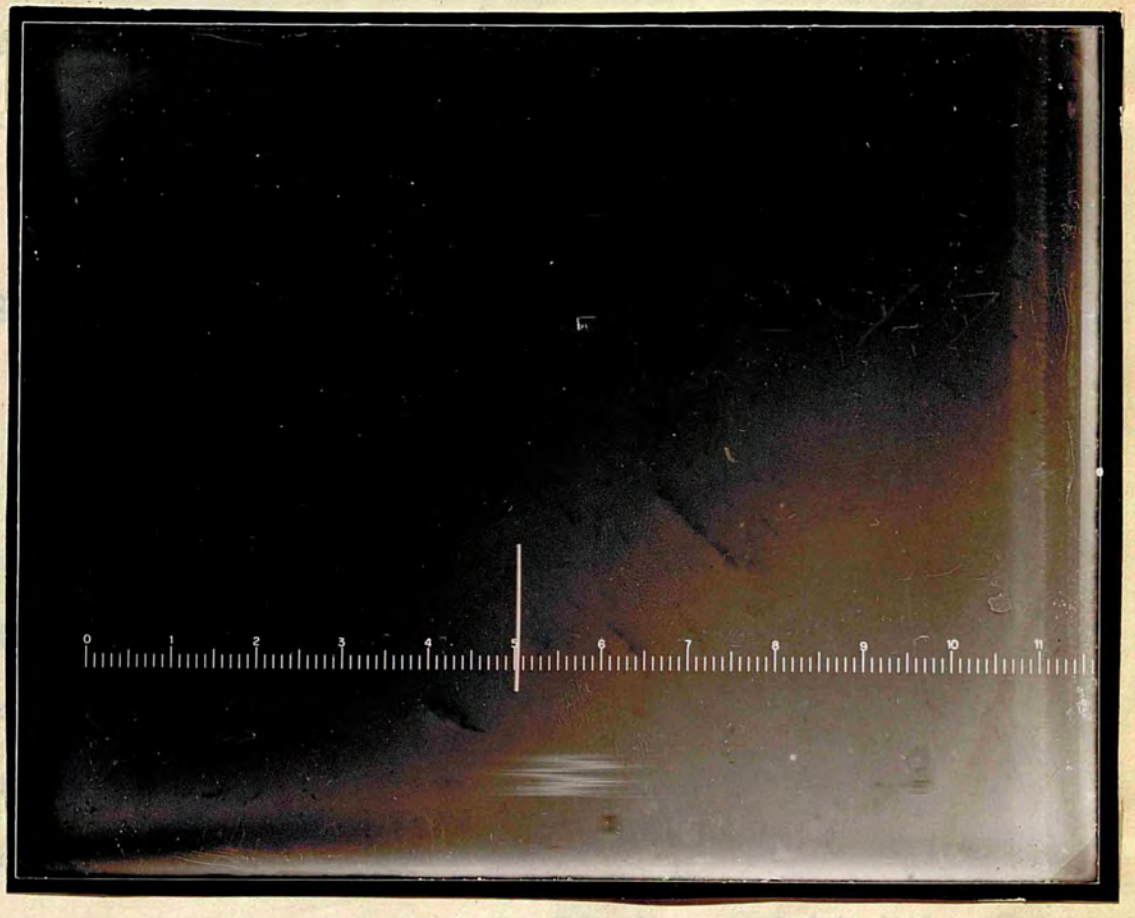

Fig. (59 b)

falls above mark 5 in fig (59b). It has been ascertained from f.e.c.o. measurement that the blue fringe is actually order number 4, while the yellow fringe is order number 3. The line appearing at 17.8 fig (59a) is the green mercury line, and it is seen that the kinks towards the red end of the spectrum are more prominent than those towards the blue. The first signify depressions, and the latter elevations; trigons and hills are in close proximity on account of the small magnification used. The kinks that represent depressions are of the same order as the separation of the mercury yellow doublet seen above i.e. 20 Å. As $2t = n\lambda \therefore 2\delta t = n\delta\lambda$. If we denote the depth of a trigon by δt, and since the order $n = 3$,

$$\therefore 2\delta t = 3 \times 20 \qquad \therefore \delta t = 30 \text{ Å}$$

The kinks due to the elevations are much less. This confirms the results reached from before. The streaks in the fringes are due to diffraction.

Phase contrast and High Dispersion.

It is clear from the above that the features are on the average in the range of 20 A deep or high, that is some ten atomic spacings , and therefore they are truly molecular in the sense that elementary layers are forming them. Phase contrast confirmed these expectations; they could only be seen and photographed under very critical illumination. Fig (60a) shows a phase contrast picture under magnification. All the inverted triangles are trigons and all the upright triangles

X330

Fig. (60 a)

are elevations i.e. hillocks. These appear with a slightly different shade and are incomplete through extension and sub-division. Every trigon is bounded by growth hillocks. This is the universal feature of diamond octahedral faces. The advantage of phase contrast over its competitor, high dispersion, is that phase contrast is more recordable photographically if the correct contrasty plate and developer are used. The high dispersion setting showed more trigons in the same area. These pass in the field of view with varying tints and beautiful shades of colour when the high dispersion is varying. Its drawback is that when these colour shades are transformed into intensity patterns no photographic plate can honestly record them. Fig (60b) is a high dispersion photograph of part of the other surface. Fig (60c) is a phase contrast micrograph of part of an extremely fine surface of crystal G. Crystal G is a type II octahedron with perfect morphology. This has been referred to in chapter 6, and is amongst the collection of Dr. Grenville Wells. Fig (60d) is also amongst the faint features studied by other workers. (8) These are extended features of the types encountered in (60a), and a further analysis of this most famous picture is necessary. It has given Tolansky and Wilcock a theory for the formation of the trigon, as due to growth and not to etch. It also illustrated the curvature of diamond surfaces as a piling of growth sheets. The picture is a combination of Fizeau (green and yellow fringes) and high dispersion and is an example of their crossed-fringe technique.

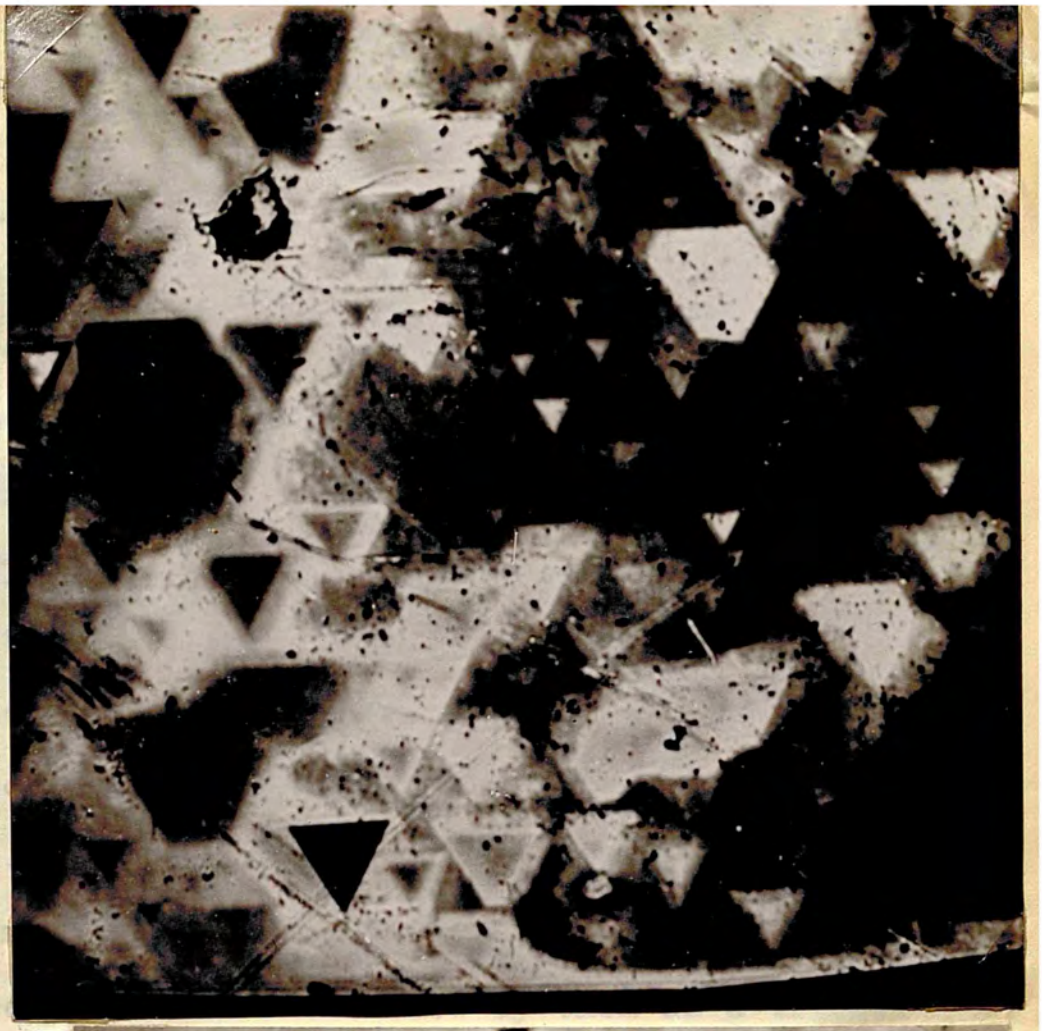

Fig. (60 b)

x 205

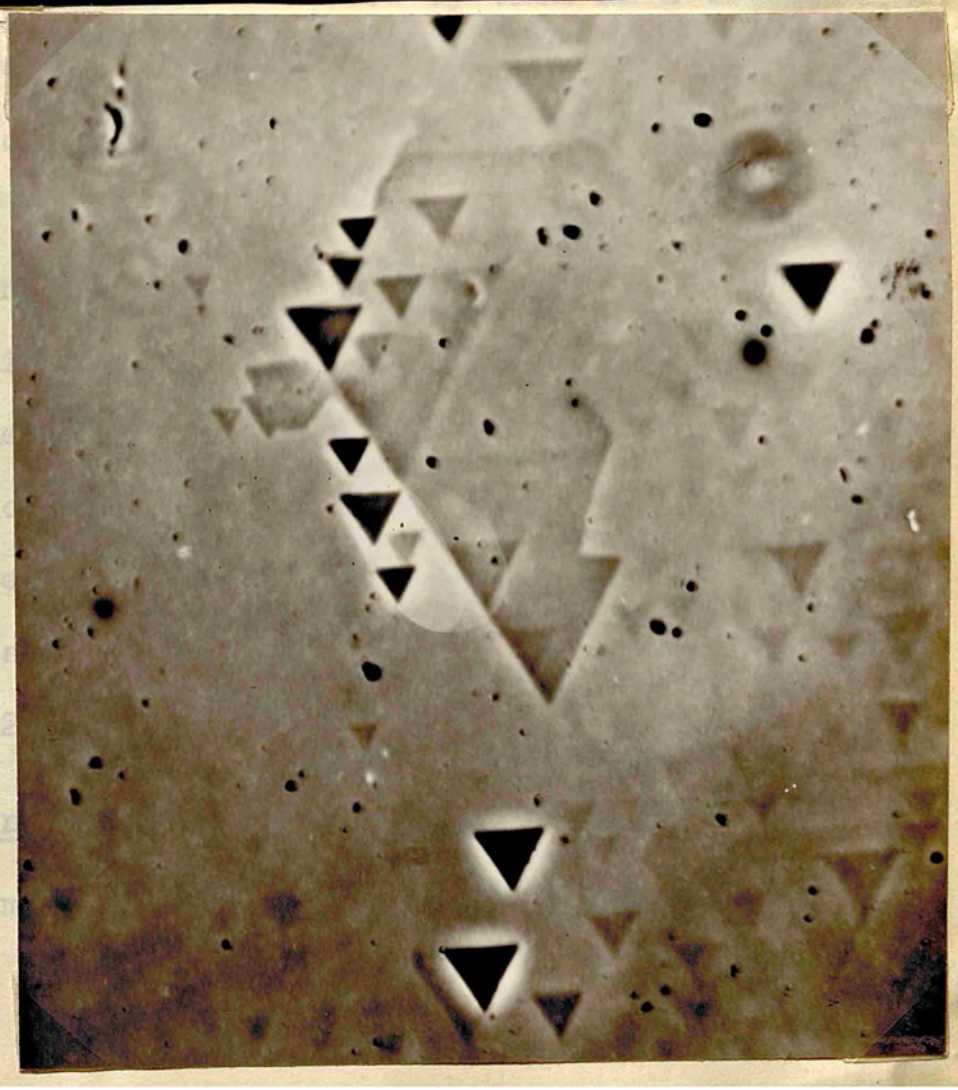

Fig. (60 c)

x 850

Only the gaps left by them will be filled.

Further Analysis of Tolansky and Wilcock's Picture.

(1) The picture contains two main centres of initiation. A and G are two growth hillocks based on these two centres.

(2) Primary growth layers from the above centres have met in stages with the formation of the descending steps E. These steps we identify as a major trigon formation. Such incomplete formations near the face edges are detected by the author in crystal E (chapter 6).

(3) The well known trigon of Tolansky and Wilcock is trigon H (c.f. chapter 6). As seen, the fringe crossing it, is a continuation of a fringe of the same order in the outer levelled area D. This area has been identified by them as a trigon. If disturbance is responsible for the formation of trigon H, such a disturbance can rarely be responsible for the major trigons D or E.

(4) F has been identified by them as an elevation with a curved surface. This fits in our model as a growth occurring at the corner of the main hillock A.

(5) From their exact and accurate description of the area surrouding H, one realizes that (H) is surrounded in the usual manner by hillocks and the question of its enclosure by three growth sheets (at 120°) cannot arise if the sheets are plane.

Conclusions reached in Part I of this Thesis.

(1) Effectively a multiple beam goniometer has been erected

Fig. (60 d_1) x 30

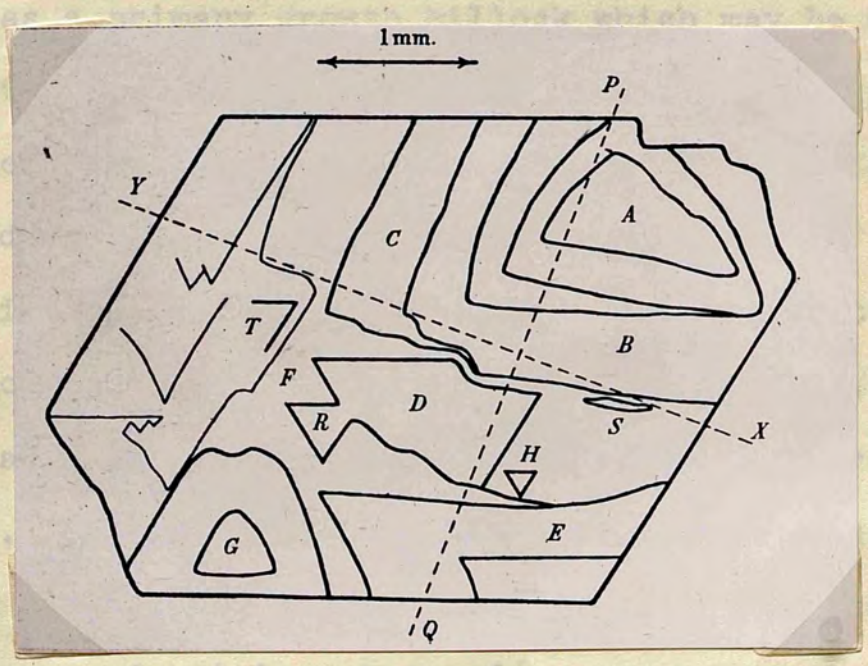

Fig. (60 d_2)

on the surface. The angles are 1° or 2° in the case of hillocks and trigons, but 1' or 2' in the case of vicinal surfaces of the whole crystal face.

(2) Cylindrical curvature of two types is the general quality of the surfaces of hillocks and partly trigons. The radius of curvature is of the order of 1 m.m. or less, but on the vicinal faces its order is a few metres up to a hundred metres.

(3) Vicinal faces are invariably lined with hillocks. The curvature of diamond surfaces is a combination of these two orders of curvature. The hillocks enclose trigons near the edges of the main growth sheets by a mechanism proposed. In this mechanism the trigon is a secondary effect and not a primary one.

(4) The mechanism accounts for the growth of vicinal faces from a primary source or several primary sources. Each main centre arises as a primary growth hillock which may be small. Further nucleation is provided at its corners. Time is an important element and all the hillocks build up in the form of a major pyramid which may occupy the whole face.

(5) The most important conclusion of the above is that no fresh nucleation is needed on the close-packed surface. Although dissected and angular, a wave front exists as issuing from the primary centre. The wave front has its own steps and directions of growth, and no dislocations are needed. The essential quality of the wave front is preserved.

(6) Although growth can be imagined to occur by wave fronts,

each part rises up vertically. If this is imitated in gross features may it not account for lineage connections and block structures?

(7) The curvature of growth hillocks which is a noticeable feature of diamond surfaces, is attributed to the curvature of the close-packed portions of the growth fronts responsible for these hillocks (also for the trigons). The order of curvature of these growth fronts is very small (of the order of 1 m.m. or less). Although extremely curved they arise from near nuclei, and $\frac{r}{\rho}$ is not unusual.

(8) The curvature is attributed to the high temperature at which the diamond formed. The binding energy in diamond is great. According to a known relation depending on concentration of kinks this should result in nearly straight edges, unless the temperature is high. Eventually the temperature at which certain diamonds were formed, has been calculated. In most cases the temperature is near the critical temperature of carbon, estimated by Crookes (110) as 5800° K. This is near to the temperature of the outer surface of the sun, so it is quite possible that the diamond crystallized when the earth was separated. Cooling of the outer crust would provide the necessary pressure.

PART II

Special New Techniques.

CHAPTER NINE

Micro-Flat Technique.

In the study of surface topography it has been adequately established (c.f. chapter 3) that the attainment of high precision depends not only on the use of the correct reflectivity, but also primarily on having a very small gap between the optical flat and the surface under consideration. Multiple beam interferometry gained ground partly by the proper choice of the samples examined. Proper choice of the material is very important in a growing science. That temporary phase is over, and its mission is now to deal with second quality surfaces. What is important in interferometry is proper approach of the flat to the surface in the area of the field of view. At a magnification of 45 the area seen is slightly over 2 m.m. in extension, and it seems a waste of good optical flat if its area is unduly extended. It is these extended areas that are likely to meet slight proturbances and small surface irregularities in the parts of the crystal not directly observed. The chances of their doing so depend upon the quality of the surface as well upon the extension of the optical flat. If the optical flat is made fairly small in extension (e.g. 1 m.m.), the chances that surface irregularities around the studied area, affecting the separation of the flat, are very much decreased as to be considered nearly non-existent. A colleague of mine, Mr. Pandya of this laboratory, and another colleague, Mr. Williams in Birmingham, found respectively that the study of

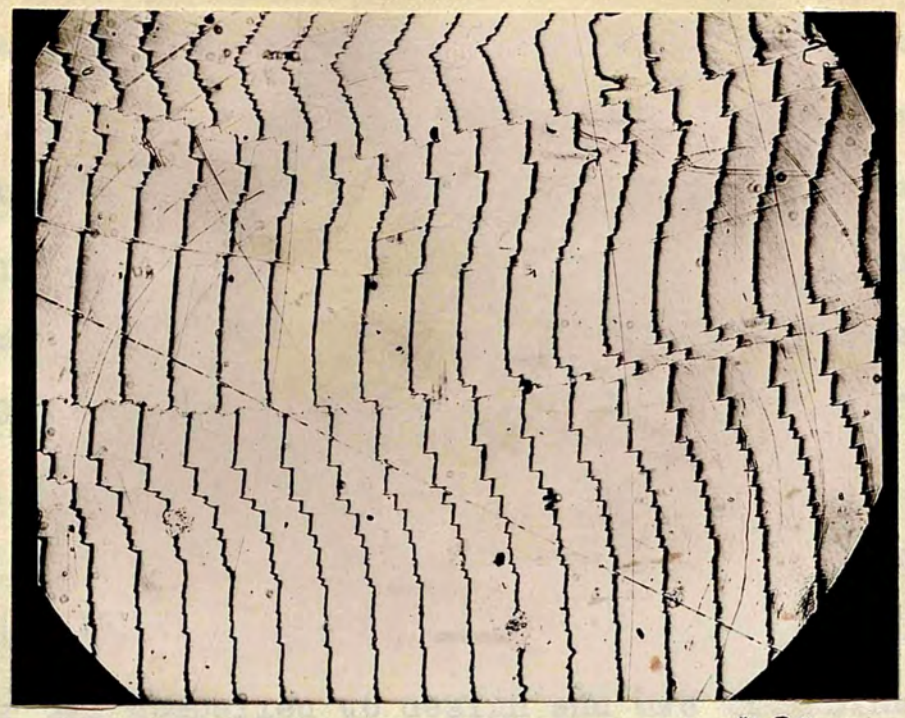

X 30

Fig. (61)

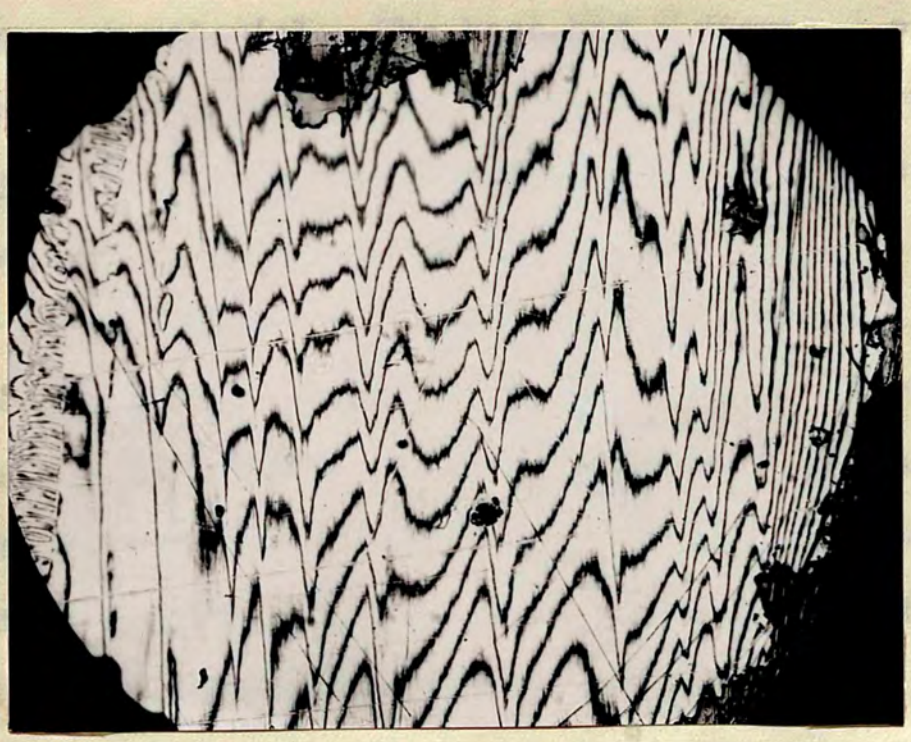

X 104

Fig. (62)

cleavage surfaces and some metal crystals, using the ordinary flat of multiple beam interferometry, a trying operation. Not only were the fringes diffuse and lacking in contrast which is a deterrent to any proper study, but in some cases no fringes could be produced at all. Fig (61) on a cleavage surface of Topaz, and fig (62) on a titanium crystal, show that exceedingly good results can be obtained by the proper choice of flat. The flat used in their study is the micro-flat which is the subject matter of this chapter. As has been mentioned before the micro-flat has been evolved during work carried out in this thesis. The writer was compelled to design and use it. Since then, it has become an indispensable instrument.

Description of the Micro-Flat.

The micro-flat is a cone of glass but it can be made of any transparent material. The base has a diameter of a few millimeters and a height of the same order but is truncated at its top by a plane parallel to the base. The truncated end may have an area of one millimeter diameter or less. It is this area which is used as an optical flat, and it is clear that it can be located sufficiently closely to the required region. A typical cone used in the present work has a base of 5 m.m. diameter polished to the normal state of plate glass. Its height is about 5 m.m. but can be made less, and the upper truncated tip surface is a disk 1 m.m. in diameter, but a smaller tip can be used. As the cone is cut from a good optical flat, its tip end needs no further polishing. The small tip-

disk is silvered and the cone is mounted in a simple manner on a brass ring which sits on a jig mounted on the inverted microscope.

The Mechanical Stage.

Owing to the small size of the reference surface of the cone, a limited area of the surface under consideration is explored at any time, and further areas may be studied by a body shift of the specimen. It is clear that the cone has to be fixed relative to the microscope objective. It was therefore necessary to construct a mechanical stage fig (63) that can rest on the stage of the projection microscope, and at the same time enable the specimen to be moved relative to the reference cone.

The cone was located by a small recess at the centre of a brass base block, A, which fitted on the microscope stage, and by adjusting the latter, the cone could be accurately centred relative to the microscope objective. A brass disc B moved on the base plate by means of a horizontal traverse C and carried a second traverse D perpendicular to the first which moved the specimen stage E. The discs and the base block had axial holes to clear the cone and the specimen was cemented to a brass disc F which could be tilted or moved vertically relative to the specimen stage by the three spring loaded nuts H. The specimen plate was also drilled axially to permit the passage of the light beam when making observations in transmission. The brass disc G, attached to the base block, served to hold the discs

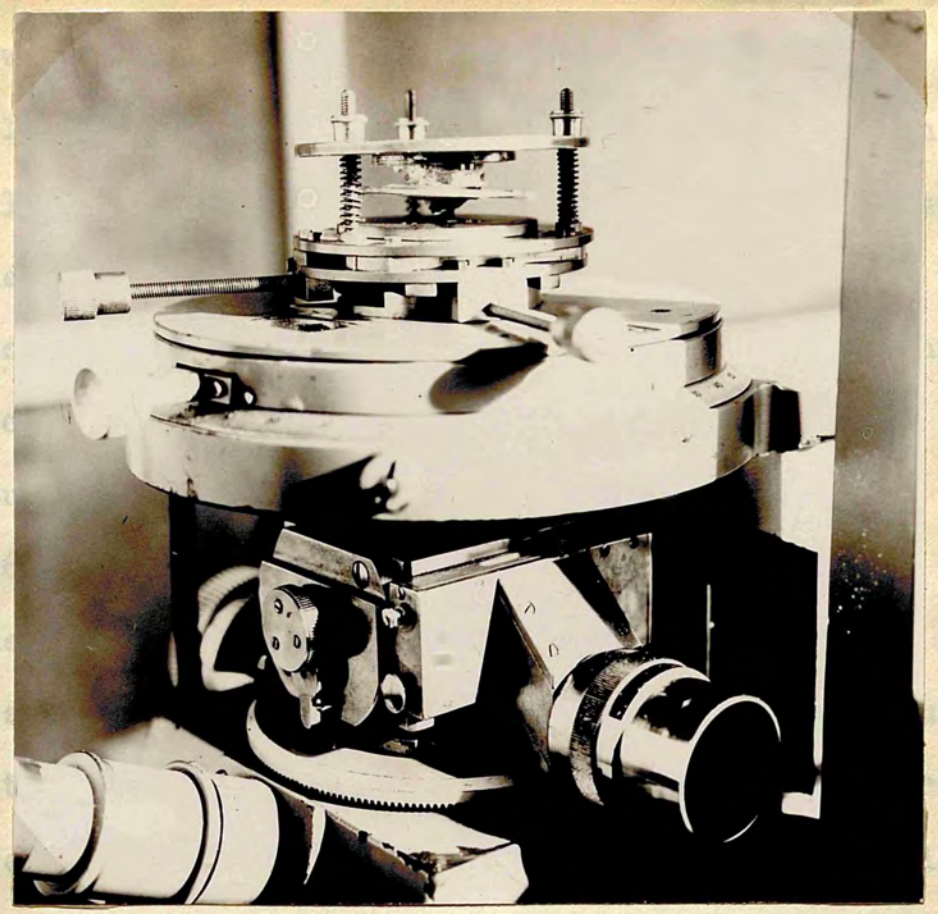

Fig: (64)

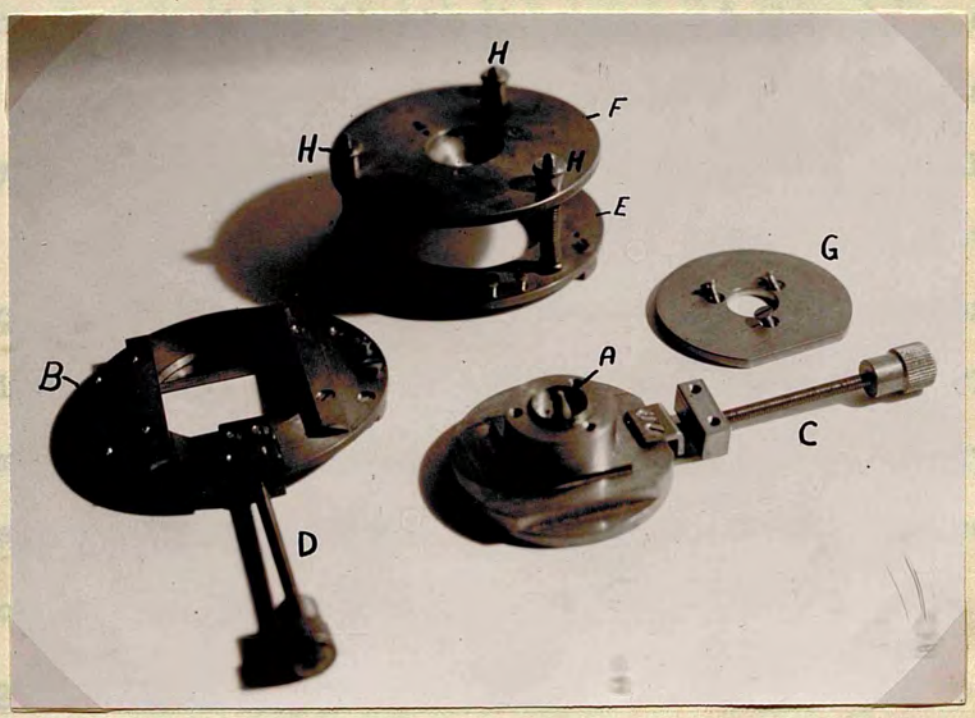

Fig. (63)

B and E down to their respective slides.

It will be seen that the specimen can be moved in two perpendicular directions on the stage, and can be brought as near to the cone tip as is desired and can further be tilted relative to the plane of the tip in order to secure any required interference fringe direction or dispersion. Fig (64) shows the jig mounted on the microscope prior to its use.

Fig (65) shows in a schematic way the advantages of the system, wherein the cone is shown closely approaching a selected region of a complex surface of a crystal. A cone is used because of its stability and ease in mounting and silvering, and as the base is wider than the tip there are no optical aperture difficulties associated either with transmission or reflection, as shown by the two sets of arrows. As one views the specimen through the cone from its base side, the optical height of the cone is the factor which limits the power of the microscope objective that can be used. With a 5 m.m. cone there is no difficulty in using a 25 m.m. objective as the optical height of 5 m.m. glass thickness is $\frac{5}{1.5} = 3\frac{1}{3}$ m.m. i.e. within the working distance of that objective. A slightly shorter cone permits the use of the 16 m.m. lens, and a glass flat cone has been made, out of a photographic glass plate, to give it the necessary thickness to be incorporated within the working distance of an 8 m.m. objective.

Interferograms Obtained by the Use of the Cone.

The cone has been found to be an indispensable instrument

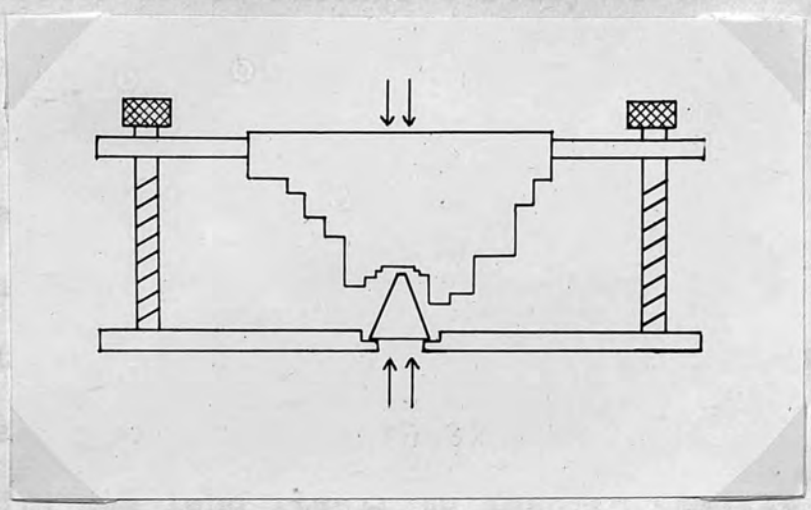

Fig. (65)

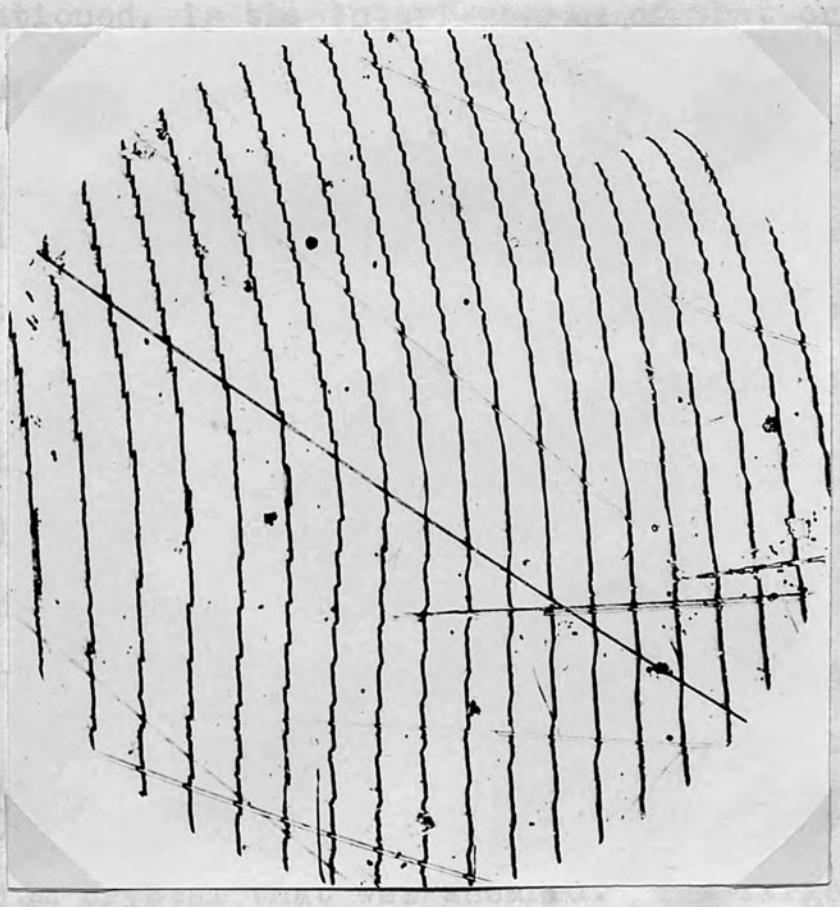

Fig. (66) x90

in the study of cleavaged surfaces, and is used now as the sole interferometer in an extensive study of cleavage by Mr. Pandya of this laboratory. By the use of the cone the author has discovered slip on diamond (chapter 13). Fig (66) shows an interfergram of spiral steps on a Si C crystal. The specimen was amongst the crystals studied by Dr. Verma in an admirable study of growth features.(111) Through these studies the dislocation theory of crystal growth received a great support. But one of the crystals did not lend itself to interferometric study. By the side of the spiral there was a bulging part that prevented the approach of the ordinary flat. As spirals are valuable the crystal could not be risked in cutting. Fig (66) , as we have just mentioned, is the interferogram of that crystal through the use of the microflat. The step height is constant and is 195 ± 10 Å. Fig (67) is another interfergram of the crystal at high dispersion, in which the spiral steps are seen by means of the scattered or diffracted light at the edges. This shows that the micro-flat can be brought into close proximity with the surface.

Fig (68) shows an interferogram of a trigon found on a diamond octahedron face. The curved fringes show a growth at the corner in an effort, perhaps, to fill the trigon. These trigons as a rule are not filled up by further growth.

Fig (69) is another of Mr. Williams' interferograms on an iodide titanium crystal that was sheared. The large and small irregularities in the fringes are supposed to show coarse and

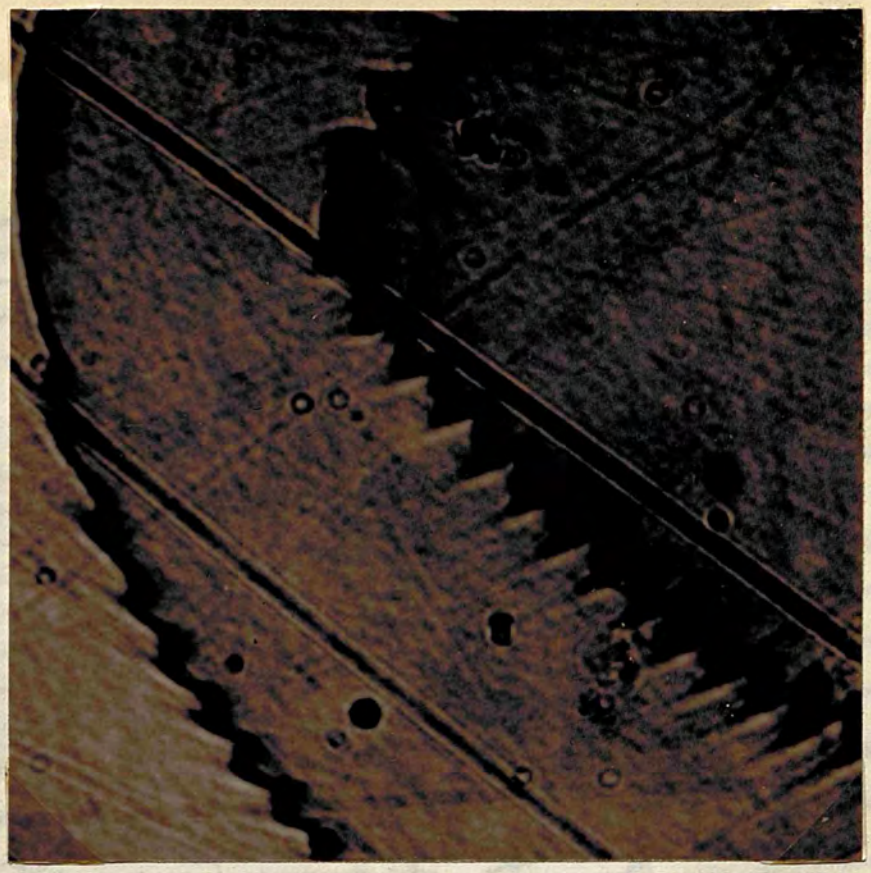

Fig. (67) ×90

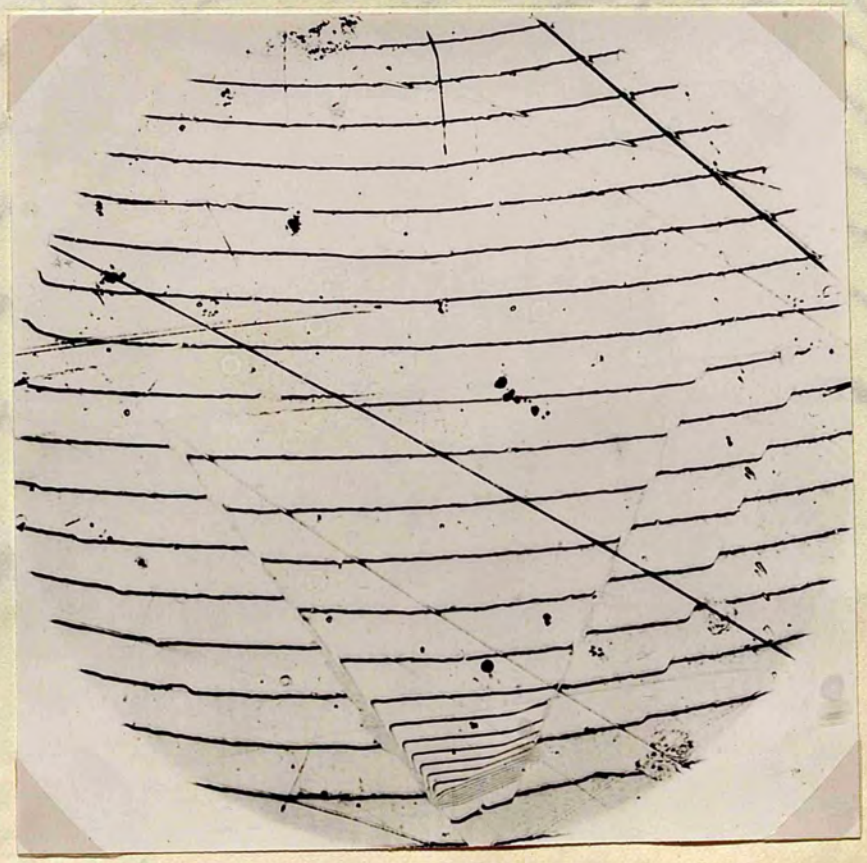

Fig. (68) ×90

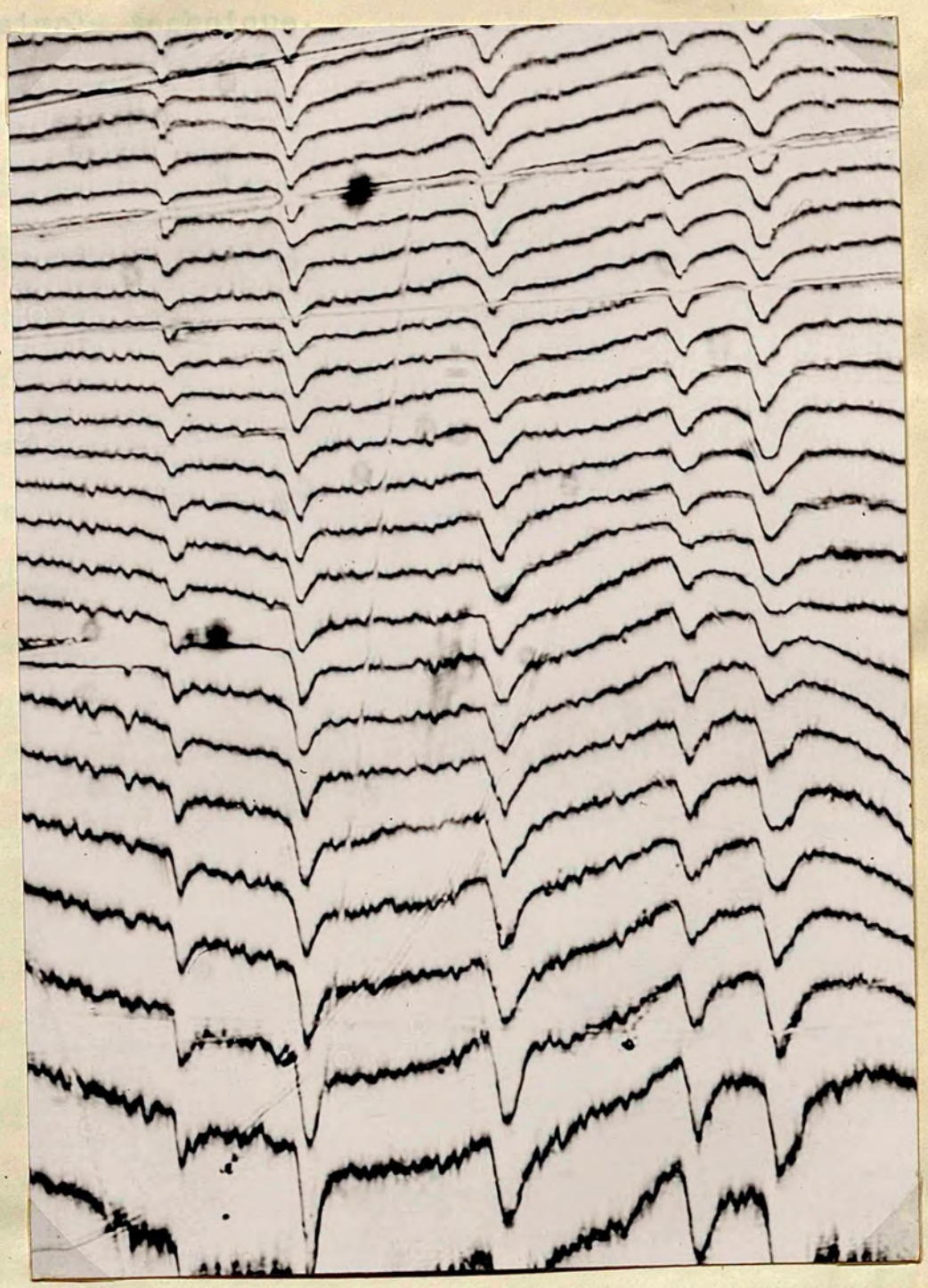

X 312

Fig. (69)

fine slip accomodation between the sheared plates (the interpretation is Mr. Williams'). Figs (61), (62) and (69) are sufficient evidence to show that a whole study can depend on such a simple technique.

CHAPTER TEN

Thin Film Technique.

Fizeau fringes are no more or less than the colours exhibited by thin transparent films, and it is no secret that multiple beam interferometry derived its first impetus from previous studies on silvered air films (e.g. the Airy summation)[59]. During work carried out in this thesis, it has been realised that diamond surfaces have a harming effect on optical glass flats in the very small gap of low order multiple beams. Liquid surfaces were tried instead of glass surfaces, and chapter 11 describes an approach using mercury surfaces as a reference flat. In the present chapter description and results of a transparent film technique are outlined. The method turned out to be of immense value in high magnification topographical studies. Since it is a new thing in interferometry that thin films as such are used, it is necessary to point out their advantages, a nd to discuss their possibilities, but first and above all, to establish the thin film technique as a method in revealing surface topography.

Description of the Method.

The method consists in covering the crystal surface by a thin transparent film, no external flat being used. Interference fringes are directly seen, in reflection, in the film, following lines of equal thickness between the crystal features and the external surface of the film, which need not be extremely flat. The success of the method depends upon depositing the film in

the appropriate thickness of the interferometric gap for two beam fringes (i.e. of the order of a few microns, not exceeding an upper limit of 10 μ). The film can be of a variety of materials, the essential qualities being transparency and stability. Stability includes non-volatibility at ordinary temperatures and pressures. Small changes in temperature as affecting the refractive index of the material of the film are generally neglected. The substance chosen was "canada balsam". This was dissolved in a volatile solvent e.g. pure xylene or benzene. A drop of the solution is placed on the crystal surface. This spreads and dries up covering the crystal with a transparent film of canada balsam. Interference takes place between the upper and lower surfaces of this film, and when mono-chromatic light is used Fizeau fringes are observed.

Interferometric Justification.

The film must be of such a thickness (depending on concentration) to fill all the cavities in the crystal surface. Since it was originally in solution it is in its capacity to do so. When it dries up its outer surface is not generally plane, and a decided convexity is sometimes experienced. The convexity of its surface is not a drawback to its use, but is one of its advantages. Under high magnification a small part of the surface is observed, and since the fringes are localised a small part of the film is used. This part will necessarily be reasonably flat and creates a wedge angle in which interference takes place. Since a residual curvature sometimes exists, the method is restricted to discontinuities, in which case any spurious topography of the upper surface of the film does not invalidate

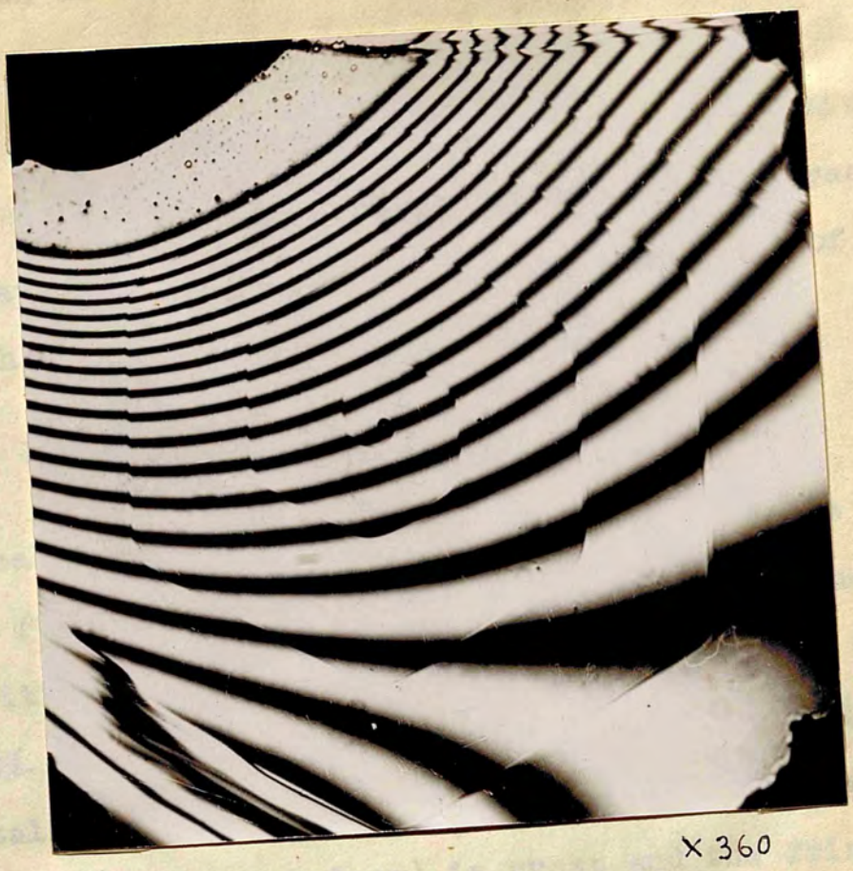

X 360

Fig. (70)

X 300

Fig. (71)

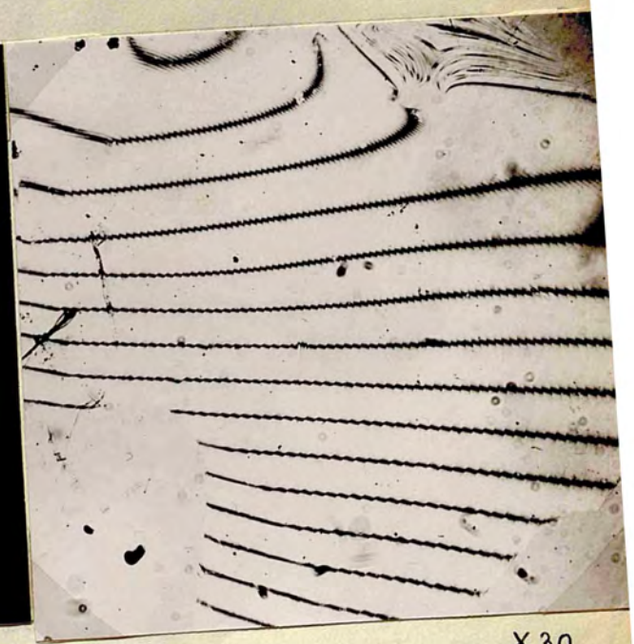

X 30

Fig. (72)

conclusions drawn as to the heights of discontinuous steps.

Success of the Un-silvered Film.

According to the electromagnetic theory the reflectivity R of a surface bounding a dielectric depends on the refractive index of its material n_2 and the refractive index n_1 of the medium in which it is embedded by the relation:

$$R = \left[\frac{n_2 - n_1}{n_2 + n_1}\right]^2$$

Theoretically the reflectivity of the outer surface of the canada balsam film ($n_2 = 1.5$ and $n_1 = 1$) would be 4%, whereas the reflectivities of several crystal faces studied are in the range 10 - 20%. The disparity in reflectivities between crystal faces and glass flats (which have the same refractive index as canada balsam) is great and the fringes obtained lack contrast. In the present case the surfaces are embedded in canada balsam ($n_1 > 1$) and therefore their reflectivities are very much decreased. As an example Si C which has a refractive index of $n_2 = 2.675$ has a theoretical reflectivity of 21% in air, but only 8% in canada balsam. The contrast is good because there is practically no absorption.

Thin Film Interferograms.

Fig (70) is an interferogram of a spiral on Si-C. It is seen how the fringes kink one way as they ascend the arms of the spiral and kink the other way as they descend. The step height is constant and is 2 10 ± 10 Å. Fig (71) is another interferogram over part of the steps of another spiral, and fig

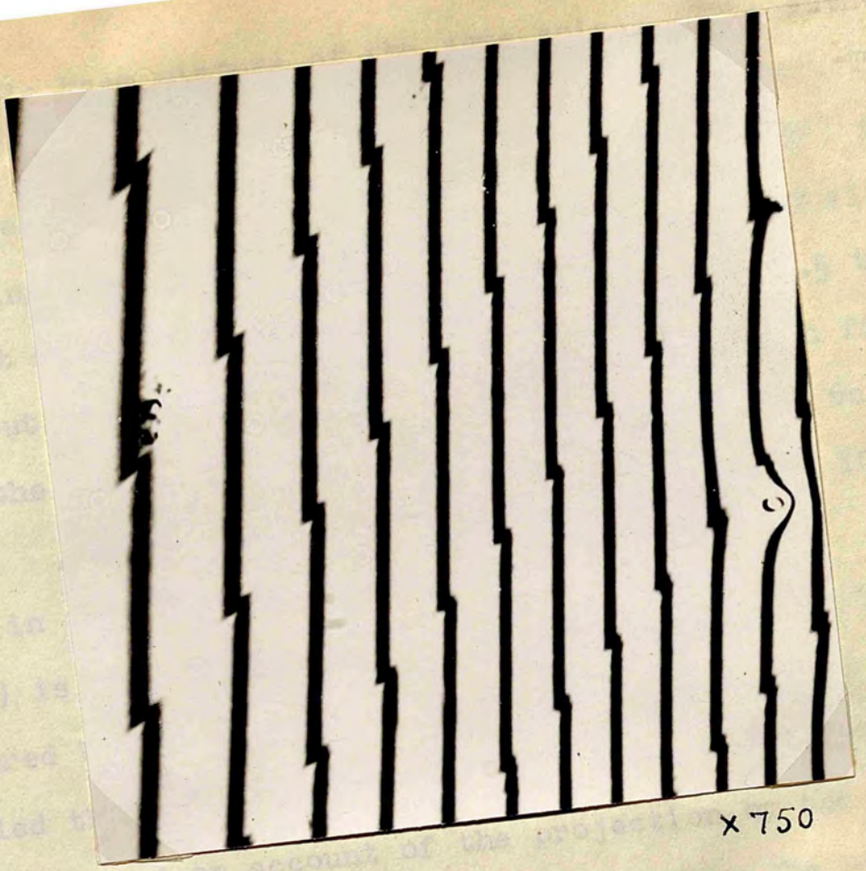

x 750

Fig. (73)

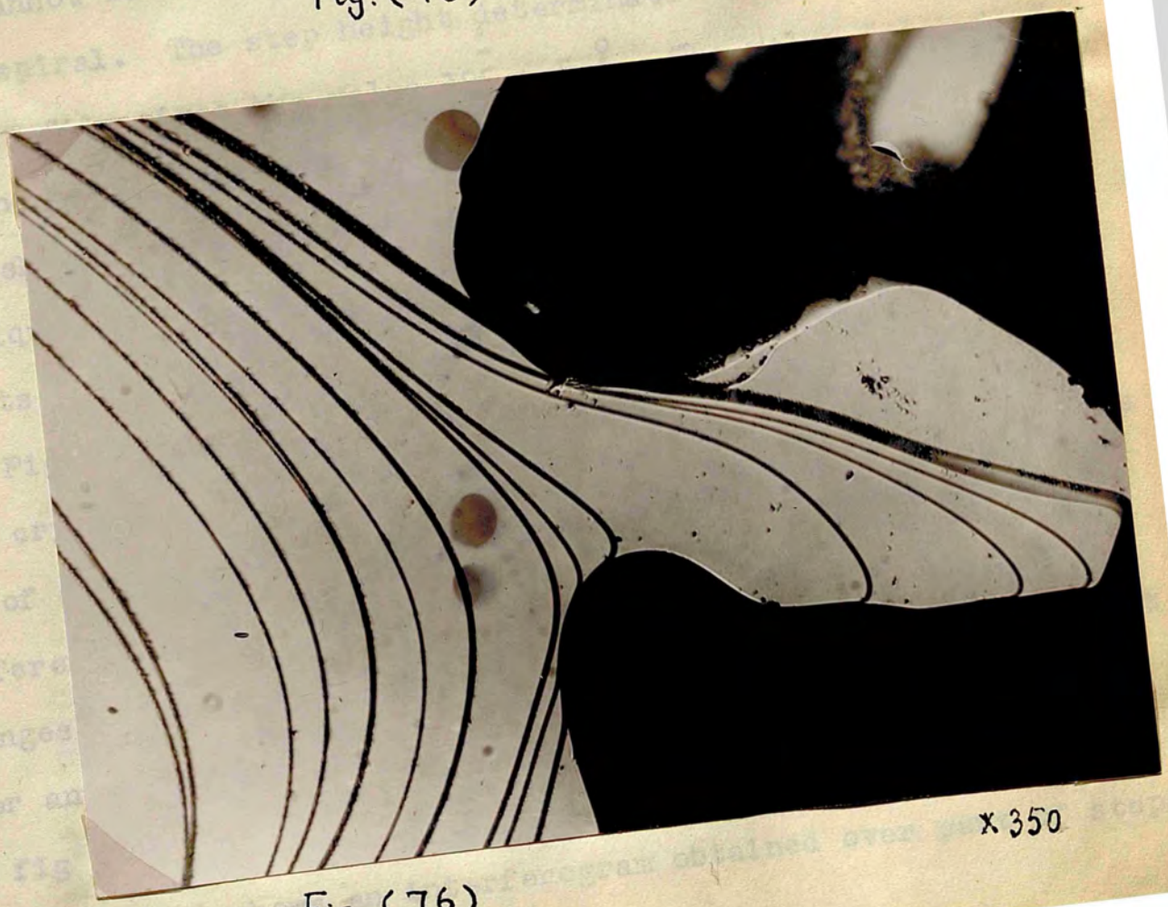

x 350

Fig. (76)

(72) is a multiple beam picture of the same spiral, (the author wishes to thank Dr. Turnbull to whom the negative belongs). The difference between the two pictures is noticeable. Fig (72) is taken by covering the crystal with multilayers instead of silver. The step height as a fraction of an order is magnified 1.5 times in fig (71), but the actual step height deduced from both figures (71 & 72) is the same. The thin film techniquegives the value 164 ± 5 Å , and multiple beam interferometry 165 ± 10 Å. The accuracy in the first method is greater.

Fig (73) is an interferogram of another spiral. It is the spiral measured by the micro-flat in chapter 8. The same reason that compelled the use of the micro-flat, exists here. Ordinary means cannot be used on account of the projection by the side of the spiral. The step height determination from the use of the thin film gives the value 195 ± 5 Å . The value determined from the micro-flat tchnique is 195 ± 10 Å. The coincidence is astonishing. Si C has been used in establishing the film technique because of its extended plateaux and constant step heights.

Figs (74) and (75), represent one and the same area in a Si C crystal (not a spiral this time). They are obtained by the use of different settings of the film. The interferograms are different, as can be judged from counting the number of the fringes over a given part. Still they give the same step height over any discontinuity. A photomicrograph of the same area is in fig (76).

Fig (77) shows an interferogram obtained over part of steps

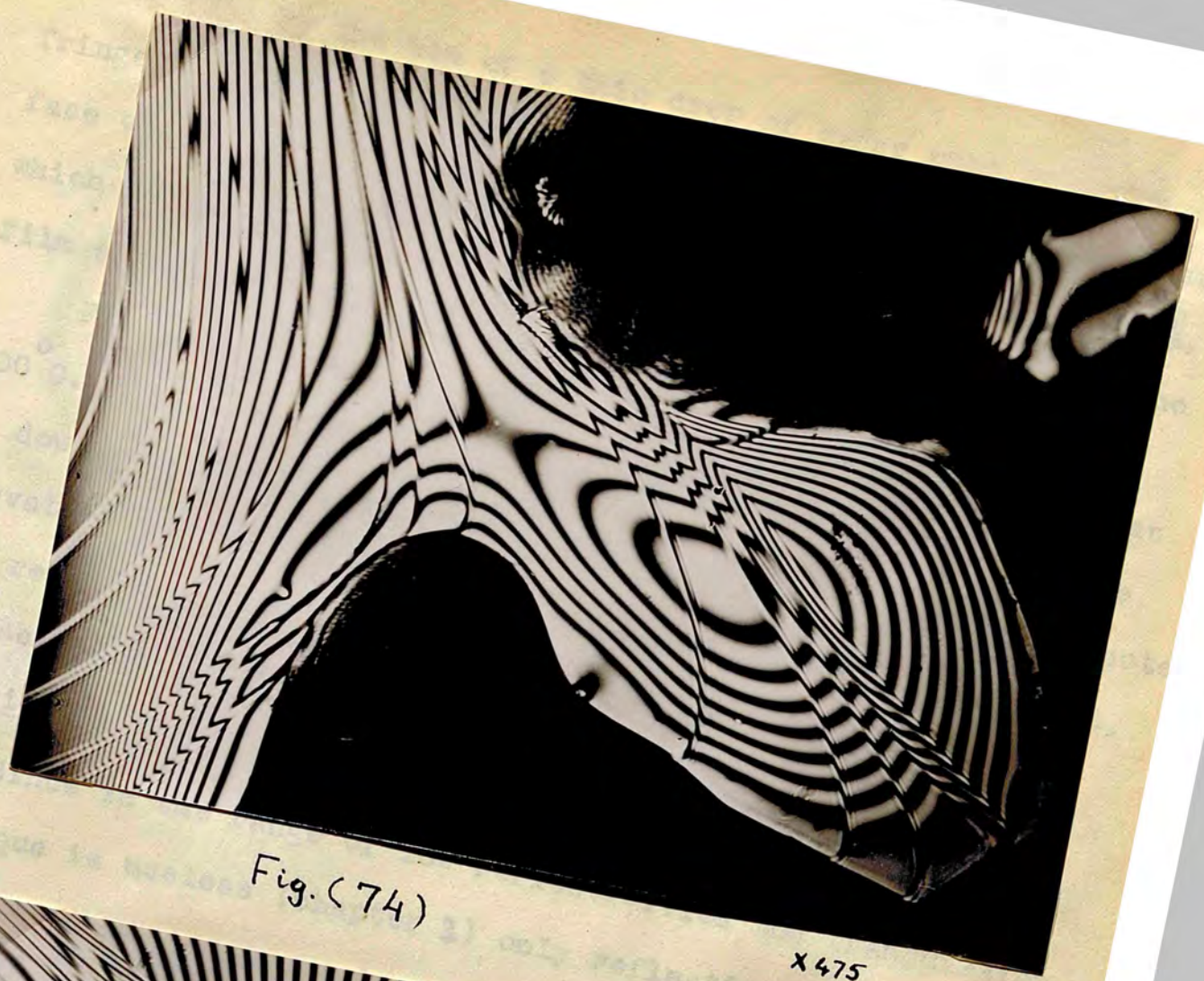

Fig. (74)

X 475

Fig. (75)

X 350

of fig (73) by the use of a thin drop of cedar wood oil. The fringes are curved on account of the topography of the outer surface of the oil. The step height determination is 200 ± 10 Å, which fits with previous results. This shows that although the film surface is not plane the results are not affected.

Fig (78) shows a part of diamond octahedral face etched at 600°C. The etch pits are rounded and pointing with their noze (P) downwards. The curvature in the fringes is genuine and denotes curvature in the pits (c.f. chapter 14). (H) is a raised area, and represents an etch-hillock. The depth of the pits varies between $\frac{1}{6}\ \mu$ and $\frac{1}{3}\ \mu$.

The Silvered Film.

Since in the range of low reflectivities the transmission technique is useless (chapter 3) only reflection fringes are obtained and the contrast is good, The method has still the further advantage that it can use multiple beams when the transmission as well as reflection techniques may be applied. For this purpose the film is deposited on the silvered surface and then silvered. As an example of the extremely thin fringes obtained under high magnification (necessary for good resolution) fig 79 shows the interferogram of a cleaved face of a diamond by applying the above method in reflection. The photograph is one of Mr. Pandya's of this laboratory and illustrates the step heights in the secondary cleavage directions. The whole photograph is comprised between two main cleavage directions. When the film is silvered it becomes subject to the multiple beam restrictions, and the equivalence of a small gap becomes here the

Fig. (77)

×300

Fig. (78)

×1000

use of a thinner film. Thinner films are best obtained by soaking a clean piece of cotton in the canada balsam solution (reasonably concentrated) and running it as quickly as possible over the surface features.

Advantages of the Thin Film Technique.

Since the method does not necessitate the use of an external flat, no space need be left between the interferometer and the objective, and high power objectives (up to 3 m.m.) may be used. The advantage is high resolution in extension. The method has the further advantage that it can be used in inaccessible parts of the crystal surface. It often happens that a bulging part of the crystal prevents the approach of an external flat to the regions of interest inside. (82) For this purpose replica techniques were invented. But replica techniques suffer from a real disadvantage: infidelity in depth. (71) If uncertainties in depth exist, the interferometric method looses its only merit. The drawback of the replica technique is that the film must be stripped from the surface. It is true that care is taken in securing an outer levelled surface, but in the act of stripping it is the copy surface that is deformed. The thin film technique is in a sense a replica technique in situ. Its power lies in the fact that if there are uncertainties about one side of the film, these uncertainties belong to the side of the film furthest from the surface features. The thin film in the thin film technique differs from the replica film in one minor respect. Its thickness cannot be any thickness, but must be of the same order as the interferometric gap.

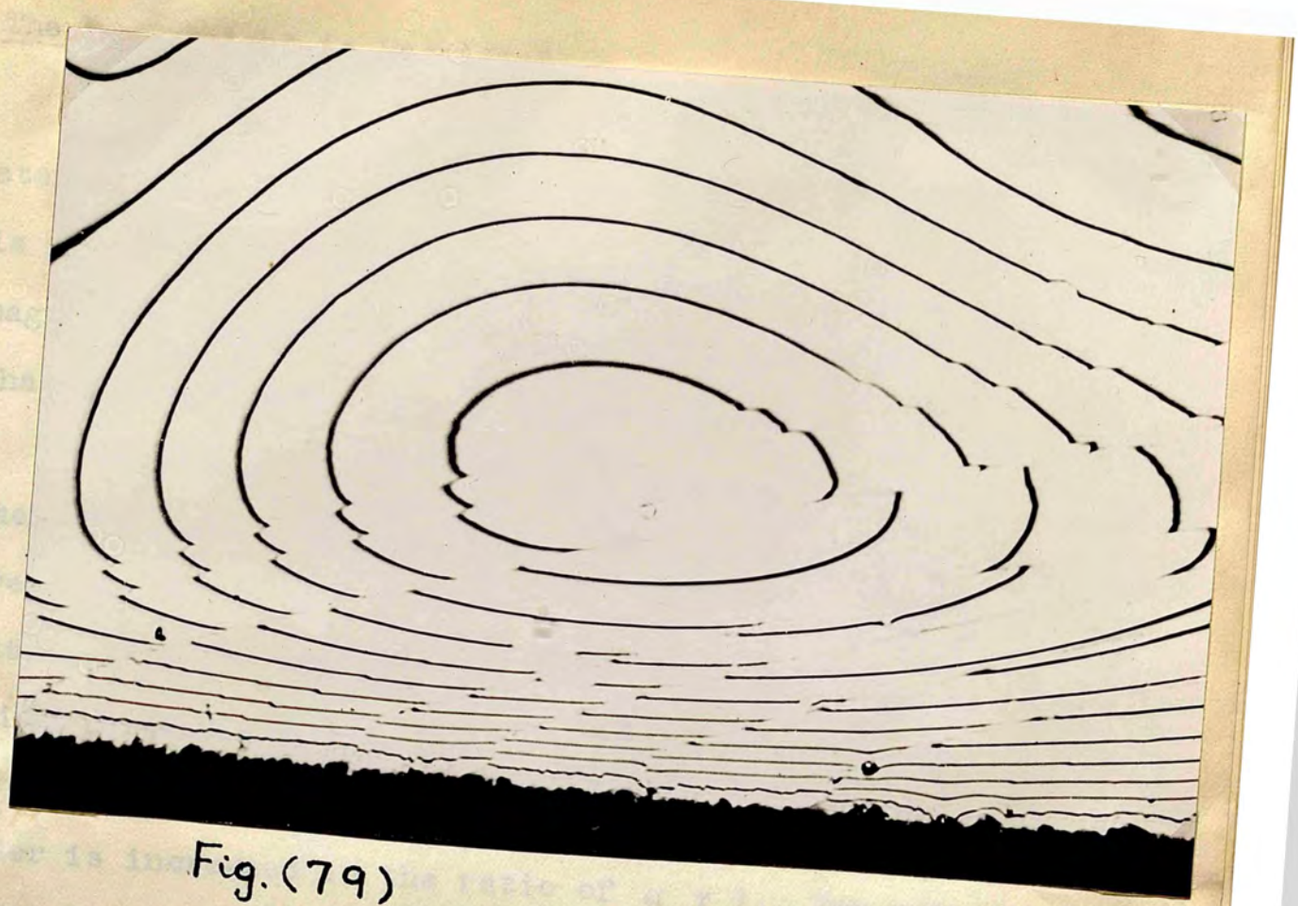

Fig. (79) X 450

Fig. (81) X 120

Fig. (80) X 190

The Step Height is Magnified.

Since the film technique is used exclusively in estimating step heights, it has the further advantage that the step height is magnified. The step height as a fraction of an order is magnified in the ratio of the refractive index of the film to that of air. This will be clear from the following analysis:

From the relation $n\lambda = \lambda\mu t$ applicable for normal incidence, the contour lines are lines of equal $\frac{\lambda}{\mu}$ i.e. they are lines of equal λ', where λ' is the wavelength in the material of the film. Since the step height is a constant thing and since the wavelength used in revealing it is reduced in the ratio $1 : \mu$, the step height as a fraction of an order is increased in the ratio of $\mu : 1$. For canada balsam films the increase is 50%. For a film of refractive index 2.5 the increase is 150%, but such films are mostly highly absorbent and moreover decrease the reflectivities of such crystals as diamond and Si C to such an extent that were the films highly transparent they would be of no use if unsilvered.

High Dispersion Thin Films.

In a second method of using the thin film technique, the canada balsam is pulled by an oil drop at the edge of the specimen before setting, under which conditions, a thin film of almost uniform thickness can be obtained on a reasonably flat surface. On illumination with an unfiltered mercury arc or white light, high interferometric contrasts appear and a wealth of detail is revealed, the system operating not as a topographical

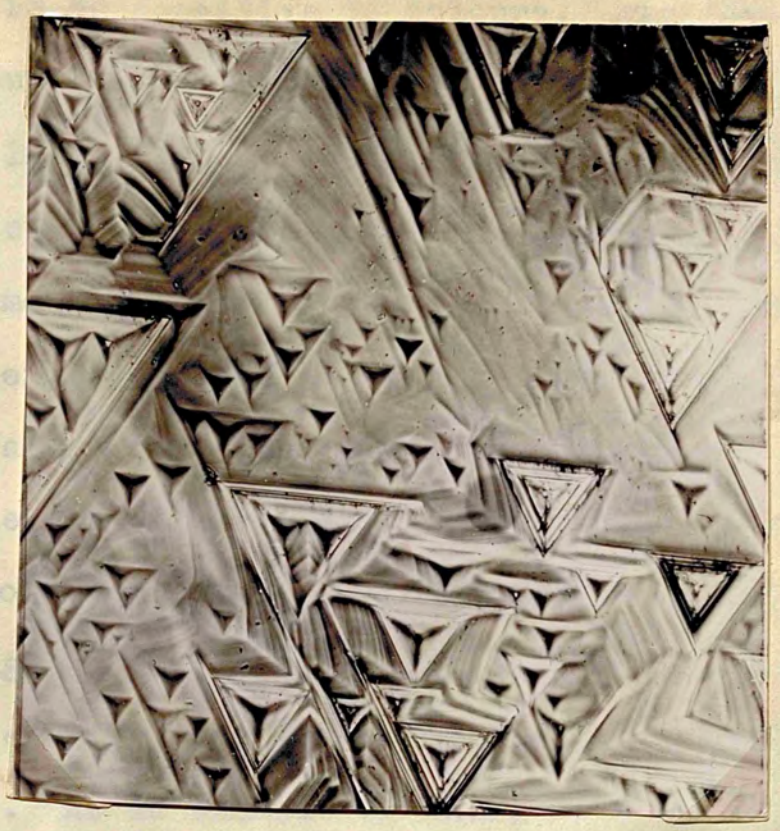

Fig. (82) ×100

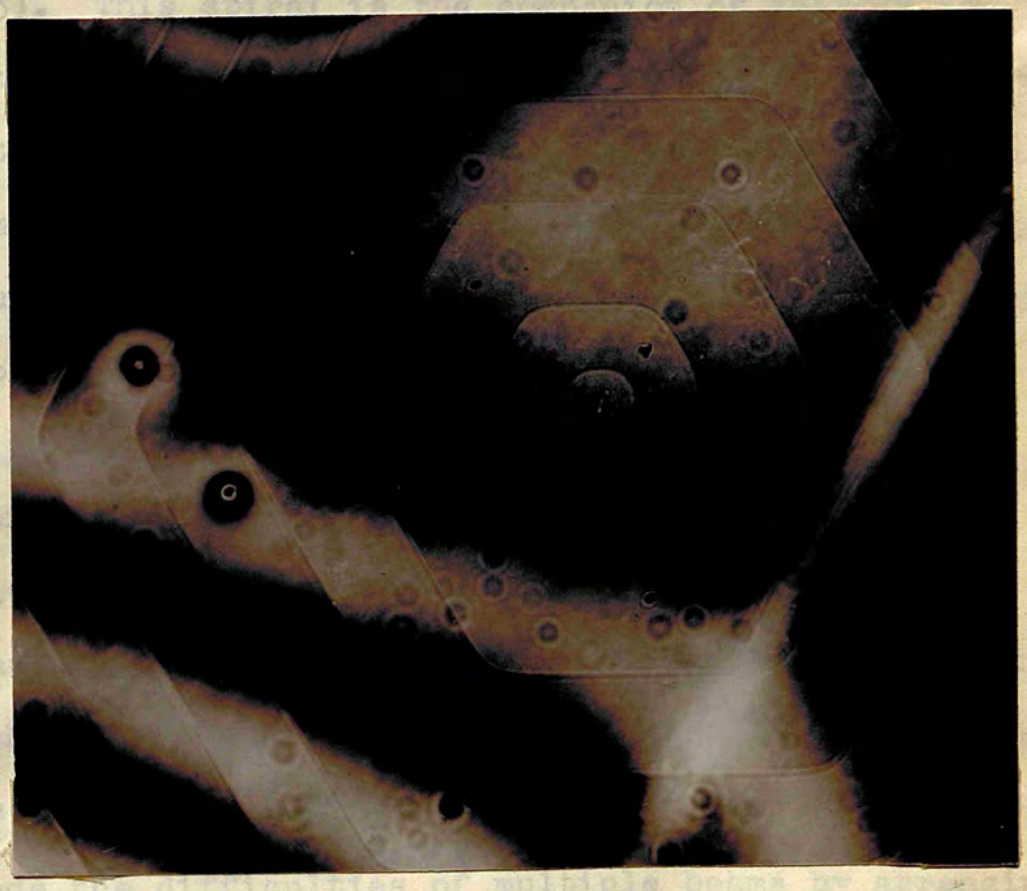

Fig. (83) ×312.

measuring device but as an enhancer of contrast, particularly to the eye which is so sensitive to colours. Fig (80) shows a region of the surface of a diamond photographed by ordinary means. Fig (81) is the interferometric contrast picture. A phase contrast picture of the same region is shown in fig (82). But it must be remembered that the interferometric contrast picture exposed here is a 'two-beam' picture as the film is used in its natural state, unsilvered, on the natural crystal surface. When the thin film is silvered on a suitably silvered crystal and the condition of high dispersion is satisfied then under the high magnifications that are possible in the case of the film, the interferometric picture is comparable with that of phase contrast. As an example of this, reference is made to fig (49) chapter 7. Another example of two-beam high dispersion is in fig (83). This spiral is the companion of that in fig (70) and is of smaller step height. Here it is seen with a good contrast that is seldom attained in ordinary micrography. The tube in the middle of the spiral appears so clearly defined not only on account of the high magnification, but also because of the high dispersion.

Appreciation of the Thin Film by Other Workers.

The advantage of the thin film is availability of high power objectives. High power means better resolution, and it is clear that the thin film, unsilvered, is not susceptible to the defects and shortcomings of multiple beams under high magnification. When it is used, silvered, on a silvered crystal, it can still evade the difficulties of multiple beams by arranging

the film to be extremely thin. This is equivalent to the good approach of an external flat in multiple beam interferometry.

For the above reasons it has been appreciated by other workers both here [83], and in the U.S.A. [84].

CHAPTER ELEVEN

Mercury Surface as a Reference Flat.

Since mercury surfaces are perfectly smooth and naturally highly reflecting and since they are not solid, they cannot be scratched, it was seriously contemplated to use mercury as a reference flat. This is very important when a hard crystal like diamond is in mind.

Since mercury is opaque it cannot be used in the transmission technique, and reflection techniques must be used. Since it is a liquid it cannot be used on the inverted microscope, as it is only the back surface which can be opaque in any interferometer, and the normal type of microscope is an obsolute necessity. Even in this type of microscope the wedge must be reversed and the crystal will have to be lightly silvered. Moreover the crystal must be transparent and its back surface must be parallel to its front surface. This condition is satisfied in diamond, as the octahedron is nearly the only form that can be studied interferometrically.

Since mercury attacks silver, normal silvering cannot be (85)
carried out and multilayers had to be used. As diamond is reasonably reflecting and as it forms the front surface of the interferometer it can be used, unsilvered, at least in an experimental stage. When the gap was small any slight touch, which is nearly unavoidable, will cause the diamond to be attracted by the mercury. This is no doubt due to surface tension effects and the angle of contact between mercury and diamond must be

less than 90°. Diamond is not wetted by water and its behaviour with respect to these two liquids is the opposite of glass.

It is this pulling effect which is the most serious objection to the use of mercury as a flat, at least with respect to diamond. The fringes could be seen with a reasonable contrast but they disappear as soon as the gap vanishes. When multilayers were used and the outer layer was cryolite this surface tension effect was very much reduced, and the most beautiful fringes were observed. The fringes were perfectly smooth and appeared in exceedingly good contrast and lasted for any length of time, moreover they were the diamond characteristic fringes. They moved with the body motion of the mercury and were damped and kept steady when cedar-wood oil was used as a barrier. Inspite of this the only attempt made to photograph and record them failed.

Feeling short of space and time, the attempt was not pursued, but the author has convinced himself that once rigid (vibrationless) supports exist and a quiet atmosphere lasts there is no safer way of observing diamond features.

The method used constitutes a simple laboratory experiment that could be carried out any time. A wide test tube nearly full of freshly distilled mercury was introduced with its upper end slightly projecting from the hole of the stand of an ordinary microscope. The specimen was fixed horizontally in a jig that rested fixed with plasticine on the stand of the microscope. The specimen was lowered and tilted until the fringes were observed. A vertical illuminator was used.

CHAPTER TWELVE

The Light Profile Method.

The light profile method or microscope as described by Tolansky,[86,87] is a development of the Schmaltz light-cut technique used in engineering practice since 1936.[88] The method depends on projecting a slit or the image of a wire on to the surface. An off centre pencil illumination is used, and the effect of the oblique incidence is to transform a profile in depth into a line pattern in extension.

The profile magnification is $M' = \frac{2M \tan i}{n}$, where i is the angle of incidence of the off-centre pencil, and n the refractive index of the medium between the specimen and the objective. The off-centre pencil causes severe chromatism and monochromatic light (generally λ 5461) is used. The above equation is usually written in the form $k = \frac{M'}{M} = \frac{2 \tan i}{n}$, when k is called the "light profile constant". This has been calculated by Tolansky, using interferometric means, for the 2 m.m. (oil immersion) and for the 4 and 8 m.m. objectives. This is done by employing a depth graticule, and for very good reasons the 16 m.m. objective k-value was not calculated - (the 16 m.m. shift is very small for ordinary graticules. For larger graticules the interferometric method does not apply). The author however, calculated this constant by employing crystallographic data when the orientation of a slip plane (chapter 13) was determined. It is true that the orientation has been carried by means of the profile, using constants of the already determined objectives. But there is always a difference between direct and indirect means.

Uses and Advantages of the Profile in the Present Work.

A list of some of the uses of the profile ampled with figures has been published by Prof. Tolansky.[87] The author has co-operated in this field and devised methods by which thicknesses of transparent films[88] and small radii of curvatures[89] may be obtained. The first of these has been used in determining the interferometric gap of canada balsam films used in chapter 10. The second in the evaluation of cylindrical curvatures of growth features. As an example of the latter use, fig (84) shows the light profile (taken with an 8 m.m. objective) over an etch hillock observed upon a rounded dodecahedron from the Belgian Congo. The crystal looks as much an octahedron as a dodecahedron. The radius of curvature of the R.H. facet of this figure is $\frac{k\ a^2}{2\ .S.M}$, where a is half the chord, s the sagitta, k the light profile constant and M the magnification. The approximate radius is roughly 0.05 m.m. (the curvature is assumed spherical).

The profile is a valuable instrument in the study of growth features on natural crystal faces. The gap in multiple beam interferometry cannot exceed a few wavelengths, and it is where the features begin to be rough for multiple beams that the need for the profile arises. It does not only measure depth or height with a fair accuracy, but it decides which feature is above, and which feature is below the surface. Connected with the above is that it decides the direction of the step. If the step direction is known and the area including this step is afterwards studied by interferometry, the direction of the

Fig. (84) × 250

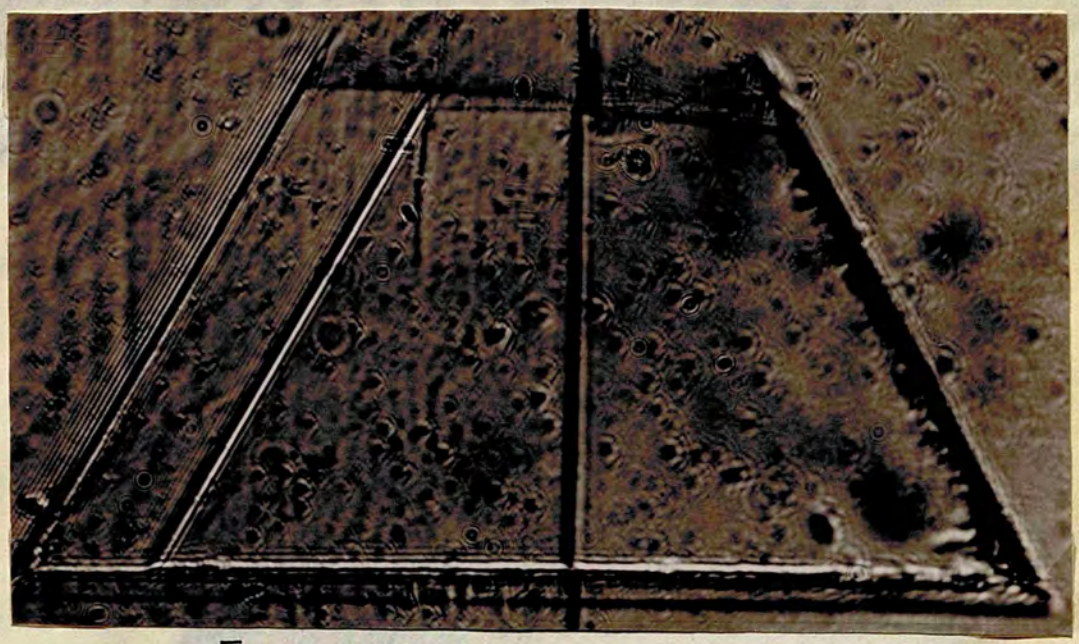

Fig. (85) × 1600

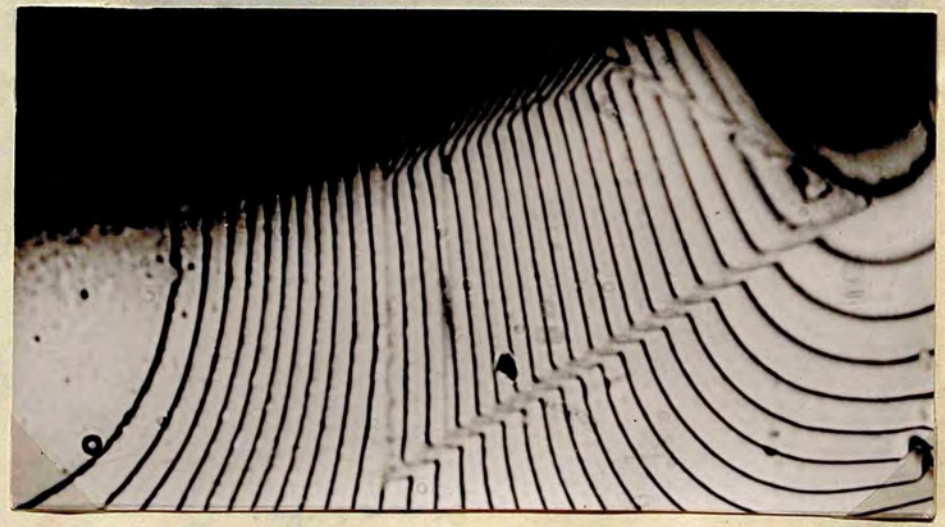

Fig. (86) × 900

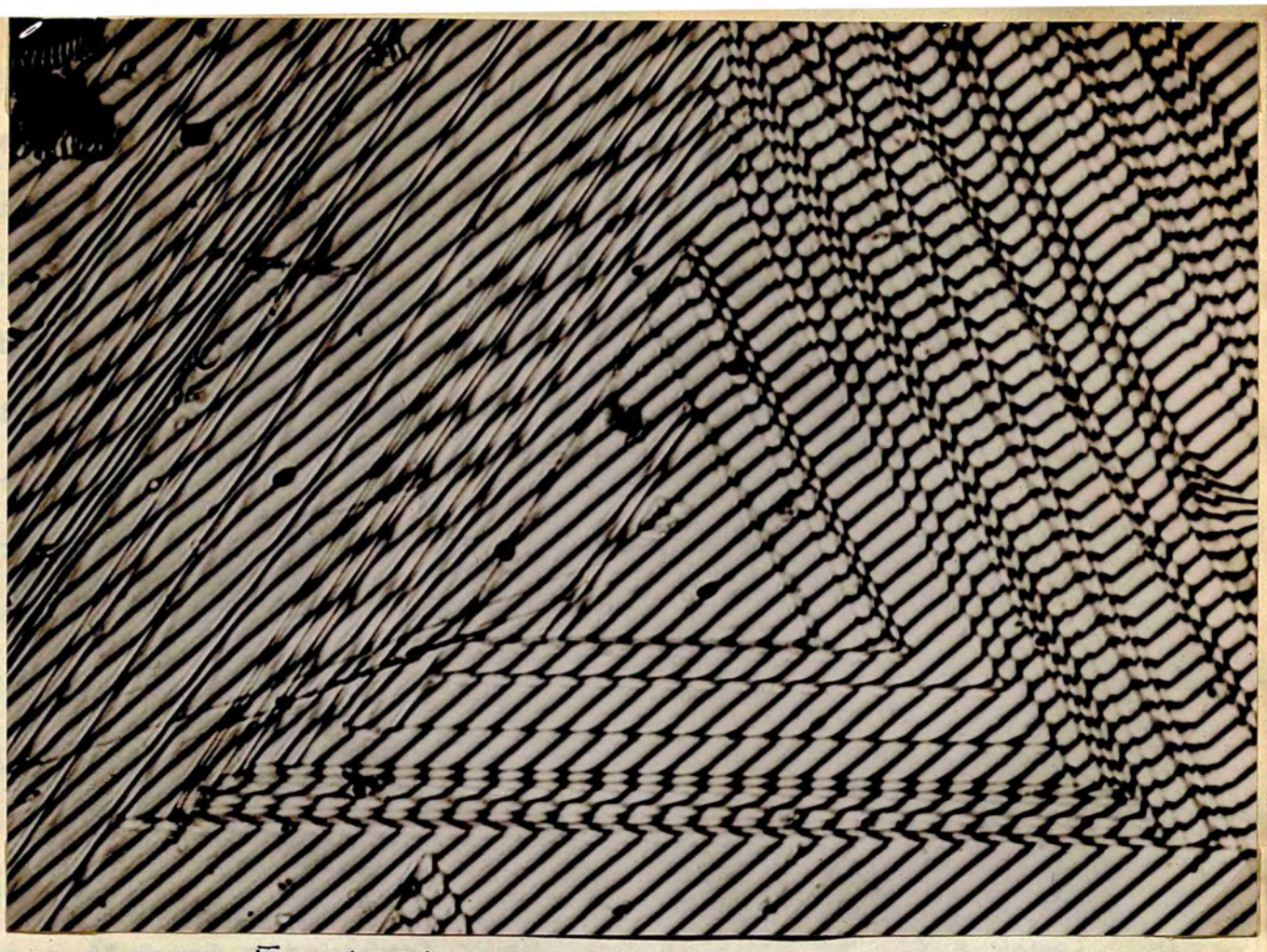

Fig. (87) X208

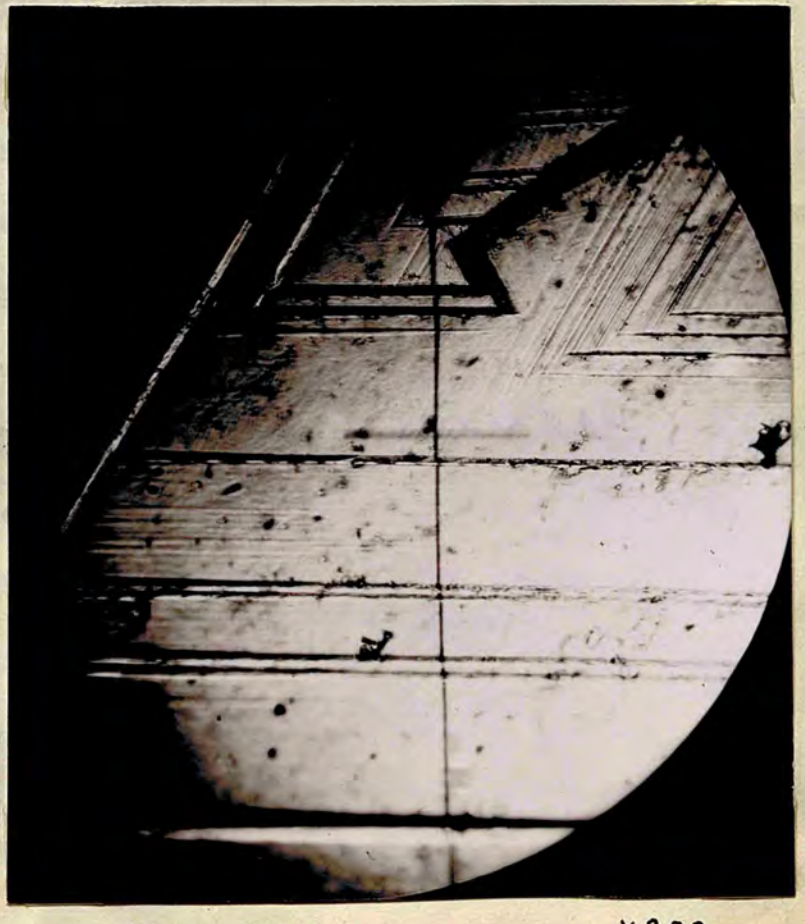

Fig. (88) X300

wedge is decided. An example of this is in chapter 13 in connection with slip. In a range far from reach with a focussing or defocussing arrangement of the microscope, flat features exist on crystal faces. It is of utmost importance to decide whether these flat features are elevations or depressions. On account of the absolute similarity of these features no guess work is possible, but the light profile line crossing their boundaries will turn one way (right or left) when they are depressions and turn the other way when they are elevations (ordinary interferometry does not tell, because the features are generally small).

Specific Examples of its Uses.

As an example of the above, fig (85) shows the light profile crossing a closed figure of trapezoidal shape. This appears on a diamond octahedral face, and as such is not a usual figure. The profile shows it to be a depression of about $\frac{1}{3}\mu$. A Fizeau interferogram, taken with the thin film technique, is in fig (86). Once Fizeau fringes are obtained F.E.C.O. methods could be used. In this manner, the figure has been proved to be a depression, the actual depth of which is 0.24μ.

Pyrite octahedral faces (chapters 6 & 7) it was mentioned, contain features that are similar to those observed on diamond surfaces. The Fizeau fringes, fig (87) were ambigious, and F.E.C.O. is an elaborate method, but the light profile over one of these features fig (88) proved they were pyramids. Triangles of opposite orientation were proved to be "trigons".

Fig (89) shows the profile over an ordinary trigon and

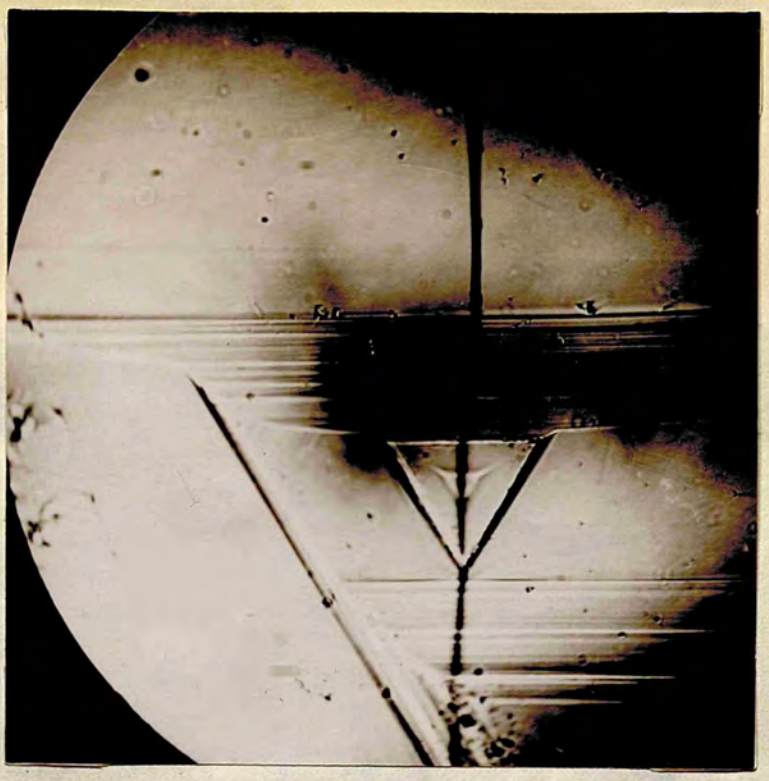

Fig. (89) x 2000

Fig. (90) x 400

Fig. (91) x 800

fig (90) over a tetragon. Fig (91) shows it over two etch pits which have been obtained at 600°C over a diamond octahedral face (c.f. chapter 14). The profile shows the upper one to have a depth of 1μ, and the lower one to have a depth of 2μ. They were taken with the 4 m.m. objective.

Limitations of the Profile.

It is true that a magnification of 2000 can be reached with an oil immersion objective using different eye pieces and different extensions of the bellows of the projection microscope. The useful magnification however is not much more than a 1000. Beyond this the profile line broadens and no net gain of accuracy is achieved. The magnification of 2000 and similar higher magnifications for the other objectives are only convenient means to magnify the scale of the effect on paper, but under no condition must the Abbe criterion for resolution be broken. To settle this question the following analysis is necessary.

Details are not discernable if their size is less than

$$e = \frac{\lambda}{2A}$$

(where A is the numerical aperture of the objective and λ the wave length used. This is .546μ for the green mercury line)

The stuctural element e under the magnification M of the microscope appears at an angle

$$\theta = M \cdot \frac{e}{250} \quad \text{radians}$$

(where 250 is the least distance of distinct vision for a normal eye)

As one radian = 3438′ $\qquad \theta' = 3438\theta$

$$M = \frac{250}{3438} \cdot \frac{\theta'}{\lambda} \cdot 2A$$

Experience tells that comfortable vision calls for θ' to have a maximum value of 4'. From this we see that the optimum magnification is $M = 1050\,A$.

PART III

Study of Slip in a Diamond.

CHAPTER THIRTEEN

Observation of Slip.

It has been realised, since the beginning of the century,(91) that the dark bands seen on the surfaces of plastically deformed metal crystals are in fact steps formed by the shearing of slabs of atoms. The slabs are imagined to have slipped with respect to each other much like cards in a pack. The planes in which the slabs have slipped are called slip planes. The steps are the outward sign of the slip phenomena and their heights measure the distance moved by the slabs. But motion does not mean the simple sliding of planes of atoms over other planes of atoms leaving the crystalline lattice undamaged apart from a translation of some parts. Instead the lattice at least around one active slip plane is supposed to be severely distorted. Slip does not usually continue at this plane until fracture occurs, but by some undiscovered means shifts on some other planes. When these planes are parallel, their trace - the slip lines - on the outer surface of the crystal form into groups which are called "slip bands".

The extensive work on non-metallic crystals carried before (1933) has been summarised in a review paper by Smekal.(92) A similar review on metallic crystals is a recent article by Brown.(93) Brown's paper is a critical account based on microscopical study of the results of experimental work of past and present investigators. The theoretical approach to the study of slip is based on the modern theory of dislocation. Leading figures in

the application of this theory include (Shockley, Barret, Seitz and Read)[94], Frank[95] and Mott[96]. Dislocations are amongst the few types of defects which occur naturally in crystalline substances. The dislocation theory is based on views first expressed by Burgers[97] but soon attracted the attention of the above scientists and in particular Frank who based on it a theory for the growth of imperfect crystals. Inspite of the excellent work achieved by the above authors this type of crystalline imperfection is far from being wholly understood.[93]

The study of slip includes:-

(1) The direction of the line which is a crystallographic direction.

(2) Identification of the slip plane with a crystallographic plane.

(3) The amount of slip, which is connected to the step height observed on the surface.

This, the author has done with respect to observations of slip found on two octahedron faces of a diamond crystal, and it is natural to enquire if similar observations had been testified by other workers, as to be due to slip in diamond.

Earlier Observations on Diamond.

It is doubtful whether earlier observers have been able fully to substantiate the existence of slip in diamond. In the literature, it is perhaps described as striations. Striæ on diamond have been observed to follow the same line of direction as cleavage.[10] Fersmann and Goldschmidt[11] describe lamellae observed

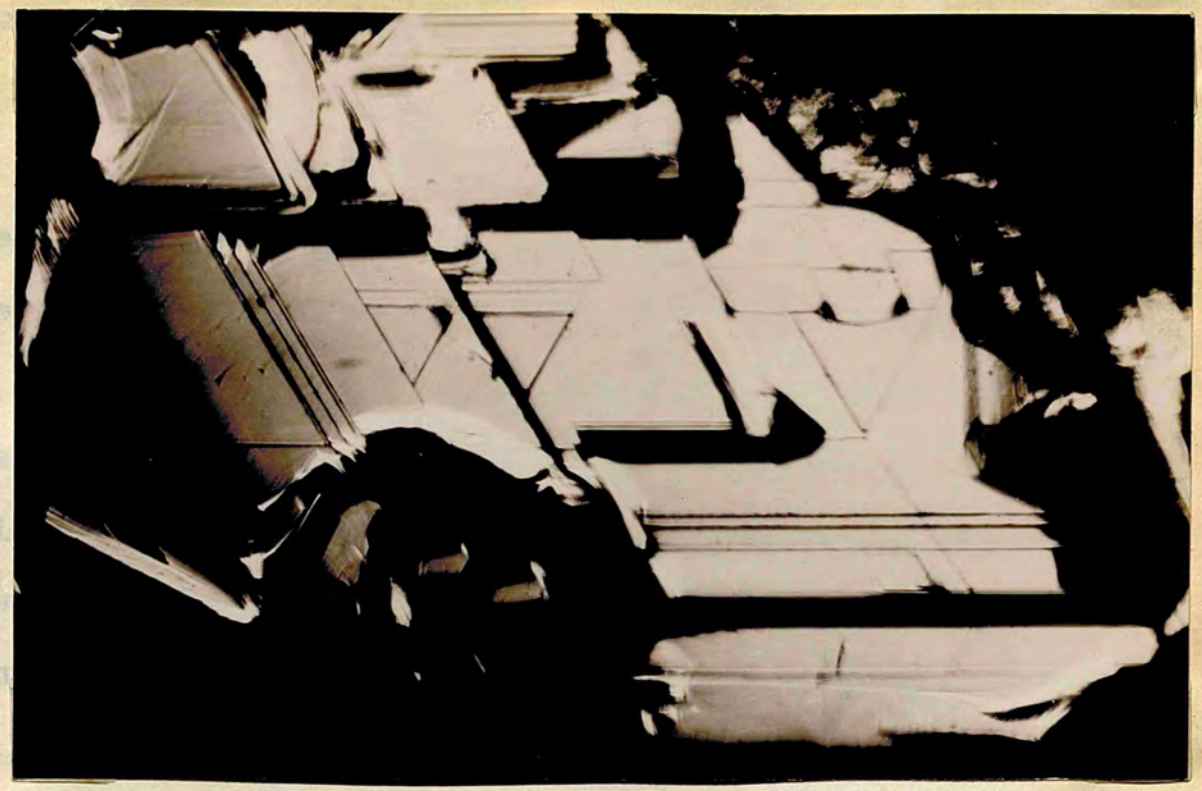

Fig. (92) x 11

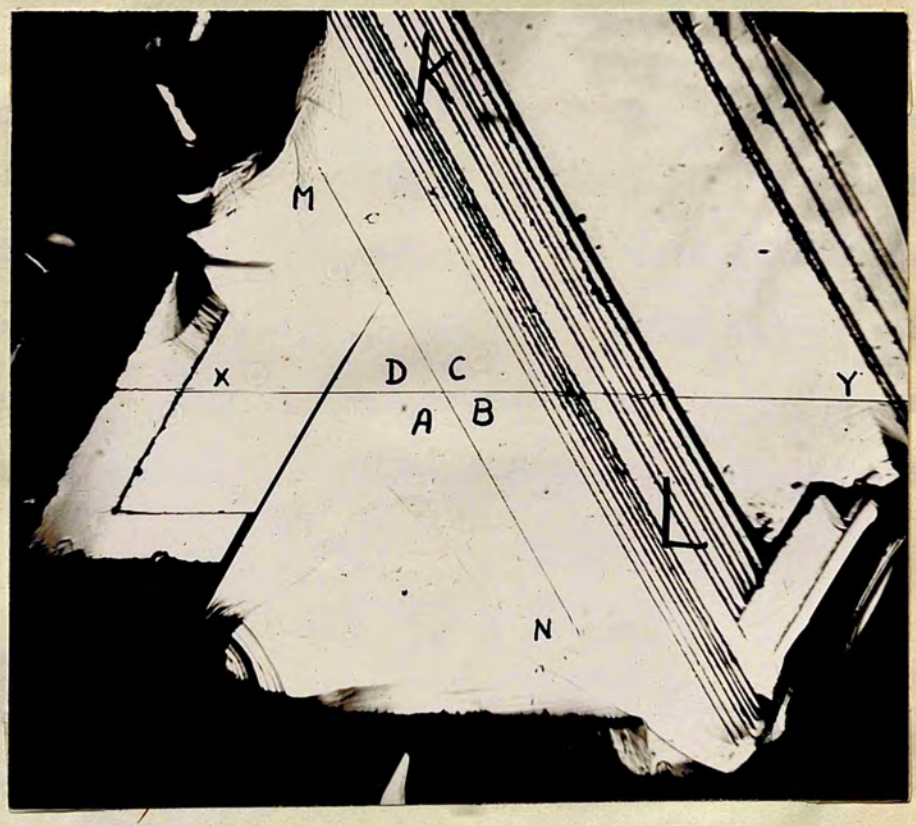

Fig. (93) x 30

on a rhombic dodecahedral crystal. The lamellæ crossed the crystal in the four octahedral directions. This phenomena they related to etch. Some striations observed on diamond octahedral faces were attributed by Williams (10) to glide planes. Williams had no evidence to offer except that this was the expressed opinion of E.D. Mountin. (98) Dr. Grenville Wells (7) discussed the hardness and brittleness of diamond and concluded that pure slip is difficult to conceive. She, however, reproduces one of Williams photo-micrographs and comments that it looks as if slip is taking place. This is all the evidence of the existence of slip in the whole literature of diamond. To establish the existence of slip in diamond is therefore an event of some importance.

Description of the Crystal.

The crystal is part of a macle, length of side 1.48 cm., and thickness 0.33 cm. The surface on which the slip was discovered first is face 1, represented by fig (92); face 2 was studied in detail before (fig 40 chapter 6). Both faces contain high growth plateaux that prevented the use of the normal flat, and had to be studied by the techniqes developed in chapters 9 and 10. Light profile methods of chapter 12, were also used.

OBSERVATIONS.

(a) Slip on the First Face.

On the one side of the crystal the slip appears as a straight line cutting right through all the growth features some 9.5 m.m. long, running right across the surface. Part of this is shown in fig (93). The series of parallel lines KL are

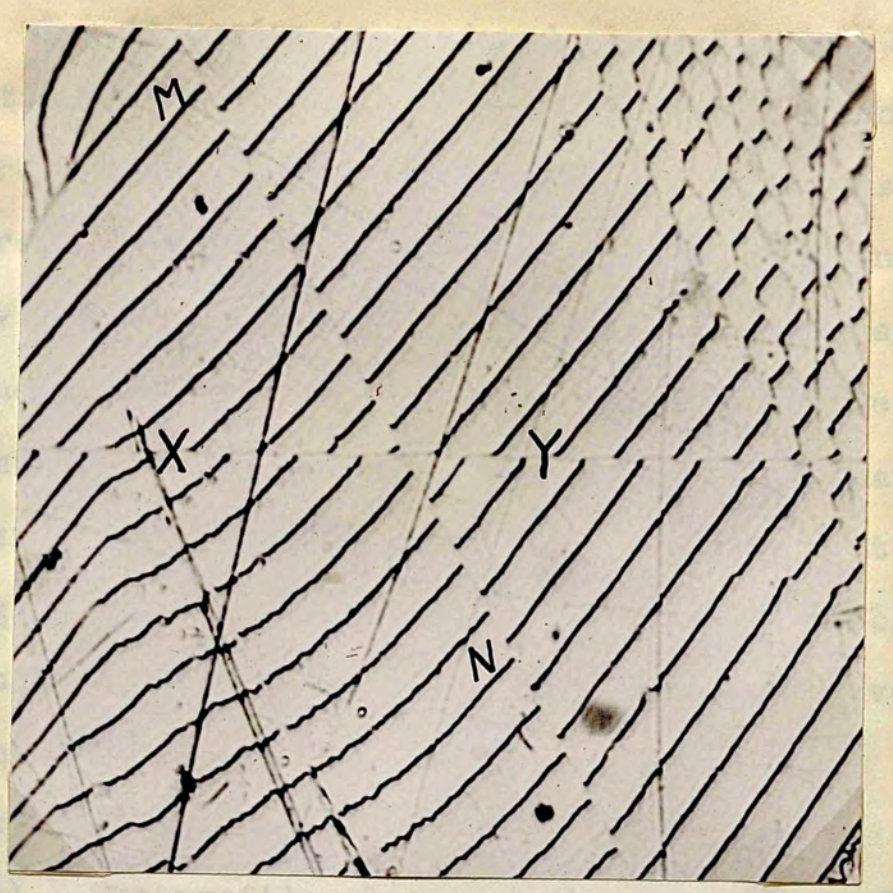

Fig. (94) ×130

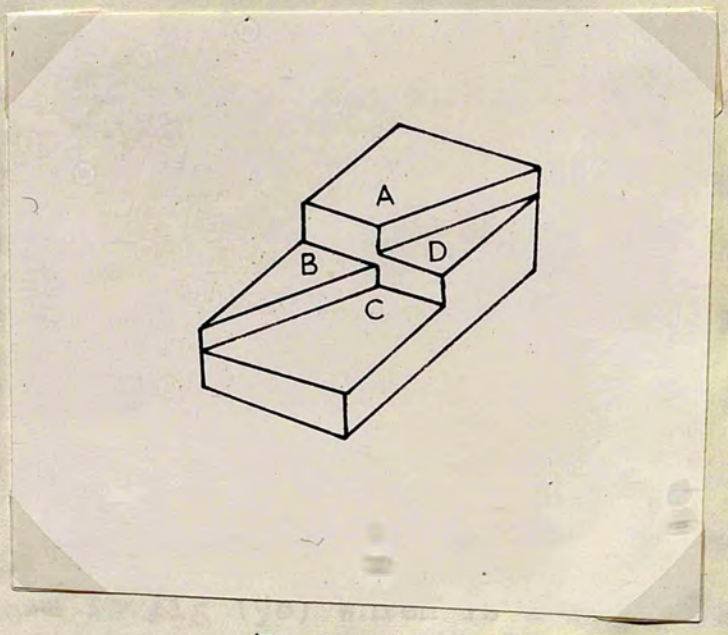

Fig. (95)

growth sheet fronts, and at 60° to these lies XY the slip line. The topography of this region is rendered clear by fig (94) which is a multiple beam interferogram taken by the cone technique. Here MN is a growth sheet step parallel to the group of steps KL and once more XY is the slip direction. From the fringes one can readily evaluate the topography, a simplified diagram being shown schematically in fig (95). The Fizeau fringes of fig (94) are ambiguous as to step directions and these have been clarified by using fringes of equal chromatic order. But even before applying this latter confirmatory method, the problem of relative heights of the four drawn segments has been solved in the following manner:

The direction of the growth step MN has been decided by the profile fig (96). The profile also gave the approximate height of step as 2/3 μ ($\sim$ 2.5 orders). This decided the direction of wedge in fig (94) and its associate fig (97) which is a transmission interferogram of the same area. Although masked partly by an opacity which will be explained later, fig (97) has the decided advantage that the fringes appear with their natural colours in the unfiltered arc. The multi-coloured fringes (and their complementary colours in reflection) combine differently and when crossing the step decide the number of orders in the step. In this manner it has been testified that the slip step XY is between 0.3 and 0.35 of an order. The variation in the value of the step in this locality is due to the existence of a low pyramid clearly seen in fig (98) which is a high dispersion picture taken with the film technique (chapter 10). It illustrates

Fig. (96) x 450

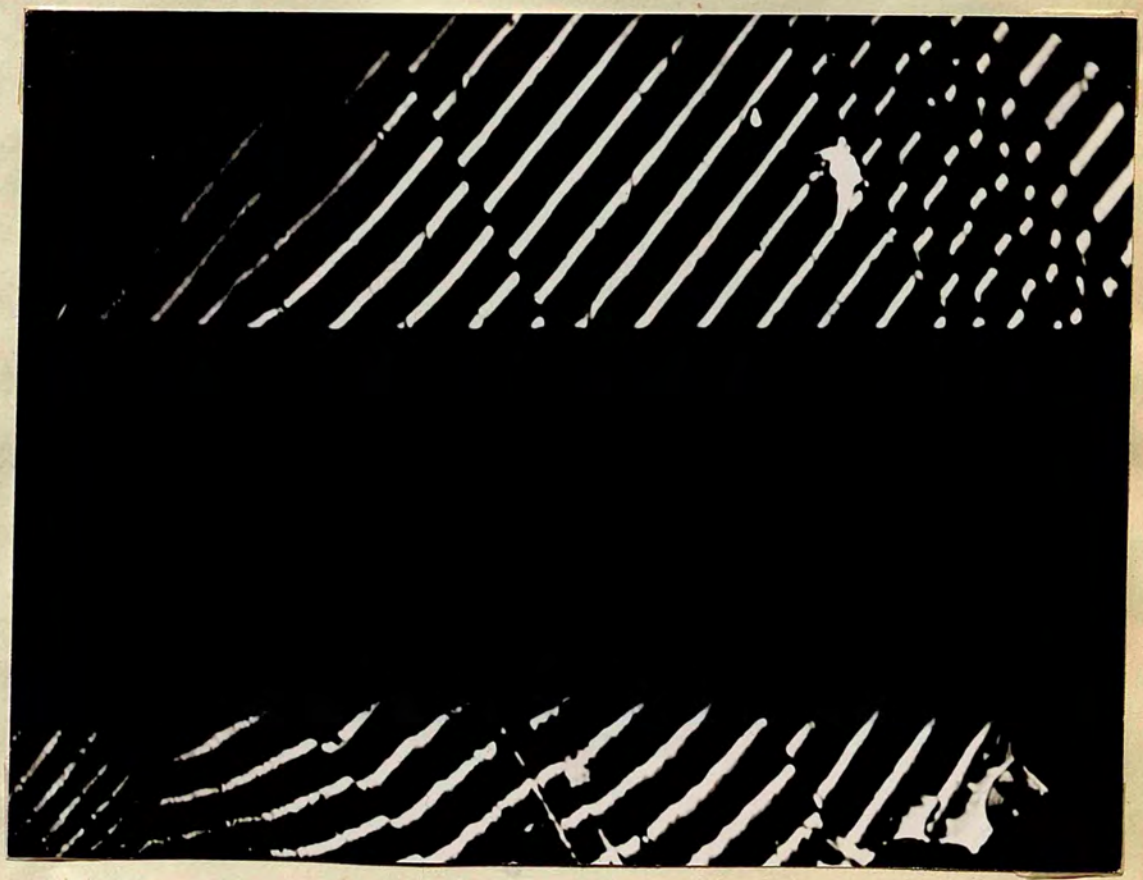

Fig. (97) x 130

X42

Fig. (98)

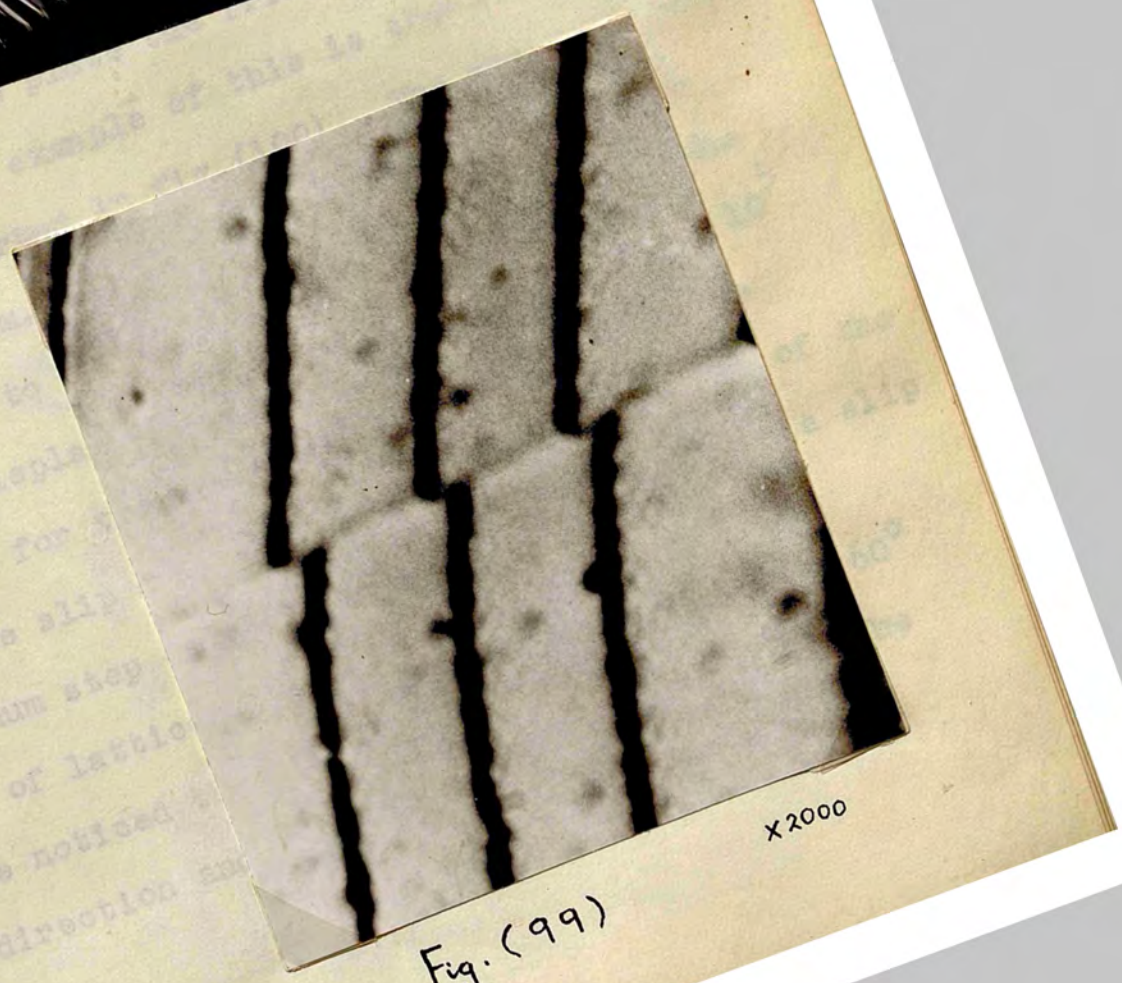

X2000

Fig. (99)

the superiority of this new method in elucidating surface structure.

An examination of the slip step over the entire length of the crystal reveals the existence of a slight slope. The step increases regularly from the left to the right. Thus at the extreme left hand side the slip is only 480 Å $\pm$ 5 Å. At a point 2 m.m. to the right it has increased to 680 $\pm$ 20 Å, and at 8 m.m. to the right to 1280 $\pm$ 20 Å. This amounts to a slope between the slipped regions with the very small angle of 10^{-5} radians i.e. merely 2 seconds of arc. These determinations are illustrated in figs (99), (100) and (101) respectively. The first two were taken with the thin film technique (chapter 10) and are multiple beam interferogram. The high magnification shows that originally on the plate the fringes are extremely thin and well defined. An example of this is shown in the contact print (M = 900) inserted in fig (100). The third is taken with the un-silvered film.

If this slip were to be taken as due to dislocation the angle would imply a displacement of one atomic lattice in 10^5 lattices, to account for the slope. However, it should be pointed out that the slip does not run to zero at one end of the crystal, the minimum step of 480 Å clearly corresponds to a slip of some hundreds of lattices.

It is to be noticed that the slip line is exactly at 60° to the growth direction and is thus parallel to an edge of the (111) face.

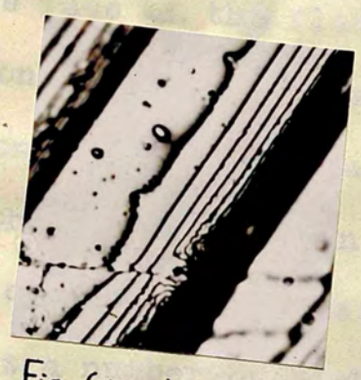

Fig. (100) x 900

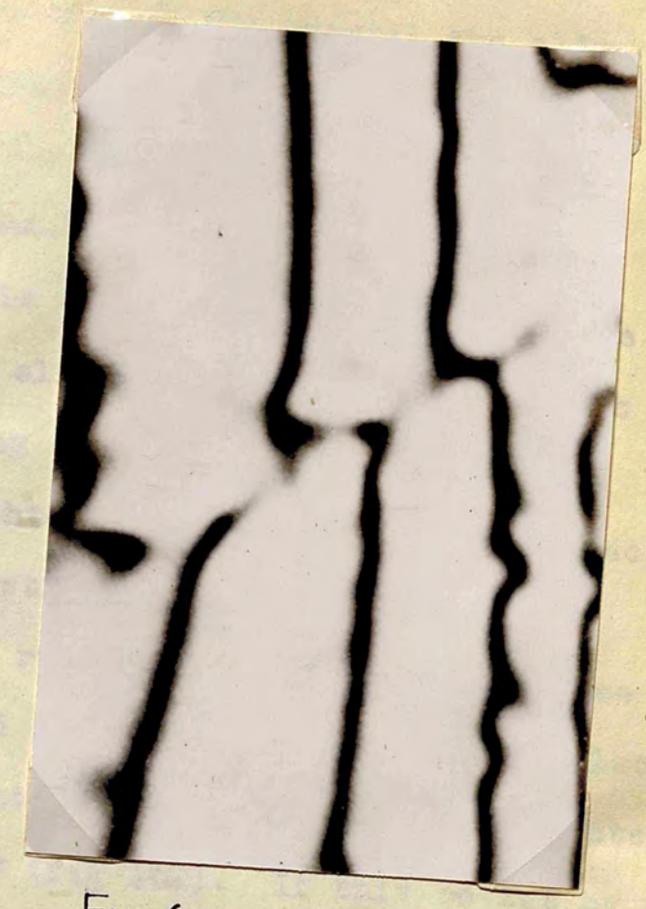

Fig. (100) x 9000

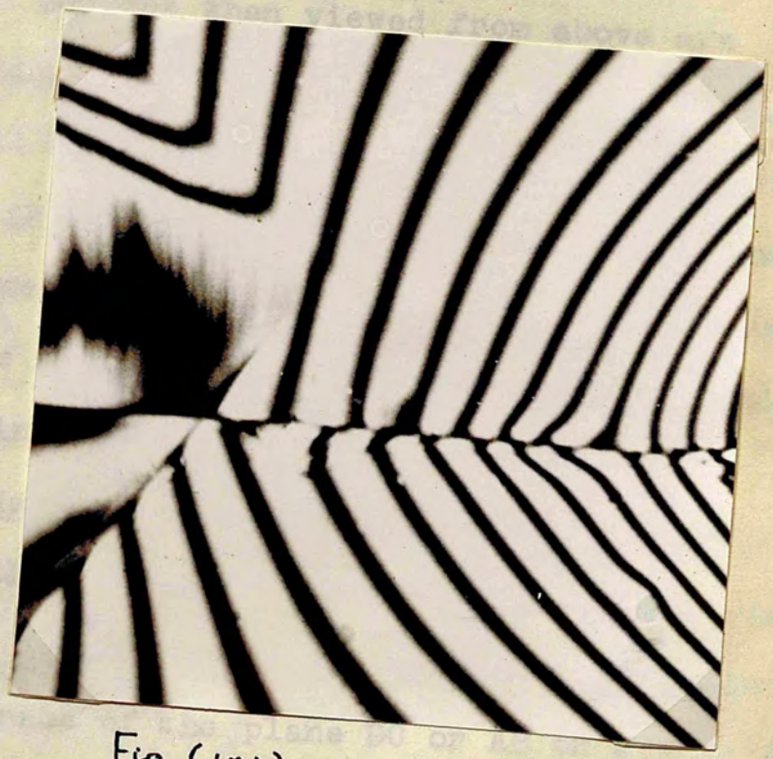

Fig. (101)

(b) Slip on the Second Face.

Because of the twinned nature of the crystal the slip cannot be expected to penetrate from one side to the other, and indeed this is the case, for the line XY does not appear on the opposite face of the flat stone. However, a slip line does appear on the second face, this being inclined at 60° to the direction of XY. This second slip line also traverses right across the crystal and in doing so very clearly reveals a feature of some considerable interest. For the second surface has on it a number of high growth plateaux as well as deep trigons. The slip in question runs right across one of these trigons (trigon B fig 40) and in doing so is clearly displaced. It is from the displacement that the slip plane can be oriented. Suppose we have a growth step P (fig 102). If this be cut by a slip plane normal to the surface, then the cut lines in the upper and lower growth regions when viewed from above are colinear. If the cutting slip plane has an angle to the surface, then the two lines will appear displaced, as shown schematically in fig (102). If the growth sheet step height be known, and is reasonably large, the measured displacement in the slip line permits the angle to be calculated. Furthermore the direction of displacement determines the direction of the angle.

Relation between Step Height (h) and Shift (p).

Fig (103)^{a} is an enlarged part of fig (102) where ABCD is the slip plane, and π is the lower (111) plane of the vertical or sharp step P. The trace of the plane DC or AB on either (111) plane is making an angle $\alpha = 60^{\circ}$ with the step direction. The

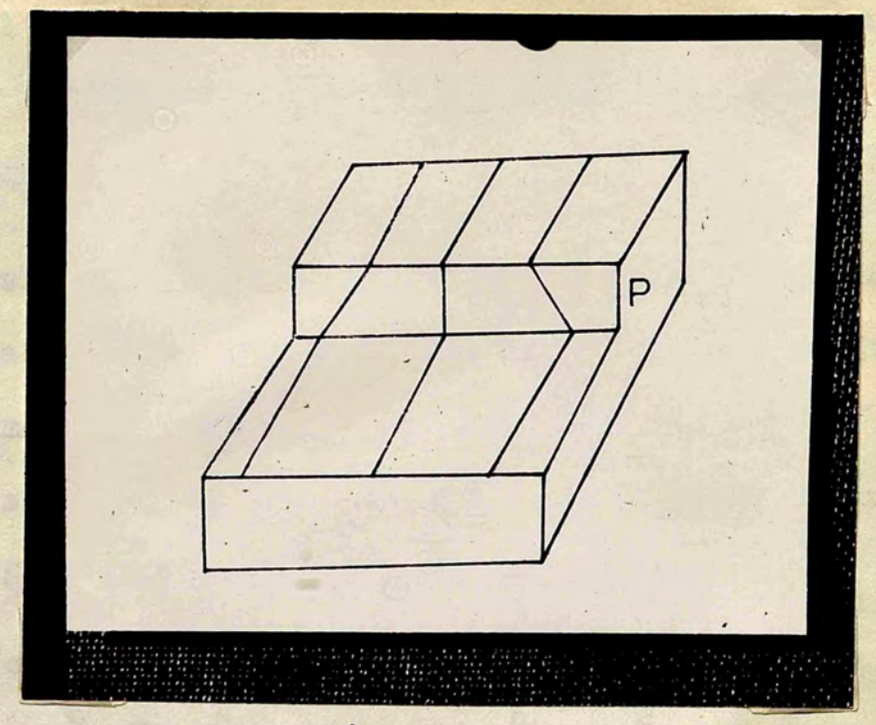

Fig. (102)

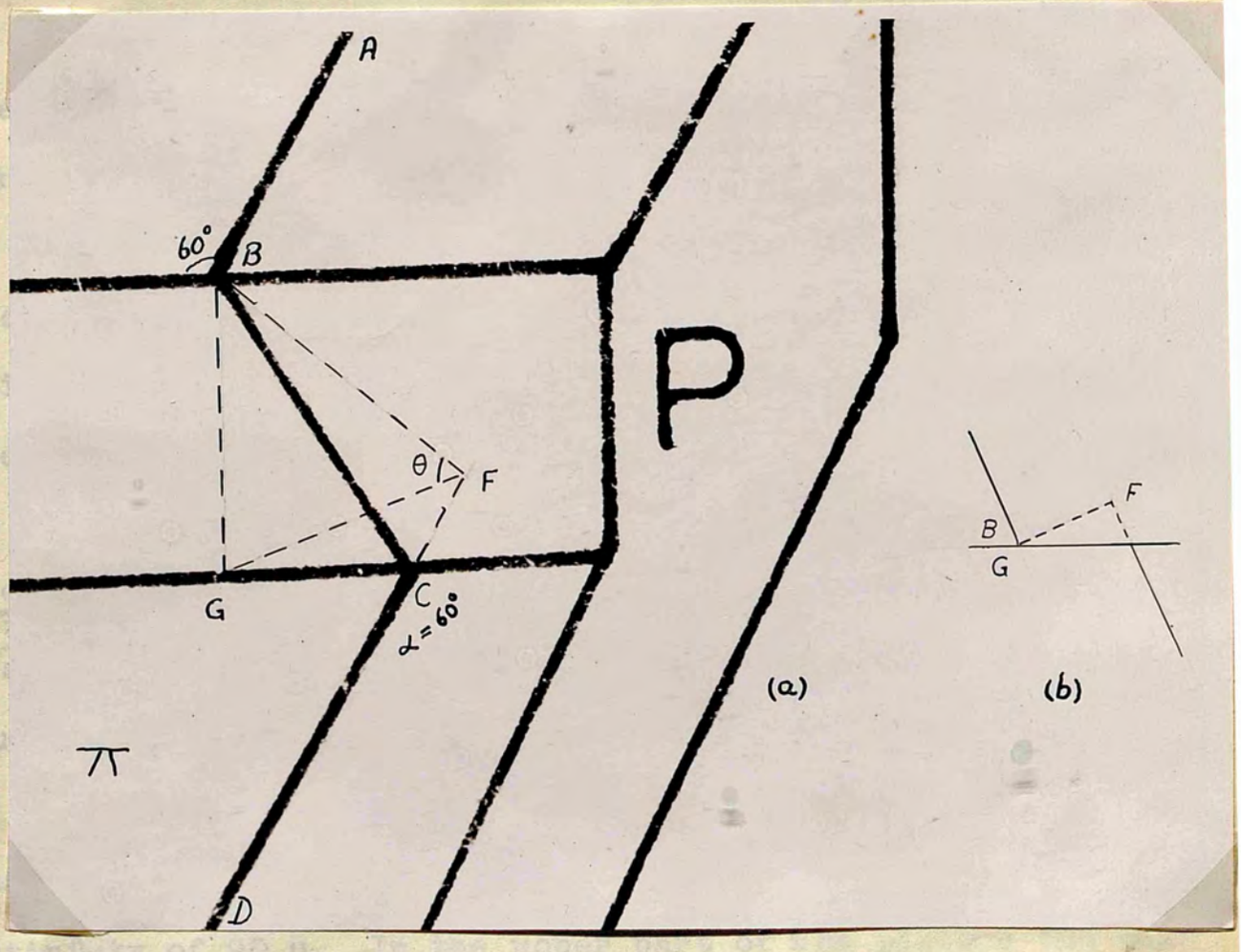

Fig. (103)

step-height BG = h, and GC = x. Draw BF $\perp^r$ to DC, and connect GF. The dihedral angle between π and the plane ABCD is $\angle$ BFG called θ.

$$\tan \theta = \frac{BG}{FG} = \frac{h}{p}$$

This dihedral angle is the angle between the slip plane and the (111) plane of the surface (the angle needed). It is seen that it is measured directly by evaluating h and p. On the surface the side of the step is not seen in this 3-dimensional sense, and B falls on top of G as it is in fig (103)b. If x is preferred for measurement, it must be noted that

$$\tan \theta = \frac{h}{x \sin \alpha} = \frac{h}{x} \cdot \frac{2}{\sqrt{3}}$$

Identification of the Slip Plane.

Fig (104) shows the slip traversing a growth trigon on face 2. The end step PQ is large and equals to 90 μ. This has been measured by the light profile and by repeated focussing and defocussing on both ends of the step using a high power objective. The results were in complete accord and the above estimate is an average. It is readily seen that the slip line experiences a lateral displacement. The displacement is 32 μ. The dihedral angle θ is calculated from the relation $\tan \theta = \frac{h}{p} = \frac{90}{32}$. This gives θ (estimated to the nearest $\frac{1}{2}^o$) as $70\frac{1}{2}^o$. This is precisely the angle made by adjoining (111) faces on diamond, and the slip plane and cleavage plane are the same.

This interesting geometrical deduction has only been made possible because of the occurrence of the very large discontinuity of 90 μ. In the upper part of the picture the slip

X 30

Fig. (104)

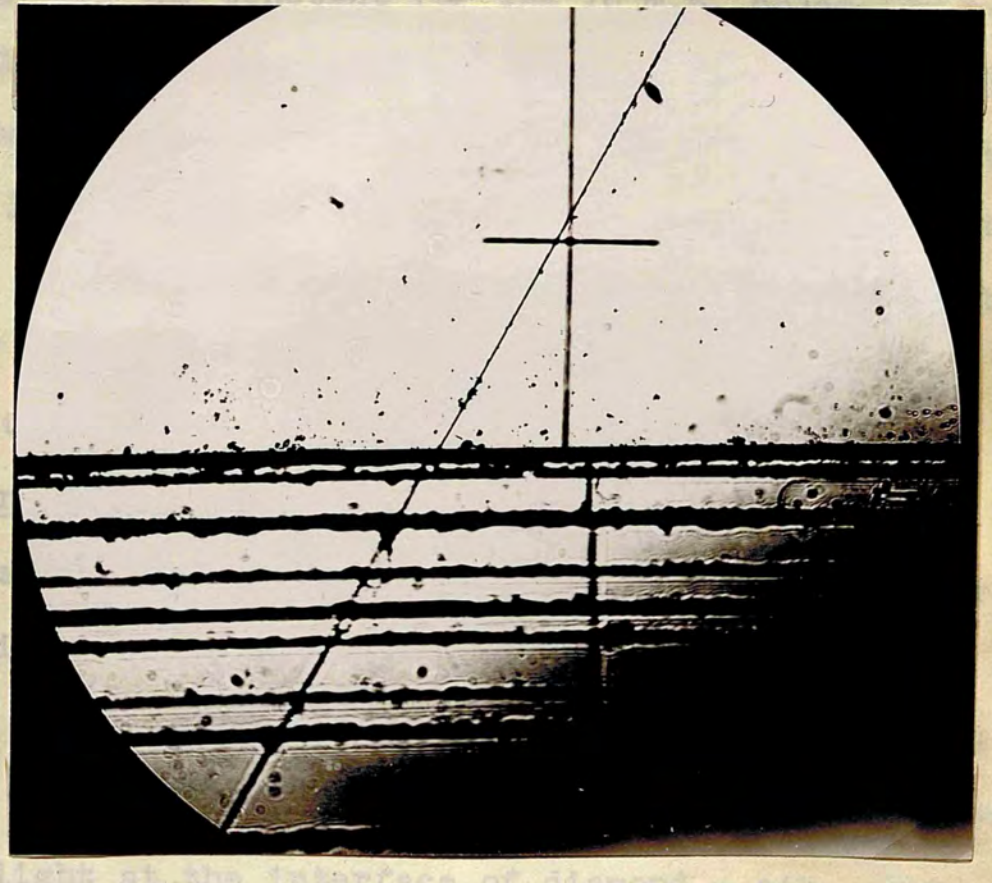

X 160

Fig. (105)

line does not appear to make an angle of 60° with the side of the trigon. As this part is made of small steps, the slip line will shift 11 μ to itself by small amounts. The apparent deviation of the slip line from the angle of 60°, is due to the unresolved shift over numerous small steps.

Further confirmation came from the other face (face 1). Here a relatively large step exists. The profile over this step, using the 8 m.m. objective calculated by Tolansky is in fig (105). The height of this step is 31.5 μ, and the slip line shift is 11 μ. The angle θ estimated to the nearest $\frac{1}{2}$° is 70°$\frac{1}{2}$ again.

Calculation of a Light Profile Constant.

Fig (106) represents the same step of fig (105) but taken with the 16 m.m. objective. This being under a different magnification confirmed the shift of 11 μ, but does not confirm the step height as the constant for the 16 m.m. objective is not known. The author took this opportunity to calculate this constant. The constant came out to be 0.283 with a probable error of $\pm$ 1%. The calculation took for granted the exact angle of 70° 31 $\frac{3}{4}$' (the 70°$\frac{1}{2}$ is sufficient) and depends on the comparison of the slip shift with the light profile shift. Being a direct method it is free from objection.

Interpretation of the Opacity.

Having established the slip plane and cleavage plane are the same, it is possible to explain the opacity of fig (97) on the following lines. If the slip plane has developed partly into a crack, then an air film in the crack would totally reflect the incident light at the interface of diamond - air. The

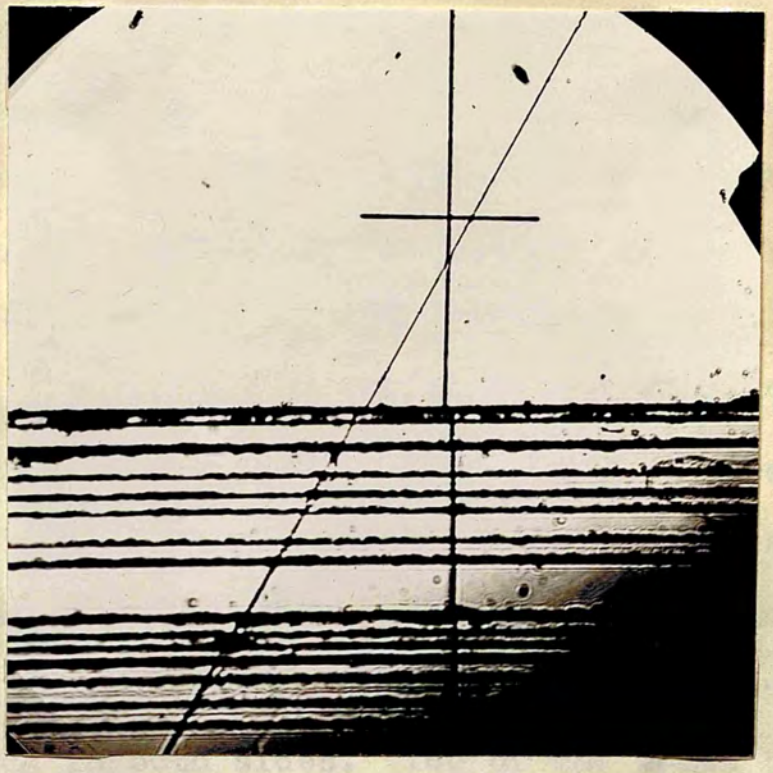

Fig. (106) ×95

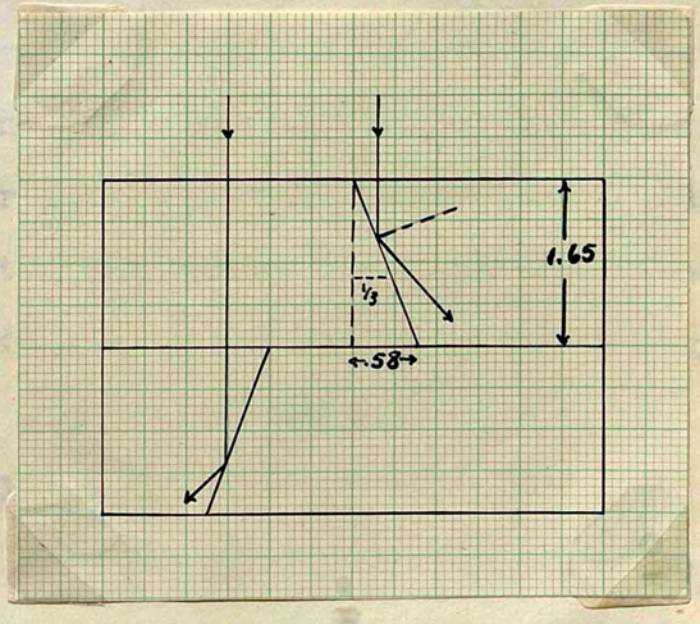

Fig. (107)

incident light would make an angle of $70\frac{1}{2}^{\circ}$ with the perpendicular to the slip plane which is greater than the critical angle of diamond ($24\frac{1}{2}^{\circ}$).

Estimation of the Depth of the Crack.

The thickness of either part of the macle is 1.65 m.m. If we assume the crack to have penetrated right down to the united plane of the two parts, the breadth of the opacity as it appears on the surface should be $1.65 \times \tan 19\frac{1}{2}^{\circ} = .58$ m.m. This is clear from fig (107). The breadth of the opacity in fig (97) is $\frac{1}{3}$ m.m. showing that the crack in this part could only have penetrated to no more than .57 the thickness. Fig (108) shows the opacity of the whole crystal in transmitted light. The non-uniform breadth of the opacity is due to the non-uniform penetration of the crack in both sides. Two of the bands belong to one face; the other two belong to the other face. The crack directions which are also the cleavage and slip directions, are mirror images to each other, and the same conditions which cause the opacity in the upper half of the horizontal crystal, will also cause the opacity in the lower half. Referring to fig (107), the interface diamond-air exists in both parts. In the upper part, the normal incident light cannot cross the crack and is reflected to the right; in the lower part it is internally reflacted to the left, and cannot pass through the crack.

Easy Cleavage of the (111) Plane.

In diamond slip has occurred in the natural cleavage plane. If it leads into a crack preparatory to fracture, this is well expected. Bragg[99] attributed the easy cleavage on diamond along

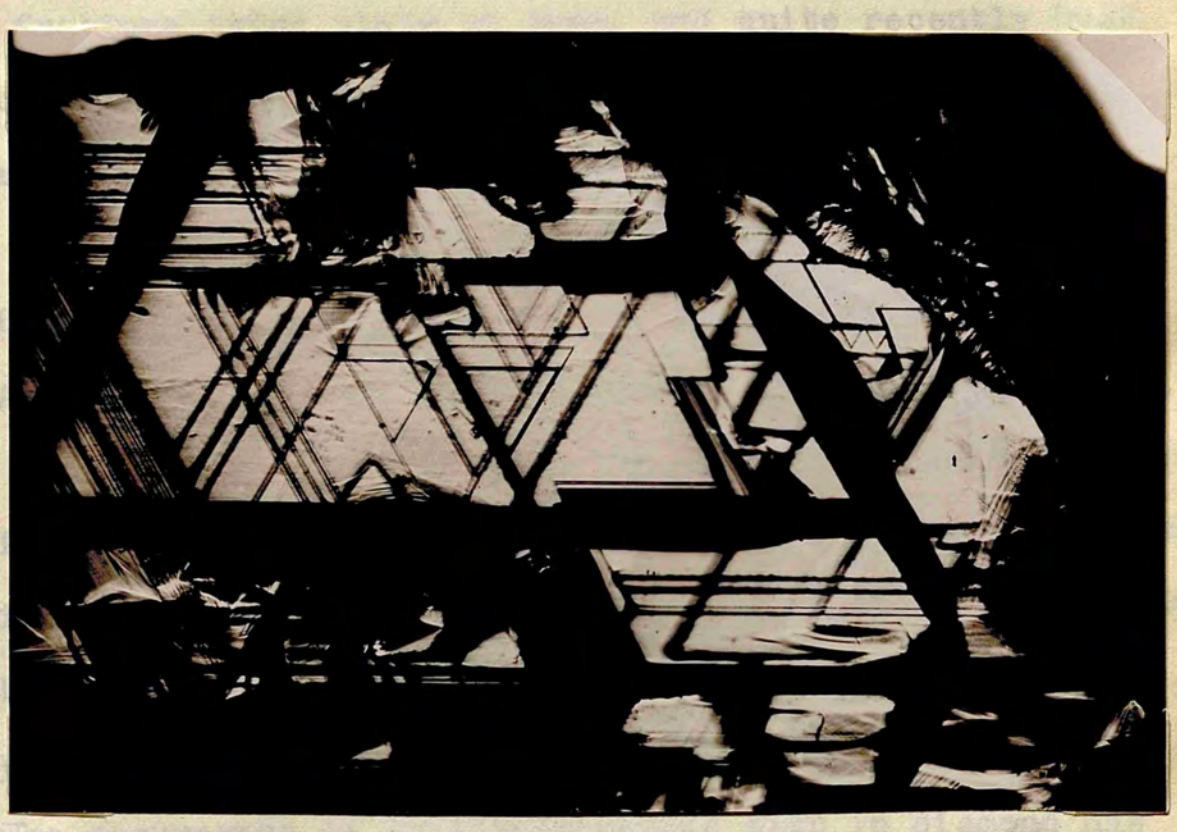

Fig. (108) X 11

the (111) planes, as due to the fact that the distance between neighbouring atom layers 111 to the cleavage plane is maximum. He has been supported in this by Wooster (100), who gives an explanation why zinc blende which has a similar structure cleaves in the (110) direction.

Slip Leading to Fracture in other Crystals.

Slip planes like cleavage planes must also be planes of weakness. Orowan (101) has demonstrated that slip planes may develpp until fracture takes place on them, and quite recently Duce (102) subjected specimens of metal crystals to high frequency torsional stresses. As the number of cycles increased more slip occurred until they resembled cracks after which fracture took place.

Slip Plane and Slip Direction.

According to Elam (103) the slip-plane is that crystal plane, which has the highest atomic density, similarly the direction of slip is along the line of greatest atomic density on this plane. The directions deduced in this chapter are in comformity with the above.

Conclusion: Thus it may be concluded that -

(a) The occurrence of crystallographic slip in diamond has been demonstrated on two faces of a twin.

(b) Slip takes place on (111) planes which are the planes of easy cleavage.

(c) The two faces on either side of one slip are inclined at the slight angle of 10^{-5} radians.

(d) The slips have associated with them regions opaque to transmitted light.

(e) The opacity has been interpreted as due to a crack.

(f) The direction of slip lines are ll! to octahedron edges i.e. to [110].

(g) The slip appears on both sides of a twinned crystal, but in neither case does the slip penetrate to the opposite side.

PART IV

Study of Etch Phenomena.

CHAPTER FOURTEEN

Etching at Low Temperatures.

When a crystal is acted upon by a solvent that physically or chemically dissolves it the first action of the solvent is to attack the faces at different isolated points with the result that the face becomes pitted with regular figures of microscopic size etched upon by the solvent. These are called 'etched figures', and are usually shallow depressions whose sloping sides are inclined to the close packed planes at small angles. The occurrence and shape of the etch-figure is connected with the different action of the solvent in different directions, and so its symmetry must have a bearing on the symmetry of the crystal as a whole.

Historical Review.

Increasing interest accompanying the etch-figure is attributed mainly to the efforts of German scientists in the latter half of the nineteenth century. These include the works of Baumhauer, Becke, Traube, Tschermak Wulf and Beckenkamp. Amongst these the works of Baumhauer seem to have been the most comprehensive. They dealt with minerals and other crystals. Some of the minerals they dealt with are still a source of considerable controversy. These researches were accompanied by theoretical studies and dealt with questions such as the conditions controlling the development of the etch pit, its relation to the crystalline molecule and to the symmetry content of crystals.

In the twentieth century possibilities arising from the

use of goniometric projection accompanied the works of leading figures such as Goldschmidt, Wright, Koller, Gaubert, McNairn and others. A complete reference to their works, as well as to the works of the above investigators, is included in an excellent work covering every aspect of the subject and illustrated by many practical examples by Honess.(104) Miers(32) made use of his special goniometer in studying the etch pit while it was developing in solution. The discovery and development of x-ray analysis of crystals solved once and for all the molecular arrangement within the crystals. The etch method as a means of determining crystal symmetry arrived at results that were mostly confirmed by x-ray analysis, but they have disagreed on the symmetry to be assigned to some species. The disagreement respecting these doubtful species arises from certain limitations in the x-ray analysis as well as from certain anamolies accompanying the shape of a stable etch pit.

Natural Etch Figures on the (111) Faces of Diamond.

Natural etch figures in the form of solution cavities produced by the magma are rarely observed on the octahedron faces of diamond. The only report of such a finding in the past is a sketch drawn by G. Rose,(105) and published in (1872). This is reproduced in fig (109). As was mentioned before (chapter 1) Fersmann and Goldsmidt(11) observed them on rare specimens. A. F. Williams who has probably seen many hundred thousand carats of diamonds reports the observation of such natural cavities on only one specimen.

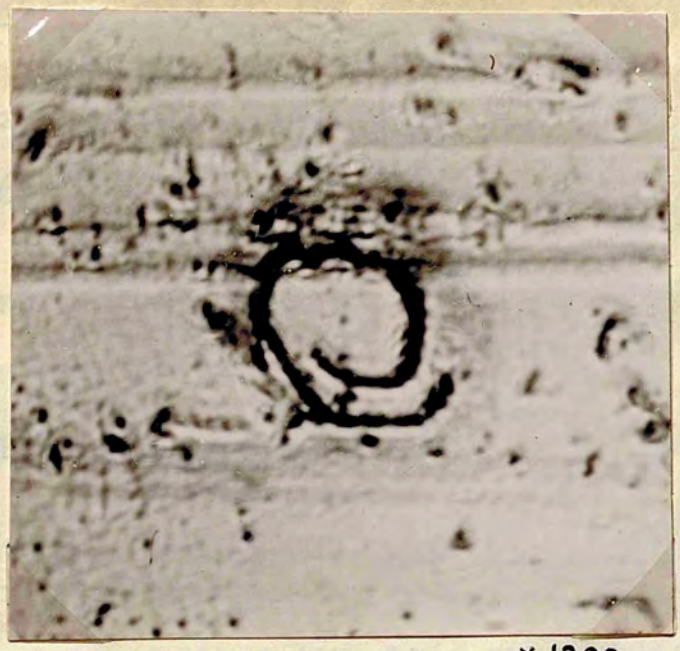

Fig. (111)

× 1300

Fig. (109.)

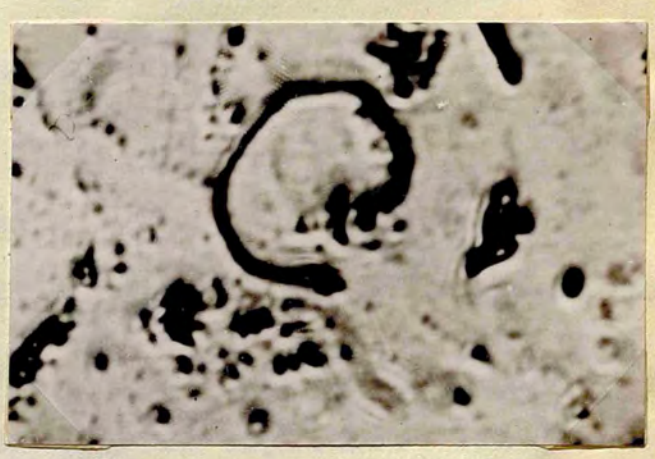

Fig. (112)

× 1800

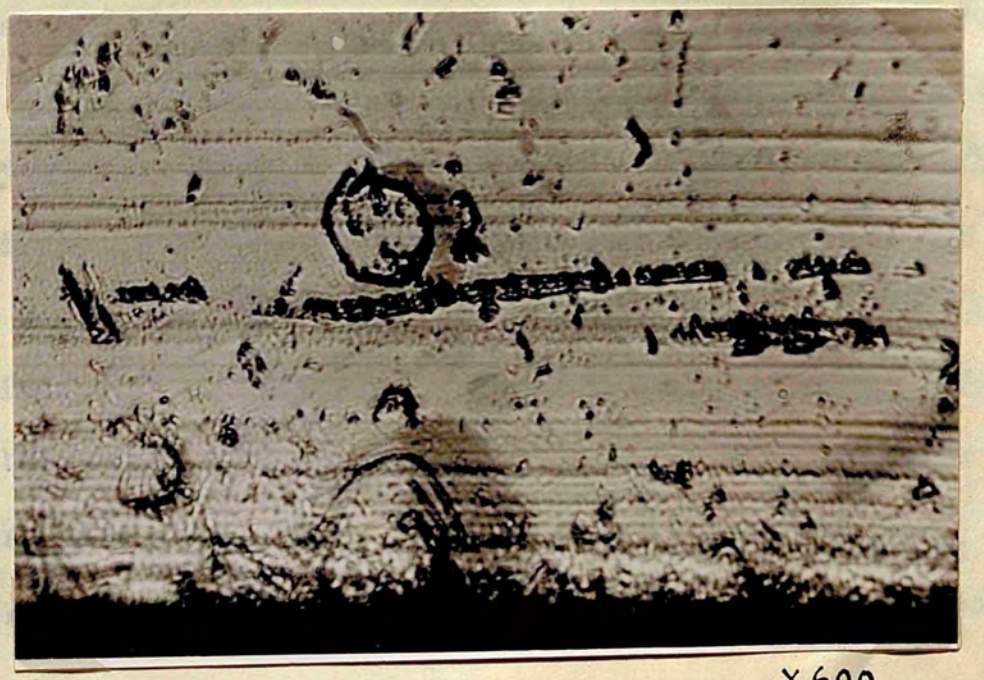

× 600

Fig. (113)

Previous Experiments on the Etching of Diamond.

(A) The Experiments of Luzi : 1892.

Luzi (106) as far back as (1892) showed that diamond could be corroded in molten blue ground. He exposed crystals for 20 to 30 minutes in a kimberlite flux at the very high temperature of 1770°C. The results obtained were very poor. Instead of getting triangular marks, he obtained irregular oval scars. This corrosion is due to the presence of oxygen in the flux, and the experiment runs against the idea that the blue ground is the original matrix of diamond.

(B) Experiments of Fersmann and Goldschmidt : 1911.

Fersmann and Goldschmidt (11) carried their experiments to investigate experimentally whether etching and solution produced the surface and reflection phenomena on diamond which they suspected to be solution phenomena on natural crystals. Their method was to plot the reflected light signals from the crystal surfaces on a goniometric projection, when growth structure was supposed to be represented by points and straight lines, and the solution structure by bent lines and patches of all shapes and sizes. They had in mind that the rounded forms of diamond were caused by solution, and the question must arise whether the Fraunhofer diffraction pattern from a small crystal surface can be trusted to give information about a surface that has already a fine structure.

They heated diamond octahedra and octahedral cleavages to

a temperature of about 900°C in potassium nitrate or soda fluxes. The attack lasted for a long time (sometimes several hours). They were mostly concerned with their theory of hemihedrism, but they certainly produced triangular and rounded etch marks. But no measurements were given, and all the drawings were made by hand.

(C) Experiments of Williams : 1932.

Williams introduced microphotography to the study of diamond surfaces and etch phenomena. He carried an experiment at the De Beers Laboratory assisted by Mr. John Parry. A diamond octahedron was subjected to the fusion of potassium nitrate (saltpeter) at the temperature of 900°C. The diamond was allowed to stay in the fuse for 2 hours during which time it lost $\frac{1}{3}$ of its weight. The photography imparted nothing new that was not known from before, and certainly the drawings made by hand looked better. (10)

Extreme importance was attached to the shape of solution cavities at the edge of the crystal. Williams connected this to an earlier observation by Rose, fig (109) and stressed the fact that his etching was nearer to Rose's observation than a similar description made by Fersmann and Goldschmidt. This peculiar edging the author has also observed in one of his etchings (c.f. chapter 15). Williams stressed the fact that the edges of the octahedron remained sharp with no rounding at the corners. We report at the end of this chapter a peculiar attack with an ultimate rounding at the corners of one specimen.

(19)

(D) Experiments of Wilcock : 1951.

The only experiment carried with the purpose of using interferometry did not materialise. Wilcock realising that previous experiments were of a damaging nature decided to carry his experiments in the cold. He began with the very low temperature of 200°C, and reached 600°C in stages. He detected the existence but not the shape of the etch pits. His only fault is that he depended too much on interferometry.

Etchings carried in the Present Investigation.

This chapter describes the results obtained by etching diamond at the comparatively low temperature of 525°C. The next chapter describes the results obtained by slightly increasing the temperature to 550°C and higher temperatures. The experimental procedure is the same, and consists in thoroughly cleaning the diamond with various reagents and the use of distilled running water. A nickel crucible was used for the lower temperatures and a platinum crucible for higher temperatures. The oven used was a small muffle furnace with controlled temperatures that remained constant within 10°C. The thermocouple registering the temperatures was tested with exact potentiometric arrangements. The etching substance was saltpeter (Potassium nitrate) and was of the purest quality obtainable "analar". These precautions were necessary in view of certain fears that impurities may change the shape of etchings. (9) Although in the case of diamond, the etching depends upon the oxidation of carbon, it is legitimate that this operation be carried out in clean

Fig. 1

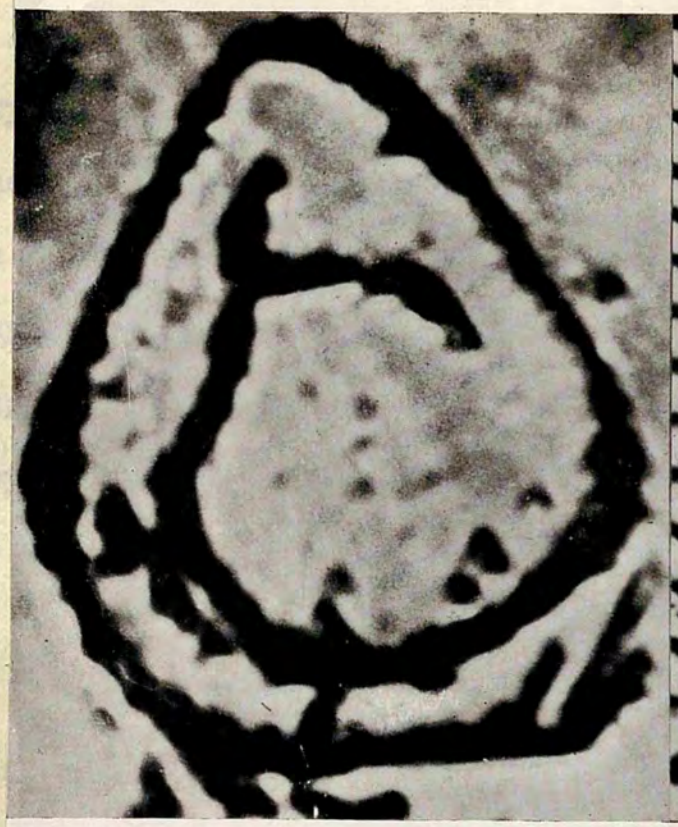

×5400

Fig. 2

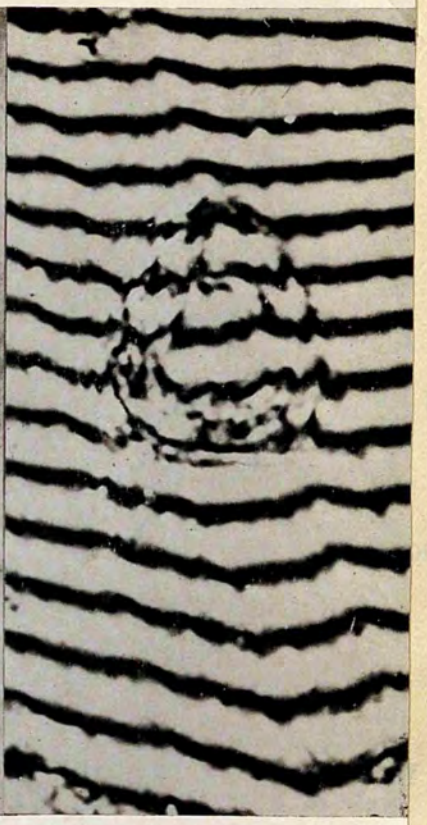

×1600

Fig. 3

×1250

Fig. 4

×1200

PLATE (110)

surroundings. The action of the melt (i.e. the nitrate or carbonate) depends on its ability of providing a limited amount of oxygen at any time. It carries its oxidizing agent, and by its fluidity permits the solution currents to follow their own rules. The process is actually a slow burning of the carbon atoms that are diamond. If advantage is to be taken of the limited supply of oxygen, the etching must be carried at the lowest temperature possible. Since the onset of etching may be detected by the use of modern means including interferometry, it is in line with the above argument to use the mildest reaction possible.

Crystal H (Etching for 2 hours at 525°C)

In contrast with earlier observations in this field very few etch pits appeared. These were exceedingly small and were as expected oppositely oriented to the trigons. In addition features have appeared of some considerable interest in connection with the recent theories of growth by spiral mechanism. The onset of etching took in many cases a spiral form, sometimes simple, sometimes complex. Fig (1), Plate 110 is a typical case. This is highly magnified in order to make clearer the fact that the spiral consists of a chain of triangular etch pits, and furthermore the spiral does not close up although it branches as it progresses. The central first turn is decidedly hexagonal. Fig (2), Plate 110 is the interferogram of the area surrounding the spiral. This is taken with the thin film (unsilvered). It should be noted that ordinary interferometric techniques are useless in front of small features. Here it is seen for example

that the fringes kink in passing over the arms of the spiral, and measurement reveals that the approximate depth is about 700 Å, and is moreover reasonably uniform in both arms.

The spirals are rarely more than one turn, and fig (3), Plate 110 shows another typical spiral. The C - shaped figure to the left is another spiral in the making. In all cases the spirals appear to consist of chains of contiguous small triangular etch pits all oriented in the same direction. In all the photographs they are made to lie with one angle upwards. Some of the spirals were right-handed and some were left-handed, but they all had their heads upward as in figs (1) and (3) Plate 110. Another spiral is in fig (111). It is a hexagonal spiral with a rounding in some parts. With respect to the spirals we are in doubt as to their origin. They may have been intended to be closed figures, and for one reason or another, they have been diverted from the closure. But why after all should a closed figure be formed. If the spiral tendency exists in the surface, why does it not endow the spiral with more turns? It is with an effort to achieve more turns that the crystal was afterwards subjected to the etching for four consecutive hours (c.f. chapter 15). Fig (112) shows another example. This is not a closed figure and appears as if it is made of two parts of a hexagon stuck together. Fig (113) shows in modern terminology the meeting of a right and left-handed spirals; somehow the R.H. tendency predominates. All these figures are perplexing and divert one's attention to other fields which may or may not give the right interpretation. In addition, exact parts of a real

Fig. (114) X 1200

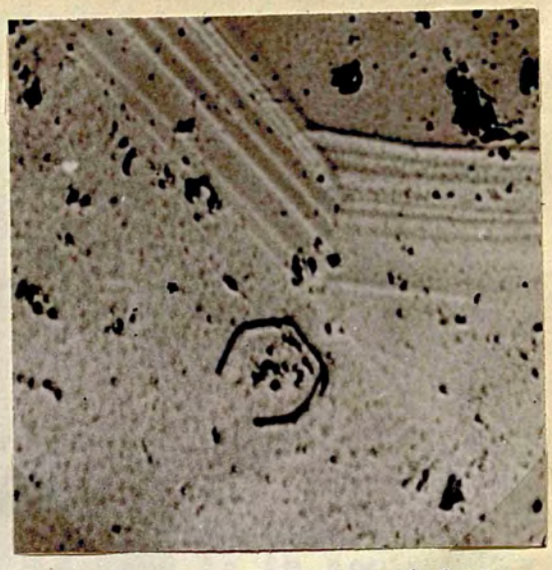

Fig. (114) X 1200

Fig. (114) X 400

Fig. (118) X 350

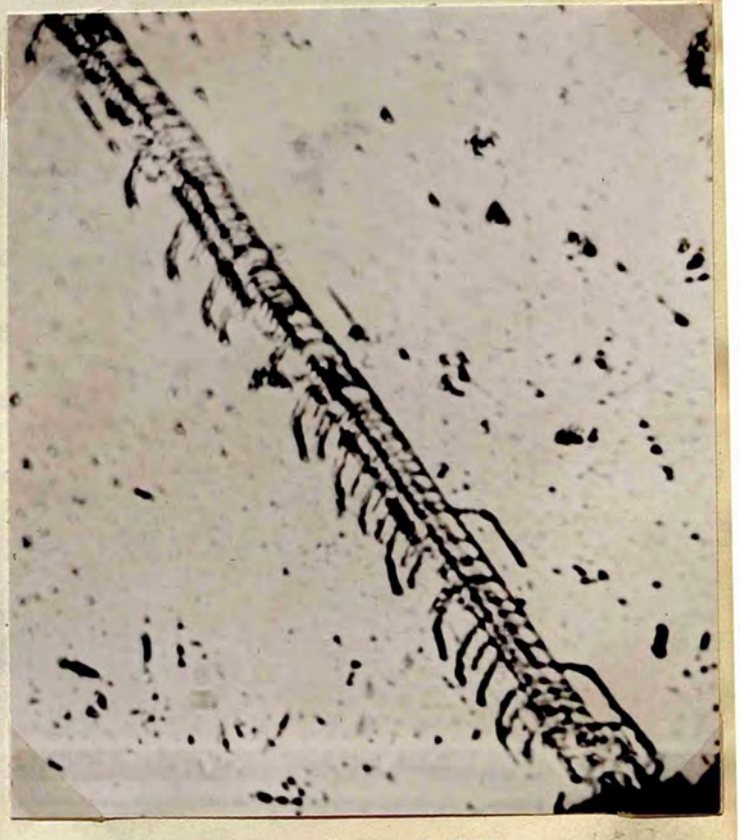

Fig. (118) X 1200

hexagon appeared. These comprised 1, 2, 3, 4 or 5 sides of the hexagon, but no complete hexagon was observed on this crystal. An example is in fig (114).

The Crystal Tested:

The crystal used is part of an octahedron, and has one well developed natural (111) face. The extent of this face is revealed by fig (116). Fig (116) is an interferogram of the face. The face contains bosses at its lower right hand corner which represent powerful centres of growth. Their united wave front appears in the upper part of the picture, and is in conformity with their outline at the bottom. The parallel lines at the top represent edges of growth fronts that primarily covered the face. From the shape of wave fronts the direction of growth in the last phase is upwards, and it may not be a coincidence that the heads of the spirals are in that direction too.

The face contains no major trigons but some very faint triangular marks were observed on one of the hillocks. Fig (117) represents the extent and shape of etch over the whole face. The bent lines and scars are actually grooves caused by the etching, and represent chains of triangular etch marks. Some of the straight or nearly straight grooves represent chains of hexagons (fig 118). The hexagons are not hexagonal etch pits, but hexagonal markings which are in fact rows of small triangular etch pits. As can be seen from fig (117) there is no preferential place for these markings on which to arise. They develop equally on the top of hillocks as well as on the planer areas beneath. The spiral marks referred to above are very small and cannot be seen in fig (117).

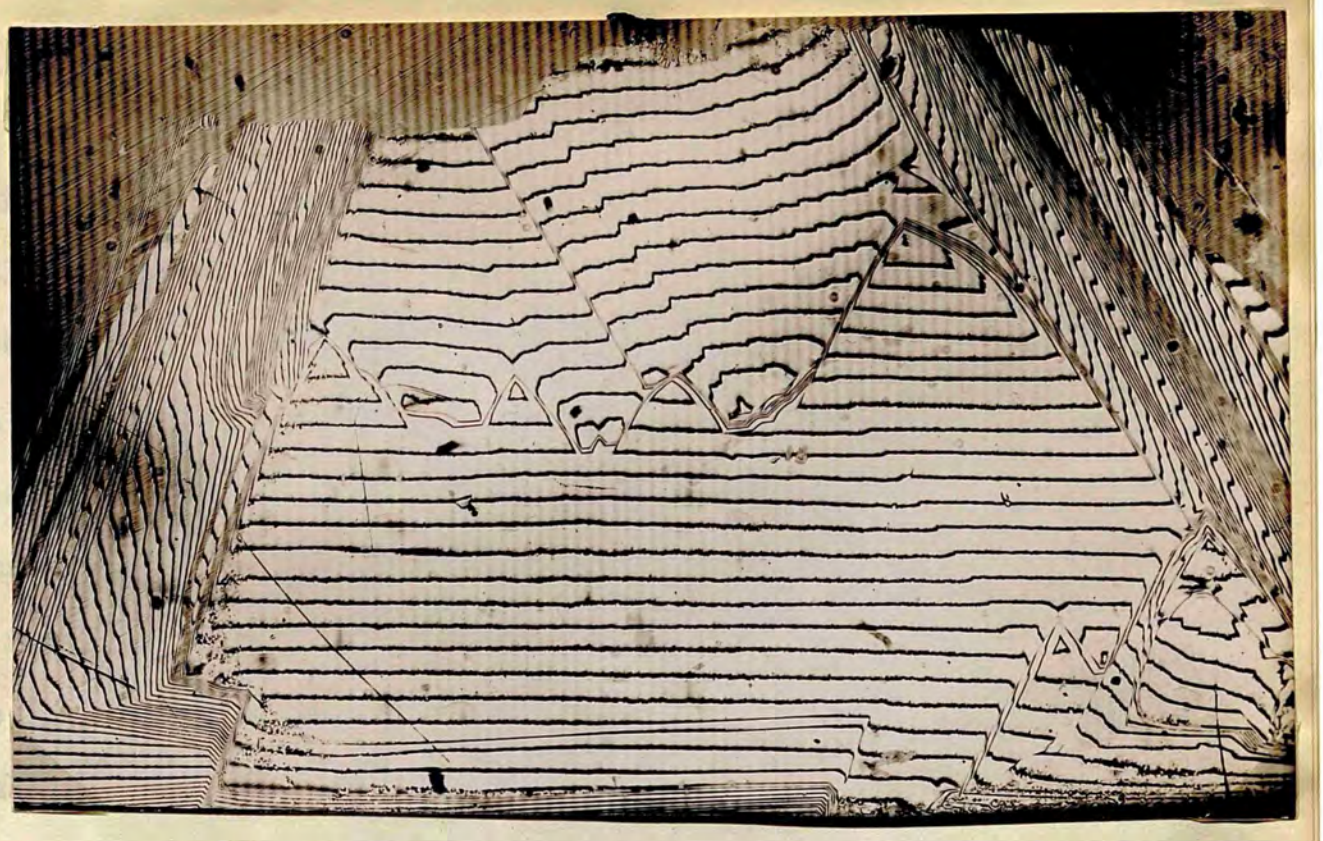

Fig. (116) X60

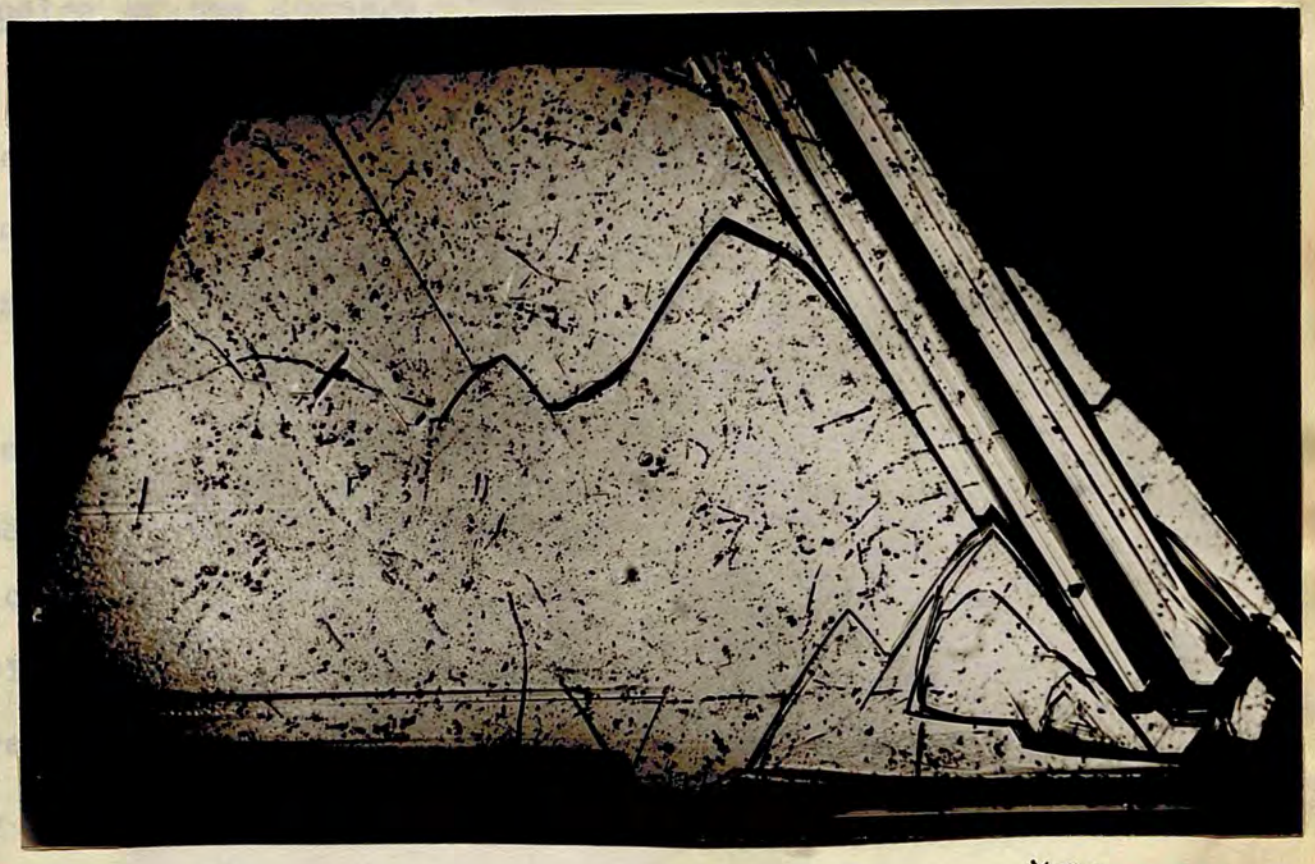

Fig. (117) X60

Solution Canals:

Etch pits in the form of straight rows have been observed on diamond by Fersmann and Goldschmidt.(11) They observed them mostly in lines $\perp^{r}$ to the sides of the triangle, and fig (119) represents their one and only drawing. Rows of etch pits have been observed by Honess on the basal plane (0001) of apatite.(104) He calls them solution canals, and comments on their rarity. According to him they may represent a line of secondary cleavage, but not necessarily so. He also discovered that they need not necessarily be straight lines and can form symmetrical curves. He also mentioned that these curves are difficult to explain. It should also be mentioned that the density of our scars on the surface is also very small.

Rounding of the Corners.

Although the reaction was not excessive, crystal H was severely attacked at both corners. This is clear in fig (120) which shows one corner.

Crystal C (Etching for 1 hour at 525°C)

The reason for choosing this temperature, is that etching at a lower temperature e.g. 450°C for as long as 16 hours at stages gave no reproducible results. Instead of choosing 500°C which is the nearest round figure to 450°C, it was thought advisable to stick to the temperature that gave visible and interesting results viz: 525°C. Another reason is that comparison may be needed later. It was also decided to shorten the time of etching to test the time factor. Crystal (C) has been studied

Fig. (119)

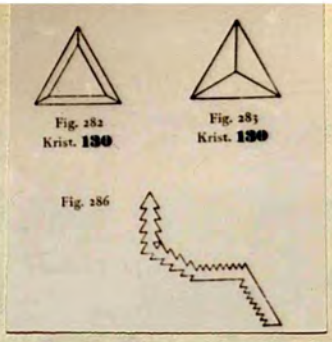

Fig. (120)

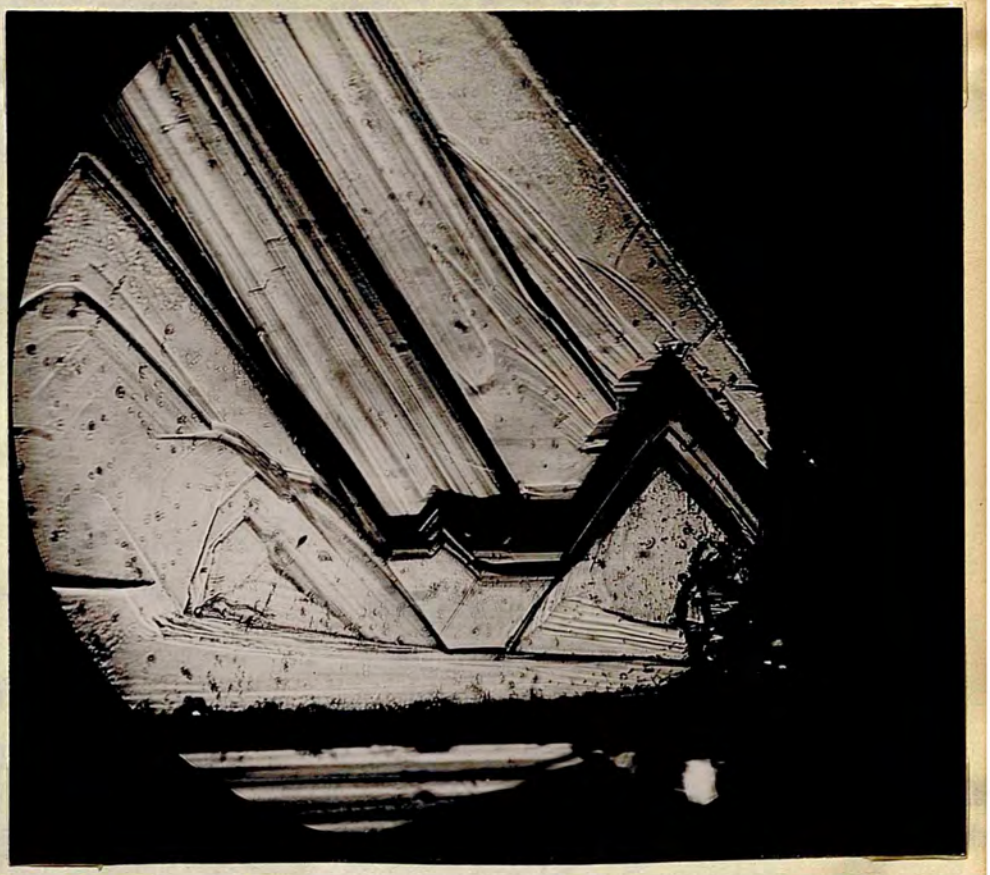

X 140

Fig. (121)

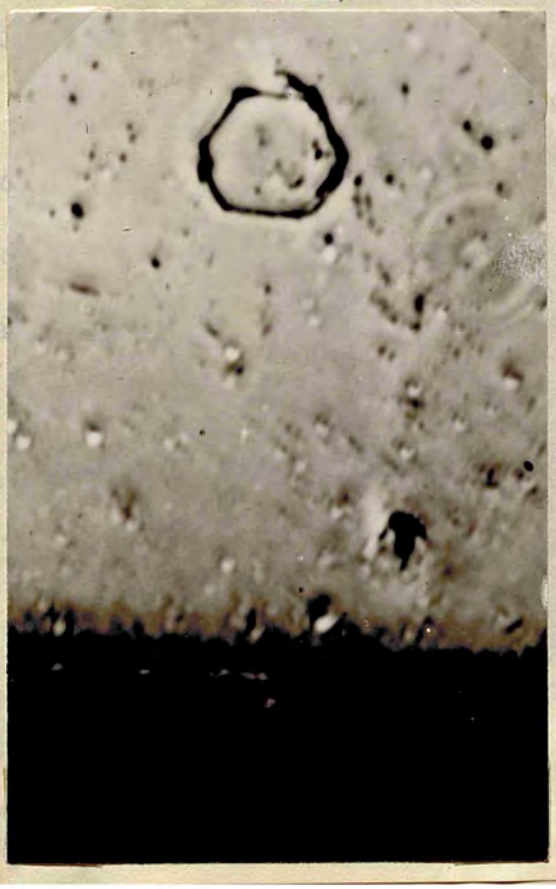

X 1800

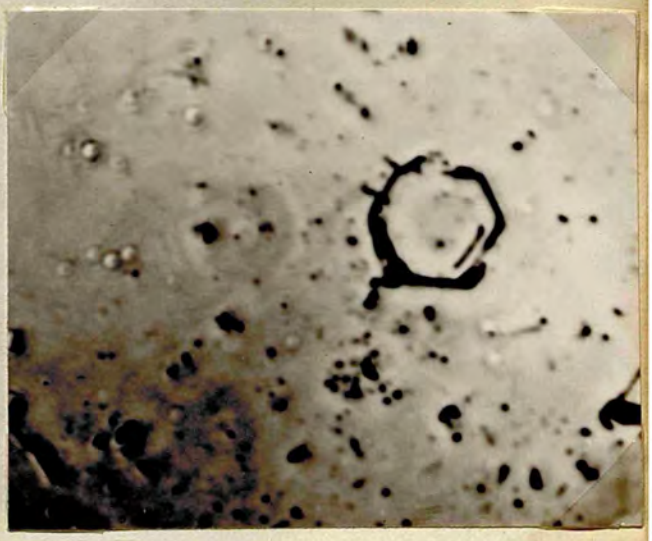

Fig. (122) X 1800

in detail in chapter 8 of this thesis. As its surface was extremely plane it affords a good specimen for study by interferometric means, if the etching is continued further on. Crystal C gave also very few and extremely small etch pits. Instead of the spirals, closed hexagons were obtained. Examples of these are in fig (121) and (122). The hexagons are regular and nearly closed. Some of the hexagons were elongated, two symmetrical curves replacing four sides of the hexagon. The short sides are nearly // to an octahedron edge, fig (123). The elongated figures either lie // to each other or take transverse positions at 60°. One of the hexagons fig (124) had a tail, and this may give a clue to the spiral. The density of these scars were much smaller than it was for crystal H (this is only a time factor).

Conclusions and Deductions.

Since the publishing of the author's article on the etching (107) of diamond, experiments were conducted both in Europe and America (80) (81) to see if similar effects can be produced on other crystals. The results came positive and spiral formations of etch pits were observed on Si-C and other crystals. Although these works were inspired by our work on diamond, there is still the basic difference that they are carried on crystals that generally produce growth spirals, and on which growth spirals were definitely seen by the observers. In a recent article Mott (96) enumerated chemical action as amongst the things influenced by dislocations. The first hint in that direction came from Lacombe (108) in a report connected with veining in aluminium. He observed that in a

Fig. (124) x1600

Fig. (123) x1400

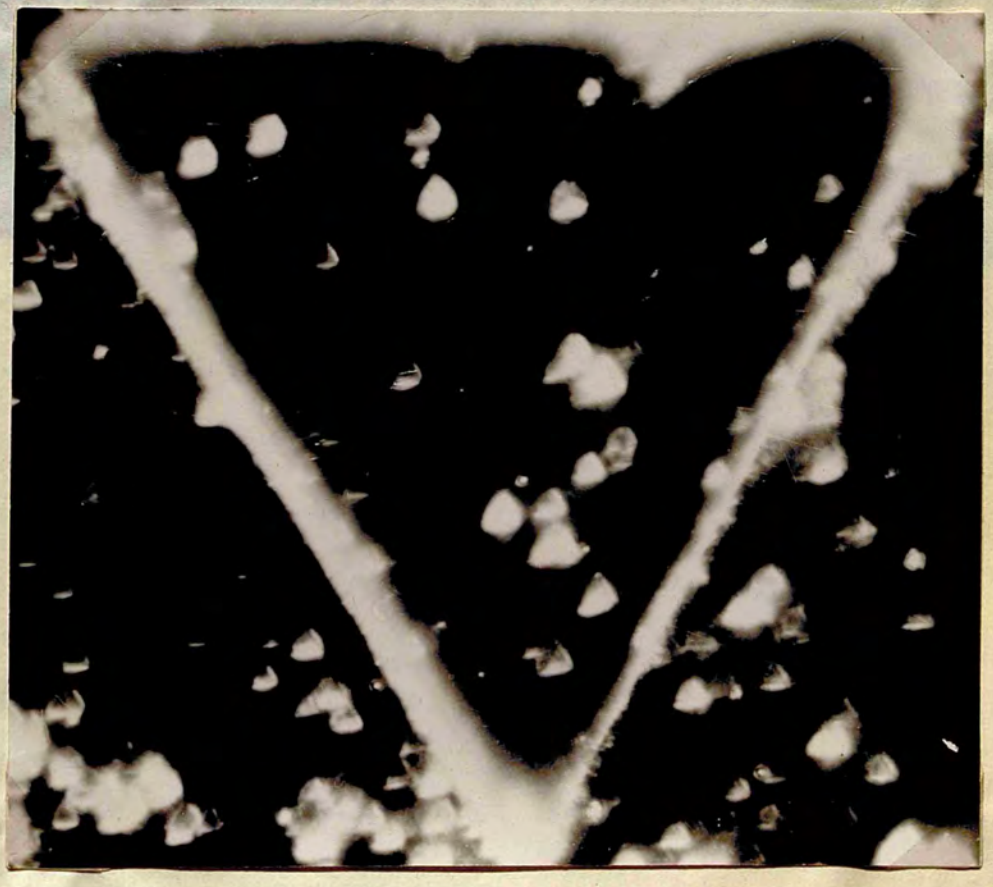

Fig. (126) x 1000

Fig. (125) X1800

single crystal grain, there are faint lines (or veins) which are revealed as rows of separate etch pits, under suitable etching conditions. Shockley and Read (109) have stressed the fact that each etch pit originates at a dislocation, where according to their view, the free energy of the stressed material will be higher than elsewhere. The pit then grows to a large size so that it is optically observed. Dislocation lines in the views of the same authors (94) can be spirally wound and can form successive closed loops.

Hexagonal figures may be expected to occur on the basal planes of hexagonal crystals but not in cubic crystals. This is not overlooking the fact that hexagonal close-packed and face centred cubic crystals are much more closely connected than would appear from their structures; both represent spheres in their closest packing. Tightly packed rows of atoms run in six directions through h.c.p. and f.c.c. structures, (73) and on the (111) face of diamond three rows of densely packed atoms exist. If the etching proceeds in a sweeping attack, eddies perhaps would be produced, and the six-sided figures and the spirals may perhaps be explained. But why should all the heads of the spirals on one face lie in the same direction?

CHAPTER FIFTEEN

Etching at Higher Temperatures.

Time and temperature are the only variants at our hand in etching with a certain reagent. Both have been tried and this chapter comments on the etching of diamond at 550°C and higher temperatures. As the same crystal is etched again for higher temperatures, time is an important element. Temperature speeds up the reaction immensely, and shortens the time of etching. However, the first crystal to be described under the category of higher temperatures was not actually etched in that sense. This is crystal H of the previous chapter. Etching it again for a long time at 525°C gave results similar to what is described in this chapter.

Crystal (H) Etched for 4 hours at 525°C.

Crystal (H) (c.f. chapter 14) gave etch spirals after two hours at 525°C. As the spirals were not complete, and as etching for shorter times would perhaps develop more incomplete spirals, it was decided to carry on the etching for a long time: 4 hours. Instead of the spirals developing an altogether different phenomena appeared. The growth features were well preserved but the long sought for etch pits appeared in a visible form. These appeared in thousands and filled the whole face. Not only did the spirals cease to grow, but no new spirals developed. Solution canals behaved in the same manner. Both appeared broader due to the increase in size of the etch pits forming them. The etch pits were difficult to photograph with

good contrast; diffraction at their edges obscured their outline too. The film technique meant for good contrast (c.f. chapter 10) was tried. The triangles appeared beautifully coloured and revealed the true outline of the etch pits. Fig (125) is the interferogram of part of the surface taken with this film technique. It shows only the triangles that appeared with green mercury light. The unsilvered film is not sensitive to small changes in depth, and cannot be a guide if a group of triangles appear with the same colour. Beyond the fact that they were less than $\frac{\lambda}{2}$ in depth, no information could be obtained as to the actual distribution of depth amongst the etch pits. The figures ranged in size from 2 to 6 μ; needless to say ordinary interferometry e.g. at high dispersion could not have detected the shape of these features. At its best dots could only appear in place of the triangles. However, high dispersion could not be applied on account of the curved nature of the face. Fig (126) is similar only in appearance to fig (125). This is a dark ground illumination picture which represents the area of a trigon on crystal C, etched under similar conditions. On account of the diffuse light the etch pits appear larger than what they actually are, and the shape of the etch pits is not clear. Fig (125) has been taken by covering the crystal with a thin layer of oil; its superiority to well established techniques needs no further comment. The density of etch pits on Crystal H differed little from place to place and is between 5 and 8×10^6 per $cm.^2$

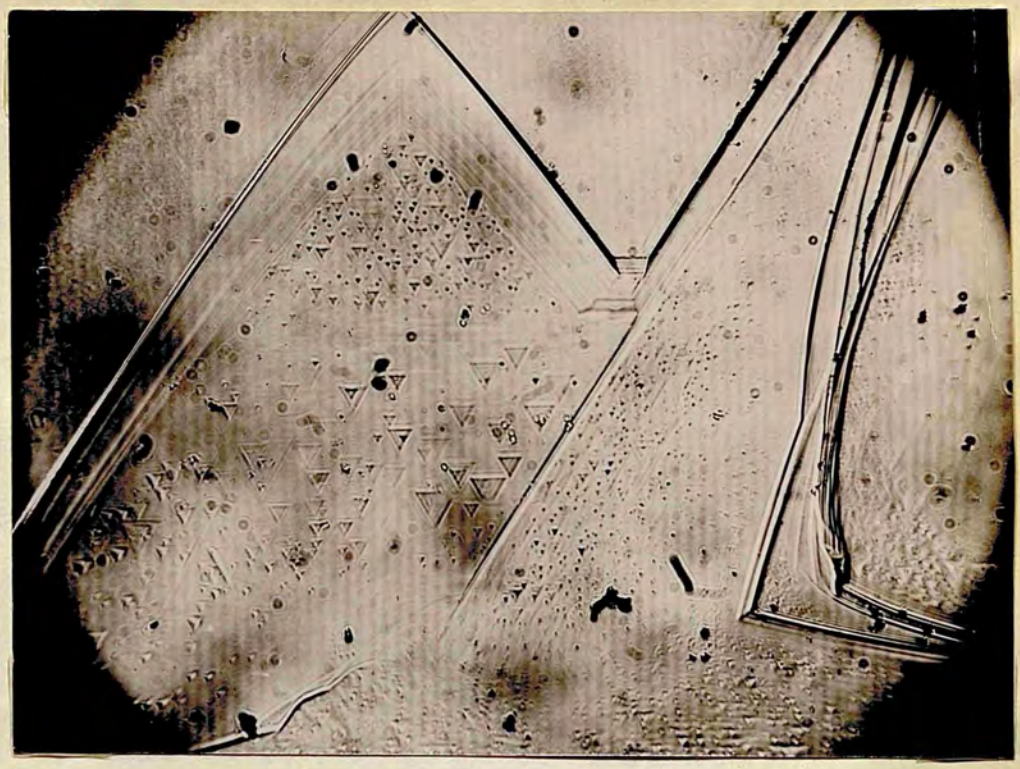

Fig. (127)

×400

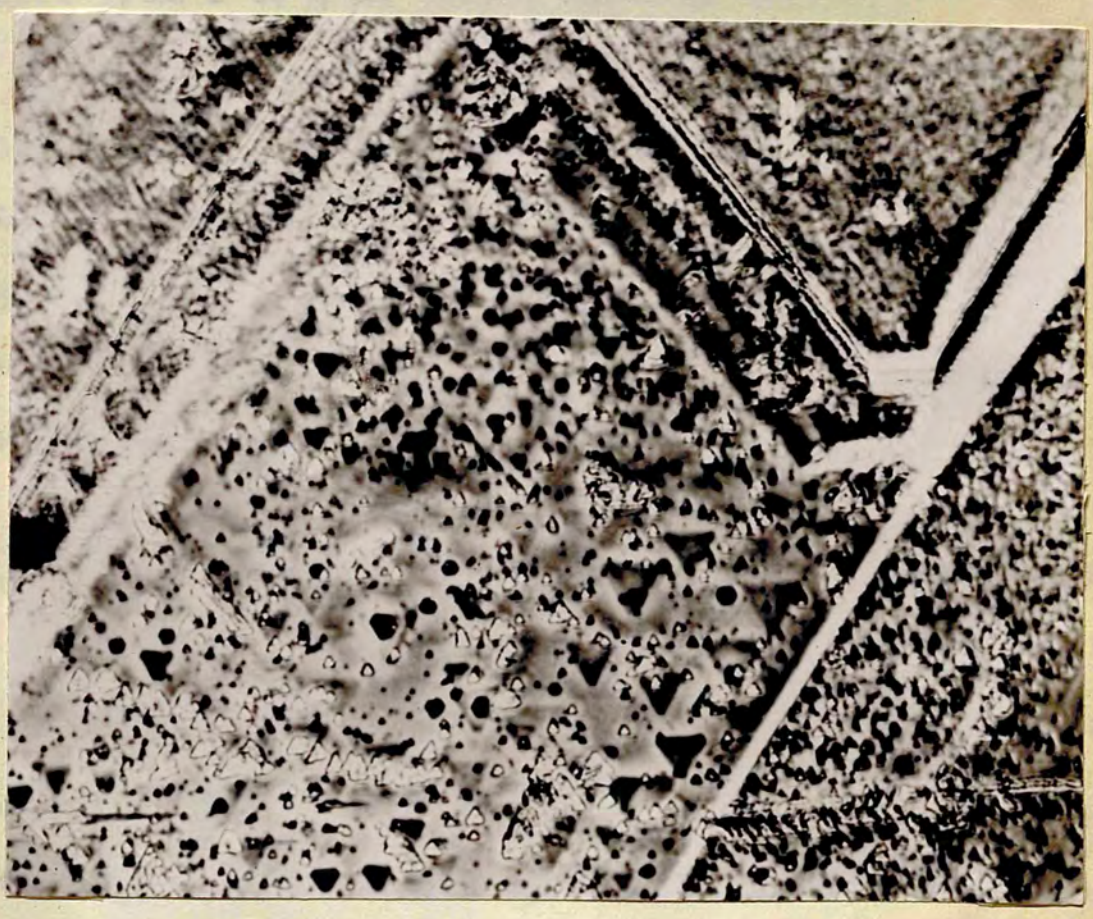

Fig. (128)

X640

One point is perhaps worth mentioning. One of the hillocks had been described (c.f. chapter 14) as having faint trigons on its surface. As they could be photograped by ordinary means they are perhaps 200 Å deep. These are shown in fig (127) before the etching took place. The black spots are failing marks in the silver. Fig (128) shows it after etching took place for 4 hours at 525°C, following the two hours of previous etching. This is a phase contrast picture, and seems to give the impression that the trigons, referred to, were lightly affected by the etching.

Crystal C Etched for 1 hour at 550°C.

Crystal C has been etched previously for 1 hour at 525°C. The etching for a further hour at 550°C produced etch pits that varied in size from 1 to 4 μ. Their density varied between 1 and 2 x 10^7 per cm^2. The average size of etch pits is a little bit less than what has been attained in Crystal H after 4 hours etching at 525°C. Also the density is slightly greater. Considering that cyrstal C has been etched only for 1 hour, the enhanced effect is due to the slight increase in temperature. As the behaviour of both crystals was nearly the same at 525°C, the effect of 4 hours etching at 525°C nearly corresponds to 1½ hours etching at 550°C. Fig (129) represents an area of the surface of crystal C before any etch took place, and fig (130) represents the same area after etching took place. It represents a trigon bounded by two hillocks near the edge of one face. Etching occurred in rows along the edges of growth sheets of

Fig. (129)

X 600

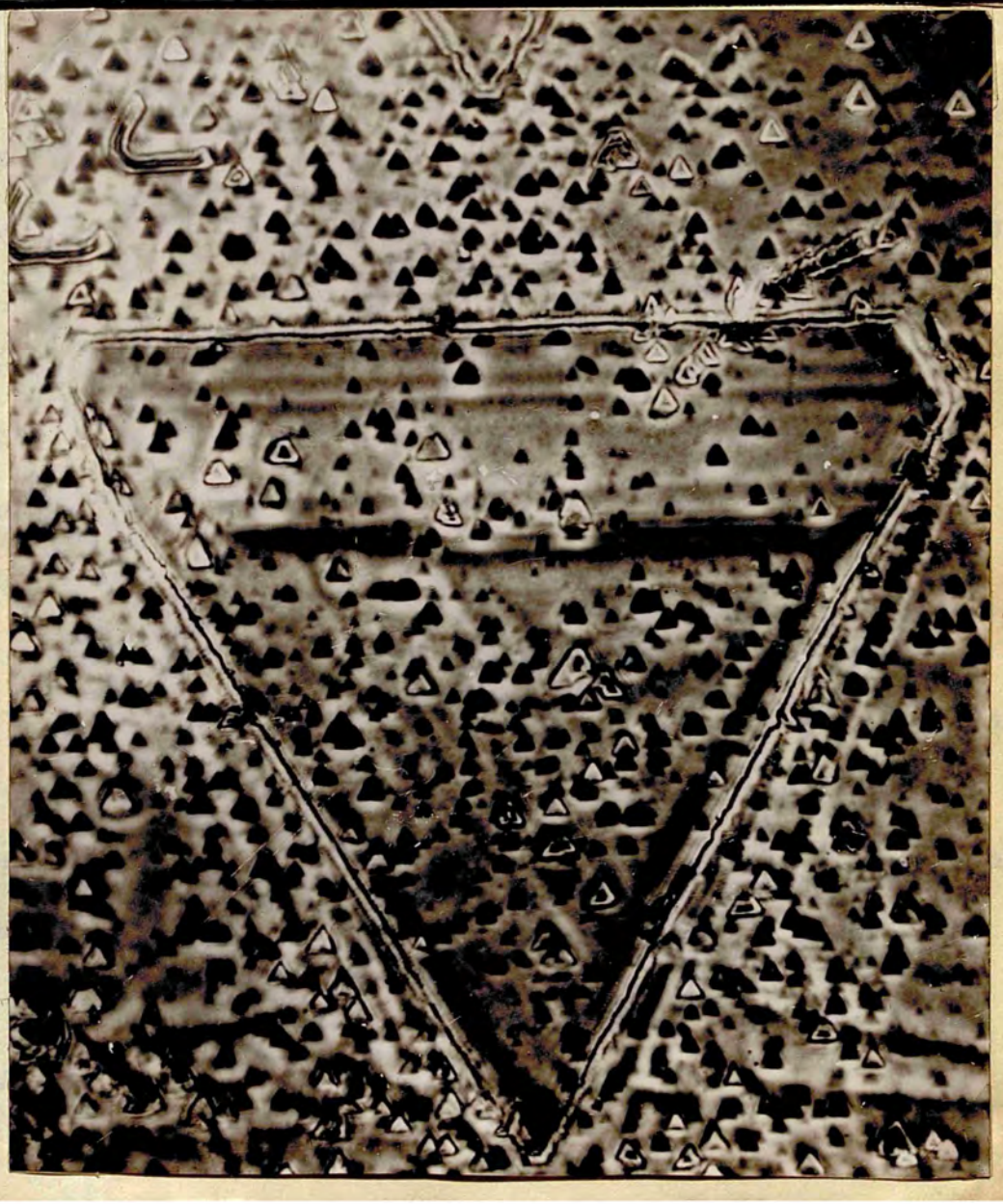

Fig. (130)

X 900

the hillocks. The apparent density of etch pits inside most of the trigon is comparable with that outside it, but the density in the higher part is very much less. On the average the proportion of mature etch pits inside the trigon is less than it is at the hillocks. The phase contrast picture shows more of the faint pits, and confuses the whole issue.

Interpretation of Results.

Fig (131) shows another area on the surface (crystal C) including a trigon, after etch took place. It is quite clearly seen that the proportion of etch pits of the same intensity is very much less inside the trigon than outside it. If we think of the etched parts as weak points in the lattice, the density of such points inside the trigons is less. If we resort to dislocation interpretations (c.f. chapter 14) the number of dislocations in the pyramids is much more than it is in the trigons. Still there is perhaps an easier interpretation: the etching is a sweeping effect, and is not of the nature of a frontal attack as thought by Buckley.(9) Being of this nature it must be very sensitive to changes in level in the form of depressions. As a rule the etching is retarded over the floors of trigons.

Crystal C, it may be remembered, has an extremely flat surface, and is characterised (c.f. chapter 8) by extremely faint trigons of the order of 25 Å deep. It is not expected that shallow features will affect the distribution of etch pits (which at 550°C are deep enough). Still, we reproduce in figs (132) and (133) an area of the surface before and after etch. From these two pictures it is easy to see that a relation does not exist.

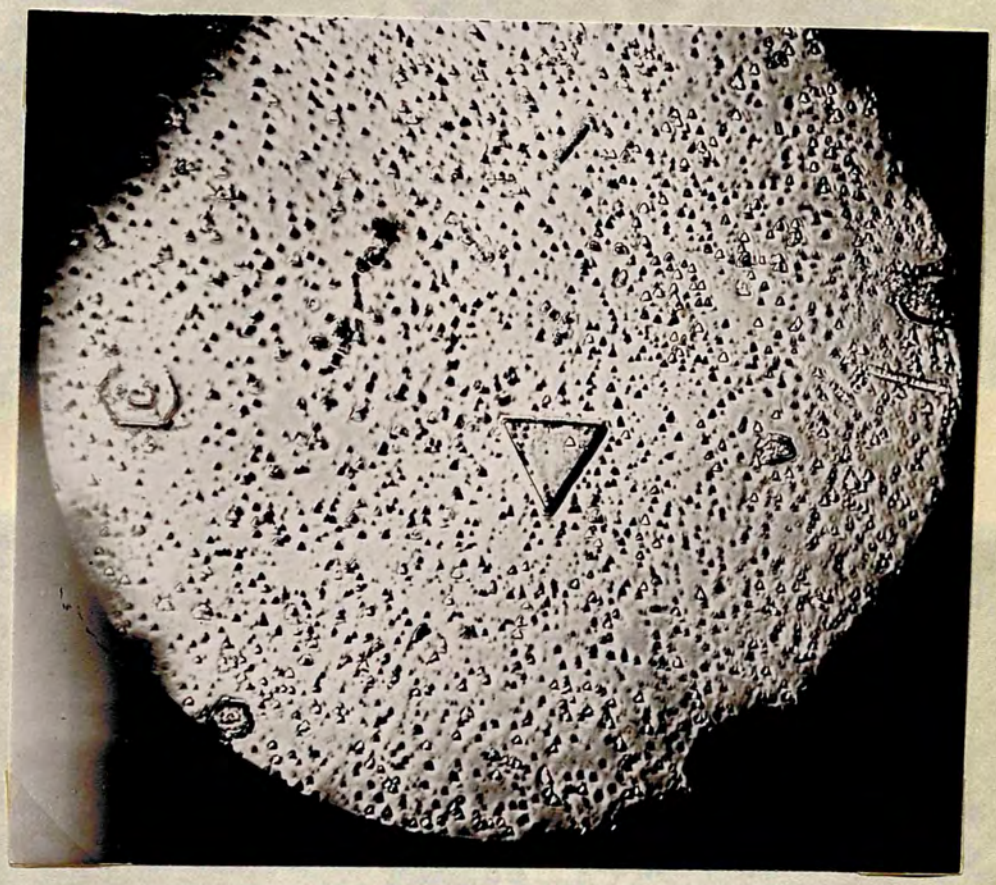

X 300

Fig. (131)

Fig. (132) X 270

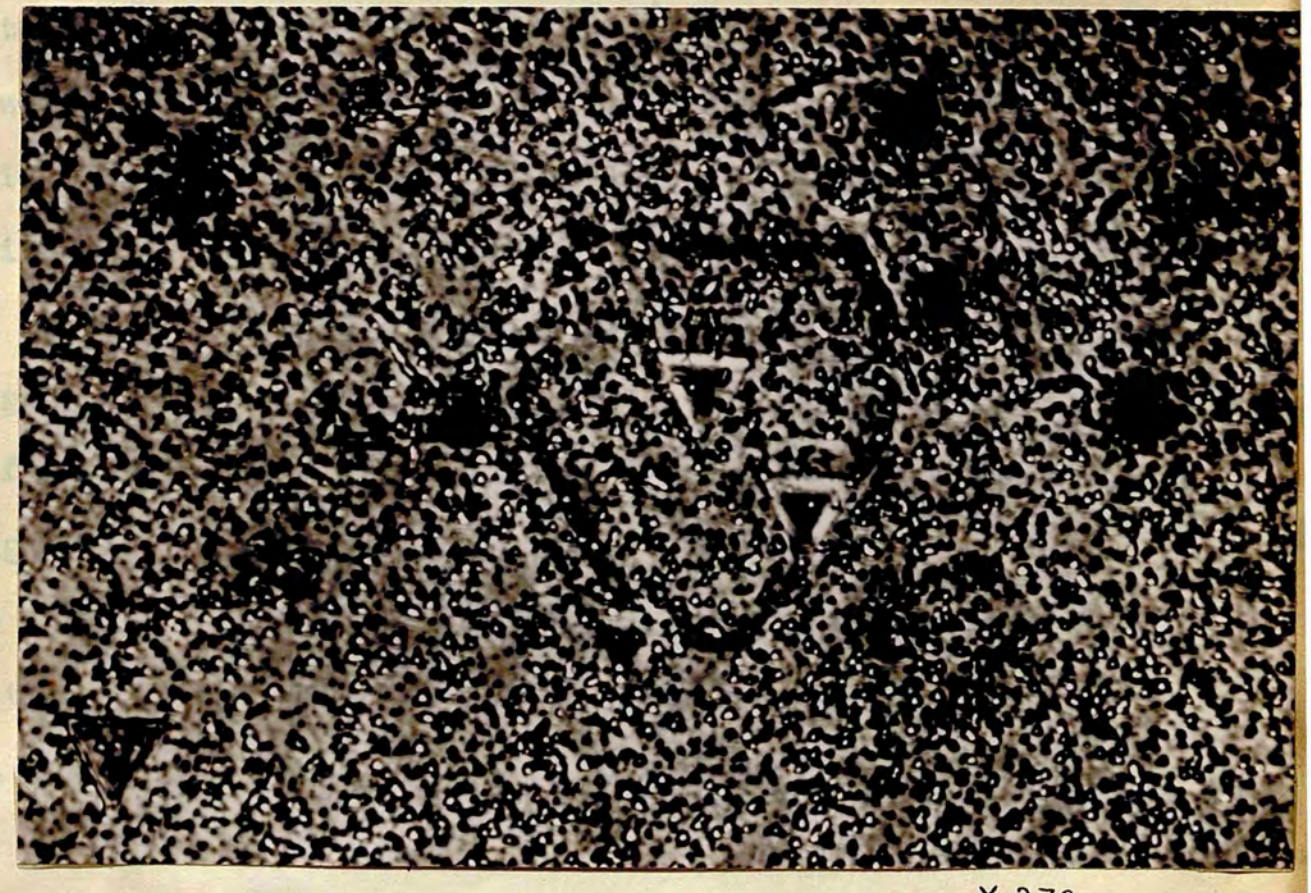

X 270

Fig. (133)

Distribution of Depth Amongst the Etch Pits.

By silvering the crystal and matching it with a $\frac{\lambda}{40}$ flat, fig (134) is the result. The wedge apex is to the left, and it is seen that pits appear as dots shifted towards the wedge apex. The silvering was 94% but the fringes appear broad on account of the small surface irregularites (the pits). Aside from this broadening it is clearly seen that the density of the etch pits in the vicinity of the fringes is greater, their number tailing off as a fringe of a previous order is reached. But the magnification exposed in fig (134) also the dispersion is not enough to give an idea of the exact distribution. For this purpose fig (135) at 575°C was obtained when two fringes existed over the entire surface of the crystal. Hypothetical lines in the highly densed areas can be made to represent the position of the fringes. The shift of any pit as a fraction of an order is a direct measure of its depth. To obtain the distribution it is only necessary to count the pits at equal distances in a strip $\perp^r$ to the fringes. The number decreases exponentially and no pit appears to be deeper than $\frac{\lambda}{2}$. This precaution in judgment is necessary. If there are pits deeper than $\frac{\lambda}{2}$, their shift to the previous order will lead to false results. A diagram representing the true distribution is drawn in fig (136). The trigons exposed in figs (134) and (135) are those revealed by the green mercury light; it is also expected that some of the small and faint pits will not appear.

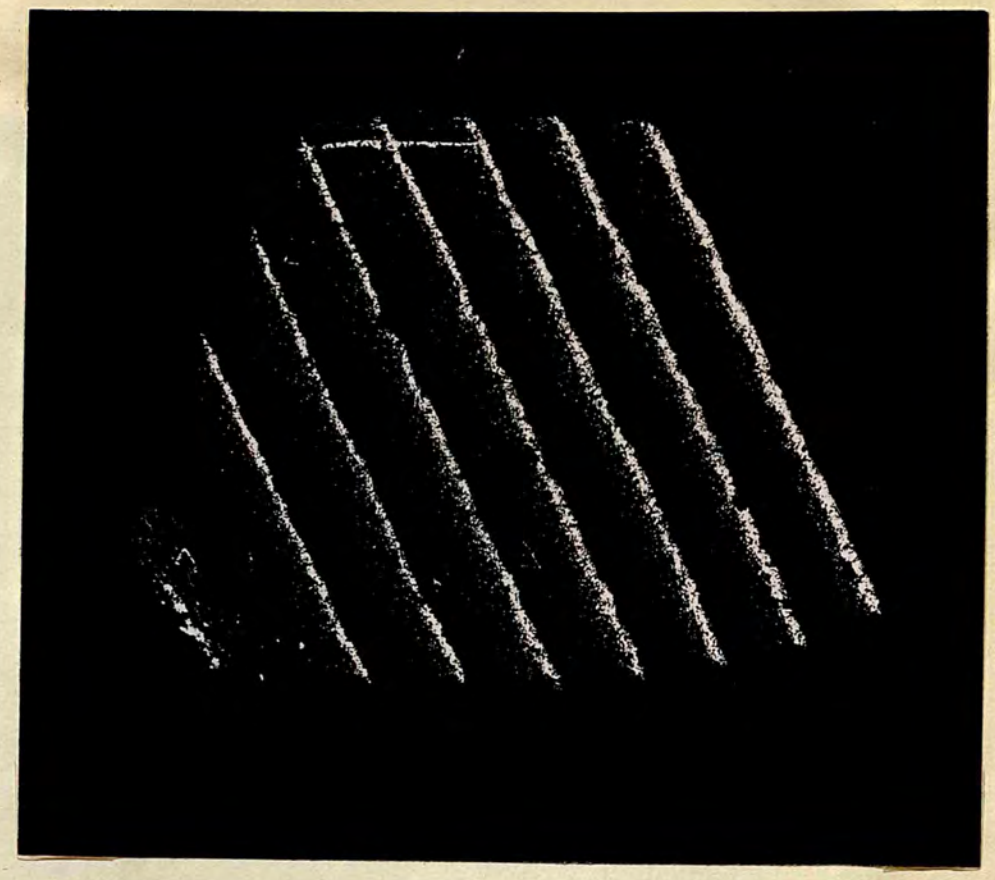

Fig. (134). X45

Fig. (135) X90

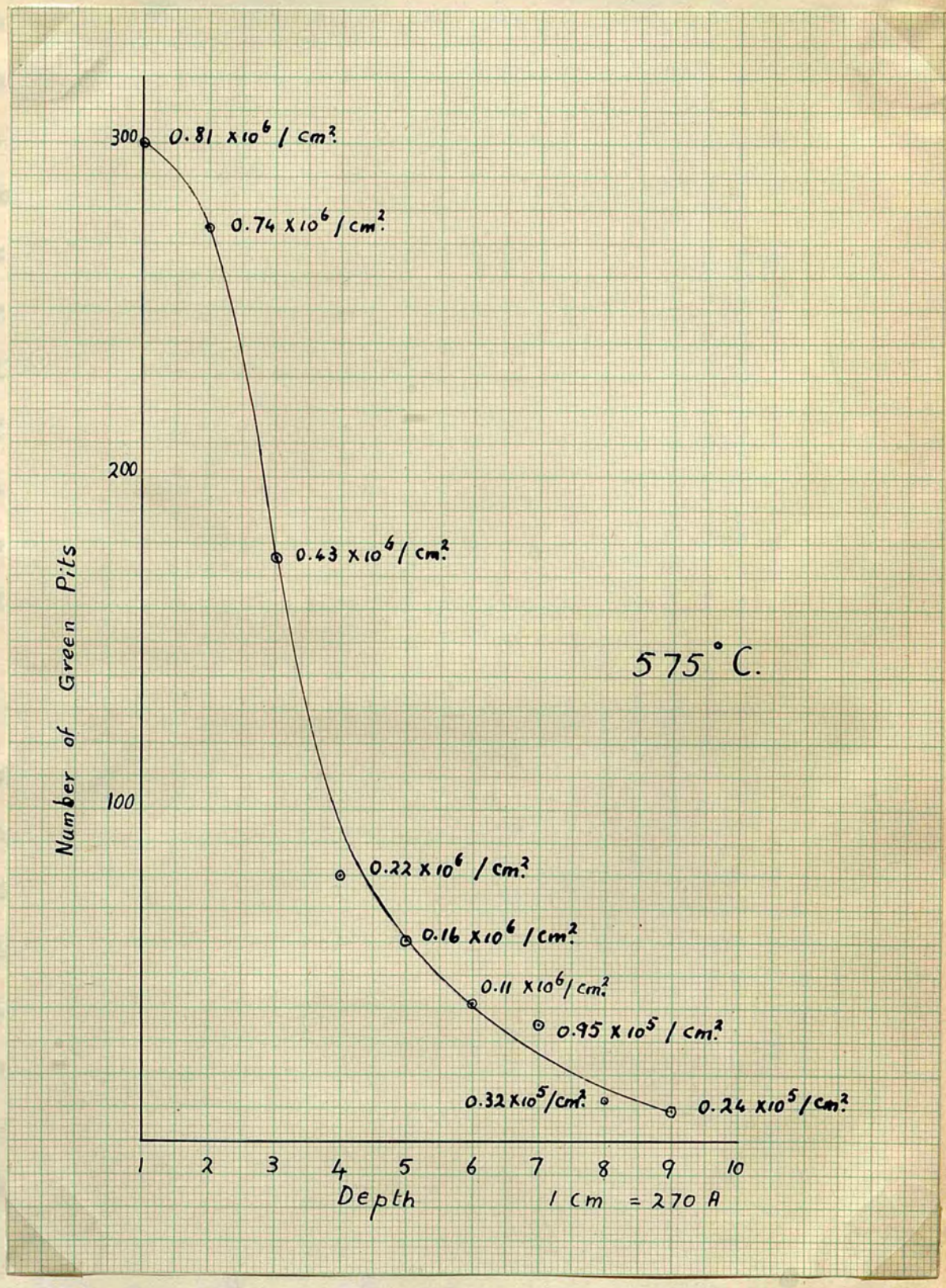
300
200
100
Number of Green Pits
0.81 x 10^6 / cm^2.
0.74 x 10^6 / cm^2.
0.43 x 10^6 / cm^2.
0.22 x 10^6 / cm^2.
0.16 x 10^6 / cm^2.
0.11 x 10^6 / cm^2.
0.95 x 10^5 / cm^2.
0.32 x 10^5 / cm^2.
0.24 x 10^5 / cm^2.
575° C.
1 2 3 4 5 6 7 8 9 10
Depth
1 cm = 270 A

Fig. (136).

Crystal C Etched at Higher Temperatures.

Crystal C was then etched at higher temperatures at intervals of 1 hour, the temperature increasing at each stage, 25°C at a time. This was continued until 650°C had been attained. Figs (137), (138) and (139) represent the whole of face 2, and figs (140), (141) and (142) represent one and the same part in face 1. Fig (137) and (138) represent etching at 600°C for two consecutive hours. Before 600°C the pits were much smaller and greater in number. Fig (139) represents the result of 1 hour etching at 650°C following the above two etchings. The etching for 1 hour at 625°C is not included. The etch pits can be followed quite easily as some of the more developed pits have deeper and thicker edges and appear black. Each pit progressively increases in size, and of course the distance between the centres of corresponding pits remains exactly the same. By following the above self-evident rule, and taking account of the shape and colour of certain pits, it is easy to see how the etching advances. At first sight the figures look quite perplexing as the number decreases progressively; also they increase in size and appear nearer. The active etch pits advance (and all the pits advance) until they devour or incorporate the less active ones in their own territory. In fig (139) they have decreased in number to such an extent they could be counted for the whole face directly by sight. Their density is now 8×10^4 per cm^2 which means that they have decreased 200 times since the onset of etching started. With

THE FACE ETCHED. X60

x 60

Fig. (137).

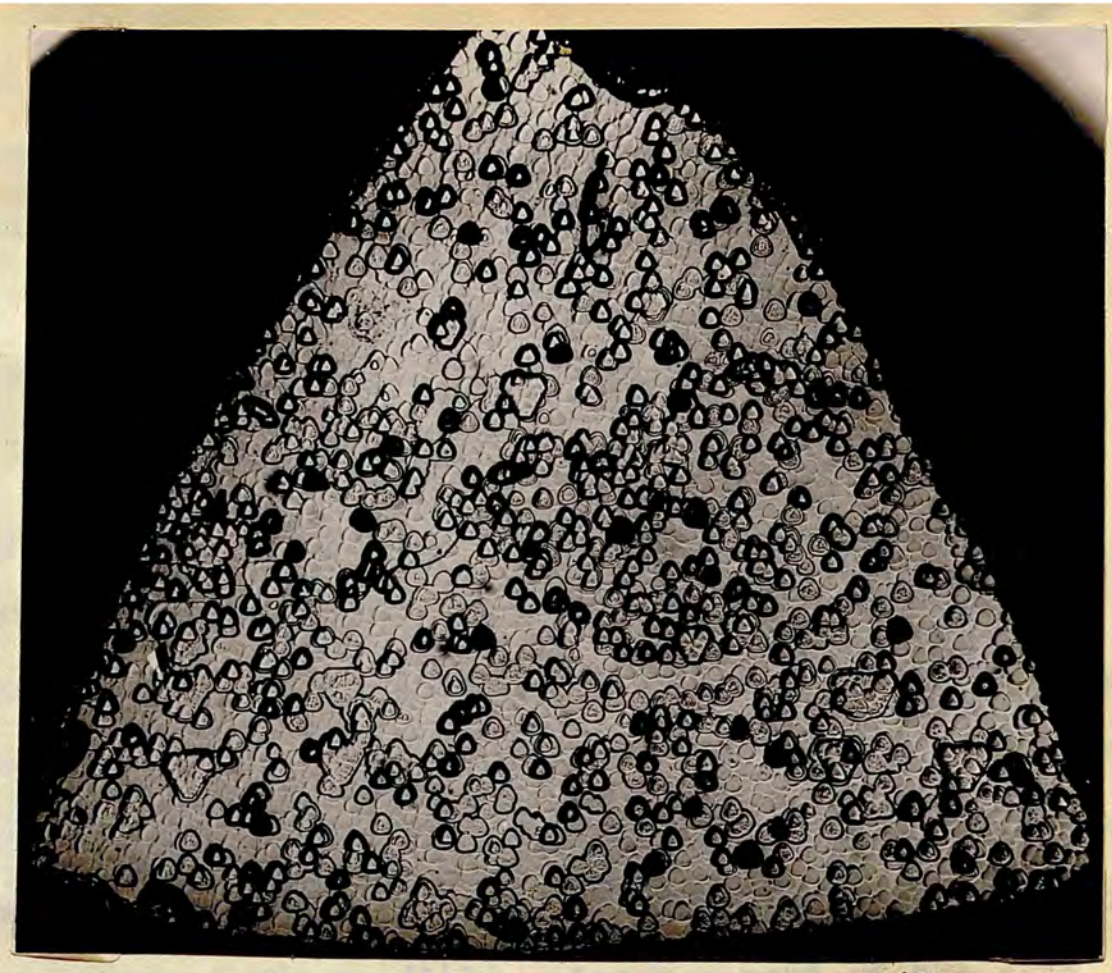

×60

Fig. (138).

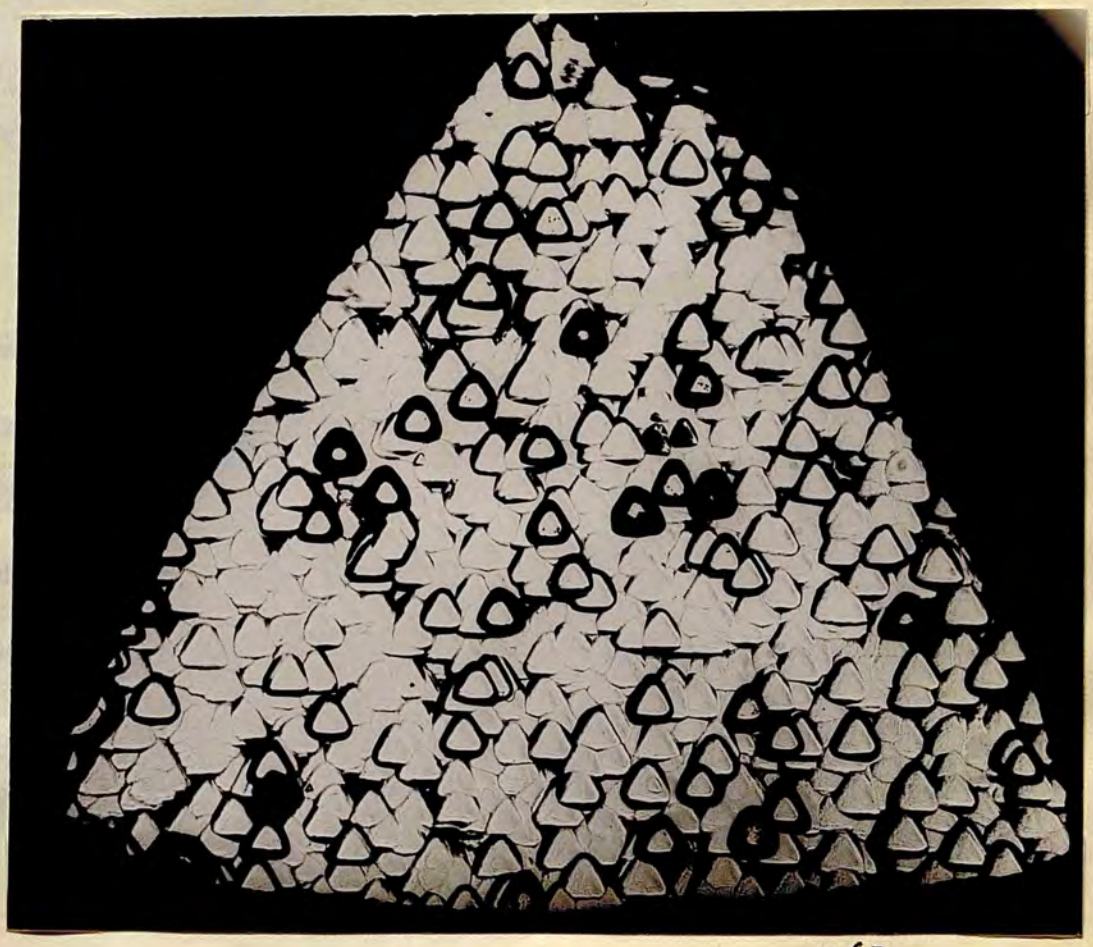

×60

Fig. (139).

the exception of one or two etch pits, they have reached now the approximately equal size of 85 μ, and since their largest size at 550°C was 4 μ they have increased in area also by about 400 times. Figs (140), (141) and (142) are enlarged parts of face 1 under similar conditions to fig (137), (138) and (139) only that the last figure occurred at 625°C instead of 650°C.

Increase in Depth.

The etch pits have not only increased in size but they have increased in depth. An example estimating their depth by the film technique has already been given in chapter 10. There they varied in depth (fig 78) from $\frac{1}{2}\lambda'$ to λ' where λ' is the wavelength in the film. It represents the 600°C further etching and is part of fig (138) or (141). Another part of the same surface is shown in fig (143) from which we see that there are other pits on the surface deeper than the above estimate. Here the depth varies between $2\lambda'$ and $3\lambda'$ i.e. between $\frac{2}{3}$ μ and 1 μ. This is by the way of an example. Fig (144) at 625 °C, represents for the first time the use of multiple beam interferometry with the help of flats. This is one of a set of four pictures from which the distribution of depth over an entire face can if desired be deduced. Fig (145) in another interferogram under larger magnification. Ordinary multiple beam interferometry could be applied because the etch pits have developed in extension. Still uncertainties in depth exist in both methods, on account of the steep sloping edges of these pits, and the light profile described by Tolansky (86) (an example

X 150

Fig. (140).

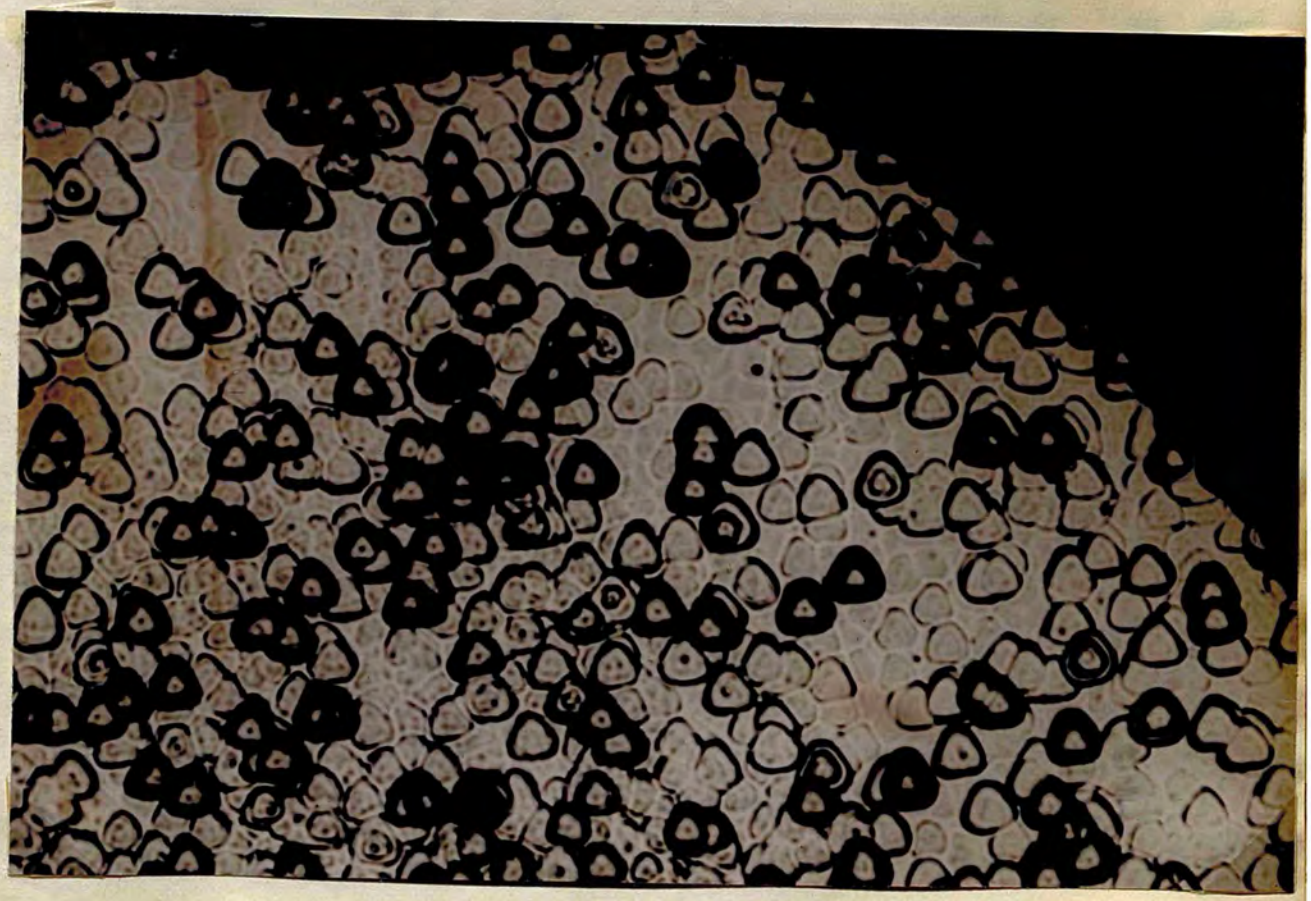

X 150

Fig. (141).

X 150

Fig. (142).

X 800

Fig. (143).

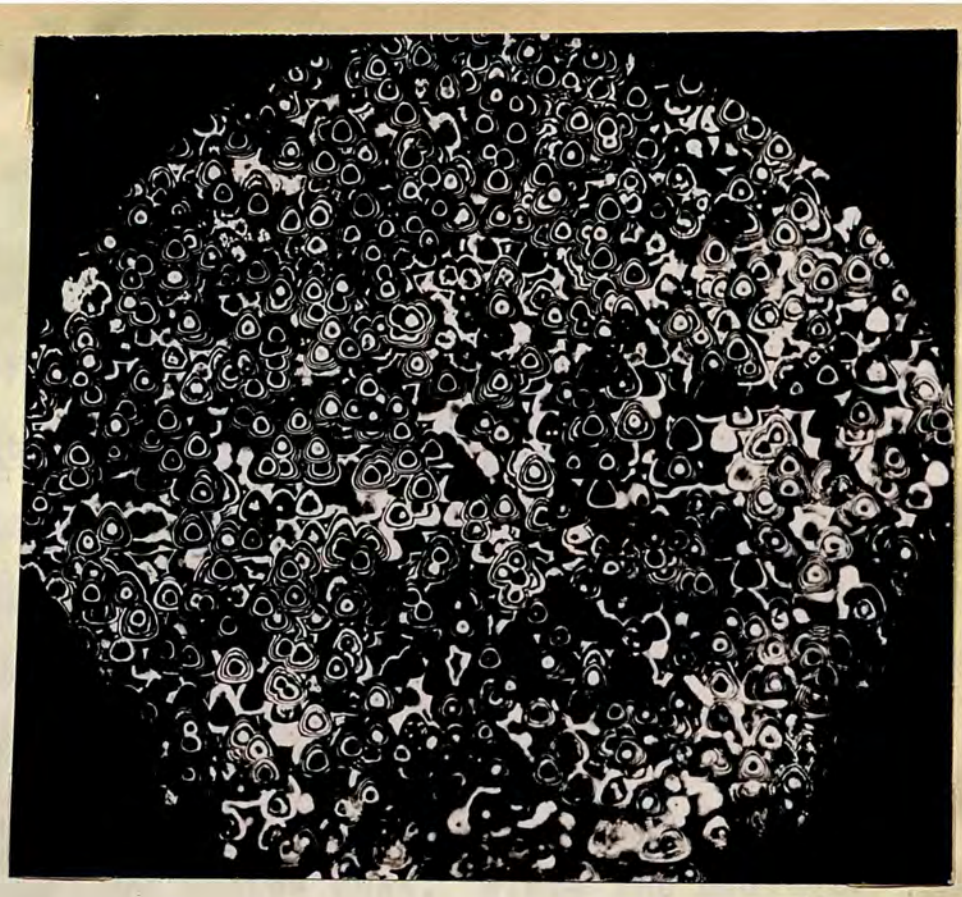

X 90

Fig (144)

X 400

Fig (145)

has already been given in chapter 11) is an outlet. On the whole the proportion of deep etch pits increases with time or temperature. Fig (146) is an example of well developed etch pits at 625°C, and fig (147) is an example of a rather small pit at 650°C. They register successively 3λ and 4λ pits.

Some Peculiarities of the Etch Pits.

The profile as well as interfacial angles of pits could be deduced from interferograms at the geographical dispersion. In this section we are interested in the rounded outline of most of the etch pits, once they develop at the expense of others. The rounding seems to be a direct result of the incorporation of etch pits in the more active ones. Since the addition comes from all directions, roundness must be superimposed on the trigonal symmetry, and we expect to meet pits something between a pyramid and a sphere. We report in fig (148) a new observation. Much smaller etch pits are developing all the time inside the etch pits. Their role is not known with certainty. They may or may not play an active part in the development of the etch pit.

Interfacial Angles of the Pits.

In fig (147) the interfacial angle differs between 10.5° at the outline of the pit to 15.5° at the bottom. The angle between the sloping sides and the close packed surface varies accordingly (c.f. chapter 5). This is not the general trend of the rounded etch pits which are steeper at the edge than at the bottom. The angles are approximate on account of the rounded nature added to the approximations used in the equations of

X 1000

Fig. (146).

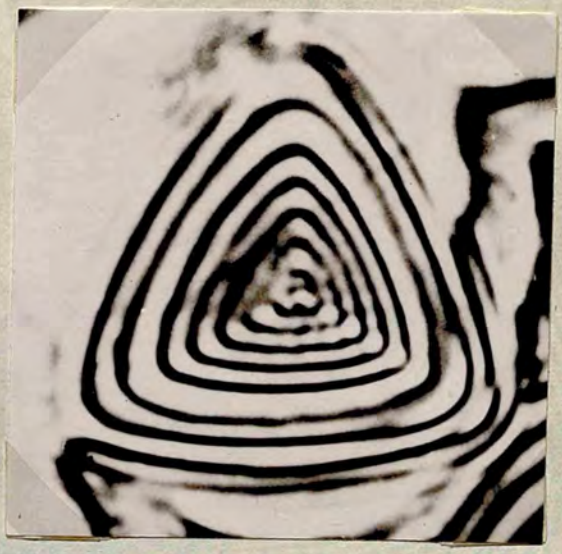

X 1000

Fig. (147).

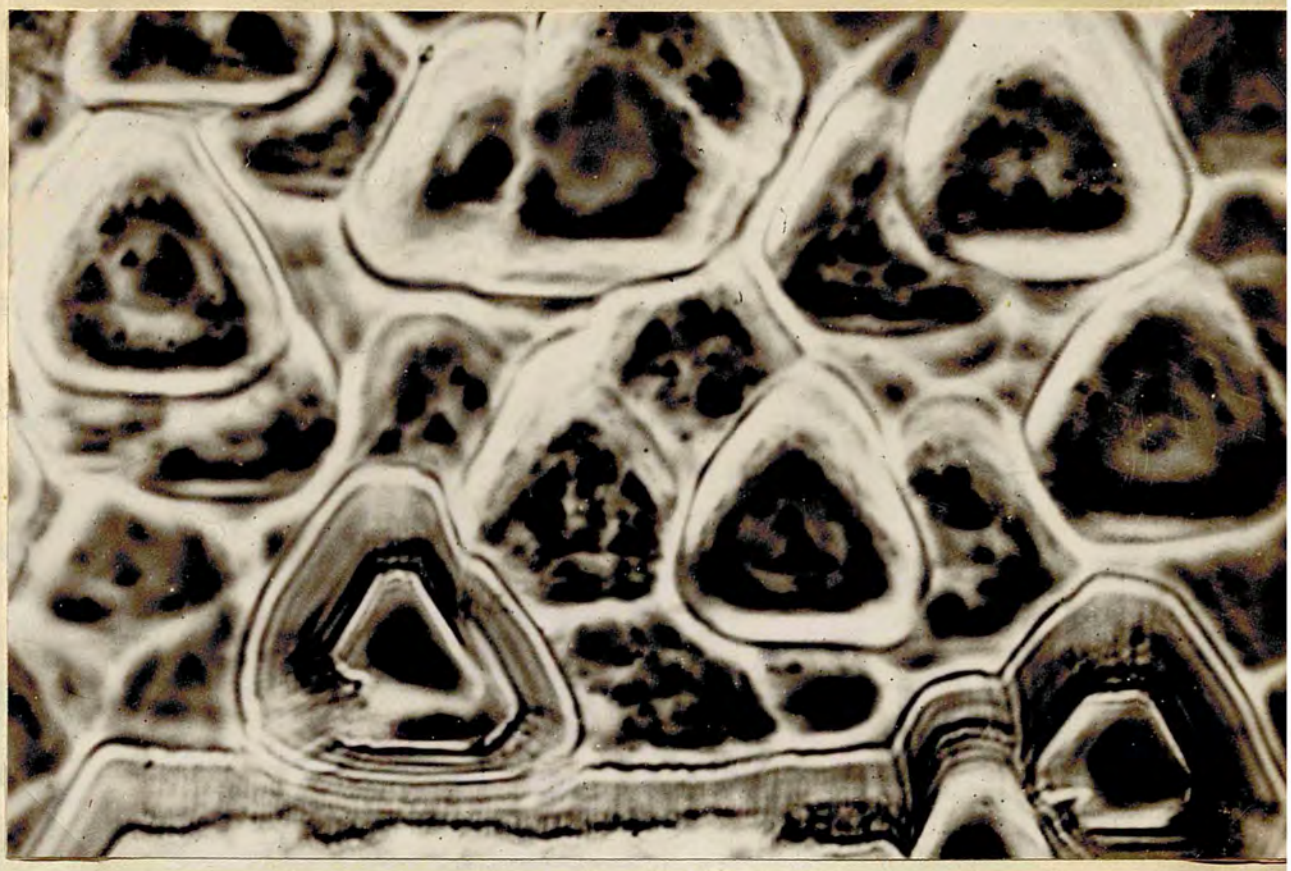

Fig. (148). X 800

Fig. (149). X 360

interferometry. A rough estimate using the equations of solid geometry (c.f. chapter 5) applicable only for a regular pyramid, gives the interfacial angle the value of 12.5°. These angles are near to crystallographic angles and are different from the range of angles encountered in the trigons. The interfacial angle in fig (146) is roughly 8° at the top.

Crystal (H) Etched for 2 hours at 700°C.

On account of the high temperature, etch pits larger than any encountered before, have appeared. Fig (149) is a typical etch pit of length of side about $\frac{1}{3}$ m.m. This is also steeper at the apex than it is at the periphery, but the difference is not great. This is a multiple beam interferogram using a $\frac{\lambda}{40}$ flat. The equations of interferometry give 9° for the interfacial angle at the top and 11.5 at the bottom. The approximate use of solid geometry gives 11.25° at the bottom.

In conformity with earlier observations of Williams,(10) a peculiar edging in the form of solution cavities appeared at the edges of the crystal $\perp^r$ to the direction of the edges of the octahedron. The light profile (using 4 m.m. objective) across one of these cavities is in fig (150a). The radius of cylindrical curvature, by a method developed by the author (c.f. chapter 12)(90) is 0.64 m.m. The film technique developed also by the author (fig 150b) gives a value of 0.65 m.m. for the right hand/lowest cavity. No attempt has beem made to study the same cavity by both techniques. The exact value reached by both techniques can either be due to chance or to a geniune constant curvature in these cavities.

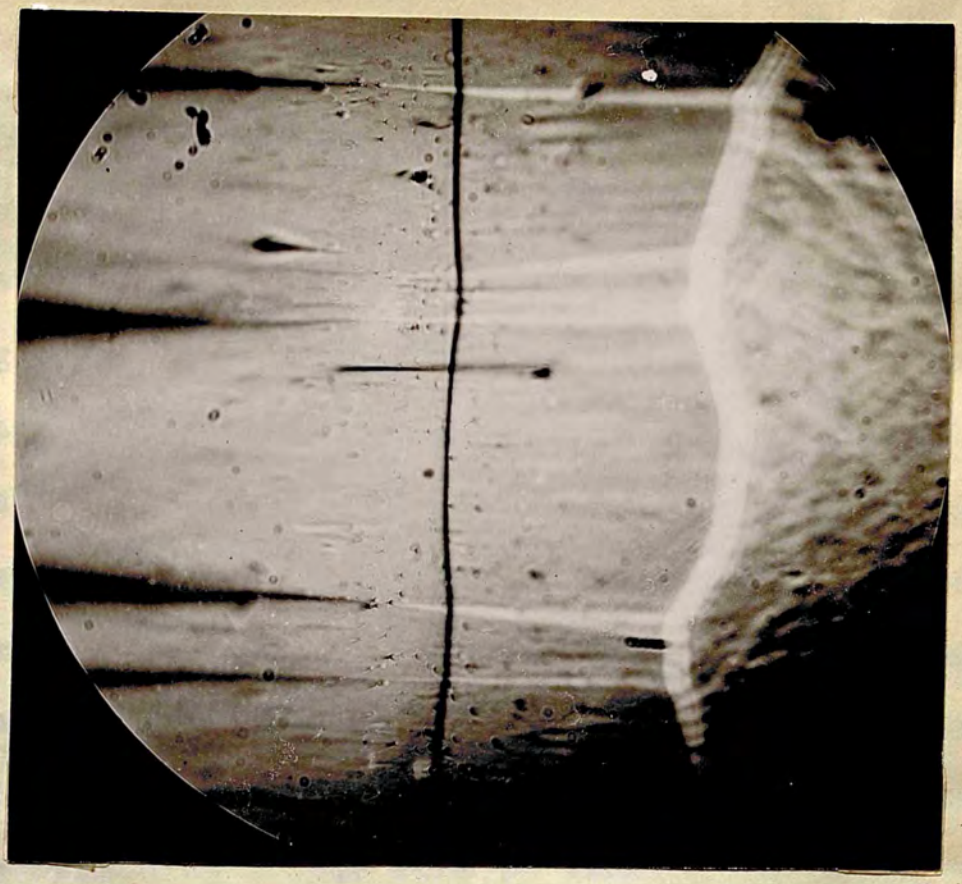

Fig. (150 a) ×300

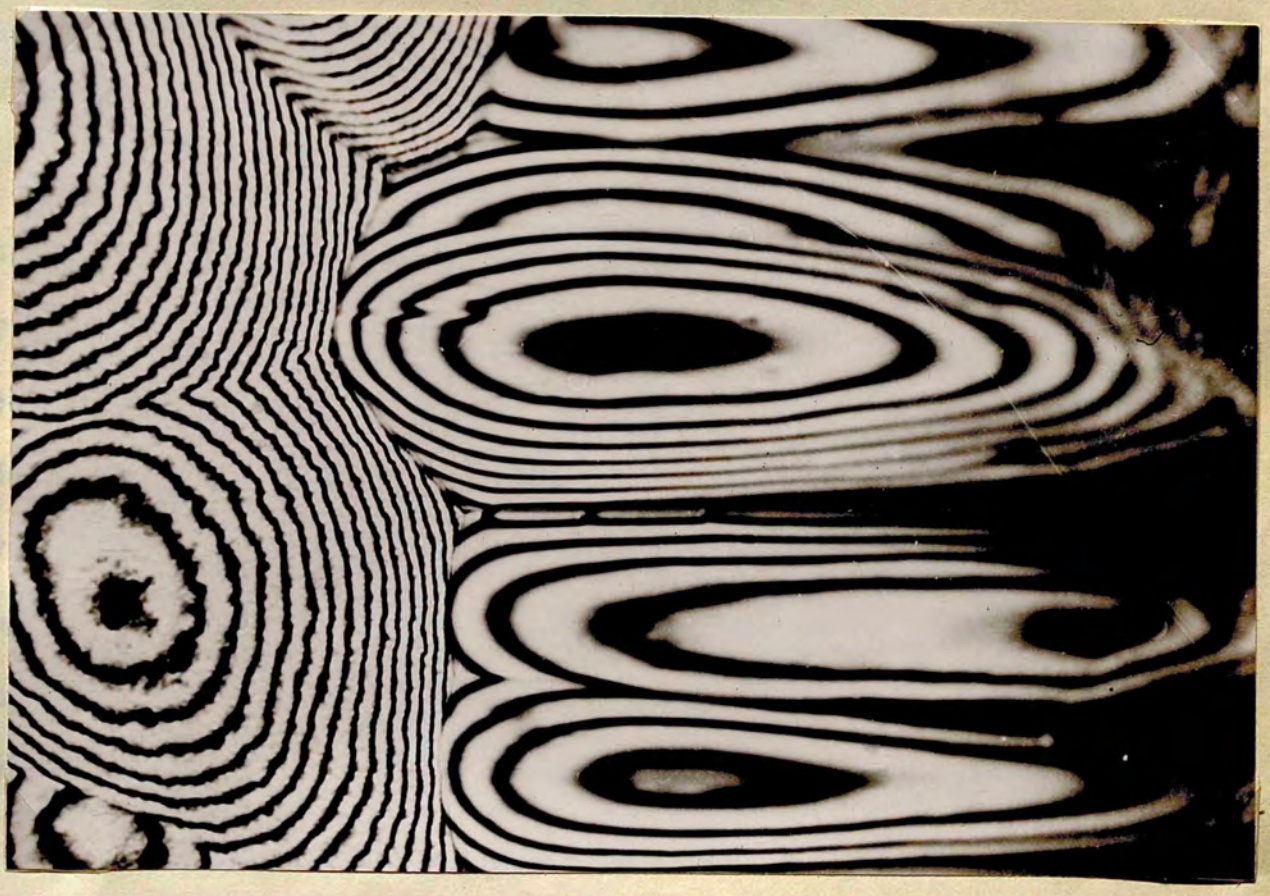

Fig. (150 b). ×470

ACKNOWLEDGMENTS

The author owes his knowledge in interferometry to Prof. S. Tolansky whose constant interest and unerring judgment have been of real help during the work carried out in this thesis. He owes his knowledge in optics to professors M. Nazif and W. L. Bragg. Any short-coming as may appear in this thesis is entirely the author's fault and cannot be attributed to them.

Amongst his colleagues and friends, he thanks J. Reed for helpful discussions in solid geometry and Dr. A. R. Verma for helpful remarks, also for valuable criticisms in the preparation of the MS and for the loan of Si C specimens. The author offers his most sincere thanks to Dr. Grenville Wells for her gracious help at the beginning of his work in lending him large pieces of diamonds. The author was always afraid of loosing small diamonds and his temporary possession of sizable pieces enabled him to proceed with his work.

He wishes to thank Mr. P. Grodzinski of the Industrial Distributors (London) for the loan of numerous diamonds and for help in various ways; his last move in that direction was his direct response in communicating with South Africa for the loan of diamonds of known origin and localities to enable the author to verify his calculation of the temperature of formation of diamond. The diamonds have just arrived but the author had no time even to see them; for the same reason no appendix is provided in the present thesis.

REFERENCES.

(1) The Story of Diamond. Gemological Inst. U.S.A., ... 1941

(2) Bragg, W.H.& W.L., Proc.Roy.Soc. 89A, 277 1913

(3) Raman, C.V., Proc.Ind.Ac.Sci.,A, 19, 1 ... 1944

(4) Krishnan, R.S., Proc.Ind.Ac.Sci.,A, 19, 298 . 1944

(5) Sutton, J.R., "Diamond" D.Van Nostrand, New York. 1928

(6) Miers, H.A., Encyc.Brit.,Minerallogy, 11 Ed.1902

(7) Grenville Wells, Thesis, Ph.D (London) 1951

(8) Tolansky, S. & Wilcock,W.L., Proc.Roy.Soc. A,191,182. 1947

(9) Buckley, H.E., "Crystal Growth" John Wiley, New York. 1951

(10) Williams, A.F., "The Genesis of the Diamond", Benn Lond .1932

(11) Fersmann,A. & Goldschmidt,V., "Der Diamant",Heidelberg,1911

(12) Shafranovsky, C.R., Acad. Sci.URSS, 26, No.7 1940

(13) Friedel, G., "Sur la birefringence du Diamant" Bull,Soc.Fran.Min. 1924

(14) Kucharenko, A., Doklady Akad, Nauk SSSR, 51, 629 . 1946

(15) Van der Veen, A., "Symmetrie Van Diamant",Leiden,1911

(16) Raman,C.V. & Ramaseshan,S., Proc.Ind.Ac.Sci. A, 24, 1, 1946

(17) Rinne, F., "Crystals and the Fine Structure of Matter" Methuen & Co, Lond..1924

(18) Harkins, W.D., Jour. Chem. Phys.,10, 268 1942

(19) Wilcock, W.L., Ph.D Thesis, Manchester 1951

(20) Wilks, E.M., Ph.D.,Thesis, London 1952

(21) Wells, A.F., Annual Reports,Chem.Soc.(London) 43, 62 .1946

(22) Gibbs, J.W., Collected Works (Longmans Green & Co.),London .. 1928

(23) Volmer, M., Z. Phys. Chem. 102, 267 1923
Kinetic der Phasen bildung (Dresden
& Leipzig: Steinkopff) 1939

(24) Kossel, W., Nachr.Ges.Wiss Gottingen p.135 1927

(25) Stranski, I.N., Z. Phys. Chem, 136, 259 1928

(26) Becker, R.,& Doring, W., Ann.Physik, 24, 719 1935

(27) Frenkel, J., J. Phys. U.S.S.R., 9, 392 1945
Kinetic Theory of Liquids (Oxford:
Clarendon Press) 1946

(28) Pfaff Sitzungber.d.Physik,10, 59 1878

(29) Brauns Neues Jahrbuch 1, 138 1887

(30) Scacchi, A., Z.deut.geol.Ges., 15, 19 1863

(31) Mallard, E., Traite de Cristallographie,Vol.2 ... 1879

(32) Miers, H.A., Phil. Trans.Roy.Soc. A, 202, 459 ... 1904

(33) Hintze, C., Z. Krist, 11, 220 1886

(34) Hedges J. Chem.Soc. 1, 791 1926

(35) Schubnikov, A., & Brunowsky, B., Z.Krist,77,337 1931

(36) Tolansky, S., Proc.Roy.Soc. A, 184, 41 1945

(37) Kalb, G., Z. Krist, 73, 266 1930
Z. Krist, 86, 439 1933
Z. Krist, 89, 400 1934

(38) Wulff, G., Z. Krist, 34, 441 1901

(39) Miers, H.A., Proc.Roy.Soc. 71, 439 1903

(40) Marcelin, R., Ann. Physique, 10, 185 1918

(41) Kowarski, J. Chim. Physique, 32, 303 1935
395 1935
469 1935

(42) Bunn, C.W., & Emett, H., Discussions of the Faraday Soc. No. 5 p. 119 1949

(43) Volmer, M., & Schultze, W., Z. Phys. Chem. A, 156, 1 1931

(44) Burton, W.K., Cabrera, N., & Frank, F.C., Nature, 163, 398 ..1949

" " " " " " Phil Trans. Roy .. Soc. A. 243, 299 ...1951

(45) Frank, F.C., Advances in Physics (Phil. Mag. Supplement) Vol:1, No. 1, p.91 1952

(46) Griffin, L.J., Phil. Mag. 41, 196 1950

Verma, A.R., Phil. Mag. 42, 1005 1951

" " Proc. Phys. Soc. B, 65, 806 1952

" " Thesis, Ph.D. (London) 1952

Verma, A.R., & Reynold P.M., Nature, 171, 486 1953

" " " " Proc. Phys. Soc. (In Press) ..1953

(47) Dawson, I.M., & Vand, V., Nature, 167, 476 1951

" " " " Proc. Roy. Soc. A, 206, 555 1951

(48) Menzies, A.W.C., & Sloat, C.A., Nature, 123, 348 1929

(49) Buckley, H.E., Private Communication.

(50) Buckley, H.E., Zeit fur Electrochemie, 56, 275 1952

(51) Buckley, H.E., Proc. Phys. Soc. B, 65, 678 1952

(52) Fizeau Ann. Chim. et Phys. (3), 66, 429 1862

" Compt. Rend., 54, 12 37 1862

(53) Duffieux, M., Rev. Opt. (theor. instrum) 11, 159 1932

(54) Boulouch Journ. de Physique, 5, 789 1906

(55) Tolansky, S., Proc. Phys. Soc. 58, 654 1946

(56) Brossell, J., Proc. Phys. Soc. 59, 224 1947

(57) Holden, J., Proc. Phys. Soc., B, 62, 405 1949

(58) Hamy, M., J. Phys. Radium, 5, 789 1906

(59) Airy Math. Tracts, 381 1831

(60) Tolansky, S., & Khamsavi, A., Nature, 157, 661 1946

(61) Verma, A.R., Nature, 167, 939 1951

(62) Griffin, L.J., Phil. Mag. 42, 775 1951

(63) Hopkins, H.H., Series of Lectures (Imp.College) London 1952

(64) Tolansky, S., Multiple Beam Interferometry of Surfaces and Films, Oxford (Clarendon Press). 1948

(65) Tolansky, S., Nature, 152, 722 1943

" " Nature, 153, (195,314,435) 1944

" " Phil. Mag. 35, (120,175) 1944

" " Phil. Mag. 36, 225 1945

" " Phil. Mag. 37, (390,453) 1946

" " Proc. Roy. Soc. A, 184 (41,51) 1945

" " Proc. Roy. Soc. A, 186, 261 1946

(66) Faust, R.C., Thesis, Ph.D. (Manchester) 1949

(67) Kuhn, H., Rep.Prog.Phys, (Physical Soc.) London 14, 64 1951

(68) Meggers, Journ.Opt.Soc.Amer., 5, 308 1921

(69) Brossell, J., Nature, 157, 623 1946

(70) Frank, F.C., Discussions of the Faraday Soc. No. 5, p. 48 1949

(71) Willis, B.T.M. Thesis. Ph.D. (London) 1952

(72) Bloom, Ann. d. Physik (4) 42, 1397 1913

(73) Barret, C.S., "Structure of Metals", McGraw Hill, New York 1943

(74) Ruzicka, P., Vestnik Ustredniho Ustavo Geolegeckeho, (5), 27, 194 - 197 1952

(75) Custers, J.F.H., Americ. Min., 35, 51 1950

(76) Grodzinski, P., Private communication.

(77) Papapetrou, A., Z. Krist. A 92, 89 1935

(78) Tolansky, S., & Omar, M., Nature, 170, 81 1952

(79) Diamond, Conference, Oxford, July 10th 1952

(80) Gevers, R., Nature, 171, 171 1952

(81) Horn, F.H., Phil. Mag. 43, 1210 1952

(82) Tolansky, S.,& Faust,R.C., Proc.Phys.Soc.,59,951 ... 1947

(83) Verma, A.R.,& Reynold,P.M., Proc.Phys.Soc.B (In press) 1953

(84) Steinburg, M.A., Nature, 170, 1119 1952

(85) Turnbull,D.T. & Belk,J.A., Laboratory Practice,1,399. 1952

(86) Tolansky, S., Nature, 169, 445 1952

(87) Tolansky, S., Zeitschrift Elektrochemic, 56, 263 . 1952

(88) Schmaltz, G., Techn. Oberflachenkunde, Berlin 1936

(89) Rahbek, H.,& Omar, M., Nature, 169, 1008 1952

(90) Tolansky, S.,& Omar, M.,Nature, 170, 758 1952

(91) Ewing,J.A.,& Rosenhain,W., Phil.Trans.Roy.Soc.A, 193, 353 1900

(92) Smekal, A., Handbuch der Physik, 24, 2 1933

(93) Brown, A.F., Advances in Physics (Phil.Mag. Supplement) Vol:1, No. 4, p.427 1952

(94) "Imperfections in Nearly Perfect Crystals (Symposium) John Wiley & Sons, New York 1952

(95) Frank, F.C., Phil. Mag., 42, 809 1951

(96) Mott, N.F., Nature, 171, 234 1953

(97) Burgers,J.M., Proc.Kon.Ned.Akad.,Amesterdam,42,293 1939

" " Proc. Phys. Soc. 52, 23 1940

(98) Mountain, E.D., Prof. Geol.Dept. Rhodes Univ. College, Grahamtown .....

(99) Bragg, W.L., "Atomic Structure of Minerals", Oxford University Press 1937

(100) Wooster, N., Science Progress, 103, 462 1932

(101) Orowan, E., Rep. Prog. Phys. 12, 185 1948

(102) Duce, A.G., Thesis, Ph.D. (Cambridge) 1951

(103) Elam, C.F., "Distortion of Metal Crystals" Oxford. The Clarendon Press..... 1935

(104) Honess, P., "The Nature, Origin and the Interpretation of the Etch Figures on Crystals" John Wiley & Sons, New York 1927

(105) Rose, G., Monthly Report of the Berlin Academy p. 493 1872

(106) Luzi, W., Berichte Deut. Chem. Ges. 1892

(107) Tolansky, S. & Omar, M., Phil.Mag. 43, 808 1952

(108) Lacombe, P., Rep.Conf. Strength of Solids, The Physical Society of London 1948

(109) Shockley,W. & Read,W.T., Phys.Rev. 75, 692 1949

(110) Crookes, Sir William "Diamonds" London 1909

(111) Verma, A.R., Thesis, Ph.D. (London) 1952

(112) Vogel, R., Z.Anorg.Chem., 116, 21 1921

5.

From the PHILOSOPHICAL MAGAZINE, Ser. 7, vol. 44, p. 514,
May 1953.

Observations on Slip Found in a Diamond

By S. Tolansky and M. Omar
Royal Holloway College (University of London), Egham, Surrey*

[Received February 17, 1953]

Abstract

Interferometric and optical studies on a twinned diamond reveal the presence of true crystallographic slip on two opposite faces of the twin. Slip occurs parallel to a (111) plane, in both cases, making thus an angle of $70\frac{1}{2}^\circ$ with the surface. An internal optical opacity is found associated with the slip. The two faces on either side of one slip line are not parallel but inclined at the very small angle of 10^{-5} radian.

§ 1. Introduction

It is doubtful whether earlier observers have been able fully to substantiate the existence of slip in diamond. Williams (1932) has suggested that certain features appearing on some microphotographs of diamond might be attributable to slip, but the evidence is somewhat tenuous. Since diamond cleaves only effectively on the (111) octahedron plane, it might be anticipated that if slip were to be found, then it should occur parallel to this natural cleavage plane.

During an extensive interferometric study of growth features on the surfaces of many diamonds, we have found on one crystal, a contact twin (i.e. ' macle ') loaned to us by Dr. Grenville-Wells, decisive evidence of crystallographic slip which we have studied quantitatively by interferometric and light profile methods (Tolansky 1952 a, b). Slip regions have been found on both the major (111) faces of the twin and it has been established also that the slip plane is indeed parallel to (111).

To study this crystal use has been made of a number of optical techniques. The surface had on it some high projecting regions and since it has long been established that multiple beam interferometry requires close approach to the two surfaces involved, a special micro-flat technique was developed, in which the flat used was the small tip of a truncated cone, which could be brought into close approach with the desired region. This technique is being described elsewhere. Again, high magnification multiple beam interferometry was desirable in some regions and we reproduce later an interferogram taken at $\times$ 2000, using for this the thin film technique we have already described (Tolansky and Omar 1952) elsewhere.

*Communicated by the Authors.

§ 2. Observations

(*a*) *Slip on the First Face*

On the one side of the crystal the slip appears as a straight line, cutting right through all the growth features, some 15 mm long, running right across the surface. Part of this is shown in fig. 1, Plate 29 (× 30). The series of parallel lines KL are growth sheet fronts, and at 60° to these lies XY the slip line. The topography of this region is rendered clear by fig. 2, Plate 29 (× 100) which is a multiple beam interferogram. Here MN is a growth sheet step, parallel to the group of steps KL and once more XY is the slip direction. From the fringes one can readily evaluate the topography, a simplified diagram being shown schematically in fig. 7. The Fizeau fringes of fig. 2, Plate 29 are ambiguous as to step directions and these have been clarified by using fringes of equal chromatic order (Tolansky 1945). With these fringes it is confirmed that in fact the level differences A–B and C–D are identical in the neighbourhood of the cross over.

Fig. 7

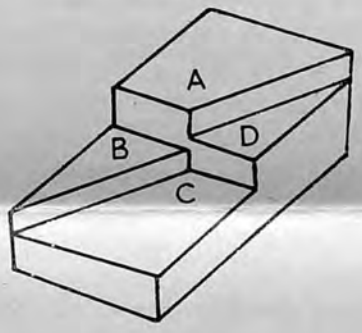

An examination of the slip step over the entire length of the crystal reveals the existence of a slight slope. The step increases regularly from the left to the right. Thus at the extreme left-hand side the slip is only 480 A. At a point 2 mm to the right it has increased to 680 A, and at 8 mm to the right to 1280 A. This corresponds to a slope between the slipped regions with the very small angle of 10^{-5} radian, i.e. merely 2 seconds of arc. Although small, this value is precise and has been confirmed by measurements on intermediate positions between ends. If this slip were to be taken as due to a dislocation the angle would imply a displacement of one atomic lattice in 10^5 lattices, to account for the slope. However, it should be pointed out that the slip does not run to zero at one end of the crystal, the minimum step of 480 A clearly corresponding to a slip of some hundreds of lattices.

Examination of the crystal in transmission with polarized light reveals a general distribution of strain other than in the slip region. Near the slip region itself and undoubtedly closely associated with it is a peculiar opacity. This is shown in fig. 4, Plate 29 (× 90). Examination with an

intense light source shows that the opaque region is sharply defined by the slip edge and then falls off somewhat, the final edge (lower) tailing away in a fuzzy manner. Inside the opaque region are some faintly transparent interference fringe regions. The difference in sharpness at the edges of the opaque region is clearly shown in the picture.

It will be shown later that the slip makes a large angle with the surface. This being so, high magnification experiments were undertaken to see whether the slip step discontinuity was sharp. To do this a silvered thin film technique (Tolansky and Omar 1952) was used. The crystal was silvered for multiple beam interferometry. A very thin film of Canada balsam was drawn over the slip boundary by means of a dilute solution of xylol. This dried rapidly and was then silvered. Multiple beam fringes are then formed in the thin film, the optical step being, of course, magnified by the ratio of the refractive index of the film to that of air. We have already demonstrated that high lateral magnification multiple beam fringes are obtainable by this procedure, fig. 3, Plate 29 shows the fringes across the slip step at $\times$ 2000. When the high lateral magnification is taken into account, it will be recognized that the fringe definition is exceptionally good.

Apart from the fact that such a picture permits accurate determination of the step, with an error of but a few angstrom units, the picture establishes that the step is discontinuous, sharply so. Now evidence will be produced later that the slip steps found on both faces have an undercut angle of $70\frac{1}{2}^\circ$ and there is every reason to believe, that the same will always be true. The sharp discontinuity observed is then only what can be expected if indeed the slip step undercuts, and is thus far a satisfactory observation.

It is to be noticed that the slip line is exactly at 60° to the growth direction and is thus parallel to an edge of the (111) face.

(*b*) *Slip on the Second Face*

Because of the twinned nature of the crystal the slip cannot be expected to penetrate from one side to the other and indeed this is the case, for the line XY does not appear on the opposite face of the flat stone. However an independent slip line does appear on the second face, this being inclined at 60° to the direction of XY. This second slip line also traverses right across the crystal and in doing so very clearly reveals a feature of some considerable interest. For the second face has on it a number of high growth plateaus, as well as deep triangular depressions (familiar features on (111) faces). The slip in question runs across some of these and in doing so becomes quite clearly displaced. It is from these displacements that the angle of undercutting can be determined, as shown in fig. 8. Suppose we have a growth step P. If this be cut by a slip plane normal to the surfaces then the cut lines in the upper and lower growth regions, when viewed from above, are colinear. If the cutting slip plane has an angle to the surface, then the

two lines will appear displaced, as in fact shown schematically in fig. 8. If the growth sheet step height be known, and is reasonably large, the measured displacement in the slip line permits the angle of undercut to be calculated. Furthermore the direction of displacement determines the direction of undercut. An example of a measurement made this way is shown by fig. 5, Plate **29**. Here the slip traverses a growth trigon. The discontinuity in the slip line as it passes over the growth step PQ, for example, is readily seen. This step height PQ measured by the light profile is large, i.e. 90 μ. The lateral displacement of the slip line measured in fig. 5, Plate **29** ($\times$ 30) is 32 μ. From a simple calculation it follows that the angle of undercut is $70\frac{1}{2}°$. This is precisely the angle made by adjoining (111) faces on diamond. We have therefore established that the slip line is not only parallel to a (111) edge, but indeed the whole slip plane is parallel to a (111) plane, i.e. to a cleavage plane.

Fig. 8

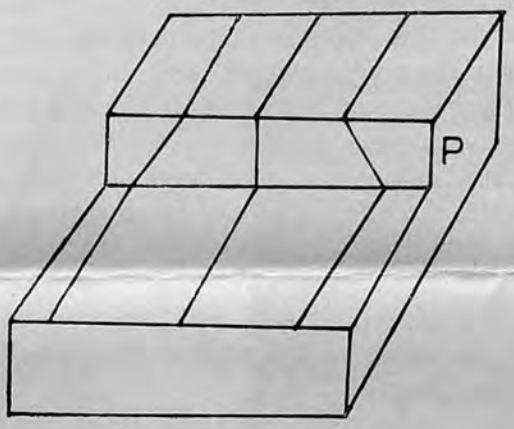

This interesting and exact geometrical deduction has only been made possible because of the occurrence of one very large discontinuity (90 μ) over which the slip traverses on the second face. Only in one position does the other slip line on the first face also pass over a relatively large discontinuity, and it is striking that from this face also it has been established to have an angle of $70\frac{1}{2}°$, exactly as in the case of the second face. The light profile picture over this part is shown in fig. 6, Plate **29** ($\times$ 90) in which the growth discontinuity is 31·5 μ and the slip line shift 11 μ. In fig. 6, the slip line is that which runs in the north-east to south-west direction crossing the group of parallel growth steps, the discontinuity appearing markedly in the last step. The optical light profile, which also shows the discontinuity at this step, is the vertical line having on it a short horizontal cross, some 1 cm from the top of the picture. The slip on the second face has also associated with it an internal opacity. Furthermore the second-face slip dose not penetrate the two twins but, as in the first case, ends within the body of the crystal.

(*c*) *A Possible Explanation of the Opacity*

Now that it is established that the slip plane is making an angle of $70\frac{1}{2}°$ with the surface it is quite possible to explain the opacity on the following lines. If the slip has developed partly into a crack, then an air film in the crack would totally reflect the incident light at the interface of diamond-air. The incident light would make an angle of $70\frac{1}{2}°$ with the perpendicular to the slip plane which is greater than the critical angle of diamond ($24\frac{1}{2}°$). As either part of the macle is 1·5 mm thick and the opacity at its maximum as estimated in different parts is $\frac{1}{3}$ mm, the crack, on this assumption, could only have penetrated to no more than two-thirds of the thickness of either part. If this interpretation of the opacity is correct it is reasonable to assume that the crack might have a finite width at its mouth where it emerges on the crystal face. Although the formation of such a small wedge crack might lead to the appearance of a small inter-facial angle between the two parts on either side of the crack, no such very small inter-facial angle has been detected. It is clear that the observed step cannot be accounted for by postulating such a mechanism for this suggested alternative would lead not to fringe steps but to fringes showing an angle kink. The fringes would appear continuous but change abrupt direction at the crack and would not, as are observed, be violently out of step.

It is emphasized that the observed angle of 10^{-5} radian referred to above applies to the fact that the slip is emerging out of the surface with a slightly increased step height as one traverses along the length of the ledge.

Thus it may be concluded that

(*a*) the occurrence of crystallographic slip on diamond has been demonstrated on two faces of a twin,

(*b*) the slips takes place on (111) planes, which are the planes of easy cleavage,

(*c*) the two faces on either side of one slip are inclined at the slight angle of 10^{-5} radian,

(*d*) the slips have associated with them regions opaque to transmitted light,

(*e*) the slip appears on both sides of a twinned macle, but in neither case does the slip penetrate to the opposite side.

References

Tolansky, S., 1945, *Phil. Mag.*, **36,** 225 ; 1952 a, *Nature, Lond.*, **169,** 445 ; 1952 *b*, *Zeitschrift für Elektrochemie*, **56,** 263.

Tolansky, S., and Omar, M., 1952, *Nature, Lond.*, **170,** 81.

Williams, A. F., 1932, *The Genesis of Diamond* (London).

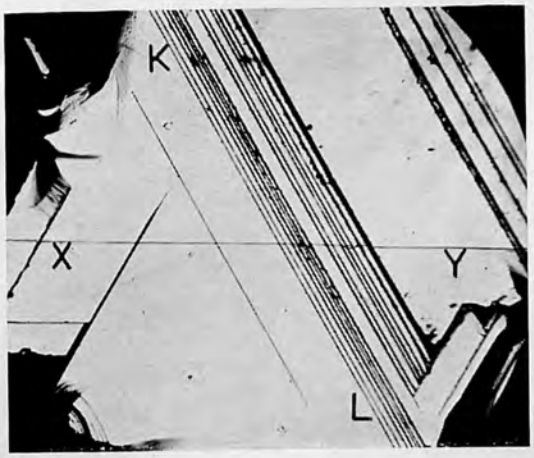

Fig. 1 ×30

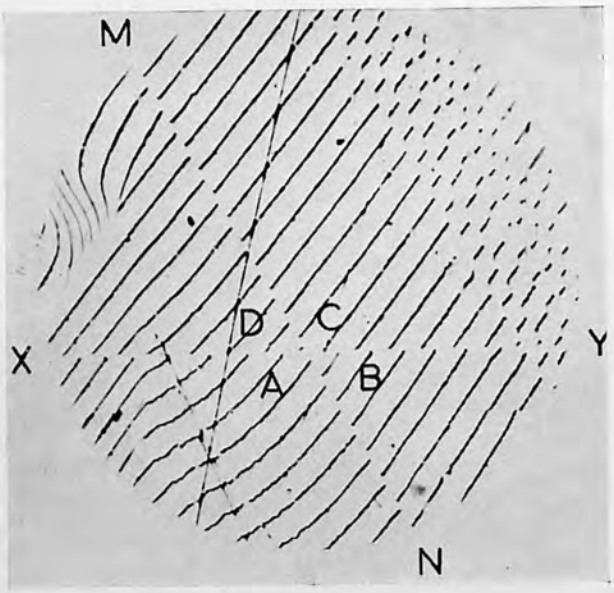

Fig. 2 ×100

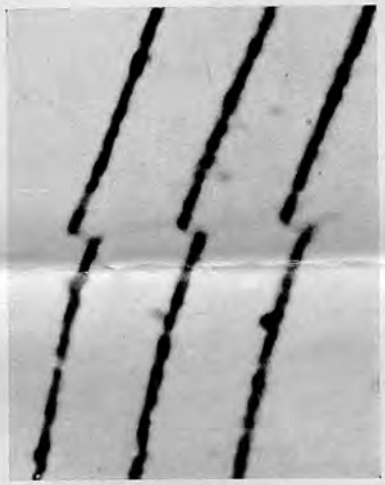

Fig. 3 ×2000

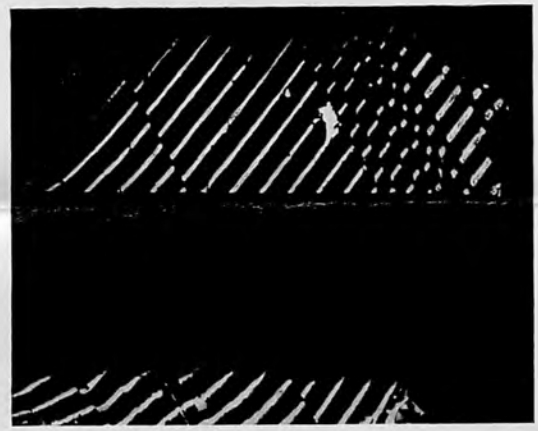

Fig. 4 ×90

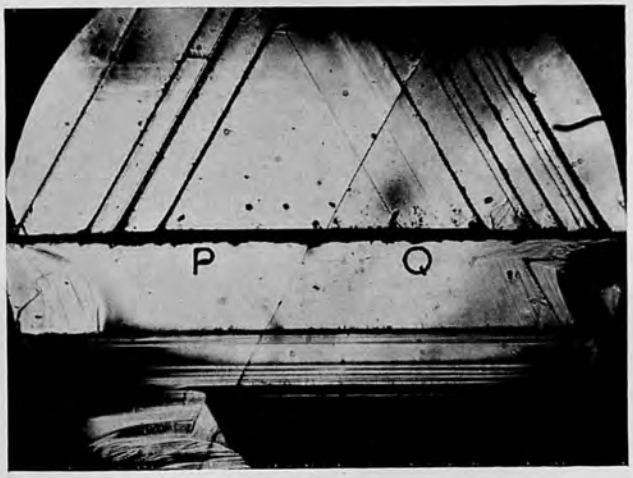

Fig. 5 ×30

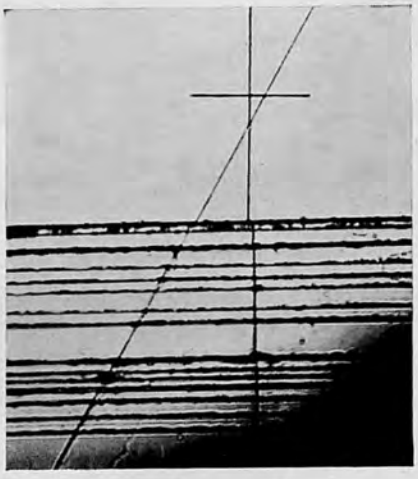

Fig. 6 ×90

Growth Temperature of Diamond

A preliminary investigation of curvature of growth fronts on diamond octahedral faces, gives a clue to the temperature of formation of diamond. As is well known (see for example Bauer and Spencer; 1904) almost every mode of origin has been brought forward to account for the existence of diamond. Some theories favour a low temperature (a few hundreds of degrees °C) while others favour a high temperature (a few tens of southands of degrees). From a limited observation on some diamonds the moderately high temperature range of 5000°C to 6000°C seems to be most probable.

The calculation is based purely on observation and is not connected with any particular mode of origin. One general and broad assumption is only made: that ~~it~~ diamond possibly has grown from solution. In two dimensions, a condition satisfied in the case of flat features, Frank (1950) has shown that the boundary of growth fronts has a radius of curvature $(1+2B)$ times its distance from the growth centre, where $B = e^{\frac{2w}{kT}}/8$. The calculation is based upon assuming imagining the rate of advance propartional to the number of kinks in the step line, a condition which according to Frank is most likely to arise in growth from solution. In the above relation w is the energy necessary to form a kink, and k is Boltzmann constant

$1 \cdot 38 \times 10^{-16}$ erg. degree^{-1}, and T the absolute temperature. In a close-packed step in a (111) face of a face centred cubic crystal, Burton, Cabrera, and Frank (1951) have shown that $w = 2\phi$ where ϕ is the nearest neighbour interaction. In diamond this is the binding energy of a carbon atom.

Denoting the radius of curvature by (ρ) and the distance to the centre by (p), the above relation, written again will be

$$\frac{\rho}{p} = 1 + \frac{1}{4} e^{\frac{\phi}{kT}} \quad \ldots \ldots (1)$$

as ρ and p can both be measured with a fair accuracy by applying multiple beam interferometry at the geographical dispersion, it is clear that if ϕ be known T could be calculated. The geographical dispersion is attained when the reference flat is symmetrically inclined to the features. The general wedge angle disappears leaving the local wedge angles to direct the fringes parallel to the features. An interferogram of this nature is contained in fig (1) Plate , while fig (2) ~~of the same plate~~ is in effect a photomicrograph of the same area. Fig (2) is actually an interference picture taken with a white light source, the filter (Wratten 77A) being retained. The growth hillocks are those marked H, and T are the trigons so familiar on diamond octahedral faces.

Fig (1) ~~only~~ differs from fig (2) in showing only the growth fronts that are separated in vertical height by $\frac{\lambda}{2}$. The growth fronts are the fringes. The percentage reflectivity must be that conducting to extremely sharp and well defined fringes. The centres of growth hillocks which are also the centres of growth are invariably marked with a fringe, but this is not a necessary condition for the identification of their exact position. The fringes being few in number and clearly defined enable both ρ and p to be accurately evaluated.

To evaluate ϕ use is made of a previous estimation due to Harkins (1942) of the energy necessary to break a C-C bond. Harkins calculated the number of bonds projecting per sq. cm. from a (111) face of diamond. He also used a reasonable estimate (90,000 calories) as the energy necessary to break the bonds of a mole of carbon. This enabled him to calculate what is effectively the cleavage energy per cm^2 of diamond. As each cm^2 becomes 2 cm^2 in the cutting, the binding energy per cm^2 would be half the cleavage energy. As one bond projects per atom it is clear from the above that ϕ is half the energy necessary to break the bond. In this manner ϕ is estimated as 3.09×10^{-12} ergs. This is an exceedingly

large amount, compared with Boltzmann constant k which is only 1.38×10^{-16}. According to equation (1) this leads ~~into~~ to an extremely large value for $\frac{\rho}{p}$, and straight wave front must necessarily arise, unless T is also high.

Measurement shows that growth fronts are highly curved, and on the crystal face of figs (1) & (2) ρ is rarely more than 2 mm while p is rarely more than 150 μ. $\frac{\rho}{p}$ attains the nearly constant ratio of 12.5 The calculated temperature is 5600°C

Ref.

Bauer and Spenser (1904), "Precious Stones", London.
Frank (1950) Phil. Mag. 41, 200.
Burton, Cabrera and Frank, 1951, Phil. Trans. Roy. Soc. ~~Part~~ of London, 243, 299.

Harkins (1942) Journ. Chem. Phys. 10, 268

4.

From the PHILOSOPHICAL MAGAZINE, Ser. 7, vol. xliii, p. 808,
July 1952.

Etch Spirals on a Diamond Octahedron Face

By S. TOLANSKY and M. OMAR
Royal Holloway College, Englefield Green

[Received May 15, 1952]

IT has long been known that etch pits appear on the octahedron faces of diamonds when treated at high temperature (900° C) with potassium nitrate and sodium carbonate (e.g. Fersmann and Goldschmidt 1911, Williams 1932). Since it was anticipated that the onset of etching might well be seen at an earlier stage by using interferometry, experiments have been carried out on the etching of diamonds at a much lower temperature and this brief note reports preliminary observations obtained at 525° C.

In conformity with early observations large numbers of very small oriented triangular etch pits have been observed but, in addition, features have appeared of some considerable interest in connection with the recent theories of crystallographic growth by the mechanism of spiral dislocations. From the considerable mass of data obtained the following are typical.

It has been found that the onset of etching in many cases takes on a spiral form, sometimes simple, sometimes complex. These spirals are rarely more than one turn. Figure 1 (figs. 1–4, Plate LIII) is a typical case. We show this here with a good deal of empty magnification ($\times 5\,400$ on the original, before reproduction) in order to make clearer the fact that the spiral consists of a chain of triangular etch pits, and furthermore the spiral does not close up although it branches as it progresses. The central first turn is distinctly hexagonal. Figure 2 ($\times 1\,600$) is an interference picture taken by means of a thin film technique especially developed for the purpose of enabling interferometry at high magnifications to be conducted. This is obtained at the expense of fringe width which, although not comparable to that obtainable by the best multiple beam methods, yet suffices to give useful information. It is seen, for example, that the fringes kink on passing over the arms of the spiral and measurement reveals that the approximate depth is some 700 Å and is, moreover, reasonably uniform in both arms.

Figure 3 ($\times 1\,250$) shows another typical spiral with a complete turn and one with an incomplete turn. It should be noted that the spirals vary in character. Some form an outline which is oriented and in the characteristic triangle shape associated with the ultimate familiar etch pits, others appear which are more nearly circular, and still others in which the outline approximates to a hexagonal character. Such indeed is partially noticeable in figs. 1 and 3.

In all cases the spirals appear to consist of chains of contiguous small triangular etch pits all oriented in the same direction. These appear occasionally in roughly straight-line chain form as shown in fig. 4 at $\times 1\,200$ which reveals more clearly the nature of the contiguous chains which in some cases ultimately become spirals.

Figure 4, it should be noted, is an interference picture taken by a thin film interference technique, specially designed to heighten contrast and with this technique details which are a small fraction of a light wave in depth can be revealed with high contrast. This thin film technique employs white light interference and involves very sensitive colour changes.

It may be noted that *no* growth spirals were detected on the diamond before etching, although sought for by interference methods. It is possible that these etch spirals in fact have developed on what were originally invisible growth spirals but we have no evidence to substantiate this. The point at issue is that in any case the anticipated height of a diamond growth spiral, if present, would probably be too small to be detectable by interferometry.

The density of these etch spirals per unit of area is relatively quite low on the surfaces etched at 525° C.

References

Fersmann, A. v., and Goldschmidt, V., 1911, *Der Diamant*, Heidelberg.
Williams, A. F., 1932, *The Genesis of Diamond*, London.

Fig. 1

×5400

Fig. 2

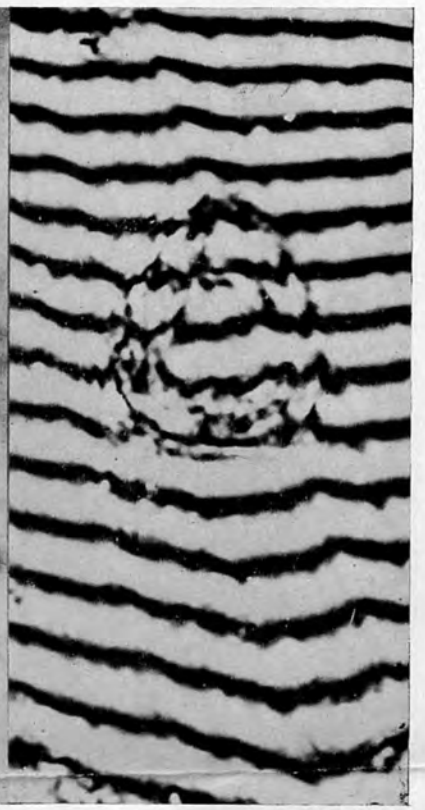

×1600

Fig. 3

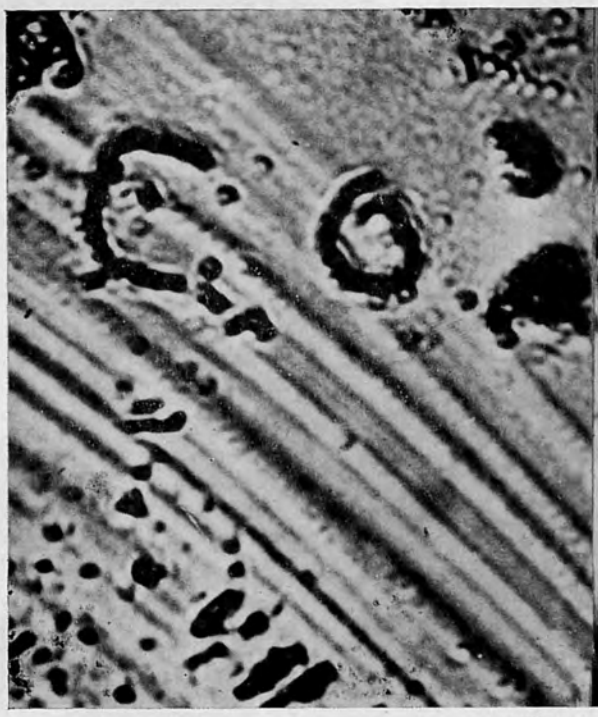

×1250

Fig. 4

×1200

(*Reprinted from Nature, Vol.* 169, *p.* 1008, *June* 14, 1952.)

Measurement of the Thickness of Transparent Films with the Light-Profile Microscope

THE light-profile microscope technique, described by Tolansky[1], has been adapted by us for the determination of the optical thickness of relatively thick transparent films. A transparent film, bounded by media with refractive indices differing from that of the film, has two reflecting surfaces; when observed with a light-profile microscope these two surfaces produce a double image, from the separation of which it is relatively easy to derive the ratio t/μ, in which t is the thickness and μ the refractive index. This is of much value in so far as direct interferometry, using, for example, fringes of equal chromatic order, gives the value μt. The combined methods thus give both μ and t.

For films exceeding a few microns in thickness, difficulties due to depth of focus prevent precise focus simultaneously on both images. We have found it satisfactory to set at an intermediate focal plane, such that both images are defocused by about the same amount. That the compromise is satisfactory is shown by a thickness evaluation of 23 microns with an 8-mm. objective (depth of focus 2 microns) for a sheet of mica of thickness known to be $22\frac{1}{2}$ microns.

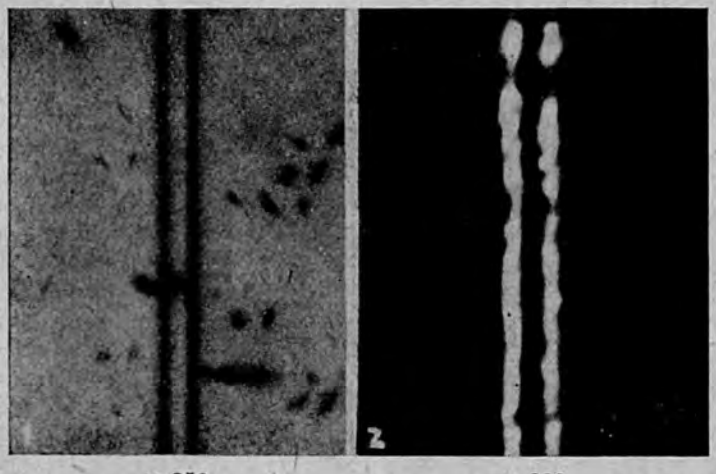

× 350 × 300

As an example of the technique, Fig. 1 shows the double image given by a sheet of mica. On making corrections for the known angle of incidence, previously determined when using the light-profile, and by combining with interference fringes, the values found were $\mu = 1{\cdot}55 \pm 0{\cdot}03$ and $t = 10{\cdot}3 \pm 0{\cdot}2$ microns.

Fig. 2 shows the slit light-cut given by a thin piece of 'Cellophane', giving $\mu = 1{\cdot}56 \pm 0{\cdot}04$ and $t = 22{\cdot}5 \pm 0{\cdot}5$ microns. It is apparent that in both cases a 2 per cent accuracy is attainable.

The method has been successfully applied to the determination of the local variation in thickness of thin collodion, Canada balsam, and liquid films on crystal surfaces, and it is clear that the method offers a useful new procedure for film thicknesses exceeding 1 micron in thickness.

H. Rahbek
M. Omar

Royal Holloway College
(University of London),
Englefield Green, Surrey.
March 10.

[1] Tolansky, S., *Nature* [**169**, 455 (1952)].

Printed in Great Britain by Fisher, Knight & Co., Ltd., St. Albans.

(*Reprinted from Nature, Vol.* 170, *p.* 81, *July* 12, 1952)

Thin-Film Interferometric Techniques for High-Magnification Topographical Studies

THIS communication describes a simple interferometric technique for examination of surface topography without the use of optical flats, the particular advantage being the possibility of using high magnification in extension across the surface without the use of a complex interference microscope. The techniques are based upon the production of a thin transparent film of Canada balsam on the surface. A drop of Canada balsam dissolved in benzine is placed on the surface and, after spreading, dries as a thin film. The spreading is assisted by a touch of cedar wood oil. The thin film appears to follow closely the contour of the lower surface, while taking on a reasonably flat upper surface, although wrinkling can at times be detected. Illumination with monochromatic light leads to the production of an interference picture which exhibits some degree of multiple-beam interference and, as the film is very thin, high resolution, using up to 3-mm. dry objectives, can be used. Thus it is possible to examine interferometrically with simultaneous high magnification in extension, a condition not normally realizable with a multiple-beam equipment employing optical flats.

The wrinkling or curvature of the surface of the film, which is irrelevant to the topography under study, restricts the application of the method largely to the study of discontinuities, at which any spurious topography due to surface curvature does not invalidate conclusions drawn as to the heights of the discontinuous steps. Order allocation is readily obtained by using different wave-lengths, and the direction of the steps by arranging the surface film to be wedged in a suitable direction. The method has the merit that it can be used on relatively inaccessible regions of crystals.

Fig. 1 ($\times$ 600 in extension) shows growth steps on a silicon carbide crystal. Fig. 2 ($\times$ 1,800 in extension) shows the interferogram given by growth trigon on a natural (111) diamond octahedron face. This is of considerable interest in that it reveals a 'trench' surrounding the trigon about half a light-wave in depth. Fig. 3 (which contains, of course, a good deal of empty magnification) shows, at $\times$ 3,000, a growth step on the surface of a hæmatite crystal, and the main feature of interest here is the fact that the step edge is shown distinctly not to be vertical but to be at an angle of some 4·4°, a feature which could not be revealed by multiple-beam methods.

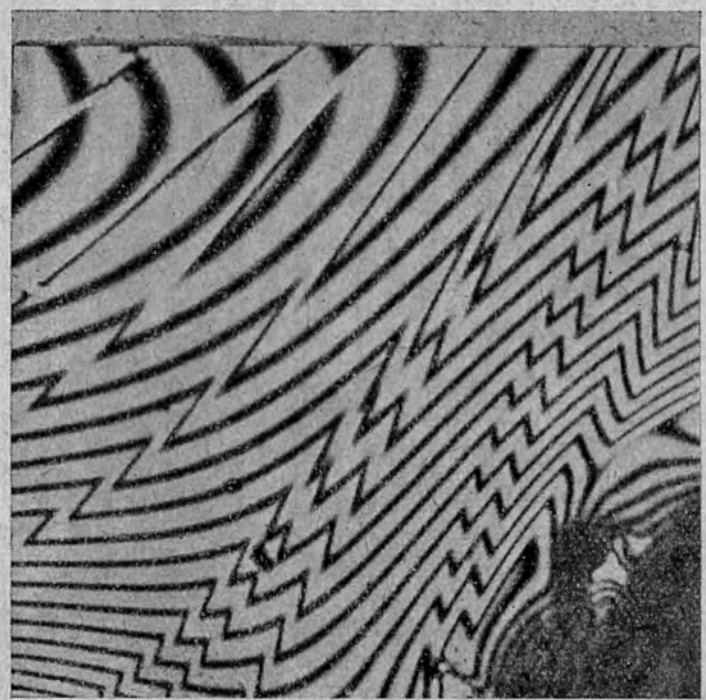

Fig. 1 (× 600)

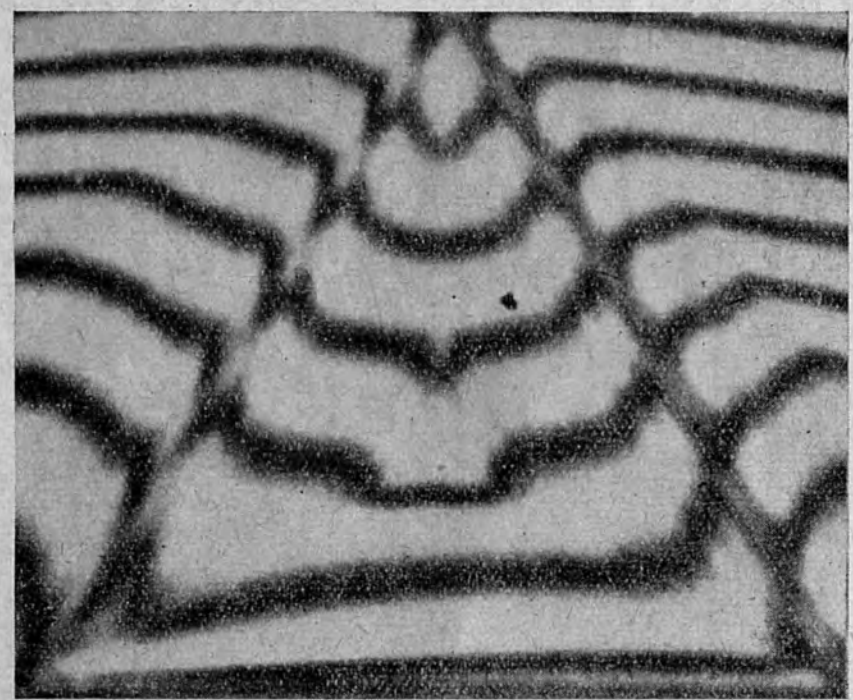

Fig. 2 (× 1,800)

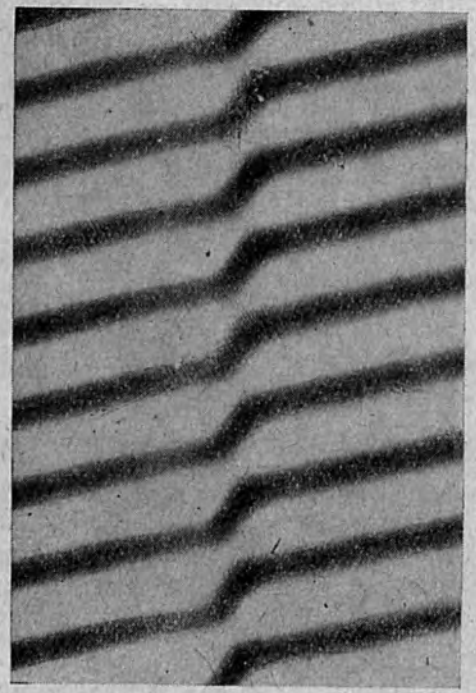

Fig. 3 (× 3,000)

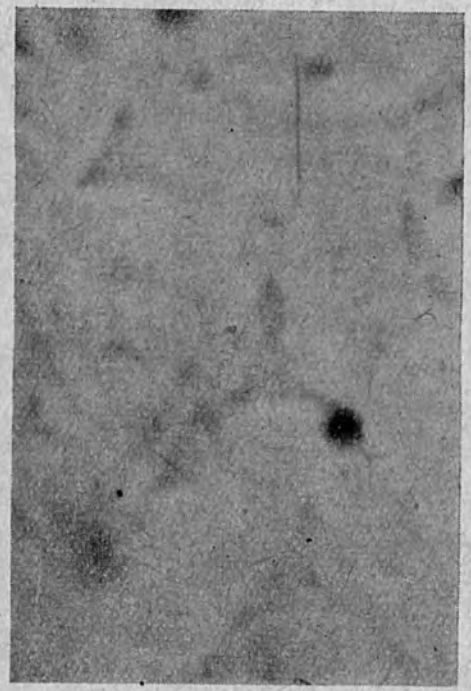

Fig. 4 (× 400)

Fig. 5 (× 400)

In a second method of using the thin-film technique, the Canada balsam is pulled by an oil drop at the edge of the specimen before setting, under which conditions a thin film of almost uniform thickness can be obtained on a reasonably flat surface. On illumination with an unfiltered mercury arc, or white light, high interferometric contrasts appear and a wealth of detail is revealed, the system operating not as a topographical measuring device but as an enhancer of contrast, particularly to the eye, which is so sensitive to colours. Fig. 4 ($\times$ 400) shows a region of the surface of a diamond photographed by ordinary means. Fig. 5 is the interferometric contrast picture. A phase-contrast micrograph of the same region does not reveal much more than is shown by this simple interferometric device.

Finally, it is possible to use multiple-beam methods by first silvering the crystal, depositing the film and then silvering the film, but so sensitive does the method become and so extremely narrow are the fringes that especial care must be taken to avoid wrinkling.

S. Tolansky
M. Omar

Royal Holloway College,
Egham, Surrey.
March 28.

Printed in Great Britain by Fisher, Knight & Co., Ltd., St. Albans.

(*Reprinted from Nature, Vol.* 170, *p.* 758, *November* 1, 1952)

Evaluation of Small Radii of Curvature using the Light-Profile Microscope

THE light-profile microscope described by Tolansky[1] is being applied in this laboratory to several fields, including the study of features of crystal growth[2], the measurement of the thickness of thin film[3] and evaluation of amplitudes of oscillation[4]. In this communication a brief description is given of a further application, whereby the radii of curvature of small spheres, droplets, cavities, etc., can be readily measured.

When the light profile passes over a curved surface, a curved profile line appears in the field of view, a spherical surface leading to a profile which approximates to part of an ellipse, the eccentricity of which is determined by the ratio of the magnifications in extension and in depth. From the curved profile and the known magnifications, the curvature of the surface can be evaluated. (Depending on the flatness of field of the particular objectives available, it may in individual cases be necessary to determine field curvature and correct for this—an easy matter.)

The reliability of the procedure has been tested by using it on a steel ball-bearing of radius 0·6 mm., for with such an object Newton's rings can readily be obtained to give a precise local value of curvature. Furthermore, a principal advantage of the light profile is the availability of high power. The steel

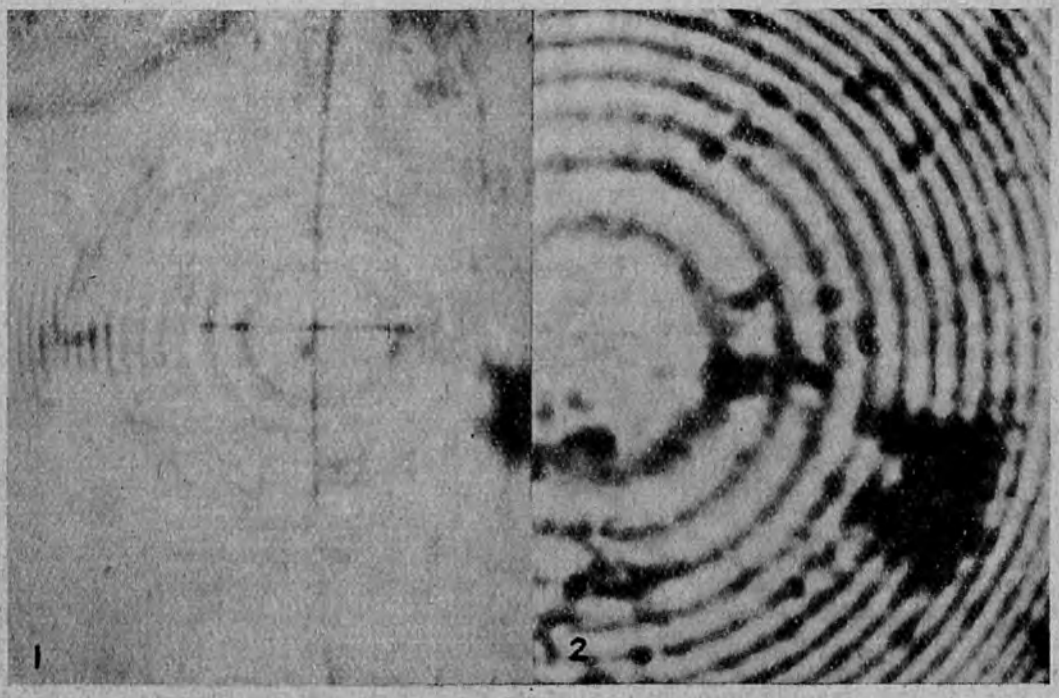

ball was placed on a cover slip and examined with λ 5,461 at $\times$ 875 (4-mm. objective). Newton's rings are seen in Fig. 2. Fig. 1 shows the light profile at $\times$ 450 in extension. The optical arrangement suited to the light profile is not the best for interferometry, hence Newton's rings can be seen only faintly, superposed on the profile. The radius of curvature calculated from the interference fringes is 0·596 mm. and from the profile 0·595 mm., the estimated error in the latter being some $\pm$ 1 per cent (that is, $\pm$ 0·005 mm.).

There is, then, complete confirmation of the reliability of the light-profile method, particularly for measuring curvature of small bodies or small cavities. Spherical cavities, such as those produced in micro-indentation by spheres or ball-ended diamonds, erosion pits, cavities produced by spark discharges on metals, etc., are but some of the features now under examination.

S. Tolansky
M. Omar

Royal Holloway College
(University of London),
Englefield Green,
Surrey. July 16.

[1] Tolansky, S., *Nature*, **169**, 445 (1952).
[2] Tolansky, S., *Zeitschrift für Elektrochemie*, **56**, 263 (1952).
[3] Omar, M., and Rahbek, H., *Nature*, **169**, 1008 (1952).
[4] Tolansky, S., and Rahbek, H., *Nature*, **169**, 1060 (1952).

Printed in Great Britain by Fisher, Knight & Co., Ltd., St. Albans.